A STUDY OF CPFSK TRELLIS MODULATION CODES ON GAUSSIAN AND NON-GAUSSIAN CHANNELS

RANUITH LIYANAPATHIRANA

A STUDY OF CPFSK TRELLIS MODULATION CODES ON GAUSSIAN AND NON-GAUSSIAN CHANNELS

by

© Ranjith Liyanapathirana, B.Sc.Eng.(Hons.), M.Eng.

A thesis submitted to the School of Graduate
Studies in partial fulfillment of the
requirements for the degree of
Doctor of Philosophy

Faculty of Engineering and Applied Science
Memorial University of Newfoundland

June 1995

St. John's Newfoundland Canada

ISBN 0-612-06131-0

ABSTRACT

The objectives of this study are to find improvements to CPFSK trellis modulation codes on AWGN channels, and to investigate the effectiveness of using suboptimum coherent phase detection of CPFSK signals on non-Gaussian channels. A simplified, time-invariant, finite-state trellis is introduced for M-CPFSK signals. Based on this, a matrix representation is formulated for M-CPFSK with $h \leq 1/M$. A class of fixed-h binary nonlinear CPFSK trellis modulation codes is constructed and analysed. Numerical results indicate that, for a given complexity, binary nonlinear CPFSK schemes can be designed so that they achieve the maximum memory length allowed by the number of trellis phase states. When $h = 1/M$, the optimum binary nonlinear CPFSK schemes exhibit coding gains of upto 2.2 dB compared with MSK signalling. The suboptimum coherent phase detection technique for CPFSK is a detection technique that has been directly adapted from PSK. Implementation of this detector is much simpler than that of the correlation receiver. Based on a code search subject to a set of heuristic design rules, self-transparent 4-CPFSK and 8-CPFSK trellis modulation codes with $h \leq 1/M$ are found for the carrier phase offset channel. It is found that the best self-transparent codes for M-CPFSK with $h \leq 1/M$ are identical with the optimum codes for the classical Gaussian channel found in the literature. Using the conventional method of computing an equivalent minimum distance, the performance of suboptimum coherent detection of CPFSK is evaluated on carrier phase offset channels. It is found that 8-CPFSK trellis modulation codes are more susceptible to carrier phase offsets than 4-CPFSK trellis modulation codes. Channel cutoff rate bounds are calculated for coherent PSK and suboptimum coherent CPFSK on (i) the AWGN channel and (ii) the mobile satellite channel modelled as a Rice fading channel with a steady line-of-sight component. It is shown that suboptimum coherent detection of 4-CPFSK is inferior to 4-PSK, but suboptimum coherent detection of 8-CPFSK with $h \geq 1/4$ and 16-CPFSK with $h \geq 1/8$ offer better coding potential than coherently detected 8-PSK and 16-PSK, respectively. This makes suboptimum coherent detection of 8-CPFSK and 16-CPFSK more attractive alternatives to PSK signalling on mobile satellite channels.

ACKNOWLEDGEMENTS

I am most grateful to Dr. S. Le-Ngoc for his guidance and supervision of my thesis. I wish to thank Dr. R. Venkatesan and Professor N. Ekanayake for serving in my supervisory committee and for providing me with valuable advice during the preparation of the thesis.

Financial support for this project was provided by Memorial University of Newfoundland Graduate Fellowship, Faculty of Engineering and Applied Science Teaching Assistantships, and Natural Sciences and Engineering Research Council (NSERC) of Canada.

My sincere thanks also go to fellow graduate students for their help, and all my family members for their encouragement and affection.

Contents

List of Figures

List of Tables

SYMBOLS

AM	Amplitude Modulation
ASK	Amplitude-Shift-Keying
AWGN	Additive White Gaussian Noise
a_n	n^{th} data symbol
C	Shannon capacity
CDMA	Code-Division Multiple Access
CCITT	International Telegraph and Telephone Consultative Committee
CPFSK	Continuous-Phase Frequency-Shift-Keying
CPM	Continuous-Phase Modulation
D	Euclidean distance
DPSK	Differential Phase-Shift-Keying
FDMA	Frequency-Division Multiple Access
d^2_{min}	Normalized squared minimum Euclidean distance
d^2_n	Normalized squared minimum equivalent distance
$x(t)$	Baseband data signal
E_b	Energy per bit
E_s	Energy per symbol
FFSK	Fast-Frequency-Shift-Keying
FM	Frequency Modulation
FSK	Frequency-Shift-Keying
f_0	Carrier frequency
h	Modulation index
$\Im$	Imaginary part of a function

ISI	Inter-Symbol Interference
k	Constraint length of a code
K	Coherent to noncoherent energy ratio (Rice factor)
L	Length of frequency pulse
λ	Chernoff bound parameter
λ_0	Optimum Chernoff bound parameter
M	Order of the modulation scheme
MAP	Maximum *a posteriori* probability
MED	Minimum Euclidean Distance
MHPM	Multi-h Phase Modulation
MLSE	Maximum-Likelihood Sequence Estimation
MSK	Minimum Shift Keying
MSS	Mobile Satellite Service
N	Number of states. Length of transmitted sequence
$N_0/2$	Double-sided noise power spectral density
N_R	Receiver path memory
$n(t)$	Noise
ν	Memory length of a code
$\nu_{\max}$	Maximum memory length of a code
p	Numerator of the modulation index
P_e	Symbol error probability
ϕ_n	Phase angle at the end of n^{th} signalling interval
PLL	Phase-Locked Loop
PSAM	Pilot Symbol Assisted Modulation
PSK	Phase-Shift-Keying
$\phi(t)$	Phase angle

q	Denominator of the modulation index
QAM	Quadrature Amplitude Modulation
QASK	Quadrature Amplitude-Shift-Keying
$r(t)$	Received signal
RC	Raised-Cosine
$\Re$	Real part of a function
R_0	Channel cutoff rate
RF	Radio Frequency
ρ	Normalized fading amplitude
σ	Standard deviation
SNR	Signal-to-Noise Ratio
$s(t)$	Transmitted signal
T	Signalling interval or symbol duration
T_b	Bit interval or bit duration
t	Time
TCT	Tone-Calibration Technique
TDMA	Time-Division Multiple Access
TTIB	Transparent Tone-In-Band technique
WARC	World Administrative Radio Conference
$\mathbf{x}$	Input symbol sequence
$\mathbf{y}$	Output symbol sequence

Chapter 1

Introduction

1.1 Digital communication systems

Communication systems are intended to convey information from one location to another or from one point in time to another. These systems include telephony, telegraphy, broadcast audio, television, cellular mobile radio, and magnetic recording, to name a few. To transmit information over a channel or to store information in a medium, many basic signal processing operations have to be performed on the baseband signal. The following operations are fundamental to all communication systems (although, in a given system, not all operations appear), source coding, channel coding, modulation, multiplexing, filtering and synchronisation. The simplified block diagram of Figure 1.1 shows only those operations of a communication system that are of concern to this study.

Modulation is an important signal processing operation that takes place in a communication system. In modulation, a parameter such as amplitude, phase or frequency of a carrier signal is varied as a function of the instantaneous value of the signal we want to transmit. It can be effectively used to match a signal with the characteristics of the transmission medium and to minimise the effects of channel noise and interference. Often, modulation is also characterised by a frequency

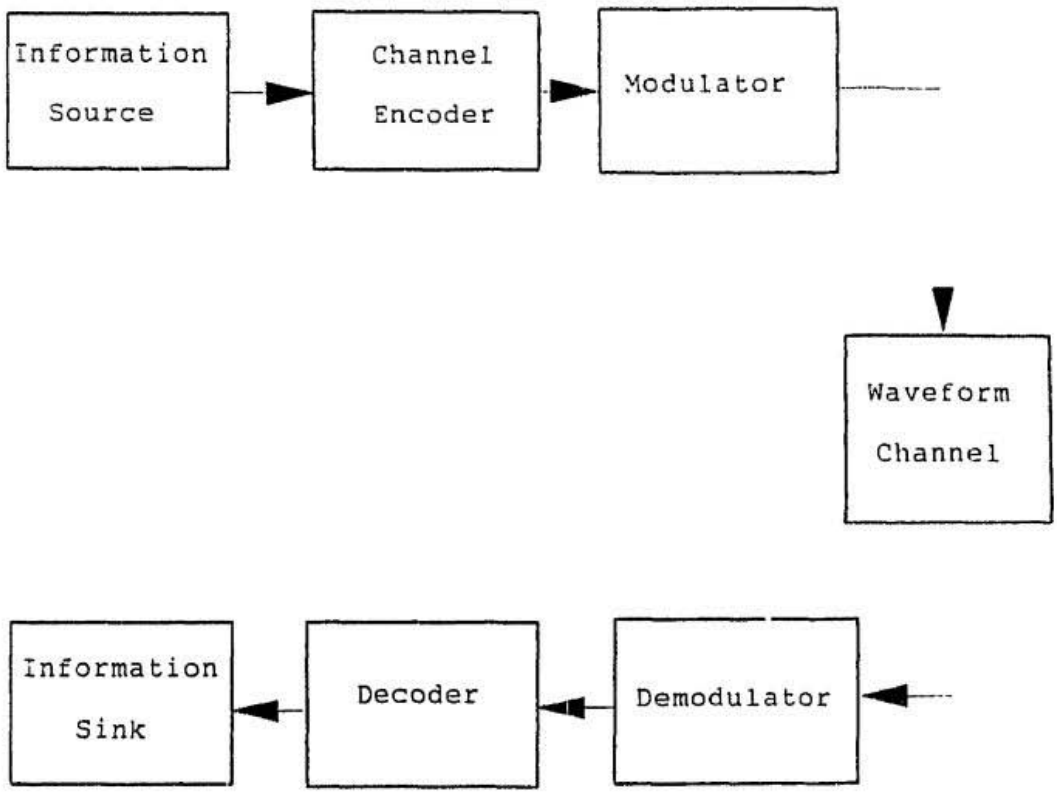

Figure 1.1 Simplified block diagram of a communication system.

translation to a new higher band of frequencies to provide the capability of multiplexing many signals. The baseband information is retrieved at the receiver by the complementary or inverse operation of modulation which is the demodulation. However, the demodulation method is not unique since there can be several distinct implementations.

Modulation can be either analog or digital. Digital equivalents of three well known analog modulation techniques, amplitude modulation (AM), phase modulation (PM) and frequency modulation (FM) are amplitude shift keying (ASK), phase shift keying (PSK) and frequency shift keying (FSK), respectively.

- **Amplitude-shift keying (ASK)**: In ASK, information is encoded in discrete amplitude levels of the carrier signal. ASK has good bandwidth-efficiency but its performance is severely degraded in nonlinear and fading channels.

- **Phase-shift keying (PSK)**: In PSK, the phase angle of the carrier signal is varied according to the message signal. PSK is a constant-envelope modulation technique and it has good bandwidth-efficiency. The bandwidth depends on the data rate and not on the number of discrete phase angles used for signalling and, therefore, PSK is commonly used in high data rate applications in nonlinear channels.

- **Frequency-shift keying(FSK)**: FSK involves changing the carrier between frequencies depending on the baseband information. This is also a constant-envelope modulation technique. In conventional FSK, the switching from one frequency to another is carried out without regard to the continuity of the phase angle of the carrier at switching times. The discontinuities in the phase angle cause undesirable discrete frequencies in the power spectrum. If the phase is maintained continuous at switching times, the resulting FSK is

known as continuous-phase FSK (CPFSK). CPFSK generally has a smooth frequency spectrum and the bandwidth depends on the data rate as well as on the number of frequencies used for signalling.

There has been a growing trend towards using digital modulation techniques in all communication systems. This is owing to the rapid advances in digital technology and the advantages these systems offer, such as the capacity to transmit different types of baseband signals (speech, video, data) in a common format and the ability to regenerate the signal, thereby minimising the adverse effects of noise and interference.

By the end of the century, most wire-line and optical fibre communication systems will be fully-digital. It is also likely that this will be true for most wireless communications. Beginning with broadcast of high quality digital audio already underway in Japan and Europe and with all-digital high-definition television systems now being tested in the U.S.A., it appears that, by the end of this decade digital will have superseded analog in all forms of broadcasting. Digital modulation techniques are also certain to become the universal choice for future personal communication systems and mobile satellite services.

In the existing digital communication systems, there is always a need for the increase of spectral efficiency. This is necessary because the radio frequency (RF) spectrum is a finite natural resource, while the user demand for spectrum steadily increases. Limitations in bandwidth have been felt in voice-band data transmission through wire-lines, point-to-point digital microwave radio, digital satellite communications and land-mobile communications. At the recently concluded World Administrative Radio Conference (WARC-92), the most important and challenging task was the allocation of additional spectrum for both existing and future

mobile communication systems [83]. Expansion of frequencies for high-frequency, satellite and terrestrial digital-audio broadcasting, and space communications was also a major topic of interest. In many of the above applications the available transmitter power is also limited. Therefore both bandwidth and power-efficiencies are desirable characteristics of digital modulation techniques. Trellis modulation codes have shown to be both power and bandwidth-efficient when compared with the conventional digital modulation techniques.

1.2 Trellis modulation codes

The conventional approach to channel coding regards coding and modulation as separate operations. Therefore the encoder and modulator are independently optimised to achieve the required error performance. The original idea of coding was to add redundant symbols (parity bits or check bits) to binary data symbols so that the receiver could exploit the redundancy to correct erroneous bits. Massey [69] and Ungerboeck [94, 95] showed that considerably lower error probabilities for the same average signal power can be achieved by combining the operations of encoding and modulation in the process of signal design. Demodulation and decoding likewise would be aspects of signal detection at the receiver.

The idea behind this alternative way of achieving redundancy was to use expanded channel signal sets with trellis-coded modulation. In trellis-coded modulation, a signal constellation with 2^{n+1} signals is used to transmit n bits of information. The constellation expansion ratio is thus a factor of two. The 2^{n+1} signal constellation is divided or partitioned into subsets, in a regular way, so that the intra-subset signal space distance is greater than that of the parent constellation. A convolutional code of rate-$n/(n+1)$ is used to select these signal points. Part of the

convolutional code output selects the subset while the other part selects the signal points from the subset. The constellation expansion of a factor of two is due to the code redundancy of one bit per symbol. This type of coding is also referred to as *set-partition coding* in the literature. In [94], it was shown that only marginal additional coding gain can be achieved by resorting to constellation expansion factors greater than two.

Today coding has an even more general definition: that is, a code is a set of sequences. Therefore, "coding is the imposition of one of a set of sequences or patterns onto the transmitted signal [10]." The receiver, having *a priori* knowledge of the set of patterns, chooses the pattern closest to the noisy received signal. The patterns impressed upon signal waveforms with the use of data sequences can be made as complex as necessary within the limits of implementation. The new definition combines the ideas of redundancy coding and modulation into one operation. Redundancy achieved by pre-coding and by expanding the signal set are both included in the new definition. By imposing coded patterns onto phase and amplitude, it has been shown that trellis modulation codes achieve higher power and bandwidth-efficiency. However, this is achieved only by increasing the receiver complexity and processing delay.

According to Viterbi [97], the complexity, which is exclusively in the digital processing, can be made as cheap and virtually as power thrifty as needed by market demand influence on economics of scale, because the phenomenal evolution of solid-state circuit integration has reduced the cost of communication electronic devices by many orders of magnitude, even while proportionately reducing their size and complexity. In the past, prohibitively complex receiver structures have been the major drawback of coherent digital signalling schemes using trellis modulation codes but, complexity is no longer the limiting factor in the practical implementation of

such schemes.

There are two broad classes of trellis modulation codes. The first includes the set-partition codes introduced by Ungerboeck [94]. As explained before, in set-partition coding, subsets of a larger signal set are associated with the transitions of a finite-state machine (usually a convolutional code.) Part of the data is carried in the choice of the subset and a part inside the subset itself. A generic trellis encoder encompassing the idea of set-partition coding is shown in Figure 1.2. Coded patterns of both phase and amplitude are present in such codes because the signal set is often Quadrature Amplitude Modulation (QAM). Thus they are non-constant-envelope codes mostly applicable to the additive white Gaussian noise channel. Several Ungerboeck codes have been adopted by the International Telegraph and Telephone Consultative Committee (CCITT) (ITU-T) as the standards for data transmission over the public switched telephone network [34].

The second class of trellis modulation codes known as continuous-phase modulation (CPM) codes have also received much attention owing to their constant-envelope property. These are based on PSK and FSK. The constant-envelope property makes them particularly suitable for applications in nonlinear channels such as the satellite communication channels. CPM signals employ coded patterns of phase within a constant amplitude signal and achieves spectral efficiency without additional filtering [8]. Thus CPM would suffer less degradation due to amplified nonlinearities (for example in a travelling-wave-tube of a satellite repeater) than would conventional PSK trellis modulation codes. Since saturating amplifiers are typically 2–3 dB more power efficient than purely linear power amplifiers, this could be counted as a gain for CPM in relation to non-constant-envelope trellis modulation codes.

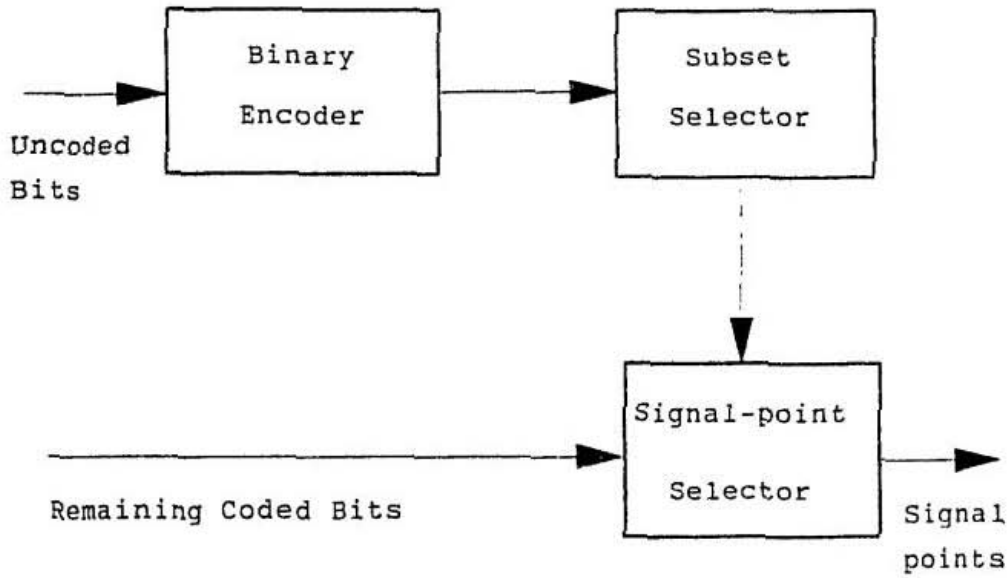

Figure 1.2 Generic trellis encoder.

1.3 Continuous-phase modulation

Trellis modulation codes based on continuous-phase modulation (CPM) carry information in the continuous coded phase of an RF carrier, therefore, the transmitted signal phase is a continuous function of time. The condition that the signal phase be continuous introduces correlation between signals in adjacent signalling intervals. The frequency of a CPM signal at any given time is the sum of frequency pulses, each delayed by a multiple of the channel symbol duration and scaled in proportion to a channel input symbol. The general signal format that will be used in this study is given below in (1.1). The notation, with minor changes, follows that of [6].

Mathematically, the CPM signal can be expressed as [6]:

$$s(t, \mathbf{x}) = \sqrt{2E_s/T}\, \cos\left[2\pi f_0 t + \phi(t, \mathbf{x}) + \phi_0\right], \tag{1.1}$$

where E_s is the symbol energy, T is the symbol duration and f_0 is the nominal carrier frequency. The phase of the signal at $t = 0$ or the phase angle accumulated over the period $-\infty < t \leq 0$ is denoted by ϕ_0. For coherent communication systems considered here ϕ_0 can be set equal to zero without any loss of generality. $\phi(t, \mathbf{x})$ is the information-carrying phase given by:

$$\phi(t, \mathbf{x}) = 2\pi \sum_{n=-\infty}^{\infty} x_n h_n q(t - nT), \tag{1.2}$$

where $\mathbf{x} = \ldots x_{-2}, x_{-1}, x_0, x_1, x_2, \ldots x_n$ is the source sequence of M-ary data symbols, each taking a value of the set $\{\mathbf{x} \mid x_n = \pm 1, \pm 3, \pm 5, \ldots, \pm(M-1)\}$ with equal probability.

The proportionality constant h_n is the modulation index of the CPM signal that may vary from signalling interval to signalling interval. Along with $q(t)$, it determines how much phase changes in the signal for each data symbol. When h_n

varies from signalling interval to signalling interval such a scheme is referred to as multi-h signalling [12]. In multi-h schemes, h_n changes cyclically through a small set of indices over consecutive signalling intervals.

In (1.2), $q(t)$ is the phase response pulse obtained from the baseband frequency pulse $g(t)$ through the relation

$$q(t) = \int_{-\infty}^{t} g(\tau)d\tau. \tag{1.3}$$

Generally, it has been shown that the highest slope in $q(t)$, which is the frequency peak of $g(t)$, affects the width of the main lobe of the frequency spectrum, while the spectral side-lobes are set by the number of continuous derivatives in the pulse [6]. The phase pulse response begins at $t = 0$ and spans a finite duration of $(L-1)$ signalling intervals, where L is the order of the CPM scheme. For $L \leq 1$, full-response CPM schemes are obtained and for $L > 1$, partial-response CPM schemes are obtained. Some commonly used phase response pulses are shown in Figure 1.3. By choosing different phase response pulses $q(t)$ and varying h_n and M, a limitless variety of CPM schemes can be realised. A list of the most common CPM signal formats can be found elsewhere [6].

The phase of CPM signal forms a tree structure. In particular the phase of an M-CPFSK signal follows a linear trajectory with one of M slopes during each signalling interval. The phase tree of a typical CPFSK signal is shown in Figure 1.4. Any trellis modulation code that can be generated with a finite-state machine has a trellis as well as a tree structure. However, this study will have little need for the tree structure since it can be simplified to form a finite-state trellis for rational value modulation indices as will be discussed later in Chapter 3.

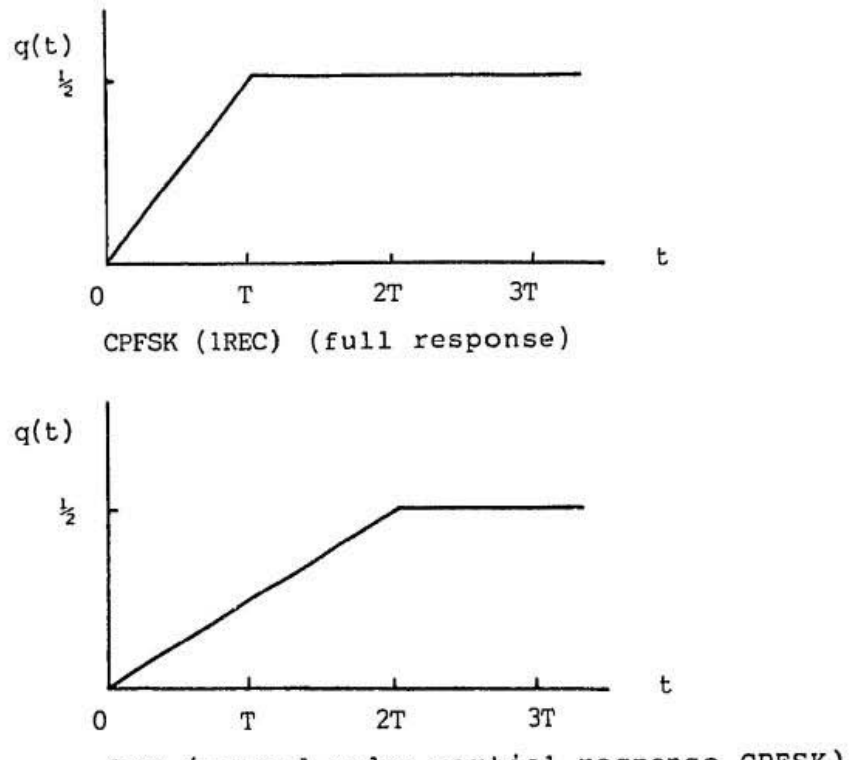

Figure 1.3 Common CPM phase response pulses.

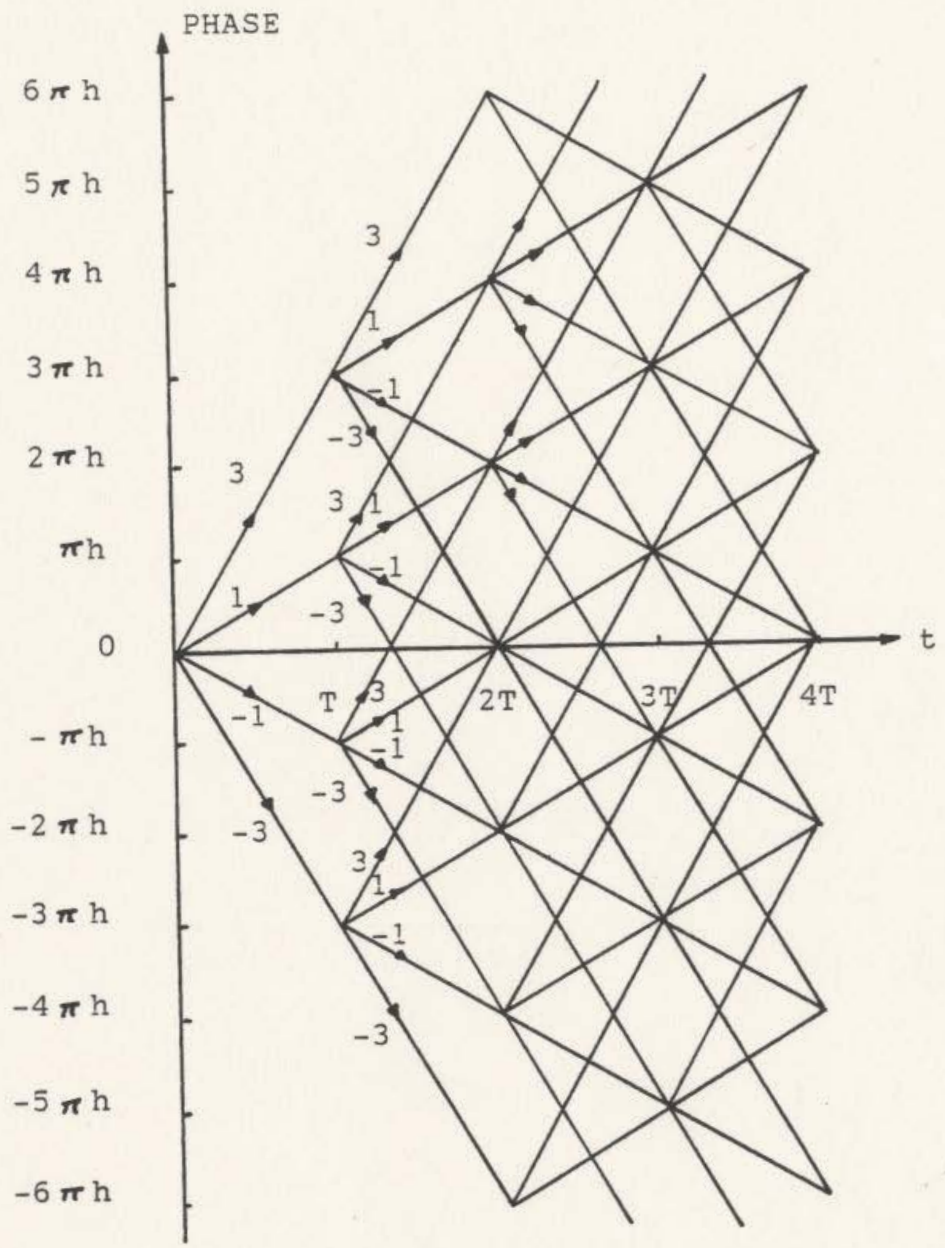

Figure 1.4 Phase tree for 4-CPFSK.

1.4 Detection of CPFSK trellis modulation codes

CPFSK trellis modulation codes can be detected either by sequence detection techniques or using symbol-by-symbol detection techniques. In practice, the maximum-likelihood sequence detector consists of a correlation demodulator followed by a trellis decoder. Typically, the Viterbi algorithm is employed in the trellis decoder to make use of the correlation between signals introduced by the phase continuity property. Most trellis decoding schemes (the notable exception being sequential decoding) operate in a way that two or more possible encoded sequences over a limited time span (known as the receiver path memory or the decoder memory) are compared to decide which sequence is most likely, given the corresponding received sequence. In an ideal situation, this decision should be maximum likelihood. In such a case, given the received sequence $y_1, y_2, \ldots, y_N$ corresponding to an input symbol sequence of $x_1, x_2, \ldots, x_N$, the decoder should select the encoded sequence that maximises the probability $P(y_1, y_2, \ldots, y_N \mid x_1, x_2, \ldots, x_N)$. The Viterbi algorithm [43] uses many such decisions, thereby selecting the maximum-likelihood sequence over the complete message rather than determining the maximum-likelihood symbol at a given time based on only one such decision (as in most decoding schemes for block codes [70]).

Well known symbol-by-symbol detection schemes available for the detection of CPFSK trellis modulation codes are coherent detection, non-coherent detection and limiter-discriminator detection. In non-coherent detection, the receiver only knows the symbol-timing while the carrier-phase is completely unknown to the receiver. Though not suitable for every channel condition, coherent detection techniques are superior to non-coherent detection techniques and to realise the full potential of trellis modulation codes, coherent detection is essential.

1.5 Correlation detection and trellis decoding

The optimum correlation receiver for coherent detection of CPFSK trellis modulation codes is shown in Figure 1.5. It can be separated into the following three tasks: demodulation, synchronisation, decoding.

1. Demodulation is accomplished by a bank of correlators (analog multiplier and integrator combination) supplied with a known set of coherent reference signals $s_1(t)$, $s_2(t)$, $s_3(t)$, ... $s_{qM}(t)$. In Figure 1.5, $r(t)$ is the received signal and $n(t)$ denotes Gaussian noise. To demodulate an uncoded M-CPFSK signal, qM such reference signals are needed, where q is the denominator of the rational value modulation index h. Correlators are replaced in practice by a set of matched-filters.

2. Synchronisation of the locally generated reference signals' phase to the carrier used in the modulator is necessary for the correct demodulation of the signal. It also includes extraction of symbol-timing information so that the received signal and the recovered clock are synchronised with the transmitter clock.

3. Decoding of the demodulated signal according to the Viterbi algorithm [43] in conjunction with a distance measure appropriate for the channel conditions results in the sequence of symbols most likely to have been transmitted.

The performance of the correlation receiver is important because it is often used as a reference with which to compare the performance of suboptimum decoding techniques. Because of the high complexity of the correlation receiver, one is motivated to study suboptimum receivers and to seek a compromise between performance and receiver complexity.

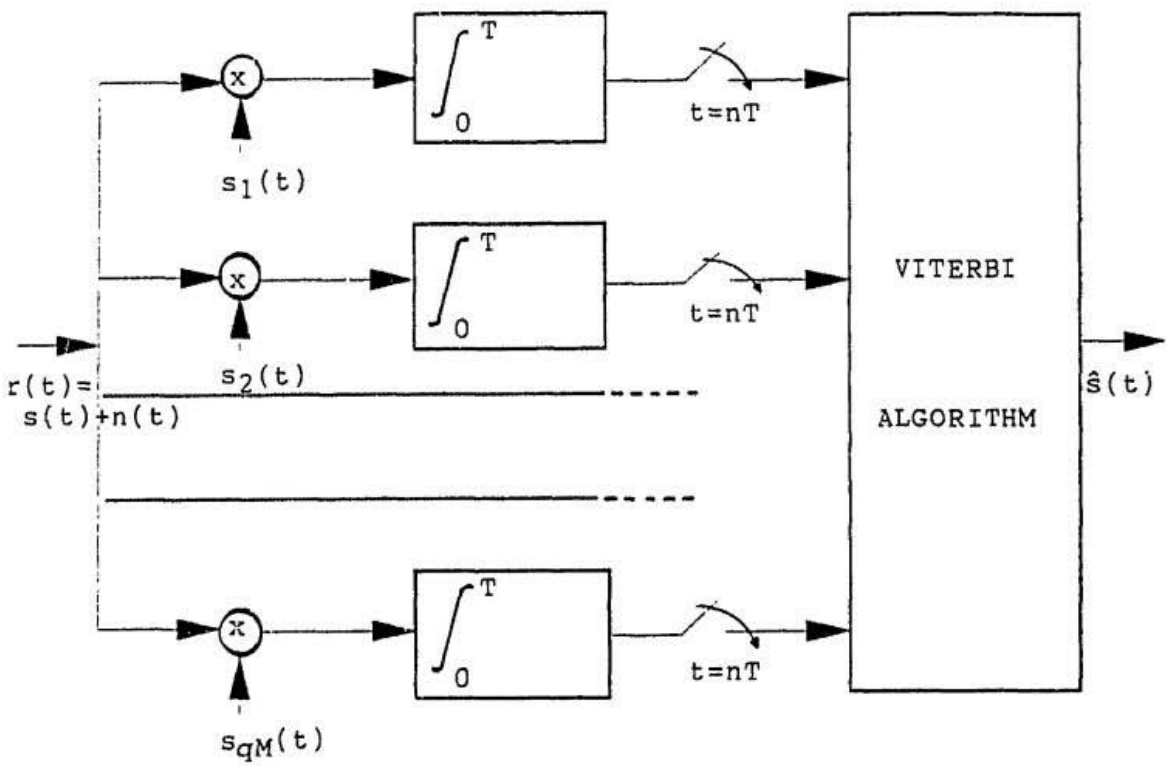

Figure 1.5 Correlation detection and trellis decoding.

1.6 Probability of error and minimum squared Euclidean distance

The usual measure of performance of a coded sytem is the average probability of error that is achieved at a specified signal-to-noise ratio (SNR). In most practical applications, we are only interested in the high-SNR performance. That is, we are interested in those situations where the probability of error is less than 10^{-3} or 10^{-4}. In this case an approximate procedure is available which makes use of the union bound [27, 105]. The union bound technique can be used with any trellis modulation code with maximum-likelihood decoding. It is based on the idea that an event can be expressed as the union of several subevents, then the probability of that event occurring is always less than or equal to the sum of the probabilities of all subevents. Thus, the probability of error can be upper-bound as the sum of the probabilities of each of the error-events. Also, it is well known that the probability of error primarily depends on the Euclidean distance or the signal space distance between the transmitted sequence and its nearest neighbour [105].

In an additive white Gaussian noise (AWGN) channel, the Euclidean distance between any two CPFSK signal sequences $s_n(t)$ and $s'_n(t)$ is given by [19]:

$$D^2[s_n(t),\, s'_n(t)] \triangleq \int [s_n(t) - s'_n(t)]^2 dt, \tag{1.4}$$

where the integral extends over an error-event (the time that the two signal sequences differ). As shown in Appendix A, (1.4) reduces to (1.5) for phase modulated signals and in the special case of CPFSK signals, (1.5) further reduces to (1.6).

$$D^2[s_n(t),\, s'_n(t)] = 2E_s/T \int \{1 - \cos[\phi_n(t) - \phi'_n(t)]\} dt \tag{1.5}$$

$$D^2(s_n,\, s'_n) \approx 2E_s\{1 - \sin[\pi h(x_n - x'_n)]/[2\pi h(x_n - x'_n)] \cos[\pi h(x_n - x'_n)/2 + \phi_n - \phi'_n]\} \tag{1.6}$$

This can be used as the decoding metric in the maximum-likelihood decoding algorithm, usually the Viterbi algorithm [43]. In (1.5) and (1.6), $o_n(t)$ and $o'_n(t)$ are the phase angles (reckoned in modulo-2π) of the two signal sequences $s_n(t)$ and $s'_n(t)$ at $t = nT$.

The minimum squared Euclidean distance (MED) is the global minimum of (1.6) over the finite-state trellis representing the trellis modulation code. That is,

$$D^2_{min} \triangleq \min \quad D^2[s_n(t), s'_n(t)] \quad \forall \; s_n(t) \neq s'_n(t), \tag{1.7}$$

where the minimisation is carried out over all possible pairs of signal sequences $s_n(t)$, $s'_n(t)$.

According to the classical signal space theory [105], the asymptotic error probability of any trellis modulation code operating over the additive white Gaussian noise channel is given by:

$$P_e \approx Q\left(\sqrt{\frac{D^2_{min} E_b}{N_0}}\right), \tag{1.8}$$

where E_b/N_0 is the bit-energy-to-noise-density ratio and $Q(\;)$ is the Gaussian error integral given by $Q(x) = \frac{1}{\sqrt{2\pi}} \int_x^\infty e^{-y^2/2} dy$. It is clear from (1.8) that the error performance of trellis modulation codes in AWGN channels can be improved by increasing the minimum squared Euclidean distance.

It is convenient if we can make the distance in (1.8) independent of energy so that comparisons can be made with codes of different alphabet size or signalling levels M. This could be done by forming the normalised minimum squared Euclidean distance,

$$d^2_{min} = D^2_{min}/2E_b, \tag{1.9}$$

where E_b is the energy per bit. According to the above normalisation the minimum squared Euclidean distance for minimum shift keying (MSK) becomes 2, which is the reference for all our numerical results.

1.7 Distance properties of CPFSK and energy-bandwidth trade-off

For coherent detection of an M-CPFSK signal with $h = p/q$, where p and q are relatively-prime positive integers, the correlation receiver needs qM correlators or matched filters [62]. Often, depending on the value of the modulation index, this number can be reduced to a number below qM. The complexity of the correlation receiver will still be high except for small M and q values. In the case of uncoded M-CPFSK signals, an M-state trellis decoder can achieve almost all the coding gain that is guaranteed by the modulation process [62]. In [90] it is shown that, for all $h < 1$, M-ary full-response CPM schemes can be decoded using a decoder of M-states with only minor degradation in error performance.

A comparison of minimum squared Euclidean distances of M-CPFSK with $h = 1/M$ and M-PSK is shown in Table 1.1. The error performance degradation of CPFSK relative to binary PSK is also shown there. The associated degradation as predicted by the minimum squared Euclidean distance is zero for the binary case, but, it is substantial for higher order modulations. However, for many nonlinear applications, this degradation is more than offset by the reduction of the envelope amplitude variation caused by bandlimiting the signal [106]. Clearly, M-PSK signals have larger minimum squared distances than the corresponding M-CPFSK signals for $h = 1/M$, though multiple-bit detection is used in the latter case. By treating the CPFSK signal as a PSK signal and sampling the phase at symbol transition instants, it is possible to decode the signal with a less complex detection technique known as phase detection and trellis decoding [61]. However, it can be shown that the performance of this suboptimum receiver depends on the phase detection process that is, in the estimation of phase at the end of signalling intervals.

Table 1.1 Error performance degradation of M-CPFSK with h=1/M relative to BPSK.

M	PSK		CPFSK (h=1/M)		Degradation (dB)
	d^2_{min}	d^2_{min} /dB	d^2_{min}	d^2_{min} /dB	
2	2.000	0.000	2.000	0.000	0.000
4	2.000	0.000	1.454	-1.385	-1.385
8	0.879	-3.570	0.598	-5.243	-1.673
16	0.304	-8.175	0.204	-9.914	-1.739
32	0.096	-13.18	0.064	-14.94	-1.756

The Euclidean distance metric given by (1.6) is no longer valid and a new metric for this suboptimum trellis decoder has to be defined, which takes into account the statistics of the errors in the estimation of phase. A more detailed description of this suboptimum receiver and its performance evaluation will be considered in Chapter 5.

In carrier modulated schemes the bandwidth is often defined as the range of frequencies about the carrier frequency within which some fixed fraction of the signal power is contained [6]. In other words it is measured in terms of the fractional out-of-band power. For instance, the 95% power containment bandwidth of a carrier modulated scheme with a carrier frequency f_0 and power spectrum $S(f)$ is the value of B such that

$$\int_{f_0-B/2}^{f_0+B/2} S(f)\,df = 0.95 \int_0^{\infty} S(f)\,df. \tag{1.10}$$

B is known as the double-sided power containment bandwidth of the signalling scheme and it is illustated in Figure 1.6.

It is well known that when the modulation index of a CPFSK signal is decreased towards zero, the bandwidth it occupies also decreases. However, a smaller modulation index generally leads to inferior error performance because of the smaller minimum squared Euclidean distance. Figure 1.7 shows minimum squared Euclidean distance ($10\log d^2_{min}$) against bandwidth for a variety of M-CPFSK schemes with different modulation indices and alphabet sizes (signalling levels). This is commonly known as the energy-bandwidth plot. Two families of curves are shown in Figure 1.7, one for 99% power containment in the double-sided RF bandwidth and the other for 99.9% inband power. Clearly, CPFSK schemes with smaller h use less bandwidth but, consume more energy. Binary CPFSK performs poorly compared with other schemes because the curves lie well to the lower right of the others.

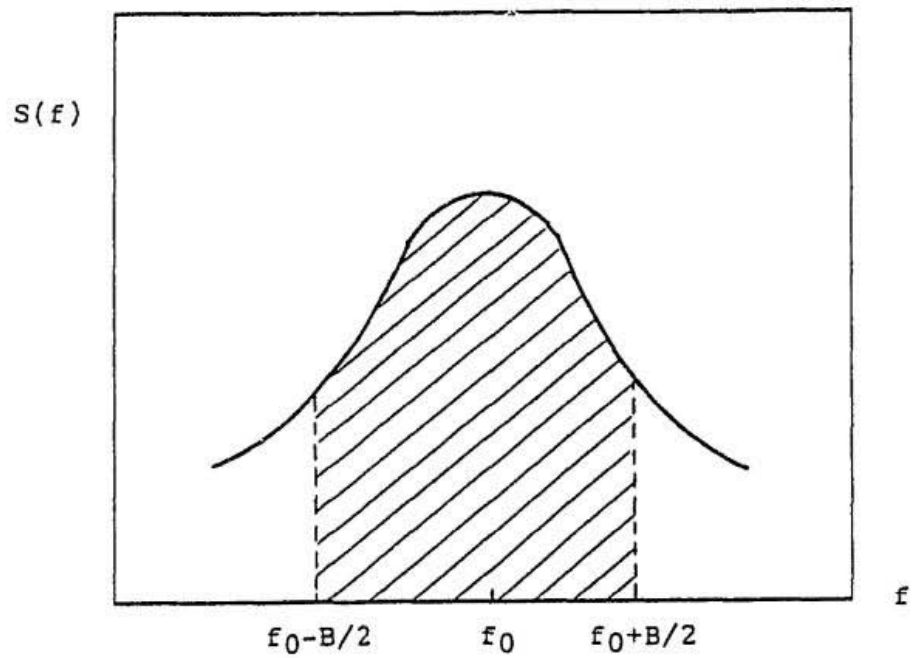

$$\int_{f_0-B/2}^{f_0+B/2} S(f)\,df = 0.95 \int_0^{\infty} S(f)\,df$$

Figure 1.6 Definition of power containment bandwidth for carrier modulated schemes.

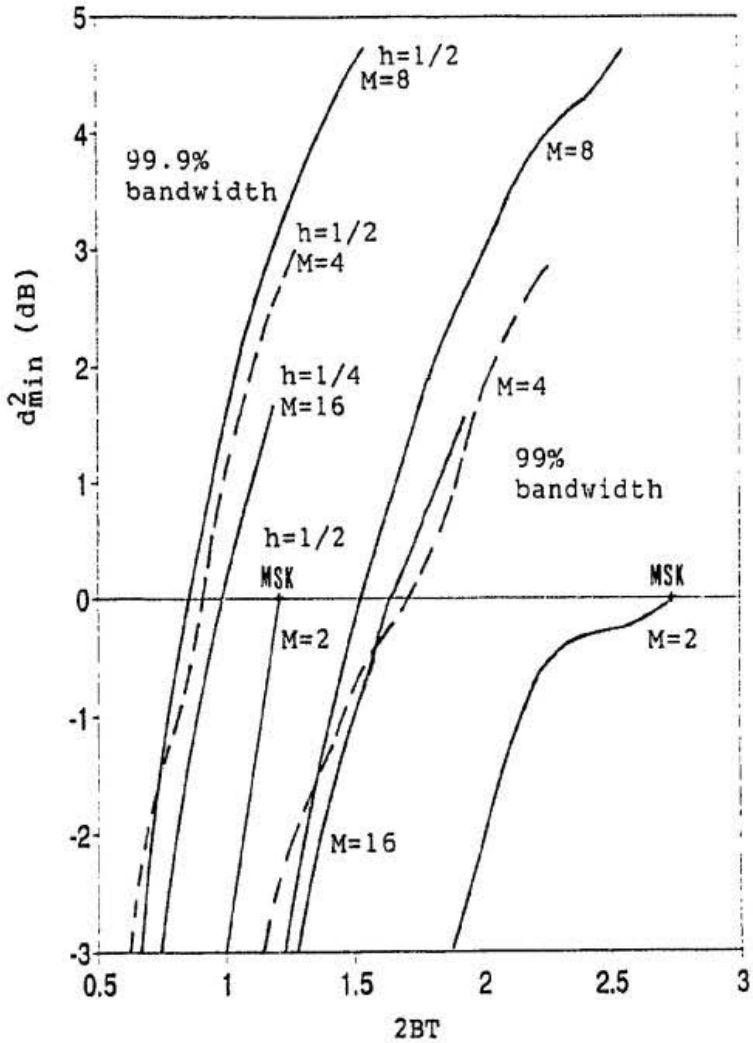

Figure 1.7 Energy-bandwidth trade-off for M-CPFSK (after Anderson et al. [6].)

The curves for 4-CPFSK and 8-CPFSK follow each other closely and both perform relatively better than 16-CPFSK. Although large distance gains are possible by choosing larger h values they are inevitably associated with wider bandwidths. Both 4-CPFSK and 8-CPFSK with small modulation indices (typically $h \leq 1/M$) have their energy-bandwidth performance curves well to the lower left of other schemes. With the small alphabet size they provide a good compromise among bandwidth-efficiency, power-efficiency and complexity.

1.8 Shannon capacity and channel cutoff rate

Shannon capacity, C, is the fundamental limit to communication in any channel. For instance, the Shannon capacity of a band-limited additive Gaussian noise channel (in bits per second) is given by,

$$C = B \log_2 (1 + SNR), \tag{1.11}$$

where B is the channel bandwidth, and SNR denotes the received signal-to-noise ratio. It sets an upper bound on the rate at which information may be transmitted through the channel without error. However, reliable transmission near capacity would only be possible with very complex coding schemes.

While the Shannon capacity gives a range of rates where reliable transmission is possible, it is now believed that the channel cutoff rate R_0 can be taken as the practical upper bound on information rate [24]. It becomes very expensive to communicate reliably over a channel when the information rate R exceeds R_0. Not only R_0 gives a range of rates at which reliable operation is possible but also it gives an exponent to average probability of error [24]. Furthermore, when combined coding and modulation is used on discrete channels the probability of error may not be meaningful because in modern trellis modulation coding there is no direct

not be meaningful because in modern trellis modulation coding there is no direct error correction involved. This was evident from the new definition of coding given in page 6.

Meaningful comparisons among discrete channels can be based on the cutoff rate R_0 [69, 105]. Moreover, bounds on R_0 can be quite useful in predicting the relative performance changes that occur when the noise process or channel model changes. The use of R_0 to assess the effectiveness of trellis modulation codes on interleaved multipath fading channels has also been recently recommended by several researchers [37, 79].

Mathematically, when finite energy M-ary signals $\{\mathbf{s}_i\}, i = 1, 2, \ldots, M$ are transmitted over the AWGN channel with probabilities $\{q_i\}, i = 1, 2, \ldots, M$, the cutoff rate is given by [69]:

$$R_0 = -\log_2\{\min_{\{q_i\}} \sum_{i=1}^{M} \sum_{j=1}^{M} q_i q_j e^{-\frac{|\mathbf{s}_i - \mathbf{s}_j|^2}{4N_0}}\}, \tag{1.12}$$

where N_0 (W/Hz) is the variance of the noise waveform. The unit of R_0 is bits per waveform or bits per signalling interval (bit/T).

Calculation of R_0 for maximum-likelihood detection of CPFSK signals on AWGN channels is given in [11]. Figure 1.8 shows the cutoff rates of 4-CPFSK and 8-CPFSK signals for several h-values plotted against the signal-to-noise ratio. These plots determine, in terms of the channel cutoff rate R_0, the relative effectiveness of each CPFSK modulation scheme on an AWGN channel. The larger R_0 is for a given average transmitted energy, the better the channel on which coding is to be used. R_0 levels-off at $\log_2 M$ bits per signalling interval, since M-ary modulation can only transmit a maximum of $\log_2 M$ bits per symbol error-free. Schemes with $h = 1/M$ exhibit almost all the coding potential of M-CPFSK signalling in the intermediate to high signal-to-noise ratio range. When the signal-to-noise ratio is

small 4-CPFSK and 8-CPFSK schemes have almost the same cutoff rates. Clearly, increasing h beyond $1/M$ does not result in significant reduction in the SNR required. Therefore based on the channel cutoff rate criterion too M-CPFSK signals with $h \leq 1/M$ provide the best combination of power-efficiency and bandwidth-efficiency for AWGN channels.

Research reported in this thesis is partly motivated by the above observations and is directed towards (i) the improvement of trellis modulation codes based on M-CPFSK signals with $h \leq 1/M$ for data transmission through the classical Gaussian channel, and (ii) the application of suboptimum coherent detection (coherent phase detection and trellis decoding) of M-CPFSK trellis modulation codes for data transmission through non-Gaussian channels. By 'non-Gaussian' we mean channels with carrier-phase offsets and channels with amplitude only multipath fading. It should be emphasized that only full response, fixed-h M-CPFSK signals with a rectangular phase response pulse will be considered and unless otherwise stated ideal coherent detection with a maximum-likelihood decoder at the receiver is assumed. The scope of the present study is given in the next chapter after the pertinent literature on the subject has been reviewed.

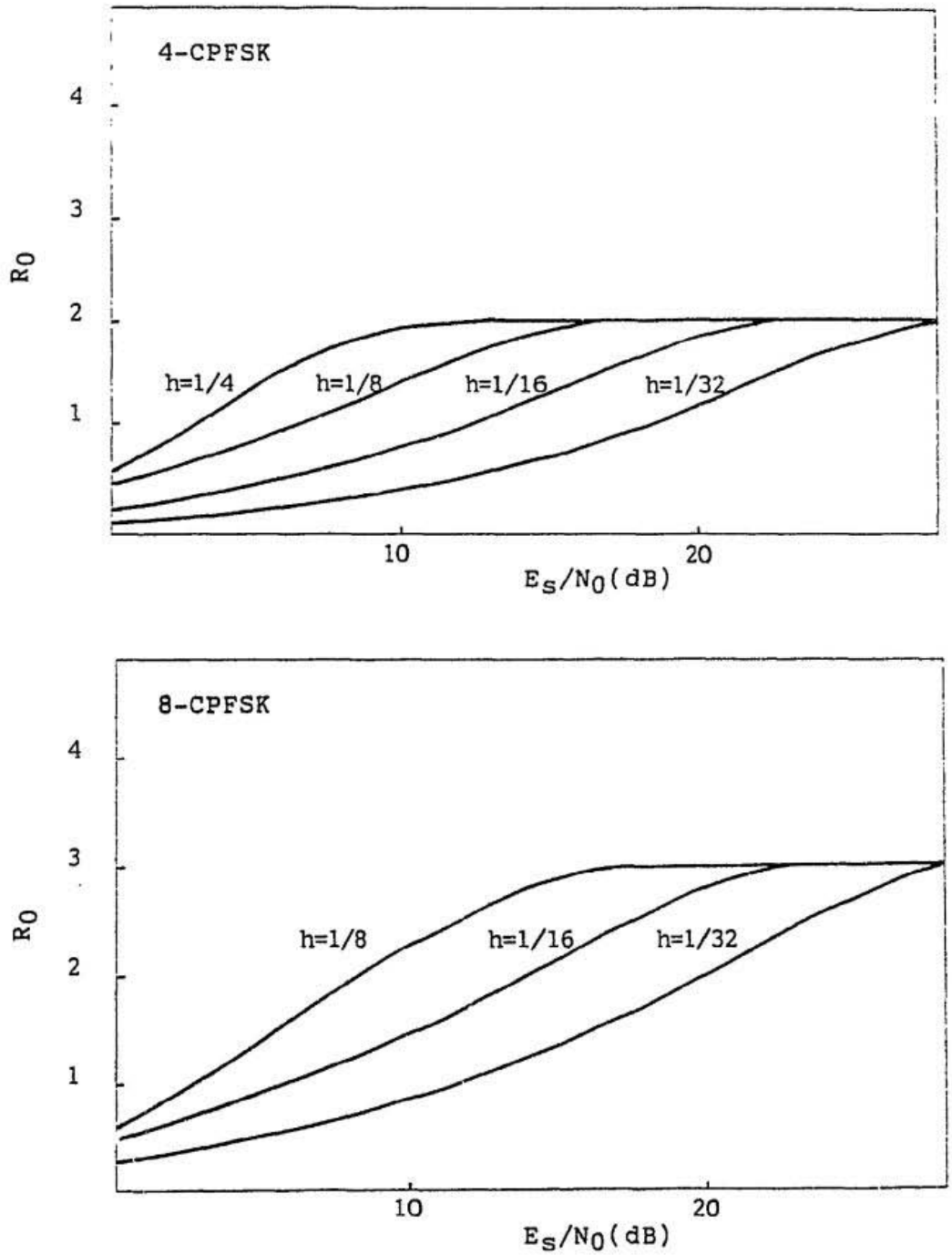

Figure 1.8 Cutoff rate R_0 of 4-CPFSK and 8-CPFSK against signal-to-noise ratio E_s/N_0 on an AWGN channel.

Chapter 2

Literature Review

2.1 Introduction

This chapter presents a review of literature on continuous-phase modulation (CPM). The literature specific to continuous-phase frequency-shift keying (CPFSK), which is a full-response subset of CPM, will be emphasised. A lot of research work has been conducted on detection, error performance, spectral performance and synchronisation of CPFSK. Regarding trellis coded CPFSK, substantially more results are available for the classical additive white Gaussian noise channel as compared to non-Gaussian channels. A survey of the current literature indicates that less amount of work has been reported on the application of CPFSK trellis modulation codes to channels with multipath fading and carrier-phase offsets.

Scope of the present study and the organisation of the thesis is given at the end of this chapter.

2.2 Continuous-phase modulation

Digital phase modulation with continuous phase first appeared in the work of de Buda [33], Osborne and Luntz [76] and Schonhoff [85]. However, the papers of Anderson, Aulin and Sundberg [12, 14, 19] summarized and generalized the previous

work, and prompted a lot of studies to be conducted in continuous-phase modulation (CPM). In particular, the two-part paper by Aulin and Sundberg [14, 19] introduced the general form of CPM. In Part-I they restricted their attention to *full-response* CPM, while in Part-II, co-authored by Rydbeck, *partial-response* CPM was considered. Relative error performance and spectral characteristics of various continuous-phase modulation formats were presented for the AWGN channel assuming ideal coherent detection. It was also shown that significant processing complexity would be required to achieve low error probabilities while retaining both power and bandwidth-efficiency. Anderson and Taylor [12] introduced multi-h CPM signalling and investigated the error and spectral properties. A practical motivation at the time for the above work was satellite transmission and digital mobile radio using nonlinear power amplifiers. A historical overview of the theory and research literature on CPM can be found in [6, 87, 101].

Among the many CPM schemes that have been reported, the class of full response signalling known as *continuous-phase frequency-shift-keying* (CPFSK) has drawn considerable attention [7, 13, 15, 38, 76, 77, 80, 85]. The special case of binary CPFSK with the modulation index 1/2, often referred to as Minimum-Shift-Keying (MSK) [22, 32, 47] or Fast-Frequency-Shift-Keying (FFSK) [32, 33, 47], has been studied extensively during the late 1960's for use on band-limited non-linear channels as an alternative to conventional quaternary PSK (QPSK). de Buda [33] has discussed the performance of MSK with a two-bit observation interval and has given a self-synchronising receiver structure for MSK. Forney [43] has given a clear exposition of the use of *Viterbi algorithm* for maximum-likelihood sequence estimation (MLSE) of coherently detected CPFSK and in particular, examined the case of MSK. The work of de Buda [33] and Forney [43] generated much interest in M-ary CPFSK signalling.

A restricted class of continuous-phase modulated signals known as multi-h signalling or multi-h phase modulation (MHPM) [11, 12, 22, 40, 41, 42, 73] also has received much attention in the literature owing to their superior error performance. In most multi-h schemes the modulation index varies cyclically from symbol interval to symbol interval. This leads to a delayed merging of neighbouring phase trellis paths, which in turn increases the minimum squared Euclidean distance and improves the error performance. The price paid for the improved error performance of multi-h signalling as compared to fixed-h schemes is the increase in the receiver complexity. This is caused by the use of more than one value of h which requires an additional type of synchronisation known as super-baud synchronisation [40]. In adaptive multi-h signalling [40, 41] the modulation index in a given symbol interval depends on both the transmitted symbol and the state of the system. Adaptive binary multi-h CPM schemes that achieve maximum constraint length allowed by the number of trellis states have been designed and they have been shown to offer better energy-bandwidth trade-off than MSK signalling [40].

2.2.1 Detection of continuous-phase modulation

It has been shown in the literature [32, 33, 43, 76] that between the two classes of detection techniques available for CPFSK signals, the Maximum-Likelihood Sequence Detection (MLSD) technique yields better performance than the symbol-by-symbol detection technique. For rational value modulation indices, the CPFSK signal can be modelled as a finite-state time-invariant Markov process [6, 14, 19], thus the Viterbi algorithm can be used for optimum demodulation in the presence of additive white Gaussian noise [43, 94]. For the particular case of MSK, coherent Maximum-Likelihood Sequence Detection can achieve the same error probability as the conventional non-coherent detection of binary FSK with 3 dB less power [33].

Osborne and Luntz [76] considered the maximum-likelihood detection of binary CPFSK for arbitrary modulation indices. Schonhoff [85] extended the approach of Osborne and Luntz [76] to M-ary CPFSK and concluded that significant power gains can be achieved by the careful selection of the modulation parameters.

There are basically two methods by which the performance of a particular detection scheme may be determined. One is an exact procedure which involves the consideration of all possible error situations or error events because the probability of error can change with a different transmitted sequence and to obtain the error rate one must average over all possible transmitted sequences. Thus it produces a result which is valid at all signal-to-noise ratios (SNR). Though CPM schemes are exactly defined, obtaining closed-form expressions for the probability of symbol error (P_e) is made impossible due to the complexity of the modulation. But in many practical situations, only the high-SNR performance is required. Therefore, in modulation schemes, where the symbol error probability is difficult to determine exactly, it has become a common practice to obtain upper and lower-bounds instead [13, 54]. At high-signal-to-noise ratios, the symbol error probability of CPM on an AWGN channel is asymptotically determined by the squared minimum Euclidean distance (d^2_{min}) given by $P_e \approx Q(\sqrt{d^2_{min}/2N_0})$ [6, 105]. This single parameter description of the detection performance has greatly simplified the problem of searching for reliable CPM schemes at high-SNR.

On additive, white Gaussian noise channels with high signal-to-noise ratios, the error probability of CPFSK schemes is dominated by the minimum Euclidean distance between any two signals. This is not always true at low and intermediate signal-to-noise ratios, because other error events with larger Euclidean distances can become significant [91]. Thus it was necessary to find methods to study the distribution of error events and their distance profiles. Several algorithms have

been discovered by a number of researchers for evaluating the minimum distance parameters of CPFSK schemes [6, 19, 75, 94]. These algorithms belong to the class of tree-search and trellis-search algorithms. A well established trellis-search algorithm is described by Mulligan and Wilson [75]. Tennant and Kingsbury [91] extended this algorithm to evaluate distances and paths of error-events other than the free distance event. The above algorithms are computationally efficient only when the number of states in the trellis is small and, therefore, performance bounds are the most common means of estimating the error probability and designing new and more complex coded-modulation schemes.

For uncoded CPFSK signals with $h \leq 1/2$ the exact formula for the minimum squared Euclidean distance has been recently obtained by Rimoldi [81]. While the above interval of h covers most of the cases of practical interest, in [59], we have derived the closed-form expression for the d^2_{min} of M-CPFSK valid for any rational modulation index. Obtaining closed-form expressions for the minimum Euclidean distance of other CPM schemes, however, is made difficult by their complexity, and computer algorithms must be used instead.

The optimum maximum-likelihood sequence detection receivers for CPFSK tend to suffer from high complexity and they are more sensitive to carrier-phase perturbations compared with receivers for QPSK and other memoryless modulations [6]. The optimum receiver is useful mostly to provide a theoretical performance reference to which other receivers could be compared. In certain applications, such as cellular land-mobile radio, non-coherent receivers and suboptimum receivers have proven useful.

The optimum non-coherent detector for CPM signals was derived in [76]. This receiver is optimum irrespective of the signal-to-noise ratio, though it is always inferior to coherent maximum-likelihood detection. In non-coherent detection the

receiver only knows the symbol-timing while the carrier-phase is completely unknown to the receiver. The performance has been analyzed by means of an equivalent distance and for CPFSK signals, upper bounds on the probability of error with non-coherent detection have been derived in [6, 16]. In the comparison of various modulation techniques in a band-limited environment like the mobile satellite channel, it is necessary to use spectral performance results in conjunction with error performance results.

2.2.2 Bandwidth of continuous-phase modulation

An important feature of any modulation scheme is its signal bandwidth. It is directly related to the power spectrum of the modulation scheme, however, bandwidth lacks a single definition. Different measures like the fractional out-of-band power (the definition of which was given in Chapter 1) and the position of the spectral nulls have been used to define the bandwidth in different contexts. The bandwidth of a CPFSK signal is normally expressed in the current literature in terms of the 99% inband power definition [6, 5]. As explained in Chapter 1 this is the range of frequencies within which 99% of the total transmitted power is concentrated. The 99% power containment bandwidths of CPFSK signals are almost all less than the 99% power containment bandwidth of PSK and QAM [6]. The 99.9% inband power definition, sometimes used in the literature [6], is a wider measure than the 99% inband power definition. For a given baseband shaping pulse and a modulation index, partial-response CPM schemes always have narrower bandwidths than their full-response counterparts [6].

Several methods of computing the power spectrum of CPFSK have been described in the literature [6, 9, 17, 38, 104]. Wilson [104] has obtained power spectrum of multi-h CPM signalling through computer simulation. In the method de-

veloped by Aulin and Sundberg [6, 17], the autocorrelation function of the CPFSK signal is first evaluated and then the Fourier transform is taken to obtain the power spectrum. Although the power spectrum is taken as the Fourier transform of the autocorrelation function, a typical CPFSK scheme driven by random data does not produce a wide-sense stationary output. An exact autocorrelation function cannot be defined for such a process [6]. Nevertheless, the above method gives accurate results because of the exponential decay characteristic of the autocorrelation function.

Closed-form expressions for the power spectrum can be found only in very simple cases. In [38], expressions for the autocorrelation function and the power spectral density function of M-CPFSK with modulation index $1/M$ have been derived in closed-form and the results compared to those of MSK. It has been shown that M-CPFSK signals with $h = 1/M$ have approximately the same autocorrelation function and the same power spectral density, regardless of the number of signalling levels for $M \geq 4$ [38].

Summarizing the work on spectral performance of CPFSK it can be stated that the power spectrum of a multilevel CPFSK signal is determined by the number of levels and the modulation index, which determines the maximum slope variation among the piecewise-continuous phase trellis. It has been shown that, decreasing the modulation index confines the transmitted power to a narrow-band around the carrier frequency. Furthermore, smoothing of the frequency pulse, as happens in raised-cosine CPM causes the tail of the spectrum to decay rapidly. A more compact spectrum also can be obtained by increasing the pulse duration. A comparison of spectral density of several CPM schemes with that of PSK is given in Fig. 2.1.

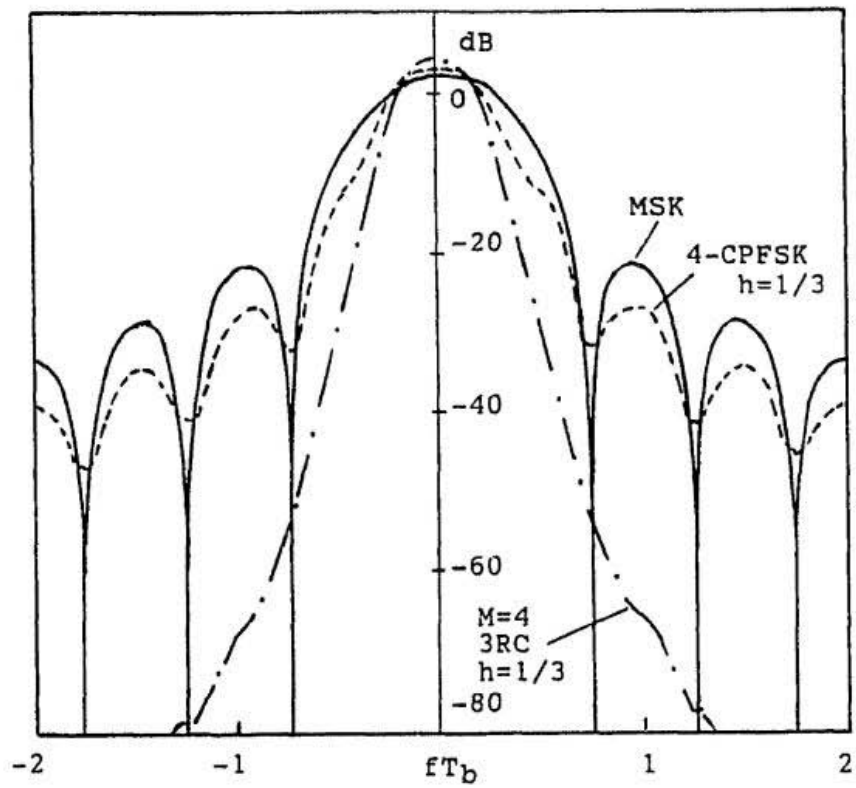

Figure 2.1 Power spectral density of MSK, 4-CPFSK (h=1/3) and M=4, 3RC (h=1/3) (after Anderson et al.[6])

2.2.3 Synchronisation of continuous-phase modulation

Another important area of research has been the synchronisation and carrier recovery of CPM signals. Coherent demodulation requires the use of a properly phased carrier at the receiver. (In coherent detection of CPFSK, for example, the implementation of the Viterbi algorithm requires knowledge of exact carrier-phase.) The carrier phase must be estimated by the receiver from the incoming signal. In addition, symbol timing must be derived from the received signal for both coherent and noncoherent detection [80]. Unfortunately, in any practical communication system the above synchronisation signals are not exactly known since they are derived at the receiver in the presence of noise. Besides random noise, impairments such as constant carrier-phase offsets (carrier-phase rotations) and accumulated phase offsets can also affect synchronisation.

Carrier-phase rotations occur in practical communication systems when synchronisation is regained after a temporary failure caused by phase jumps or noise. Accumulated phase offsets can occur in a mobile radio communication system when fixed Doppler frequency shifts owing to the relative motion of the vehicle exist in the demodulator operation. Usually, in the case of imperfect synchronisation of a coded-modulation scheme, a signal-space rotation caused by a shift in carrier-phase may result in the received sequence falling outside the valid code space. The above imperfections clearly cause degradations in the system performance and these are known to affect coded-modulation schemes more than they affect uncoded-schemes.

A self synchronisation technique for CPFSK signals has been suggested in [51] by passing the received signal through a nonlinearity. This is an extension of the synchroniser first proposed by de Buda [33] for minimum-shift-keyed (MSK) signals. In [18], it has been shown that the same circuit can be adapted for any CPM

signal. The above methods use nonlinear operations on the received signal, coupled with narrow-band phase-locked loops (PLLs) to estimate the carrier-phase. The basis of the nonlinear technique is the presence of discrete spectral components in the spectrum whenever the modulation index is an integer. A different approach to carrier-phase and symbol-timing recovery using maximum *a posteriori* probability (MAP) estimation has been introduced in [103]. While these techniques can successfully be applied to CPFSK when the signal-to-noise ratio is high and the modulation index is large, efficient synchronisers for general CPM schemes (especially partial response CPM schemes with narrow frequency spectra) are still not available.

Rotationally invariant trellis modulation codes also have received considerable attention in the current literature [24, 58, 78, 96, 99, 100, 102]. They are also sometimes referred to as self-transparent trellis modulation codes. These are designed such that they can tolerate (or are transparent to) carrier-phase ambiguities of the reconstructed reference signals at the demodulator. This simplifies the receiver design, because there is no need for ambiguity-resolving circuitry in the receiver and allows fast recovery after losses of carrier-phase synchronisation. Self-transparent codes should be especially useful for transmission over mobile communication (both land-mobile and satellite-mobile) channels where Rayleigh and Rician fading can lead to frequent losses of carrier-phase synchronisation in the receiver.

2.3 Application of trellis modulation codes to Gaussian channels

Performance of a digital communication system is intended to include the quality of end-to-end transmission. Whenever uncoded signalling techniques alone could not satisfy the performance specifications, it is customary to employ combined coded-

modulation to achieve the required performance. This is often referred to as channel coding, and channel coding always results in a more complex communication system.

The conventional approach to channel coding regards encoding and modulation as separate operations. Accordingly, the encoder and modulator are independently optimised to achieve the required probability of error in a given coded digital communication system. The code is designed to maximise the minimum Hamming distance between the generated code-words at the modulator input without consideration to the modulator signal constellation.

Massey [69] and Ungerboeck [93, 94] questioned the conventional approach and showed that considerable performance gain can be obtained by treating encoding and modulation as a single entity. In the latter approach, the code and the modulation scheme are selected jointly instead of independently such that the minimum Euclidean distance between coded signal sequences at the modulator output is maximised. This work laid the foundation for the design and development of power and bandwidth-efficient coded-modulation schemes.

Continuous-phase modulation itself has been viewed as a coding operation since the continuity of phase exhibits memory inherent to coded systems. Rimoldi [82] has decomposed CPM to a continuous-phase encoder and a memoryless modulator thereby separating the coding and modulation operations. The continuous-phase encoder can be represented as a nonlinear system with finite memory [25]. This inherent memory can be further enhanced by encoding the modulator input symbol sequence with convolutional codes [27, 39, 52, 53, 56, 79, 98] or more generally with trellis codes [20, 21, 92, 93, 94]. Conventional modulation schemes like QPSK when coupled with convolutional codes yield modest coding gain, but at the expense of bandwidth. In contrast, the set-partition coding technique due to Ungerboeck

[94] and continuous-phase modulation schemes enable improved error performance without increasing the bandwidth.

Ungerboeck, through the technique of 'mapping by set partitioning [94],' used a 2^{m+1} point signal constellation combined with binary convolutional codes to send m bits per symbol with two-dimensional signal constellations such as QAM and PSK. The concept of set-partition coding was later extended to higher-dimensional signal constellations by Wei [44, 99]. While higher-dimensional signal constellations offered only marginal increase in coding gain, they have been used to design good rotationally invariant trellis codes [24]. The Viterbi algorithm has been used to decode Ungerboeck codes [24, 44, 92, 93]. On ideal Gaussian channels (white Gaussian noise, no intersymbol interference), asymptotic coding gains of the order of 3 dB have been obtained with simple four-state codes combined with 8-PSK, while up to 6 dB have been obtained with more complex 128-state codes. A variant of Ungerboeck's eight-state trellis code mapped on to a 32-point signal constellation has been adopted by the CCITT (ITU-T) as the international standard for both 9.6 kb/s and 14.4 kb/s voice-band modems [36]. More complicated trellis modulation codes have allowed the development of modems that operate at speeds from 19.2–24 kb/s on telephone channels. Still, such high-speed data transmission over telephone channels is made possible only with adaptive linear equalisation techniques that remove a considerable portion of amplitude and delay distortion.

Since Ungerboeck's work [94], most research on coded-modulation for power-limited satellite channels have been concentrated on combining convolutional codes or trellis codes with various bandwidth-efficient modulation techniques [99, 44]. Trellis codes for 8-PSK and 16-QASK were presented in [94]. Wilson et al. [104] investigated rate-3/4 convolutional coding of 16-PSK. They performed a computer search for good codes and showed that for the AWGN channel, 32-state codes can

achieve 4.8 dB over uncoded 8-PSK. Rate-5/6 trellis coded 8-PSK has been the subject of [102] and an eight-state code was shown to produce 6.2 dB coding gain over uncoded 8-PSK. Spectral performance of above codes has also been evaluated using computer simulation. Though trellis coded QAM is more bandwidth-efficient than trellis coded PSK, the latter is particularly suitable for nonlinear satellite channels due to its constant-envelope property. The performance of 16-PSK, 32-PSK and 16-QAM trellis codes have also been analyzed and shown to provide substantial improvement on nonlinear satellite channels [20, 21, 23]

CPM signals may be precoded by a block code or a convolutional code followed by a mapping rule. The result is often a more powerful trellis modulation code than CPM alone. Convolutional codes are more suited for encoding CPM than block codes since their memory can be easily combined with the inherent memory of these signals. Several studies [53, 55, 56, 57, 62, 79, 104] have shown that CPM schemes when combined with suitable convolutional codes can both be more power and bandwidth-efficient than uncoded CPM. All of these studies assumed high signal-to-noise ratio (SNR) ideal additive white Gaussian noise (AWGN) channel conditions. Knowledge of binary convolutional codes could not be exploited in these studies, because cascading convolutional codes with maximum free Hamming distance do not in general produce the largest minimum squared free Euclidean distance with CPM signalling.

Lindell [53], Lindell and Sundberg [56], and Pizzi and Wilson [79] have conducted detailed studies on the distance properties of rate-1/2 convolutional coded CPFSK signalling for AWGN channels. Using heuristic rules to reduce the number of codes to be searched, they also found the best rate-1/2 convolutional codes for 4-CPFSK and 8-CPFSK. Rate-2/3 convolutional coded 8-CPFSK has been studied in [61, 79, 53]. The combined effect of partial response CPM and convolutional

coding has been considered in [55, 53, 57]. Lindell et al. [56] have extended the above results to high rate convolutional codes combined with octal, 16-ary, and 32-ary CPM. To observe the improvement gained by convolutional coding, in Fig. 2.2, we have compared the minimum squared Euclidean distance results for optimum rate-1/2 convolutional coded 4-CPFSK signalling with those of uncoded 4-CPFSK signalling.

2.4 Application of trellis modulation codes to fading channels

Trellis modulation codes are just beginning to be considered for application to channels other than the AWGN channel, such as radio channels and mobile satellite channels. Each of these applications presents its own problems and consequently requires the development of new types of codes.

Code design and error performance of various trellis modulation codes on fading multipath channels have been considered because the conventional uncoded digital modulation techniques, such as BPSK, MSK and QPSK perform very poorly on such channels. Most of the modulation and detection techniques that have been designed for use over fading multipath channels attempt to minimise the effects of time-dependent impairments of the channel in a number of ways. The various approaches can be divided into the following categories [67]:

1. Non-coherent and differentially-coherent detection of constant-envelope digital modulation. This minimises the adverse effects of the time-dependent amplitude and phase of the received signal on the detector.

2. Coherent detection of constant-envelope digital modulation. At the receiver, a replica of the transmitted carrier is regenerated with the aid of a reference

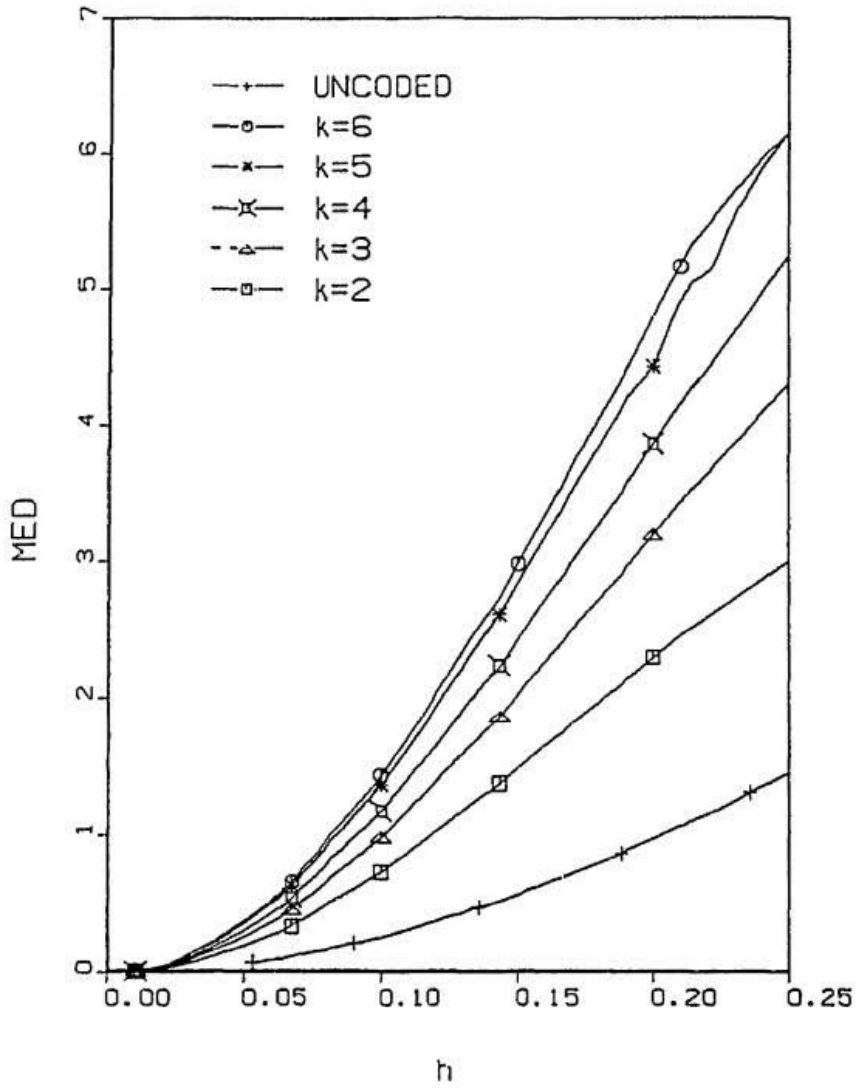

Figure 2.2 Minimum Euclidean distance of optimal rate-1/2 convolutional coded 4-CPFSK.

signal.

3. Introduce time diversity to the transmitted signal. Trellis modulation codes have been used to introduce time diversity to the transmitted signal and it has been shown to be very effective on fading multipath channels. However, improved performance has been achieved with a corresponding increase in the computational complexity and signal processing delay at the transmitter and the receiver. Symbol interleaving and de-interleaving have been used to combat the effect of the fading.

Data and voice transmission for the satellite-based mobile communication channel has received much attention recently [30, 34, 36, 48, 50, 66, 72, 74]. As both power and bandwidth limitations are simultaneously imposed in the mobile satellite channel, in many cases, it is not possible to achieve the desired throughput with bandwidth-efficient digital modulation alone [36], thus the mobile satellite channel has become an important present day application of bandwidth efficient trellis modulation codes.

Fading in the mobile satellite channel severely degrades the performance of data transmission [48]. To combat fading, it is required to use fading compensation techniques. Due to the small size of the mobile terminals it is not possible to use antenna diversity (spatial diversity) [48] and also the large coherence bandwidth [30] makes frequency diversity unsuitable. However, time diversity can be incorporated through coded-modulation schemes. Long or deep fades cause burst errors when MLSE decoding is used. To spread the burst errors caused by fading in the channel, it is customary to use symbol interleaving and de-interleaving, but de-interleaving destroys the memory of the channel. Therefore, research on coded-modulation schemes for interleaved channels has concentrated on memoryless modulations such

as PSK and DPSK.

Fading channel performance and code construction for PSK and DPSK have been the subject of several studies [34, 35, 36, 72, 86]. Divsalar and Simon [36] studied trellis coded M-PSK with non-symmetrical signal sets for the mobile satellite channel. It was shown that introducing non-uniformity to the spacing between the signal points in a constellation improves error performance over the more conventional symmetrical signal sets. In [66, 74], the performance of uniformly-spaced codes is compared with non-uniformly-spaced codes. For the classical AWGN channel and lightly faded channels it has been shown that both types of codes perform equally well. However, according to Lodge [66], for heavily faded channels the uniformly-spaced codes with greater time diversity performed better.

The performance of multilevel DPSK for the mobile satellite channel has been considered in [72, 86]. A summary of performance criteria and optimum code design strategies for memoryless modulations can be found in [34, 35]. A common assumption made in these studies is that, the time-varying phase of the received signal is fully compensated for fading either by tracking with some form of PLL or by employing pilot-aided coherent detection techniques [29, 36, 71]. Thus these results reflect the performance degradation due to amplitude fading only. Furthermore, the analysis has been simplified by assuming ideal interleaving and de-interleaving to convert the bursty channel into a memoryless channel. 8-PSK trellis codes for fading channels constructed using the design parameters suggested in [34, 35] can be found in [84]. These studies have shown that the well known Chernoff bounding technique can be used to obtain performance bounds for bandwidth efficient trellis modulation codes on fading channels. It has also been demonstrated that channel coding and trellis decoding provide a bandwidth-efficient means for obtaining time diversity over such channels.

2.5 Application of CPFSK trellis modulation codes to multipath fading channels

Literature on the application of trellis coded CPFSK to fading multipath channels is sparse. Optimum and suboptimum coherent detection of CPM on a two-ray multipath fading channel has been considered by Svensson [89]. Sundberg [88] also investigated CPM for Rayleigh fading channels. Coherent maximum-likelihood detection of trellis coded CPFSK in fading environments is rendered difficult due to the memory inherent in the modulation. Abrishamkar and Biglieri [4, 3] have considered differential detection of trellis coded CPFSK, and Kerr and McLane [50] have investigated coherent detection of trellis coded CPFSK.

In [4], time diversity with maximal ratio combining has been used to combat the effects of fading. Time diversity was achieved by the simple means of repeating each coded sequence once. To compensate for the resulting reduction in the data rate, trellis coded 32-CPFSK has been used instead of 16-CPFSK that would have been used without coding. Since no interleaving was used in the above scheme, coherent Viterbi detection was possible. In the same work they considered differential detection of CPFSK with block interleaving. In differential detection, the delayed signal itself provides a phase reference. Without phase tracking the receiver is simpler to implement.

In both [4] and [3], because of using differential detection, the CPFSK trellis has not been used in the decoding process hence the inherent memory of CPFSK has not been exploited by the decoder. In contrast, the scheme recently considered by Kerr and McLane [50] partially exploits the memory of the CPFSK signals by using a new decoding algorithm that can cope with the interleaving of CPFSK. Their simulation results suggest that coherent detection of interleaved CPFSK gives

a significant performance advantage for lightly-shadowed mobile satellite channels such as the Canadian mobile satellite (MSAT) channel. The channel model used in above studies is described in [30, 68, 80].

Proof-of-concept modems using coherent CPFSK signalling for both high data rate and low data rate applications have been reported recently [28, 49, 106]. A trellis-coded 16-CPFSK digital modem using coherent detection and Viterbi decoding has been reported in [28]. This modem is designed for 200 Mb/s time-division multiple access (TDMA) applications in nonlinear AWGN channels with 100 MHz adjacent channel spacing. A 300 Mb/s modem using trellis-coded 16-CPFSK has been implemented by the NASA for linking the proposed Space Station with ground stations [106]. The above modems use data-derived carrier recovery techniques. Low data rate binary CPFSK modems for mobile satellite applications have been tested by the Jet Propulsion Lab, Pasadena CA, U.S.A. in connection with the MSAT-X project [49]. The typical data rates of these modems were between 4800–9600 b/s.

These modems use pilot-aided coherent detection, for which there are at least three approaches: (i) the Transparent Tone-Inband Technique (TTIB) [71], (ii) the Tone Calibration Technique (TCT) [29] and (iii) Pilot Symbol Assisted Modulation (PSAM) [26, 74] which multiplexes a time-domain pilot sequence to permit coherent detection. The basic idea behind all these techniques is to transmit a pilot at a convenient frequency in the data spectrum and extract this pilot at the receiver assuming that the effect of the fading on the pilot and the data are the same. The extracted pilot can be used as a coherent reference in the demodulator. Pilot-aided and pilot symbol assisted coherent detection techniques have received renewed interest recently because, to realize the full potential of trellis modulation codes it is essential that we use coherent detection.

2.6 Scope of the thesis

The two main goals of this research are to find ways of improving the error performance of CPFSK trellis modulation codes on AWGN channels and to study the effectiveness of suboptimum coherent phase detection of CPFSK signals on non-Gaussian channels.

We consider digital transmission over a nonlinear, power and bandwidth-limited channel. Such channel conditions exist, for instance, in satellite-based land-mobile communication systems. The transponders in satellite communication systems operate in the nonlinear region, therefore in such applications constant envelope digital modulation techniques are generally preferred to schemes with significant amplitude variations. The frequency spectrum allocated by the WARC'92 [83] for mobile satellite communications is extremely limited and, therefore, bandwidth and power-limitations are simultaneously imposed on the channel. Thus, for efficient and reliable transmission of information on such channels digital modulation techniques should be constant-envelope, power and bandwidth-efficient. When coherently detected, CPFSK trellis modulation codes have shown to possess all the above desirable properties; but, they are only achieved at the expense of excessive signal processing delay and high receiver complexity.

CPFSK trellis modulation codes with large modulation indices have a broad frequency spectrum. They are also more power-efficient owing to the larger minimum Euclidean distances that they achieve. Since the frequency spectrum allocated to mobile satellite communication is narrow, schemes with smaller modulation indices are necessary in such channels. To realize the full potential of any CPFSK scheme, it is essential that we use coherent detection. To achieve coherence, one may take advantage of the synchronisation properties of CPFSK, though as the spectrum of

the signals becomes narrow, the problem of finding the carrier (carrier-phase synchronsiation) becomes difficult. This is exactly the case when the modulation index is small as considered in this study (typically $h \leq 1/M$, where M is the number of signalling levels of the CPFSK scheme). It was pointed out in the literature survey that rotationally-invariant or self-transparent trellis modulation codes are more suitable in such situations because resynchronisation can be quickly restored.

In Chapter 3 we show how CPFSK signals can be represented by a simplified, finite-state trellis, whose states have a one-to-one relationship to the phase of the CPFSK signal (reckoned modulo-2π.) In most of the literature, it is claimed that the number of phase states in full response CPFSK is equal to q if p is even and $2q$ if p is odd, where the modulation index $h = p/q$ and, p and q are relatively prime positive integers. It is shown that the number of trellis phase states can always be made equal to q irrespective of whether p is odd or even. Based on the above finite-state trellis representation, a state transition matrix and a state location matrix are defined which leads to a matrix description of CPFSK signals. This enables us to consider all merging events of the trellis within a single matrix. Such a matrix approach simplifies trellis search algorithms that computes the minimum Euclidean distance and other trellis parameters.

In Chapter 4 we construct and analyse a class of binary nonlinear CPFSK trellis modulation codes based on higher-order M-ary CPFSK with fixed modulation index h ($h \leq 1/M$) for the additive white Gaussian noise channel. They achieve the maximum memory length for a given number of phase states in a binary trellis. To distinguish these schemes from general CPFSK schemes they are referred to as nonlinear CPFSK schemes. Binary nonlinear CPFSK involves the use of a finite-state machine to decrease the connectivity of the conventional CPFSK trellis such that merging of path-pairs (error events) is delayed beyond two. The memory length

or the time diversity of CPFSK is increased by overcoming the inevitable merging event. These fixed-h binary nonlinear CPFSK schemes achieve coding gains ranging from 0.3 dB to 2.2 dB relative to MSK signals. It is also shown that the optimum binary nonlinear CPFSK schemes lack the important property of transparency to carrier-phase ambiguities. Thus they are rotationally non-invariant. However, since they are outcomes of a legitimate CPFSK signal, the bandwidth is not much changed.

Chapter 5 is concerned with the application of M-CPFSK trellis modulation codes to non-Gaussian channels. By 'non-Gaussian' we mean channels with carrier-phase offsets and channels with multipath fading. The channel models used in the study are first described. Then the suboptimum coherent phase detection and trellis decoding receiver for CPFSK signals is introduced. Realisation of this suboptimum receiver is significantly simpler than that of the correlation receiver and unlike the latter the complexity does not grow with the number of signalling levels M. It has the additional advantage that it can be used on interleaved multipath fading channels to introduce time diversity to the CPFSK signal thereby reducing the effect of the fading. Next, the well known Chernoff bounding technique is used to derive a suitable decoding metric (equivalent distance) for the receiver on channels with finite memory. In Chapter 6 this equivalent distance is used to search for the best self-transparent 4-CPFSK and 8-CPFSK trellis modulation codes for channels with carrier-phase offsets.

In Chapter 6, we investigate rotationally invariant or self-transparent CPFSK trellis modulation codes when $h \leq 1/M$ and present a generalized state transition matrix that could be used to obtain optimal trellis modulation codes at any even number of states. By using trellis outer codes of longer memory length, it is often possible to obtain more powerful CPFSK trellis modulation codes. The matrix rep-

resentation could be used to search for better codes (if any) based on more general finite-state machines than the convolutional code generator usually employed in the literature. Following this idea and subject to a set of heuristic design rules, the matrix approach is used to find the best self-transparent 4-CPFSK and 8-CPFSK trellis modulation codes for channels with carrier phase offsets. Generalized state transition matrices that can be used to construct rotationally invariant 4-CPFSK and 8-CPFSK trellis modulation codes for $h \leq 1/M$ are also presented. All CPFSK trellis modulation codes found are constant-envelope and self-transparent, and neither they require a post modulation filter nor they require any ambiguity-resolving circuitry in the coherent demodulator. The equivalent distance derived in Chapter 5 is used to study the effect of static carrier phase offsets on the performance of CPFSK trellis modulation codes.

Application of CPFSK trellis modulation codes for data transmission through mobile satellite channels is considered in Chapter 7. As stated before, satellite channels are inherently nonlinear and communication with mobile terminals via satellite suffers from signal shadowing and multipath fading that result in strong fluctuations of the received signal. The characteristic of multipath fading depends on the presence or absence of the direct path and the mobile satellite channel is modelled as a Rician distribution.

Constant-envelope modulations such as PSK and CPFSK are generally impervious to channel nonlinearities and fading, because the information is not carried in the amplitude of the transmitted signal. However, multipath fading causes burst errors in the channel. For narrowband communications the fading can be assumed to be frequency-non-selective or 'slow' fading. Furthermore, the fading in mobile satellite channels is not as severe as that encountered in land-mobile communication channels, because of the presence of a strong line-of-sight component (direct path)

between the satellite and the mobile unit. This simplifies the detection problem considerably because the channel can be assumed to have only amplitude fading.

Trellis modulation codes that have originally been designed for the random (memoryless) noise channels are generally not effective on burst noise channels (with finite memory) and, therefore, it is necessary to use channel symbol interleaving and de-interleaving to convert the burst noise channel to a memoryless channel with random noise, so that trellis modulation codes can be effectively used on multipath fading channels. However, the process of de-interleaving at the receiver destroys not only the channel memory but also the memory inherent in CPFSK, thereby making it difficult to use coherent maximum-likelihood detection. Therefore, we resort to the suboptimum coherent phase detection and trellis decoding scheme for CPFSK which also allows channel symbol interleaving to combat fading.

Several studies have shown that the cutoff rate R_0 of the discrete channel created by the modulation system is the appropriate performance measure for interleaved multipath fading channels where trellis modulation codes have been used to provide time diversity. The higher the cutoff rate for a given channel the better the coding potential would be. The widely used error probability criterion is difficult to be used on such channels because of the nonlinear signal processing involved. In this study, the channel cutoff rate R_0 for suboptimum coherent detection (phase detection and trellis decoding) of CPFSK signals and coherent PSK signalling will be compared to estimate the effectiveness of CPFSK trellis modulation codes on the mobile satellite communication channel.

The main contributions of the research are summarized in Chapter 8. Finally, the thesis is concluded with some suggestions for future work in this area.

Chapter 3

Matrix Description of CPFSK Signals

3.1 Introduction

In this chapter it is shown how CPFSK signals can be represented by a simplified, time-invariant finite-state trellis whose states have a one-to-one relationship to the phase of the CPFSK signal. According to the traditional finite-state trellis representation the number of phase states in CPFSK is equal to q if p is even and $2q$ if p is odd, where the modulation index $h = p/q$, with p and q relatively prime integers. By assuming that the lowest tone of the CPFSK signal goes through an integer multiple of cycles during one signalling interval, we show here that the number of phase states can always be made equal to q, irrespective of whether p is odd or even. Based on the simplified finite-state representation, it is also shown how a state transition matrix and a state location matrix for CPFSK can be defined. This makes it possible to describe CPFSK in the form of a matrix, and all signal paths through the trellis can be considered together within one matrix. This novel matrix approach simplifies trellis search algorithms that compute the minimum Euclidean distance.

3.2 Trellis structure of CPFSK signals

The general format of any M-CPFSK signal was given in Sec. 1.3. In this study, we restrict our attention to the finite-state representation of full response M-CPFSK with a fixed modulation index h and a rectangular frequency pulse $g(t)$ given by

$$g(t) = \begin{cases} 1/2T, & 0 \leq t < T \\ 0, & \text{otherwise.} \end{cases} \tag{3.1}$$

A typical CPFSK phase tree or the plot of phase trajectories against time was given in Chapter 1. The phase has physical significance because it is closely related to the finite-state representation of the signal and carries the coded information. Unless otherwise stated, the phase is reckoned only in modulo-2π.

For rational modulation indices such as $h = p/q$, where p and q are relatively prime positive integers, the phase tree collapses to a periodic phase trellis that is necessary for maximum-likelihood sequence detection [6]. To select the most-likely transmitted sequence, the decoder determines the path through the trellis that is nearest to the received waveform using the Euclidean distance metric (in the case of AWGN channels), which may be effected recursively using the Viterbi algorithm.

In most of the literature (see [6] and references therein), it is claimed that the number of trellis phase states in CPFSK is equal to q if p is even, and $2q$ if p is odd, where the modulation index $h = p/q$. This is a consequence of the conventional finite-state representation of CPFSK, which causes the phase trellis to be time varying, in the sense that the transitions in the even-numbered signalling intervals are not the same as those in the odd-numbered signalling intervals. In this section, we show how this can be reduced to a more efficient, time-invariant finite-state trellis representation, where the states are obtained by a one-to-one mapping of the phase of the signal, and hence show that CPFSK always has q phase states irrespective of whether p is odd or even. The important part of the CPFSK trellis

is its phase deviations, not its absolute phase. Therefore, the distance properties are preserved.

In (1.1), we have given the conventional definition of CPFSK, which leads to the well known trellis of size $2pM^{L-1}$, where $L(\geq 1)$ is the length of the frequency pulse in signalling intervals. Since, by assumption, p and q have no common factors, the phase $\phi(t, \mathbf{x})$ during the interval $nT \leq t \leq (n+1)T$ can be written as

$$\phi(t, \mathbf{x}) = 2\pi h \sum_{i=n-L+1}^{n} x_i q(t - iT) + \phi_n, \tag{3.2}$$

in which

$$\phi_n = \pi h \sum_{i=-\infty}^{n-L} x_i \quad \text{(modulo-}2\pi\text{)} \tag{3.3}$$

can assume only $2p$ different values $(0, \pi p/q, 2\pi p/q, \ldots\ldots, (2q-1)\pi p/q)$ if p is odd, and p different values $(0, \pi p/q, 2\pi p/q, \ldots\ldots, (q-1)\pi p/q)$ if p is even.

The phase tree and the corresponding phase trellis that is obtained by reducing the phase tree modulo-2π for fixed-h binary CPFSK signals are shown in Figure 3.1(a) ($h = 1/2$) and Figure 3.1(b) ($h = 3/4$). Since the phase is unique when reckoned in modulo-2π, actually they form a cylindrical trellis as shown in Figure 3.2. Thus, the phase tree eventually wraps around onto itself and certain nodes will merge and so become indistinguishable. This is true for all CPM schemes with rational h values, and it is considered as the conventional definition of a phase trellis. The simplified trellis representation used in this thesis is given in the next section.

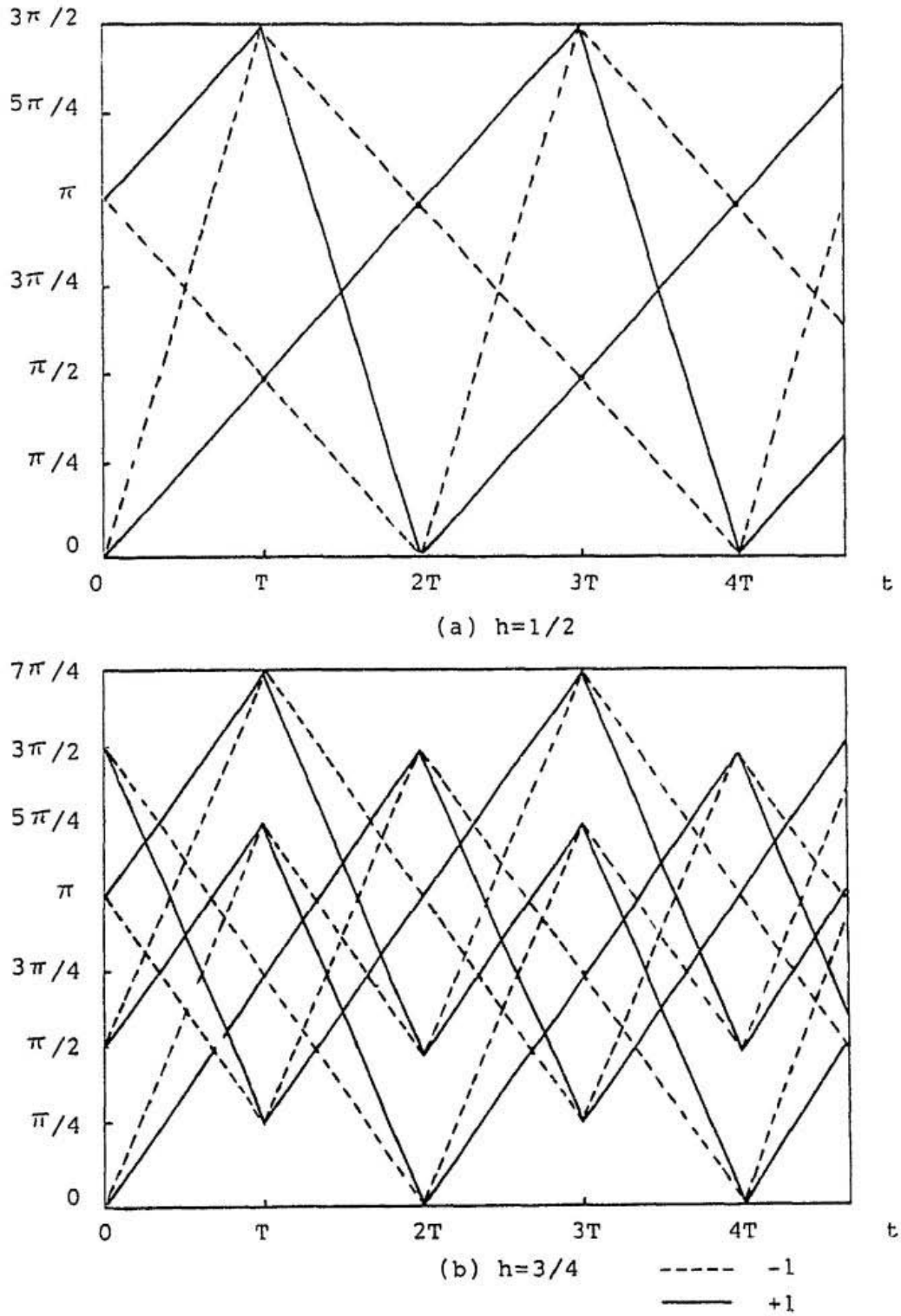

Figure 3.1 Phase trellis for binary CPFSK signals.

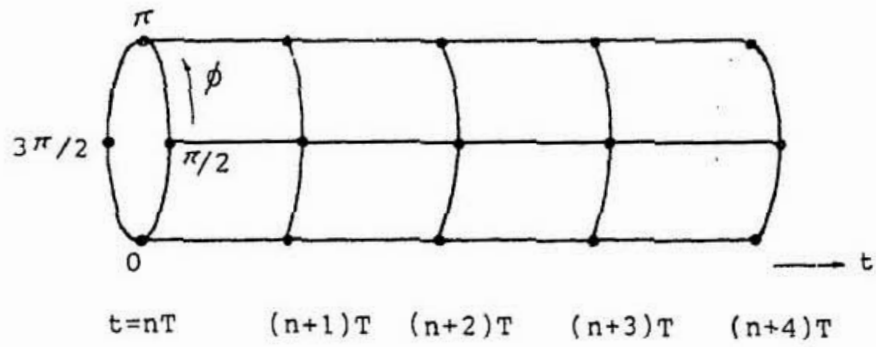

Figure 3.2 Phase cylinder for binary CPFSK when $h=\frac{1}{2}$.

3.3 Simplified finite state representation of CPFSK signals

For full response CPFSK (*i.e.*, when $L = 1$ and $q(t) = \frac{t}{2T}$, $0 \leq t \leq T$) (3.2) can be written as

$$\begin{aligned} o(t, \mathbf{x}) &= \sum_{i=-\infty}^{n-1} x_i \pi h + 2x_n \pi h q(t - nT) \\ &= \pi h \sum_{i=-\infty}^{n-1} x_i + x_n \pi h (t - nT)/T \\ i.e.\ o(t, \mathbf{x}) &= \pi h x_n t/T + \pi h \sum_{i=-\infty}^{n-1} x_i - n\pi h x_n. \end{aligned} \tag{3.4}$$

Therefore, the transmitted CPFSK signal $s(t)$ is given by

$$s(t) = \sqrt{2E_s/T} \cos(2\pi f_0 t + \pi h x_n t/T + o_n), \tag{3.5}$$

where

$$o_n = \pi h \sum_{i=-\infty}^{n-1} x_i - n\pi h x_n. \tag{3.6}$$

o_n is constant over a signalling interval and its value in a given signalling interval should satisfy the phase continuity property at the symbol transition instant. In other words, the phase of the signal after the $(n-1)^{\text{th}}$ signalling interval must equal the phase of the signal at the beginning of the n^{th} signalling interval. Referring to Figure 3.3 the phase at the end of the $(n-1)^{\text{th}}$ signalling interval is given by

$$2\pi f_0(nT) + \pi h x_{n-1}(nT)/T + o_{n-1}. \tag{3.7}$$

Similarly, the phase of the signal at the beginning of the n^{th} interval is given by

$$2\pi f_0(nT) + \pi h x_n(nT)/T + o_n. \tag{3.8}$$

Equating the above two expressions, we have

$$o_n = o_{n-1} + n\pi h(x_{n-1} - x_n). \tag{3.9}$$

Clearly ϕ_n depends upon the value of ϕ_{n-1} during the preceding signalling interval and the symbol transmitted during that signalling interval.

As stated earlier, the channel symbols x_n of M-CPFSK can take on any value of the set $\{(2i - M - 1),\ i = 1, 2, 3, \ldots, M\}$, that is,

$$\{\pm 1, \pm 3 \pm 5, \ldots\ldots, \pm(M-1)\}$$

with equal probability. M distinct tones are transmitted in relation to each of the M symbols in the above set. The lowest tone transmitted has a frequency of $\{f_0 - h(M-1)/2T\}$. Following Forney [43] we assume that this lowest tone goes through an integer multiple of cycles during one signalling interval. This assumption simplifies the phase trellis but does not in anyway alter the spectral characteristics or the distance properties of CPFSK signals [43]. Corresponding to the M tones we have

$$\begin{aligned}
-(M-1): &\quad 2\pi T[f_0 - \frac{h}{2T}(M-1)] = \quad 2n\pi = 0 \quad \text{(modulo-}2\pi\text{)} \\
-(M-3): &\quad 2\pi T[f_0 - \frac{h}{2T}(M-3)] = \quad 2\pi h \quad \text{(modulo-}2\pi\text{)} \\
-(M-5): &\quad 2\pi T[f_0 - \frac{h}{2T}(M-5)] = \quad 4\pi h \quad \text{(modulo-}2\pi\text{)} \\
&\ldots\ldots\ldots\ldots\ldots\ldots\ldots\ldots\ldots\ldots \\
&\ldots\ldots\ldots\ldots\ldots\ldots\ldots\ldots\ldots\ldots \\
+(M-1): &\quad 2\pi T[f_0 + \frac{h}{2T}(M+1)] = \quad 2(M-1)\pi h \quad \text{(modulo-}2\pi\text{)} \qquad (3.10)
\end{aligned}$$

where n is an integer. Therefore, ϕ_n in (3.9) assumes the values of the set

$$\Phi = \{0, 2\pi h, 4\pi h, \ldots, 2(M-1)\pi h\}.$$

With the assumption we have already made that h is a rational number such that $h = p/q$, where p and q are relatively prime positive numbers, coupled with the modulo-2π rendition of the phase, the elements of the set Φ reduces to q distinct

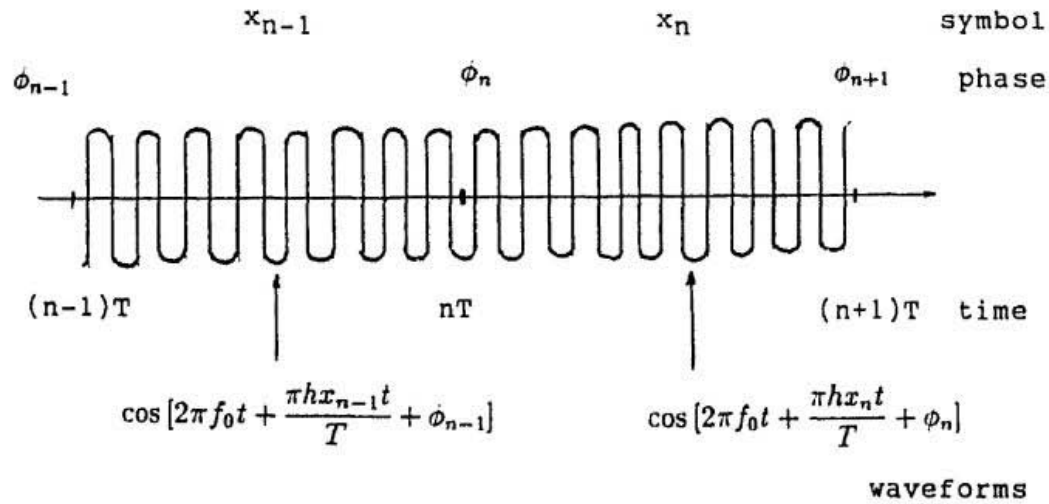

$$\phi_n = \phi_{n-1} + n\pi h(x_{n-1} - x_n)$$

Figure 3.3 Phase continuity condition for CPFSK signalling.

values. The important observation we make here is that, this reduction in the number of states takes place irrespective of whether p is odd or even enabling us to always describe M-CPFSK signalling waveform by a q-state trellis, where the q states are obtained by a one-to-one mapping of the phase values ϕ_n.

In the case of M-ary signalling, every state has M branches leaving and M branches merging. Each branch is associated with a symbol in the M-ary alphabet. Also, a total of qM branches connect the states of any two adjacent levels and, therefore, each branch is associated with a distinct waveform of the qM waveforms. Hence we make the observation that when $q < M$, the number of states in the trellis at a given level is less than the number of branches leaving a state, implying that there are parallel branches in the trellis. When $q \geq M$ the number of distinct states is greater than the number of branches leaving each state; therefore, no parallel branches exist between the states of adjacent levels. For integer valued modulation indices

$$2\pi h = 4\pi h = \ldots\ldots\ldots\ldots = 2(M-1)\pi h = 0 \quad (\text{modulo} - 2\pi)$$

Therefore, the set Φ has only one element, and the trellis collapses to a single-state trellis. Thus there are M parallel branches between the states. In the following section we give examples of simplified finite-state trellis representations for the three cases: $q \geq M$, $q < M$, and integer h. For illustration we choose 4-CPFSK with $h = 1/5$, $h = 1/3$, and $h = 1$ for each case, respectively. Other examples can be found in [60].

Case 1: q ≥ M

For 4-CPFSK signals, x_n can take on any value of the set $\{\pm 1, \pm 3\}$ with equal probability. Rewriting (3.9) with $h = 1/5$,

$$\phi_n = \phi_{n-1} + \frac{n\pi}{5}(x_{n-1} - x_n). \tag{3.11}$$

where $x_n, x_{n-1} \in \{\pm 1, \pm 3\}$ for all integer values of n. Then

$$\phi_n = 0, 2\pi/5, 4\pi/5, 6\pi/5, 8\pi/5 \quad \text{(modulo-}2\pi\text{)}.$$

Therefore, ϕ_n can take only five different values in the case of 4-CPFSK with $h = 1/5$.

Four different tones of frequency $(f_0 - 3/10T)$, $(f_0 - 1/10T)$, $(f_0 + 1/10T)$ and $(f_0 + 3/10T)$ are transmitted in relation to the four symbols -3, -1, 1 and 3. Assuming that the tone with the lowest frequency, $(f_0 - 3/10T)$, goes through an integer multiple of cycles during a signalling interval, we have

$$\begin{aligned}
-3: \ & 2\pi(f_0 - 3/10T)T = \ 2n\pi = 0 \ \ (\text{modulo} - 2\pi) \\
-1: \ & 2\pi(f_0 - 1/10T)T = \ 2\pi/5 \ \ (\text{modulo} - 2\pi) \\
+1: \ & 2\pi(f_0 + 1/10T)T = \ 4\pi/5 \ \ (\text{modulo} - 2\pi) \\
+3: \ & 2\pi(f_0 + 3/10T)T = \ 6\pi/5 \ \ (\text{modulo} - 2\pi)
\end{aligned} \tag{3.12}$$

Therefore, the transmission of symbols -3, -1, 1 and 3 would result in phase changes of 0, $2\pi/5$, $4\pi/5$ and $6\pi/5$, respectively, in the CPFSK signal. Using the results of (3.11) and (3.12) the phase trellis of 4-CPFSK with $h = 1/5$ can be drawn as shown in Figure 3.4(a). The corresponding state diagram is drawn in Figure 3.4(b). There are twenty transitions connecting states of adjacent levels. Therefore, twenty different waveforms are possible at the modulator output in any signalling interval.

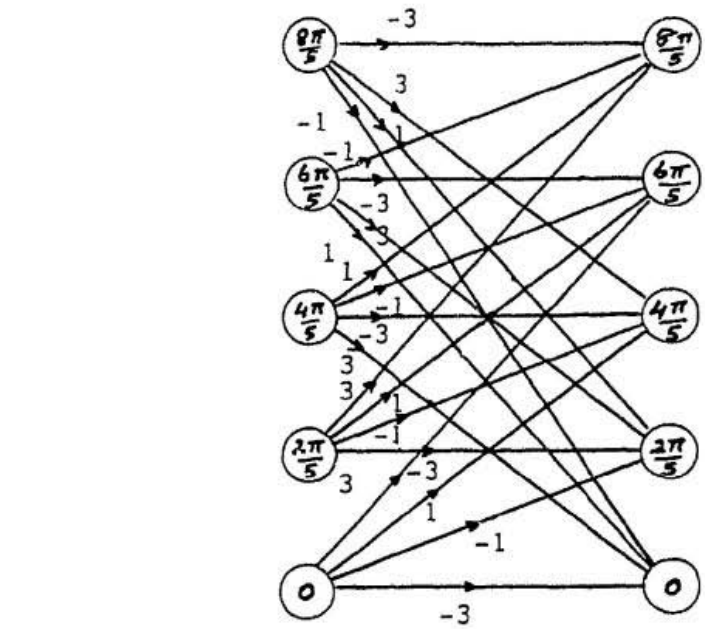

(a) trellis

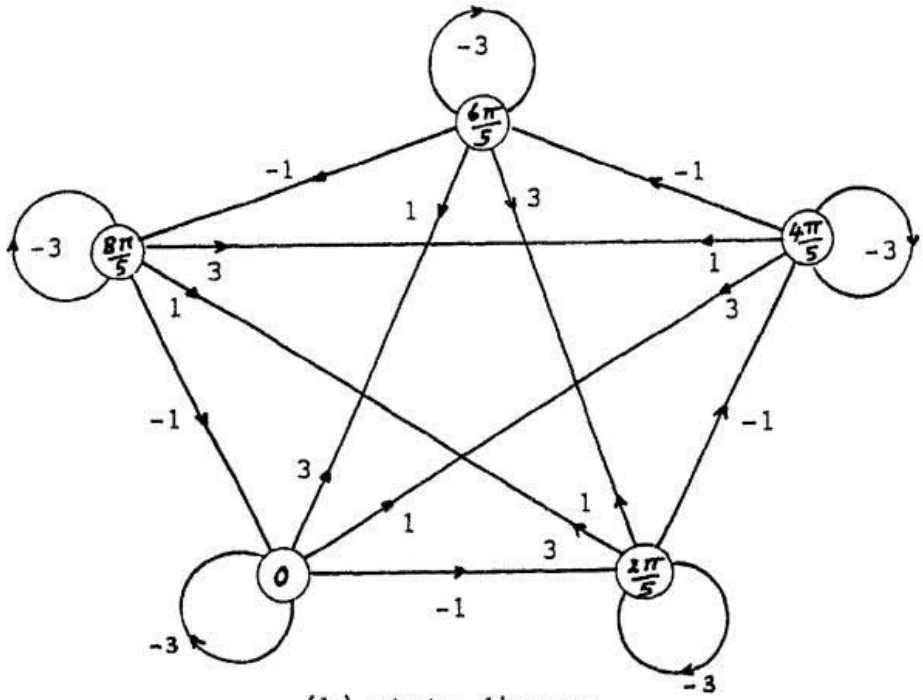

(b) state diagram

Figure 3.4 Finite-state representation of 4-CPFSK with h=1/5.

Case 2: q < M

Consider 4-CPFSK with $h = 1/3$. Substituting $h = 1/3$ in (3.9),

$$\phi_n = \phi_{n-1} + \frac{n\pi}{3}(x_{n-1} - x_n). \tag{3.13}$$

where $x_n, x_{n-1} \in \{\pm 1, \pm 3\}$ for all integer values of n. It is easy to show that

$$\phi_n = 0, 2\pi/3, 4\pi/3 \quad \text{modulo-}2\pi.$$

Therefore, ϕ_n can take only three values when $h = 1/3$. The symbols -3, -1, 1 and 3 correspond to the four tones of frequency $(f_0 - 1/2T)$, $(f_0 - 1/6T)$, $(f_0 + 1/6T)$ and $(f_0 + 1/2T)$, respectively. As before if the frequency of the lowest tone, $(f_0 - 1/2T)$, is fixed such that

$$-3: \ 2\pi(f_0 - 1/2T)T = 2n\pi = 0 \quad (\text{modulo} - 2\pi) \tag{3.14}$$

then the phase change in each signalling interval for the other three tones are:

$$\begin{aligned} -1: \ & 2\pi(f_0 - 1/6T)T = \ 2\pi/3 \quad (\text{modulo} - 2\pi) \\ +1: \ & 2\pi(f_0 + 1/6T)T = \ 4\pi/3 \quad (\text{modulo} - 2\pi) \\ +3: \ & 2\pi(f_0 + 1/2T)T = \ \ 0 \quad\ \ (\text{modulo} - 2\pi) \end{aligned} \tag{3.15}$$

With the above results, the phase trellis and the state diagram of 4-CPFSK with $h = 1/3$ can be drawn as shown in Figure 3.5(a). Since the number of states in the trellis is less than the number of trellis transitions, there are parallel branches between the states of adjacent levels. The presence of parallel branches affect adversely on the distance properties of CPFSK [59].

Case 3: Integer h

Consider 4-CPFSK with $h = 1$. In this case (3.9) becomes

$$\phi_n = \phi_{n-1} + n\pi(x_{n-1} - x_n). \tag{3.16}$$

where $x_n, x_{n-1} \in \{\pm 1, \pm 3\}$ for all integer n. Clearly ϕ_n reduces to a single phase angle:

$$\phi_n = 0 = 2n\pi(\text{modulo} - 2\pi).$$

Thus, the trellis collapses to a single state trellis. The number of parallel transitions would be equal to the number of signalling levels, which is four. The trellis and the state diagram of 4-CPFSK with $h = 1$ are shown in Figure 3.5(b). (Though it is unconventional to have two or more arrow-heads on the same branch of a state diagram, we have used it to simplify the state diagrams.)

The finite-state representation technique that has been discussed so far with uncoded CPFSK signalling can also be extended to the case, where CPFSK signals are precoded with a convolutional code or more generally with any trellis code.

The state of a trellis encoded signal is determined by the symbol state $C_n = (x_{n-1}, x_{n-2}, \ldots, x_{n-\nu})$ of the code and the phase state ϕ_n of the CPFSK modulator, and can therefore, be expressed as $X_n = \{C_n, \phi_n\}$. The parameter ν is the memory length of the trellis code. The total number of states N of the combined coded-modulation scheme is equal to 2^ν times the number of phase states q; that is, $N = q\,2^\nu$. An illustrative example is given below.

Consider $r = 1/2$, $\nu = 1$ coding of 4-CPFSK with $h = 1/4$, the general block diagram of which is given in Figure 3.6(a). The data sequence is encoded by a rate-1/2 trellis code and mapped onto the quaternary set $\{\pm 1, \pm 3\}$. The mapping function chosen will decide the trellis labelling. The above encoder generates a simple eight-state CPFSK trellis modulation code. The eight states are the combinations of the

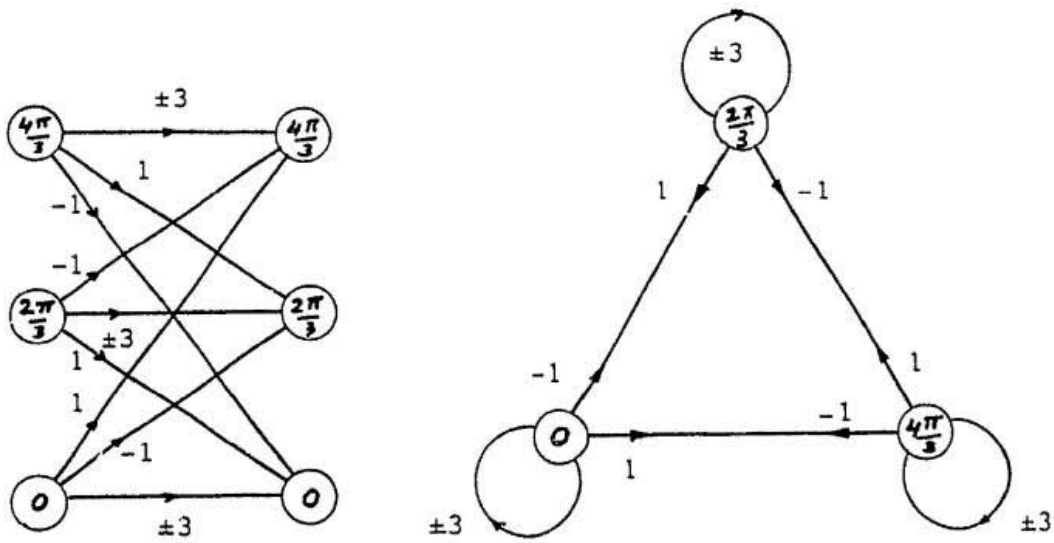

(a) h=1/3

(b) h=1

Figure 3.5 Finite-state representation of 4-CPFSK with h=1/3 and h=1.

two states $C_n = \{0, 1\}$ of the trellis code and the four states $\phi_n = \{0, \pi/2, \pi, 3\pi/2\}$ of the 4-CPFSK modulator. Each state of the trellis-modulation code thus has two parts: one, corresponding to the phase of the signal, and the other corresponding to the symbol state of the code. The symbol states are represented by integers equal to binary equivalents of the contents of delay cells of the trellis code. In the finite-state trellis of the trellis modulation code shown in Figure 3.6(b) there are only two branches leaving each state. But in the uncoded 4-CPFSK trellis there were four branches leaving each state. Clearly the connectivity of the trellis has been increased due to trellis encoding.

For a given rate-1/2 trellis code of memory length $\nu = 1$ twenty-four different trellis labellings are possible. In other words the pair of outputs of the code can be mapped onto the 4-ary set $\{\pm 1, \pm 3\}$ in twenty-four different ways. However, most of these are equivalent and can be obtained simply by inverting the symbol states 0 and 1. The finite-state diagram is also rotationally symmetrical, which has important implications in the practical implementation of trellis modulated CPFSK signalling schemes. The rotational symmetry property of CPFSK trellis modulation codes will be described in detail later in Chapter 4.

3.4 Matrix description of CPFSK signals

The conventional method of analysis of trellis modulation codes is by using the finite-state trellis that we have described in previous sections. Recently, Fonseka [40] has taken a matrix approach to analyze binary multi-h CPFSK signalling. He has pointed out that it is more convenient to use a state transition matrix and a state location matrix to describe trellis modulation codes so that the progression of phase states through the trellis can be considered together within a single matrix.

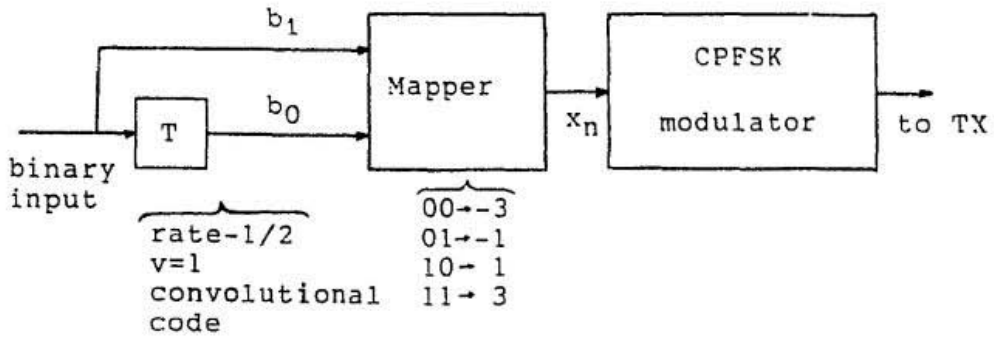

(a)

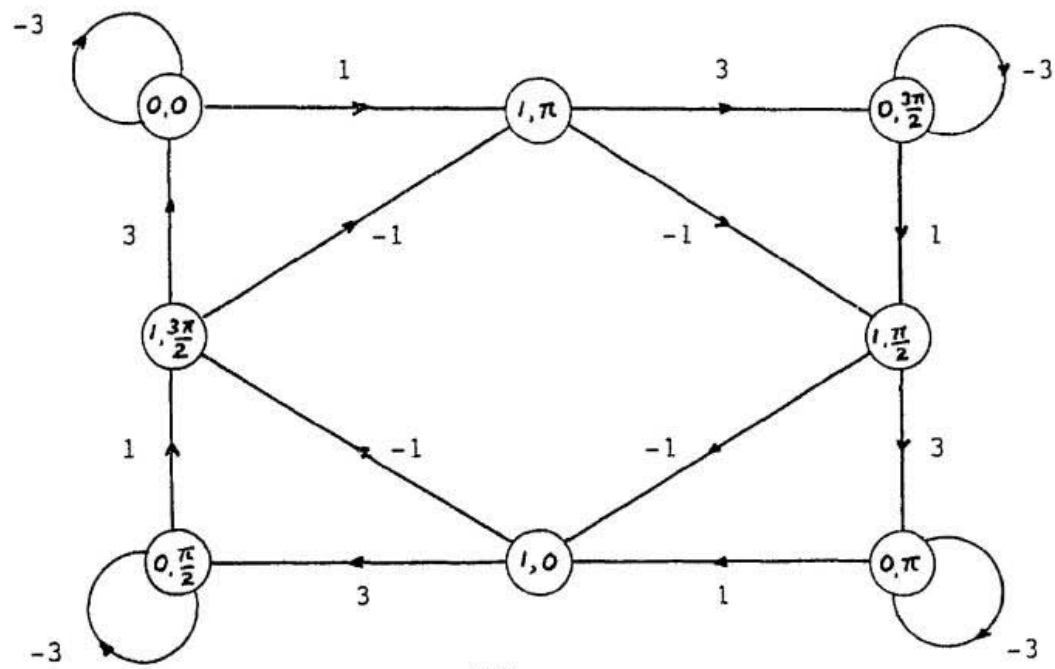

(b)

Figure 3.6 Trellis-coded CPFSK (a) block diagram
(b) finite-state representation.

This method simplifies trellis search procedures because all signal paths, and hence all error events, can be tracked through matrices. Based on the simplified finite-state trellis derived for CPFSK signals in the previous section, here we present a matrix representation for fixed-h M-CPFSK trellis modulation codes. This is applicable to any M-CPFSK trellis modulation code when $h \leq p/q$, where $q \geq M$.

3.4.1 State transition matrix

By definition the state transition matrix S_N during the n^{th} signalling interval is a N by N matrix with elements x_ns and zeros corresponding to the presence or absence of paths between the N trellis phase states, where $x_n \in \{(2i - M - 1),\ i = 1, 2, 3, \ldots, M\}$. For uncoded CPFSK with $h = p/q$ we have shown in Section 3.3 that N can always be made equal to q. Thus the state transition matrix of CPFSK with $h = p/q$ is always a q by q matrix. The rows and columns of S_N will correspond to the q phase states:

$$0,\ 2\pi h,\ 4\pi h,\ \ldots,\ 2(M-1)\pi h \quad \text{(modulo-}2\pi\text{)}.$$

For example, the finite-state system of 4-CPFSK, $h = 1/4$ consists of four phase states 0, $\pi/2$, π, $3\pi/2$ and has the state transition matrix:

$$S_4 = \begin{bmatrix} -3 & 3 & 1 & -1 \\ -1 & -3 & 3 & 1 \\ 1 & -1 & -3 & 3 \\ 3 & 1 & -1 & -3 \end{bmatrix}.$$

The convention used here is that, the rows and columns of S_4 correspond to the phase angles in the reverse order. Therefore row one of S_4 corresponds to the phase state $3\pi/2$ while row four corresponds to the phase state 0. Similarly, column one of S_4 corresponds to the phase state $3\pi/2$ and column four to the phase state 0.

As other examples, the finite-state system of 4-CPFSK, $h = 1/5$ consists of the

five phase states 0, $2\pi/5$, $4\pi/5$, $6\pi/5$, $8\pi/5$ and has the state transition matrix:

$$S_5 = \begin{bmatrix} -3 & 0 & 3 & 1 & -1 \\ -1 & -3 & 0 & 3 & 1 \\ 1 & -1 & -3 & 0 & 3 \\ 3 & 1 & -1 & -3 & 0 \\ 0 & 3 & 1 & -1 & -3 \end{bmatrix}.$$

Similarly, the finite-state system of 8-CPFSK with $h = 1/8$ consists of the eight phase states 0, $\pi/4$, $\pi/2$, $3\pi/4$, π, $5\pi/4$, $3\pi/2$, $7\pi/4$ and has the state transition matrix:

$$S_8 = \begin{bmatrix} -7 & 7 & 5 & 3 & 1 & -1 & -3 & -5 \\ -5 & -7 & 7 & 5 & 3 & 1 & -1 & -3 \\ -3 & -5 & -7 & 7 & 5 & 3 & 1 & -1 \\ -1 & -3 & -5 & -7 & 7 & 5 & 3 & 1 \\ 1 & -1 & -3 & -5 & -7 & 7 & 5 & 3 \\ 3 & 1 & -1 & -3 & -5 & -7 & 7 & 5 \\ 5 & 3 & 1 & -1 & -3 & -5 & -7 & 7 \\ 7 & 5 & 3 & 1 & -1 & -3 & -5 & -7 \end{bmatrix}.$$

16-CPFSK with $h = 1/16$ has the state transition matrix S_{16}:

$$\begin{bmatrix} -15 & 15 & 13 & 11 & \dots & 1 & -1 & -3 & -5 & -7 & -9 & -11 & -13 \\ -13 & -15 & 15 & 13 & \dots & 3 & 1 & -1 & -3 & -5 & -7 & -9 & -11 \\ -11 & -13 & -15 & 15 & \dots & 5 & 3 & 1 & -1 & -3 & -5 & -7 & -9 \\ -9 & -11 & -13 & -15 & \dots & 7 & 5 & 3 & 1 & -1 & -3 & -5 & -7 \\ -7 & -9 & -11 & -13 & \dots & 9 & 7 & 5 & 3 & 1 & -1 & -3 & -5 \\ -5 & -7 & -9 & -11 & \dots & 11 & 9 & 7 & 5 & 3 & 1 & -1 & -3 \\ -3 & -5 & -7 & -9 & \dots & 13 & 11 & 9 & 7 & 5 & 3 & 1 & -1 \\ -1 & -3 & -5 & -7 & \dots & 15 & 13 & 11 & 9 & 7 & 5 & 3 & 1 \\ 1 & -1 & -3 & -5 & \dots & -15 & 15 & 13 & 11 & 9 & 7 & 5 & 3 \\ 3 & 1 & -1 & -3 & \dots & -13 & -15 & 15 & 13 & 11 & 9 & 7 & 5 \\ 5 & 3 & 1 & -1 & \dots & -11 & -13 & -15 & 15 & 13 & 11 & 9 & 7 \\ 7 & 5 & 3 & 1 & \dots & -9 & -11 & -13 & -15 & 15 & 13 & 11 & 9 \\ 9 & 7 & 5 & 3 & \dots & -7 & -9 & -11 & -13 & -15 & 15 & 13 & 11 \\ 11 & 9 & 7 & 5 & \dots & -5 & -7 & -9 & -11 & -13 & -15 & 15 & 13 \\ 13 & 11 & 9 & 7 & \dots & -3 & -5 & -7 & -9 & -11 & -13 & -15 & 15 \\ 15 & 13 & 11 & 9 & \dots & -1 & -3 & -5 & -7 & -9 & -11 & -13 & -15 \end{bmatrix}.$$

In the general case of M-CPFSK, each row of the state transition matrix will have M symbols corresponding to the paths originating from the state representing that row. In particular, the state transition matrix S_M of M-CPFSK with $h = 1/M$ is

given by

$$\begin{bmatrix} -(M-1) & (M-1) & (M-3) & \dots & \dots & -(M-5) & -(M-3) \\ -(M-3) & -(M-1) & (M-1) & (M-3) & \dots & -(M-7) & -(M-5) \\ -(M-5) & -(M-3) & -(M-1) & (M-1) & \dots & \dots & -(M-7) \\ -(M-7) & -(M-5) & -(M-3) & -(M-1) & \dots & \dots & -(M-9) \\ -(M-9) & -(M-7) & -(M-5) & -(M-3) & \dots & \dots & \dots \\ \dots & \dots & \dots & \dots & \dots & \dots & \dots \\ \dots & \dots & \dots & \dots & \dots & \dots & \dots \\ (M-1) & (M-3) & (M-5) & \dots & \dots & \dots & -(M-1) \end{bmatrix}.$$

The M rows (columns) of S_M correspond to the trellis phase states

$$0, \frac{2\pi}{M}, \frac{4\pi}{M}, \dots\dots \frac{2(M-1)\pi}{M} \quad (\text{modulo} - 2\pi).$$

The above matrix representation for uncoded M-CPFSK with $h \leq 1/M$ can be trivially extended to trellis encoded CPFSK.

As considered already in Section 3.3 the state of a trellis-coded CPFSK signal consists of a symbol state $C_n = (x_{n-1}, x_{n-2}, \dots, x_{n-\nu})$ and a phase state φ_n, where

$$\varphi_n \in \{0, 2\pi h, 4\pi h, \dots, 2(M-1)\pi h\} \quad (\text{modulo} - 2\pi).$$

Therefore the combined state can be expressed as $X_n = \{C_n, \phi_n\}$. The total number of states and hence the total number of rows (columns) in the state transition matrix is equal to $q\,2^{\nu}$, where q is the denominator of the rational value modulation index h, $h = p/q$, and ν is the memory length of the trellis modulation code. The trellis modulation code of Figure 3.6(a), for example, has the state transition matrix:

$$S_8 = \begin{bmatrix} -3 & 1 & 0 & 0 & 0 & 0 & 0 & 0 \\ 0 & 0 & 3 & -1 & 0 & 0 & 0 & 0 \\ 0 & 0 & -3 & 1 & 0 & 0 & 0 & 0 \\ 0 & 0 & 0 & 0 & 3 & -1 & 0 & 0 \\ 0 & 0 & 0 & 0 & -3 & 1 & 0 & 0 \\ 0 & 0 & 0 & 0 & 0 & 0 & 3 & -1 \\ 0 & 0 & 0 & 0 & 0 & 0 & -3 & 1 \\ 3 & -1 & 0 & 0 & 0 & 0 & 0 & 0 \end{bmatrix}.$$

Row (column) one of S_s corresponds to state $(0, 0)$, row (column) two to state $(1, \pi)$, row (column) three to state $(0, 3\pi/2)$, row (column) four to state $(1, \pi/2)$ and so on as shown in Figure 3.6(b). The state transition matrix along with the state location matrix to be defined in the next section provides a convenient means of analyzing trellis modulation codes.

3.4.2 State location matrix

A state location matrix $L_{N,i}$ (also an $N \times N$ matrix) can be defined at the end of every signalling interval [40]. It keeps track of the paths merging at every trellis state at a given signalling interval. The state location matrix at the end of any signalling interval can be obtained by multiplying that at the beginning of the signalling interval by the state transition matrix with all its non-zero elements replaced by 1s. That is the state location matrix at the end of the i^{th} signalling interval $L_{N,i}$ is given by

$$L_{N,i} = L_{N,i-1} T_N = (T_N)^i, \tag{3.17}$$

where T_N is obtained by replacing all non-zero elements of S_N by 1s, and $L_{N,0}$ is an $N \times N$ unit matrix.

The state location matrix at the end of a signalling interval can be used to check for merging of paths (error events) up to that signalling interval. If any of the elements of the state location matrix $L_{N,i}$ is greater than 1, that indicates at least one merging event has occurred at the end of the i^{th} interval. The combination of state transition matrix and state location matrix gives rise to a matrix description for fixed-h M-CPFSK signals, which simplifies the checking for merging events in the trellis search algorithms used to obtain the minimum squared Euclidean distance and other trellis parameters. All the trellis states are considered together within

a single matrix, which avoids the necessity to consider the paths originating from every trellis state separately.

3.5 Conclusions

In this chapter, we have shown how CPFSK signals can be represented by a simplified, time-invariant finite-state trellis, where the trellis states have a one-to-one relationship to the phase of the CPFSK signal. It was also shown that the number of phase states in M-CPFSK can always be made equal to q, irrespective of whether p is odd or even, where p is the numerator and q is the denominator of the rational value modulation index h. By defining a state transition matrix and a state location matrix, a convenient method for analyzing trellis modulation codes was presented. The matrix description may be used to simplify trellis search procedures because all merging events can be considered within a single matrix.

Chapter 4

Binary Nonlinear CPFSK Trellis Modulation Codes for Gaussian Channels

4.1 Introduction

This chapter considers a class of fixed-h binary nonlinear CPFSK trellis modulation codes for the additive white Gaussian noise channel. They differ from general CPFSK signals in that all the transitions of general CPFSK are not allowed in binary nonlinear CPFSK and the symbols are selected from a higher order alphabet. Construction of the nonlinear trellis modulation codes is based on the state transition matrix for CPFSK signals defined in Chapter 3.

In general, a nonlinear CPFSK trellis modulation code can be constructed by selecting an appropriate state transition matrix with a reduced number of transitions, thereby decreasing the connectivity of the trellis and delaying the merging of path-pairs. In this study we allow only two transitions per state and consequently the signalling schemes are binary. Delaying of merging events does not necessarily lead to a larger minimum squared Euclidean distance, although it results in a larger memory length or time diversity. The choice of minimum squared Euclidean distance as the performance measure is justifiable when the channel is

perturbed only by additive, white Gaussian noise and the receiver signal-to-noise ratio is high. It is also assumed that perfect symbol timing information is available at the maximum-likelihood decoder.

Numerical results indicate that, for a given complexity, binary nonlinear CPFSK *trellis modulation codes* can be designed so that they achieve larger minimum squared Euclidean distances and memory lengths than general binary CPFSK signals. A systematic method is given for the construction of binary nonlinear CPFSK schemes with $h = 1/M$ that achieve the maximum memory length allowed by the number of trellis phase states. Since all signals in a binary nonlinear CPFSK scheme are legitimate outcomes of an M-ary CPFSK scheme the bandwidth is unchanged. It is shown that the above binary nonlinear CPFSK schemes lack the important property of transparency to carrier-phase ambiguities of the reconstructed reference signals of the trellis decoder. In other words they are rotationally non-invariant.

4.2 Nonlinear CPFSK trellis modulation codes

Codes can be classified as *block codes* and *tree codes*. The distinguishing feature between the encoders for these codes is the presence or absence of memory. Block encoders are memoryless devices, while tree encoders are devices with memory. Trellis modulation codes are tree codes.

Codes can also be classified as *linear* or *nonlinear*. It is well known that linear codes have the important property that any two code words can be added using a suitable definition for addition to produce another valid code word. This property has implications in simplifying encoding and decoding as well as in computing the performance. In linear codes the distance between any two code words is equivalent to the distance between the all-zero code word and some other code

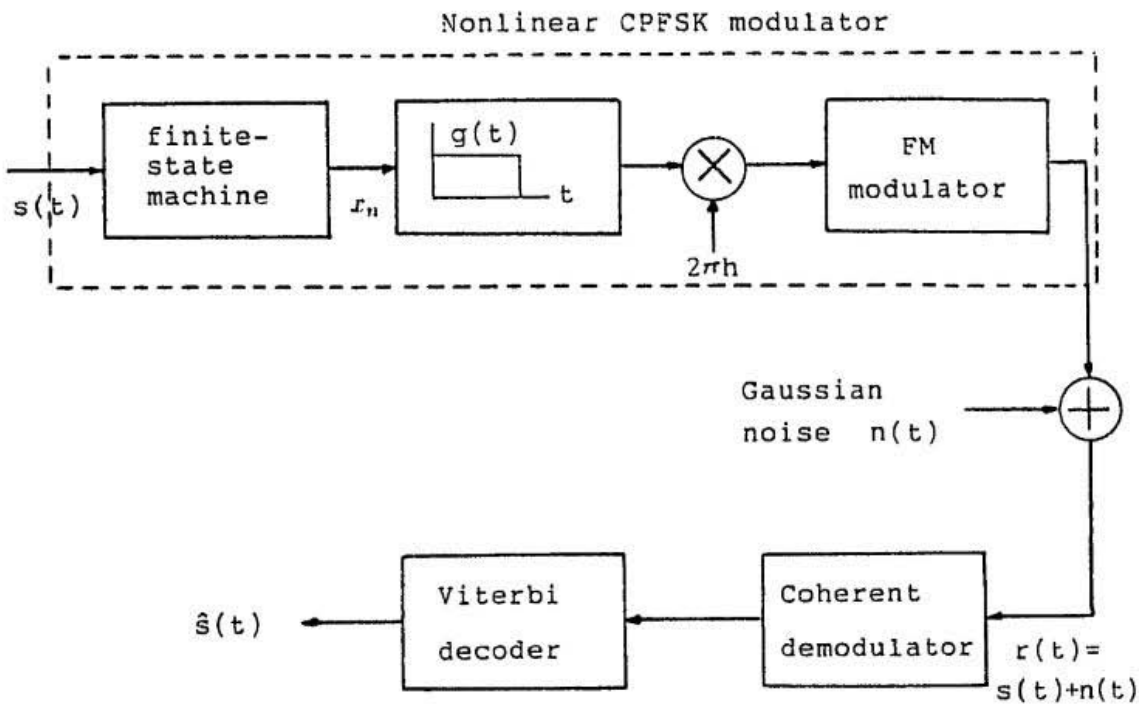

Figure 4.1 Nonlinear CPFSK system model.

word. Therefore, when computing performance, it is sufficient to consider the effect of transmitting only the all-zero code word. CPFSK trellis modulation codes do not have this important property.

The difference between CPFSK trellis modulation codes and *nonlinear* CPFSK trellis modulation codes as considered in this chapter is that, in the latter only two transitions per phase state of the original M-ary CPFSK trellis are permitted, whereas in CPFSK signals there are the same M transitions from every phase state. Moreover, the labelling of transitions depends on the current phase state. Thus, *nonlinear* refers to the labelling of the trellis branches of the modulation scheme rather than to the overall trellis code which is nonlinear anyway (in a coding sense).

4.2.1 System model

The nonlinear CPFSK system model under consideration in this chapter is shown in Figure 4.1 [63, 65]. The input data symbols are sent through a finite-state machine that maps binary data to symbols x_n from a higher-order M-ary alphabet according to the state transition matrix of a given binary nonlinear CPFSK scheme (construction of the state transition matrix is considered in the next section). In other words, the function of the finite-state machine is to implement the state transition matrix, where the mapping of binary symbols to the higher-order alphabet depends on the current state of the finite-state machine. There is no fixed natural binary mapping rule employed.

The output of the nonlinear finite-state machine is the M-ary sequence $\{x_n\}$, where x_n can take any value of the set

$$\{(2i - M - 1),\, i = 1,\, 2,\, 3,\, \ldots,\, M\}$$

with equal probability. The sequence is convolved with the impulse response $g(t)$

of the baseband frequency shaping filter. Feeding this PAM signal to the FM modulator leads to the nonlinear CPFSK signal. Whereas, in CPFSK signalling, $g(t)$ is rectangular in shape it can take other shapes such as the half-cycle sinusoid (HCS) with $g(t) = \frac{\pi}{4T} \sin(\pi t/T); 0 \leq t \leq T$ or the raised-cosine (RC) with $g(t) = \frac{1}{2T}[1 - \cos(2\pi t/T)]; 0 \leq t \leq T$. These are trivial extensions of CPFSK signalling schemes.

The channel is expected to be corrupted only by additive, white Gaussian noise and perfect symbol timing synchronisation is assumed. The error performance of any trellis modulation code on such a channel at high signal-to-noise ratios can be predicted by computing the minimum squared Euclidean distance (d^2_{min}). At the receiver, the binary nonlinear CPFSK trellis modulation codes can be optimally detected using correlation detection and Viterbi decoding. The decoding metric is the Euclidean distance defined in Section 1.5 and Appendix.

4.3 Binary nonlinear CPFSK trellis modulation codes: $h = 1/M$

This section describes the construction and analysis of binary nonlinear CPFSK trellis modulation codes when the modulation index is $1/M$.

The basic idea behind nonlinear CPFSK is to delay the first inevitable merge, thereby creating a possibly large minimum squared Euclidean distance between neighbouring path-pairs through the trellis. (Inevitable merging events correspond to pairs of information sequences or signal paths through the trellis which split at a given state only to remerge after two signalling intervals, remaining identical thereafter. The minimum squared Euclidean distances associated with these inevitable merging events provide an upper-bound to the overall minimum squared Euclidean distance of the CPFSK scheme, and it leads to a closed-form expression for same

[6, 59]).

We take the approach of first examining the matrix description of M-ary CPFSK before taking the step of constructing binary nonlinear CPFSK. The method is illustrated for several simple cases and then generalised for any M, where $M = 2^n$ and n is an integer. Unlike in the case of general M-ary CPFSK, n is not the average number of bits carried in one signalling interval. In our case the number of bits carried in one signalling interval is always equal to one.

In Chapter 3 we have shown that when $h = 1/M$ the finite-state machine representing M-CPFSK has M distinct states. The maximum memory length, ν_{max}, allowed by the number of states (i.e. the trellis phase states) of any binary trellis is given by [40]:

$$\nu_{max} = \lfloor 1 + \log_2 M \rfloor. \tag{4.1}$$

To ensure the maximum memory length, the state transition matrix of the binary nonlinear CPFSK scheme S_M has to be selected so that the state location matrix $L_{M,i}$, $i = 1, 2, 3, \ldots .(\nu_{max} - 1)$ has no elements greater than one [40]. If one or more elements of the state location matrix are greater than one, it indicates that merging events have taken place. After $(\nu_{max} - 1)$ signalling intervals the state location matrix is given by:

$$L_{M,\nu_{max}-1} = T_M{}^{(\nu_{max}-1)}, \tag{4.2}$$

where T_M is obtained by replacing all non-zero elements of S_M by ones. This condition ensures that up-to the level of $(\nu_{max} - 1)$ no merging of trellis paths has taken place. At the end of $(\nu_{max} - 1)$ signalling intervals, all elements of the state location matrix $L_{M,\nu_{max}-1}$ will be equal to one. In other words, $L_{M,\nu_{max}-1}$ is an all 1s matrix of size $M \times M$.

4.3.1 Binary nonlinear CPFSK ($M = 4$, $h = 1/4$)

In this section we consider binary nonlinear CPFSK trellis modulation codes based on quaternary CPFSK signals with modulation index 1/4. Rewriting (3.9) with $h = 1/4$, we have

$$\phi_n = \phi_{n-1} + \frac{n\pi}{4}(x_{n-1} - x_n), \tag{4.3}$$

where $x_n, x_{n-1} = \{\pm 1, \pm 3\}$ for all integral values of n. Then it can be easily shown that $\phi_n = 0, \pi/2, \pi, 3\pi/2$ (modulo-2π). Therefore ϕ_n can take only four phase values for 4-CPFSK signals with $h = 1/4$.

Four different tones are transmitted in this case and the 4-CPFSK signal is given by (with usual notation):

$$s(t) = \sqrt{2E_s/T}\cos(2\pi f_0 t + \pi x_n t/4T + \phi_n). \tag{4.4}$$

The quaternary symbols -3, -1, 1 and 3 correspond to the tones of frequencies $(f_0 - 3/8T)$, $(f_0 - 1/8T)$, $(f_0 + 1/8T)$ and $(f_0 + 3/8T)$ respectively. It is assumed that the lowest tone [*i.e.* $(f_0 - 3/8T)$] goes through an integral number of cycles during one signalling interval. Thus

$$\begin{aligned}
-3: \ 2\pi(f_0 - 3/8T)T &= 2n\pi = 0 \quad (\text{modulo} - 2\pi) \\
-1: \ 2\pi(f_0 - 1/8T)T &= \pi/2 \quad (\text{modulo} - 2\pi) \\
+1: \ 2\pi(f_0 + 1/8T)T &= \pi \quad (\text{modulo} - 2\pi) \\
+3: \ 2\pi(f_0 + 3/8T)T &= 3\pi/2 \quad (\text{modulo} - 2\pi)
\end{aligned} \tag{4.5}$$

Clearly the symbols -3, -1, 1 and 3 are associated with phase changes of 0, $\pi/2$, π and $3\pi/2$ respectively.

The above results can be used to obtain the phase trellis, and hence the state transition matrix can be deduced. Every state has four transitions (branches)

leaving, each of which is related to one of -3, -1, 1 or 3. This amounts to a total of sixteen transitions between adjacent signalling intervals. Consequently sixteen different waveforms are possible depending on the state of the modulator and the input signal. The phase trellis and the state diagram are as shown in Figure 4.2. The resulting state transition matrix S_4 is given by:

$$S_4 = \begin{bmatrix} -3 & 3 & 1 & -1 \\ -1 & -3 & 3 & 1 \\ 1 & -1 & -3 & 3 \\ 3 & 1 & -1 & -3 \end{bmatrix}. \tag{4.6}$$

For 4-CPFSK with $h = 1/4$ the state sequence can be $(0, \pi/2, \pi, 3\pi/2)$; $(\pi/2, \pi, 3\pi/2, 0)$; $(\pi, 3\pi/2, 0, \pi/2)$ or $(3\pi/2, 0, \pi/2, \pi)$. All the above state sequences produce identical finite-state systems with the same minimum squared Euclidean distance. Moreover, in trellis search algorithms it is sufficient to consider the path-pairs originating at only one set of the states since all states produce the same distance profile.

Consider the trellis and the state diagram of $h = 1/4$, 4-CPFSK shown in Figure 4.2. Any rotational shift of the states by an integer multiple of $\pi/2$ radians does not change the trellis and the state diagram. The reason for this important property is the phase angles of the transmitted signal and the states of the system having a one-to-one mapping, thereby making a rotational shift to the trellis equivalent to adding $\pi/2$ radians to the incoming signal phase, or alternatively, to the reference tone phase angles. This observation leads us to the conclusion that the Viterbi decoder is unaffected by the phase ambiguities of the regenerated reference tones. In general, M-CPFSK with $h = p/q$ are transparent to q-fold ambiguities of the reference tones. Thus the Viterbi decoder successfully resolves phase ambiguities of $2\pi h, 4\pi h, \ldots, 2(M-1)\pi h$. As we shall see later, this property is not present in most binary nonlinear CPFSK trellis modulation codes.

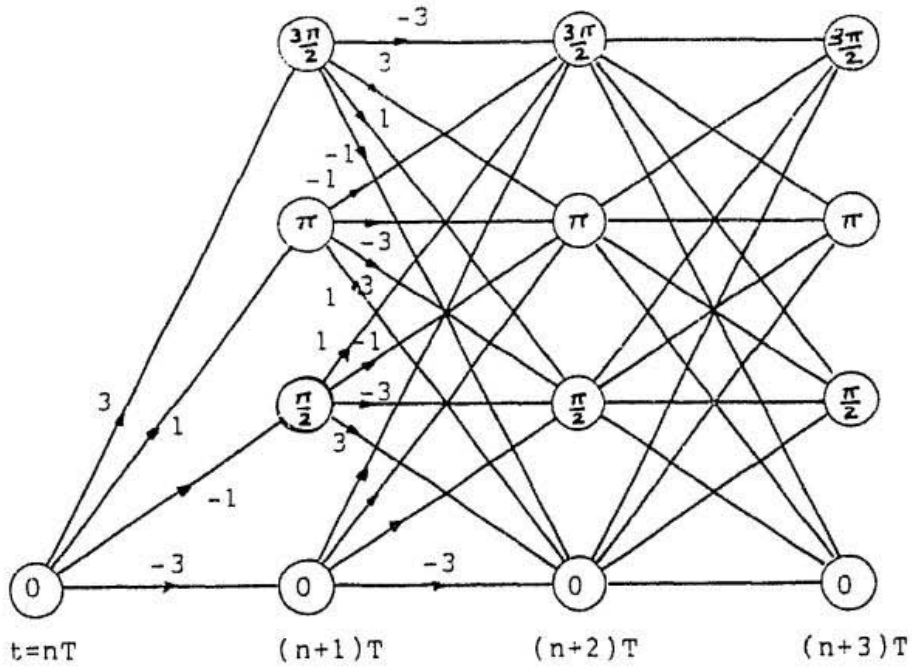

Trellis

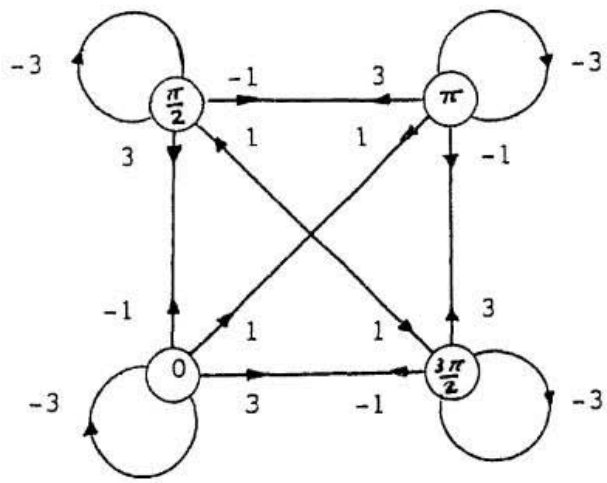

State diagram

Figure 4.2 Trellis and state diagram of 4-CPFSK, h=1/4.

Owing to the rotational symmetry property, order of the states does not affect the distance properties; therefore, in this chapter unless otherwise stated the state sequence is considered to be $0, 2\pi h, 4\pi h, \ldots, 2(M-1)\pi h$. Thus the state transition matrix has its rows and columns labelled in that order from bottom to top, and right to left, respectively. This systematic and natural state formulation enables us to concentrate only on the transition matrix without paying attention to the different state arrangement sequences.

To construct a binary nonlinear CPFSK scheme with $M = 4$ and $h = 1/4$ it is necessary to find a 4×4 matrix T_4 with two ones in every row, which satisfies (4.2). That is

$$L_{4,2} = (T_4)^2 = \begin{bmatrix} 1 & 1 & 1 & 1 \\ 1 & 1 & 1 & 1 \\ 1 & 1 & 1 & 1 \\ 1 & 1 & 1 & 1 \end{bmatrix}. \tag{4.7}$$

It can be seen that

$$T_4 = \begin{bmatrix} 1 & 0 & 1 & 0 \\ 1 & 0 & 1 & 0 \\ 0 & 1 & 0 & 1 \\ 0 & 1 & 0 & 1 \end{bmatrix} \tag{4.8}$$

satisfies (4.2). T_4 is identical with the state transition matrix of a binary convolutional code of constraint length two. And ν_{max} here is equal to $\lfloor 1 + \log_2 4 \rfloor = 3$. The corresponding state transition matrix for the nonlinear 4-CPFSK scheme is given by:

$$S_4 = \begin{bmatrix} -3 & 0 & 1 & 0 \\ -1 & 0 & 3 & 0 \\ 0 & -1 & 0 & 3 \\ 0 & 1 & 0 & -3 \end{bmatrix}. \tag{4.9}$$

The above realisation of the binary nonlinear CPFSK scheme ($M = 4$, $h = 1/4$) has $\nu = 3$, $d^2_{min} = 2.151$. This scheme has a coding gain of 0.316 dB over MSK signalling. Figure 4.3 shows the phase trellis and the state transition diagram of the above binary nonlinear CPFSK trellis m dulation code and the corresponding

minimum distance path. Clearly, the first merging takes place after three signalling intervals, indicating that the memory length is three. This is the maximum memory or time diversity achievable with any four-state binary trellis. In contrast, all general CPFSK schemes have a maximum memory length of only two. The inevitable merging event that takes place after only two signalling intervals has been overcome in the above nonlinear scheme.

Two other binary nonlinear CPFSK ($M = 4$, $h = 1/4$) trellis modulation codes were also found to have similar properties to the best code given above. But they have different transition matrices as shown in Figure 4.4. The trellis search program that computes the minimum squared Euclidean distance is based on the algorithm found in [75] in conjunction with the matrix description of CPFSK signals that we have described in Chapter 3.

As the spectral properties are also important in the comparison of various trellis modulation codes, it is proper to discuss briefly the spectrum of the above nonlinear CPFSK trellis modulation codes. As mentioned before in the review of literature, the spectrum of any CPFSK signal is determined by the maximum slope variation among the piecewise-continuous phase trellis [38]. It has been shown that M-CPFSK with $h = 1/M$ have approximately the same power spectral densities for all $M \geq 4$ [38]. M-PSK on the other hand has the same power spectral density for all M. For all practical purposes the power spectral density of 4-CPFSK could be used to roughly predict the power spectral density of CPFSK for any other value of M. It can be conjectured that the spectrum of the above binary nonlinear CPFSK scheme would not differ much from that of quaternary CPFSK with $h = 1/4$.

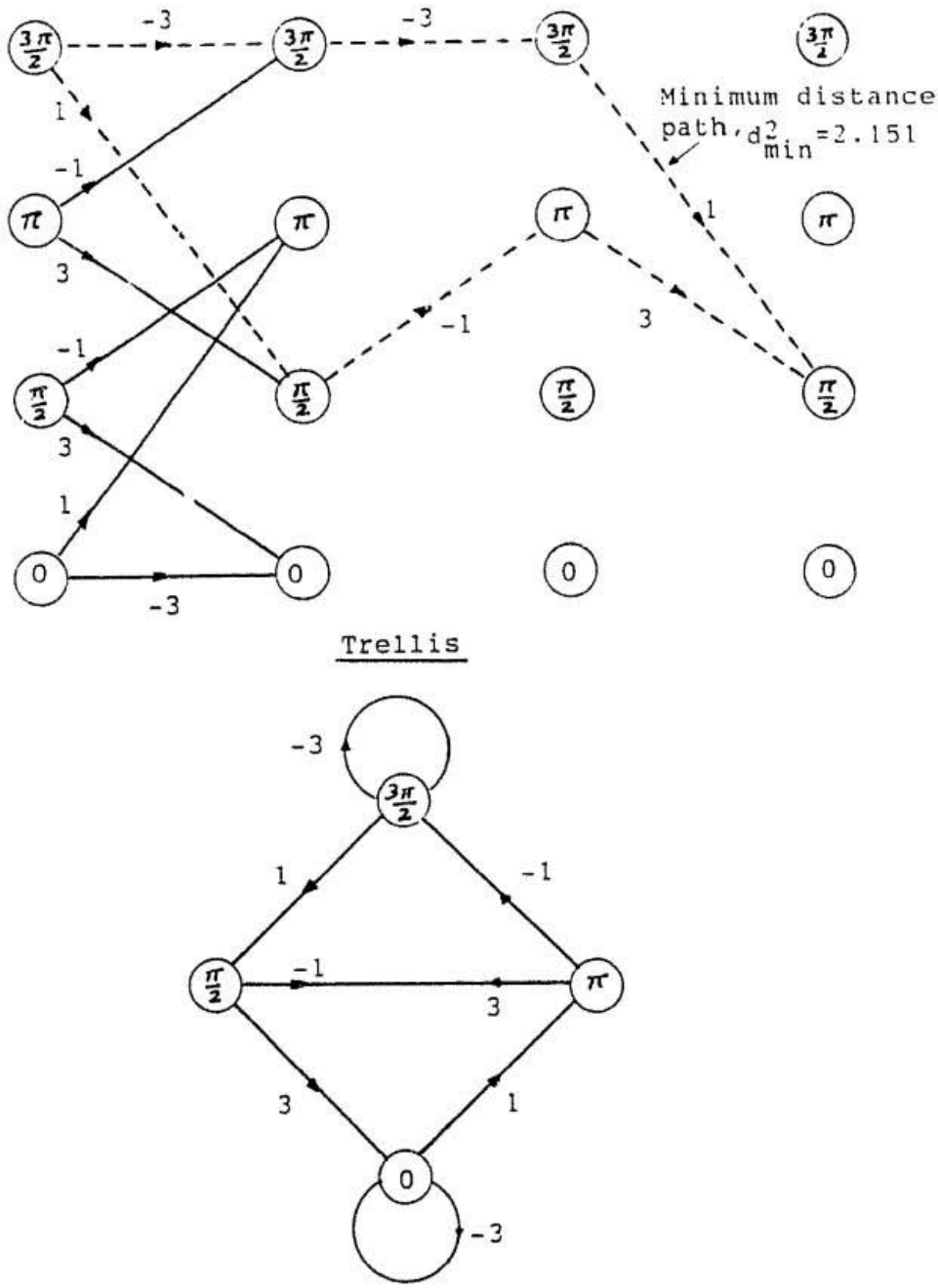

Figure 4.3 Optimum binary nonlinear CPFSK (M=4, q=4).

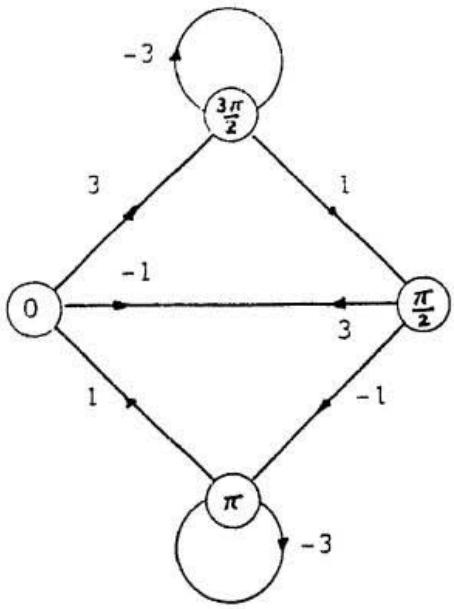

$$S_4 = \begin{bmatrix} -3 & 0 & 1 & 0 \\ 0 & -3 & 0 & 1 \\ 0 & -1 & 0 & 3 \\ 3 & 0 & -1 & 0 \end{bmatrix}$$

Minimum distance path:

x_n:	-3	-3	1
x_n':	1	3	-1

$$d^2_{min} = 2.151$$

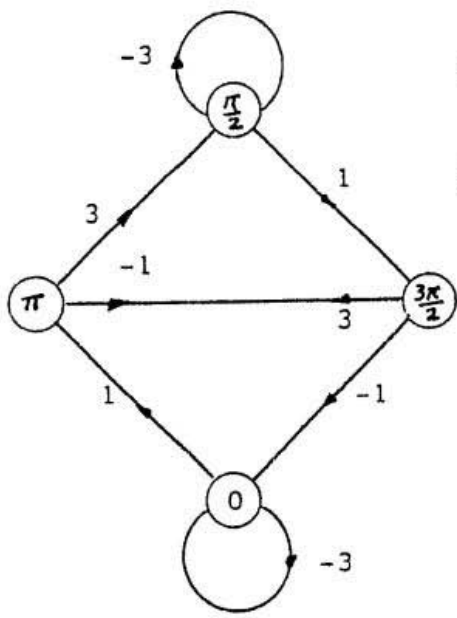

$$S_4 = \begin{bmatrix} 0 & 3 & 0 & -1 \\ -1 & 0 & 3 & 0 \\ 1 & 0 & -3 & 0 \\ 0 & 1 & 0 & -3 \end{bmatrix}$$

Minimum distance path:

x_n:	-1	3	-1
x_n':	3	-3	1

$$d^2_{min} = 2.151$$

Figure 4.4 Equivalent binary nonlinear CPFSK (M=4, q=4).

4.3.2 Binary nonlinear CPFSK ($M = 8$, $h = 1/8$)

Here we construct and analyze binary nonlinear CPFSK schemes based on octal CPFSK with $h = 1/8$. The eight-state binary nonlinear CPFSK trellis modulation code that achieves the maximum memory length is deduced.

From (3.9) we have, for $h = 1/8$, 8-CPFSK

$$\phi_n = \phi_{n-1} + \frac{n\pi}{8}(x_{n-1} - x_n), \tag{4.10}$$

where $x_n, x_{n-1} \in \{\pm 1, \pm 3, \pm 5, \pm 7\}$ for all integral values of n. Then it can be shown that $\phi_n = 0, \pi/4, \pi/2, 3\pi/4, \pi, 5\pi/4, 3\pi/2, 7\pi/8$ (*modulo-2π*). Therefore ϕ_n can take only eight phase values for 8-CPFSK signals with $h = 1/8$.

Eight different tones are transmitted in this case. The octal symbols -7, -5, -3, -1, 1, 3, 5 and 7 correspond to the tones of angular frequencies $(f_0 - 7/16T)$, $(f_0 - 5/16T)$, $(f_0 - 3/16T)$, $(f_0 - 1/16T)$, $(f_0 + 1/16T)$, $(f_0 + 3/16T)$, $(f_0 + 5/16T)$ and $(f_0 + 7/16T)$ respectively. It is again assumed that the lowest tone [*i.e.* $(f_0 - 7/16T)$] goes through an integer multiple of cycles during one signalling interval. Thus we have

$$\begin{aligned}
-7 &: 2\pi(f_0 - 7/16T)T = 2n\pi = 0 \quad (\text{modulo} - 2\pi) \\
-5 &: 2\pi(f_0 - 5/16T)T = \pi/4 \quad (\text{modulo} - 2\pi) \\
-3 &: 2\pi(f_0 - 3/16T)T = \pi/2 \quad (\text{modulo} - 2\pi) \\
-1 &: 2\pi(f_0 - 1/16T)T = 3\pi/4 \quad (\text{modulo} - 2\pi) \\
+1 &: 2\pi(f_0 + 1/16T)T = \pi \quad (\text{modulo} - 2\pi) \\
+3 &: 2\pi(f_0 + 3/16T)T = 5\pi/4 \quad (\text{modulo} - 2\pi) \\
+5 &: 2\pi(f_0 + 5/16T)T = 3\pi/2 \quad (\text{modulo} - 2\pi) \\
+7 &: 2\pi(f_0 + 7/16T)T = 7\pi/8 \quad (\text{modulo} - 2\pi)
\end{aligned} \tag{4.11}$$

Clearly the symbols -7, -5, -3, -1, 1, 3, 5 and 7 are associated with phase changes of 0, $\pi/4$, $\pi/2$, $3\pi/4$, π, $5\pi/4$, $3\pi/2$ and $7\pi/8$ radians respectively. The 8-CPFSK signal in this case is given by:

$$s(t) = \sqrt{2E_s/T}\cos(2\pi f_0 t + \pi x_n t/8T + \phi_n). \tag{4.12}$$

Using the above results the phase trellis and the state transition matrix of $h = 1/8$, 8-CPFSK can be obtained. Every state has eight transitions (branches) leaving, each of which is related to one of -7, -5, -3, -1, 1, 3, 5 or 7. Thus a total of sixty-four different waveforms are possible depending on the state of the modulator and the data symbol. The phase trellis and the state transition diagram for 8-CPFSK with $h = 1/8$ is shown in Figure 4.5 and the corresponding state transition matrix is given by:

$$S_8 = \begin{bmatrix} -7 & 7 & 5 & 3 & 1 & -1 & -3 & -5 \\ -5 & -7 & 7 & 5 & 3 & 1 & -1 & -3 \\ -3 & -5 & -7 & 7 & 5 & 3 & 1 & -1 \\ -1 & -3 & -5 & -7 & 7 & 5 & 3 & 1 \\ 1 & -1 & -3 & -5 & -7 & 7 & 5 & 3 \\ 3 & 1 & -1 & -3 & -5 & -7 & 7 & 5 \\ 5 & 3 & 1 & -1 & -3 & -5 & -7 & 7 \\ 7 & 5 & 3 & 1 & -1 & -3 & -5 & -7 \end{bmatrix}. \tag{4.13}$$

When designing binary nonlinear CPFSK with $M = 8$ and $h = 1/8$, it is necessary to find an 8×8 matrix, T_8, with two ones in every row that satisfies (4.2).

Observing that

$$L_{8,3} = (T_8)^3 = \begin{bmatrix} 1 & 1 & 1 & 1 & 1 & 1 & 1 & 1 \\ 1 & 1 & 1 & 1 & 1 & 1 & 1 & 1 \\ 1 & 1 & 1 & 1 & 1 & 1 & 1 & 1 \\ 1 & 1 & 1 & 1 & 1 & 1 & 1 & 1 \\ 1 & 1 & 1 & 1 & 1 & 1 & 1 & 1 \\ 1 & 1 & 1 & 1 & 1 & 1 & 1 & 1 \\ 1 & 1 & 1 & 1 & 1 & 1 & 1 & 1 \\ 1 & 1 & 1 & 1 & 1 & 1 & 1 & 1 \end{bmatrix} \tag{4.14}$$

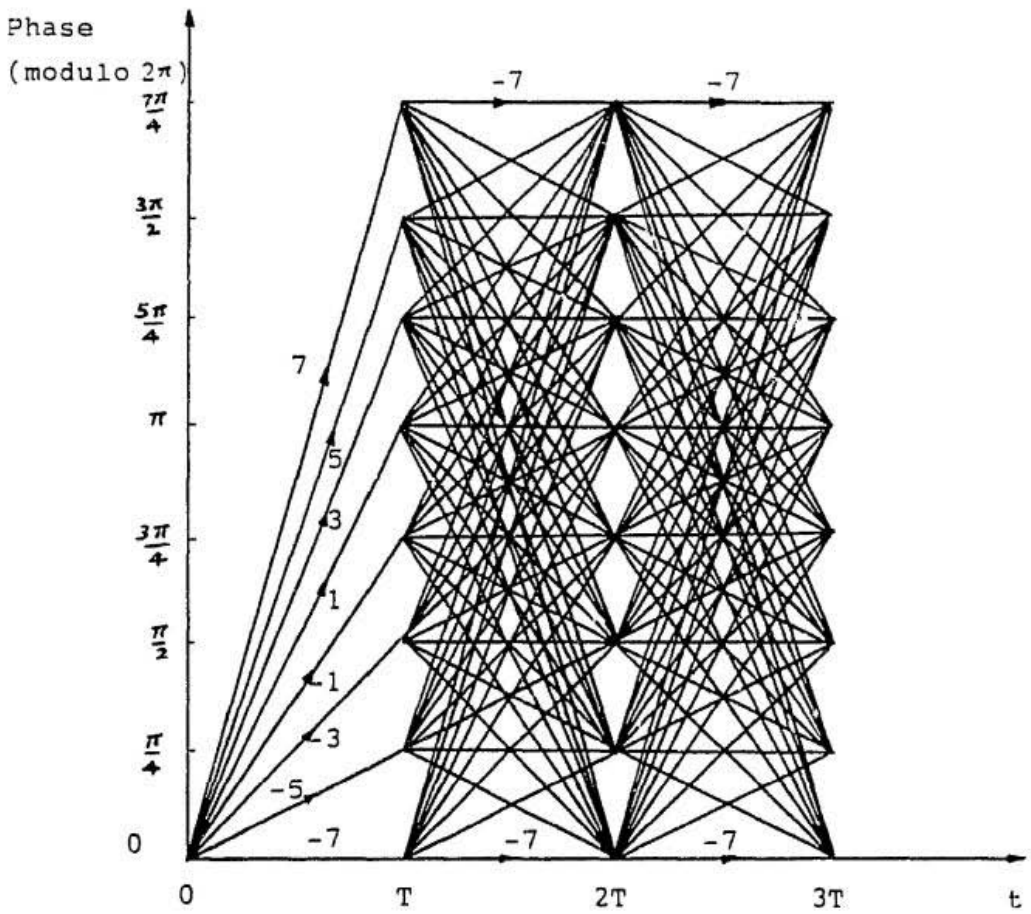

(a) Trellis

Figure 4.5 Trellis and state diagram of 8-CPFSK, h=1/8.

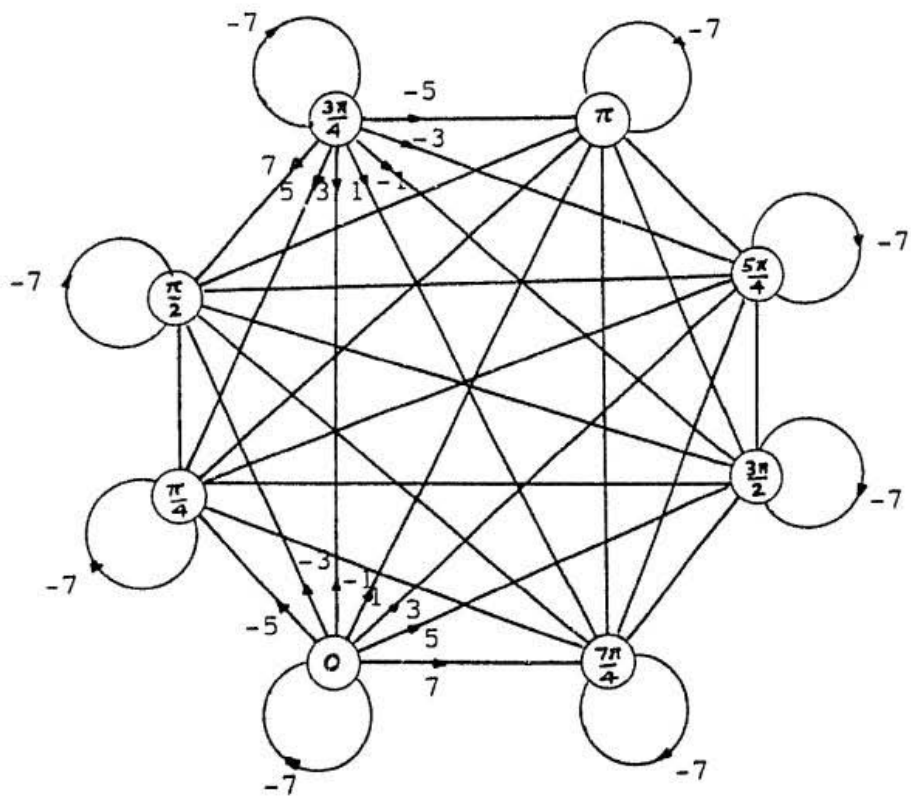

(b) State diagram

Figure 4.5 (Contd.) Trellis and state diagram of 8-CPFSK, h=1/8.

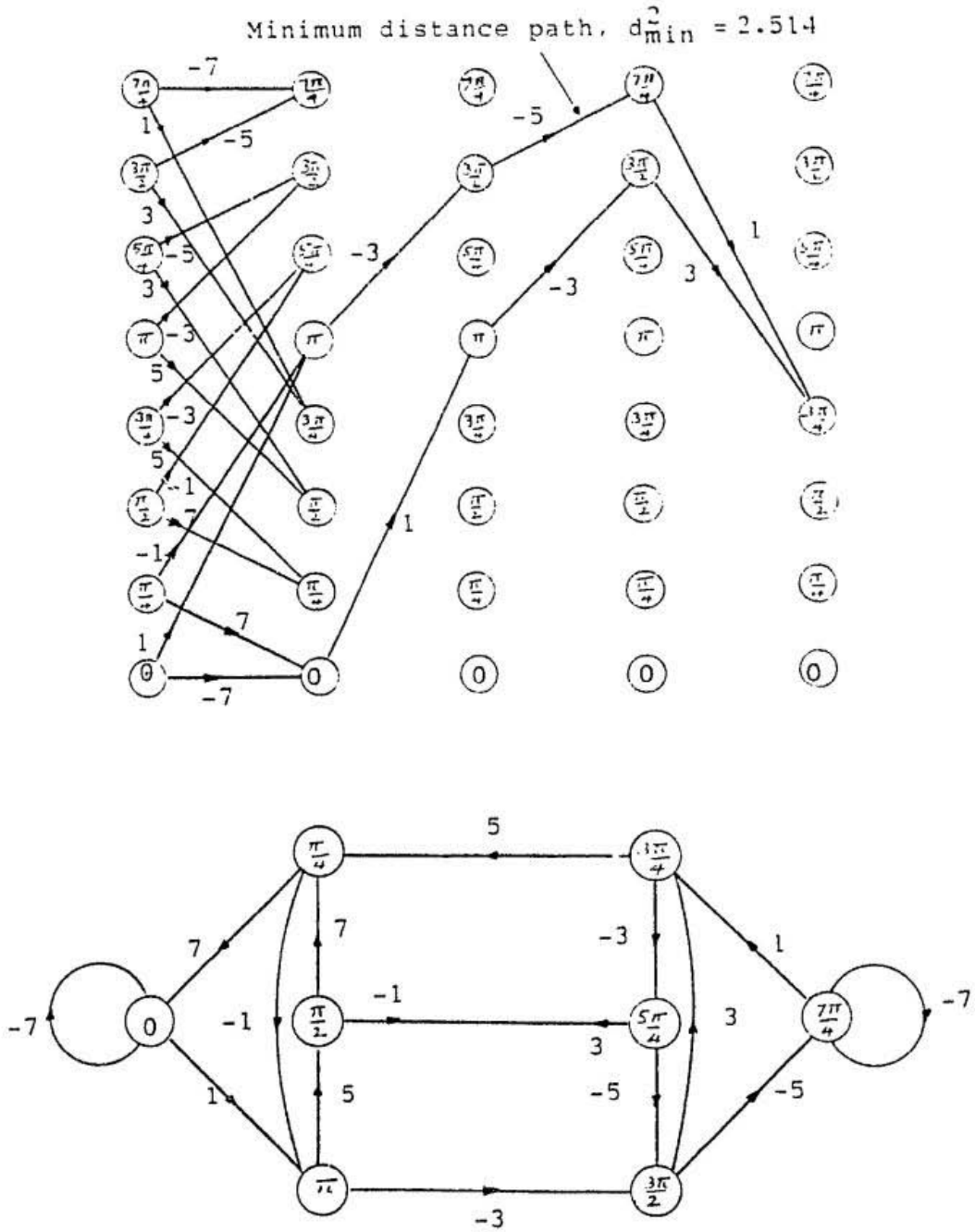

Figure 4.6 Optimum binary nonlinear CPFSK (M=8, q=8).

is satisfied by

$$T_8 = \begin{bmatrix} 1 & 0 & 0 & 0 & 1 & 0 & 0 & 0 \\ 1 & 0 & 0 & 0 & 1 & 0 & 0 & 0 \\ 0 & 1 & 0 & 0 & 0 & 1 & 0 & 0 \\ 0 & 1 & 0 & 0 & 0 & 1 & 0 & 0 \\ 0 & 0 & 1 & 0 & 0 & 0 & 1 & 0 \\ 0 & 0 & 1 & 0 & 0 & 0 & 1 & 0 \\ 0 & 0 & 0 & 1 & 0 & 0 & 0 & 1 \\ 0 & 0 & 0 & 1 & 0 & 0 & 0 & 1 \end{bmatrix}. \tag{4.15}$$

we have the required state transition matrix for the binary nonlinear CPFSK ($M = 8$, $h = 1/8$) scheme as:

$$S_8 = \begin{bmatrix} -7 & 0 & 0 & 0 & 1 & -0 & -0 & 0 \\ -5 & 0 & 0 & 0 & 3 & 0 & 0 & 0 \\ 0 & -5 & 0 & 0 & -0 & 3 & 0 & 0 \\ 0 & -3 & 0 & 0 & 0 & 5 & 0 & 0 \\ 0 & 0 & -3 & 0 & 0 & 0 & 5 & 0 \\ 0 & 0 & -1 & 0 & 0 & 0 & 7 & 0 \\ 0 & 0 & 0 & -1 & 0 & 0 & 0 & 7 \\ 0 & 0 & 0 & 1 & 0 & 0 & 0 & -7 \end{bmatrix}. \tag{4.16}$$

The above realisation of binary nonlinear CPFSK with $h = 1/8$ results in a minimum squared Euclidean distance of 2.514. This is a coding gain of approximately 1 dB over MSK signalling. The state diagram and the phase trellis of the above nonlinear CPFSK scheme with $M = 8$ and $h = 1/8$ are shown in Figure 4.6. Also shown is the minimum distance path-pair for this case. The memory length of the trellis modulation code is equal to four, which is the maximum that can be achieved with eight states.

The spectrum of the above binary nonlinear CPFSK signal will be close to that of octal CPFSK with $h = 1/8$, which is again not much different from that of quaternary CPFSK with $h = 1/4$.

4.3.3 Binary nonlinear CPFSK ($M = 16$, $h = 1/16$)

For $h = 1/16$ binary nonlinear CPFSK the optimum state transition matrix is given by:

$$\begin{bmatrix}
-15 & 0 & 0 & 0 & 0 & 0 & 0 & 0 & 1 & 0 & 0 & 0 & 0 & 0 & 0 & 0 \\
-13 & 0 & 0 & 0 & 0 & 0 & 0 & 0 & 3 & 0 & 0 & 0 & 0 & 0 & 0 & 0 \\
0 & -13 & 0 & 0 & 0 & 0 & 0 & 0 & 0 & 3 & 0 & 0 & 0 & 0 & 0 & 0 \\
0 & -11 & 0 & 0 & 0 & 0 & 0 & 0 & 0 & 5 & 0 & 0 & 0 & 0 & 0 & 0 \\
0 & 0 & -11 & 0 & 0 & 0 & 0 & 0 & 0 & 0 & 5 & 0 & 0 & 0 & 0 & 0 \\
0 & 0 & -9 & 0 & 0 & 0 & 0 & 0 & 0 & 0 & 7 & 0 & 0 & 0 & 0 & 0 \\
0 & 0 & 0 & -9 & 0 & 0 & 0 & 0 & 0 & 0 & 0 & 7 & 0 & 0 & 0 & 0 \\
0 & 0 & 0 & -7 & 0 & 0 & 0 & 0 & 0 & 0 & 0 & 9 & 0 & 0 & 0 & 0 \\
0 & 0 & 0 & 0 & -7 & 0 & 0 & 0 & 0 & 0 & 0 & 0 & 9 & 0 & 0 & 0 \\
0 & 0 & 0 & 0 & -5 & 0 & 0 & 0 & 0 & 0 & 0 & 0 & 11 & 0 & 0 & 0 \\
0 & 0 & 0 & 0 & 0 & -5 & 0 & 0 & 0 & 0 & 0 & 0 & 0 & 11 & 0 & 0 \\
0 & 0 & 0 & 0 & 0 & -3 & 0 & 0 & 0 & 0 & 0 & 0 & 0 & 13 & 0 & 0 \\
0 & 0 & 0 & 0 & 0 & 0 & -3 & 0 & 0 & 0 & 0 & 0 & 0 & 0 & 13 & 0 \\
0 & 0 & 0 & 0 & 0 & 0 & -1 & 0 & 0 & 0 & 0 & 0 & 0 & 0 & 15 & 0 \\
0 & 0 & 0 & 0 & 0 & 0 & 0 & -1 & 0 & 0 & 0 & 0 & 0 & 0 & 0 & 15 \\
0 & 0 & 0 & 0 & 0 & 0 & 0 & 1 & 0 & 0 & 0 & 0 & 0 & 0 & 0 & -15
\end{bmatrix} \tag{4.17}$$

The rows and columns of S_{16} correspond to the phase sequence 0, $\pi/8$, $\pi/4$, $3\pi/8$, $\pi/2$, $5\pi/8$, $3\pi/4$, $7\pi/8$, π, $9\pi/8$, $5\pi/4$, $11\pi/8$, $3\pi/2$, $13\pi/8$, $7\pi/4$, $15\pi/8$. The minimum squared Euclidean distance for this binary nonlinear CPFSK scheme is equal to 3.356. This reflects a coding gain of 2.25 dB over MSK signalling. The memory length is equal to five, which is the maximum for any sixteen-state binary trellis code.

4.3.4 Generalisation

The preceding examples establish a pattern towards a general conclusion. The state transition matrix that achieves the maximum memory length for the general case

of binary nonlinear CPFSK with $h = 1/M$ can be deduced as:

$$T_M = \begin{bmatrix} 1 & 0 & \dots & \dots & 0 & 1 & 0 & \dots & 0 & 0 \\ 1 & 0 & \dots & \dots & 0 & 1 & 0 & \dots & 0 & 0 \\ 0 & 1 & 0 & \dots & \dots & 0 & 1 & \dots & 0 & 0 \\ 0 & 1 & 0 & \dots & \dots & 0 & 1 & \dots & 0 & 0 \\ 0 & 0 & 1 & \dots & 0 & \dots & 0 & 1 & \dots & 0 \\ 0 & 0 & 1 & \dots & 0 & \dots & 0 & 1 & \dots & 0 \\ \dots & \dots & \dots & \dots & \dots & \dots & \dots & \dots & \dots & \dots \\ \dots & \dots & \dots & \dots & \dots & \dots & \dots & \dots & \dots & \dots \\ 0 & 0 & 0 & \dots & 1 & 0 & 0 & \dots & 0 & 1 \\ 0 & 0 & 0 & \dots & 1 & 0 & 0 & \dots & 0 & 1 \end{bmatrix} \tag{4.18}$$

with the phase state sequence $0, 2\pi/M, 4\pi/M, \dots\dots, 2(M-1)\pi/M$. The above matrix satisfies the most general form of (4.2), given by:

$$T_M{}^{\nu_{max}-1} = [\text{all ones}]_{M \times M} \tag{4.19}$$

Since these binary nonlinear CPFSK signals are outcomes of a legitimate M-ary CPFSK scheme, the spectrum would not be much different from that of the corresponding M-ary CPFSK scheme with modulation index $1/M$. However, it should be noted that, since all the above CPFSK schemes are driven by random data the spectrum, in practice, will also be dependent on the input symbol sequence.

4.4 Binary nonlinear CPFSK trellis modulation codes: $h \neq 1/M$

In this section binary nonlinear CPFSK trellis modulation codes are constructed and analyzed when the modulation index is not equal to $1/M$. Due to spectral considerations, we are only interested in trellis modulation codes with $h < 1/M$. That is modulation indexes of the form $h = p/q$, where $q > M$. While it is theoretically possible to have an odd number of states in binary nonlinear CPFSK, the condition that all M-ary symbols occur equiprobably cannot be satisfied when

the number of states is odd. Thus, we restrict our study to even number of states. In other words q is assumed to be an even integer.

In the following examples we construct and analyze simple fixed-h binary nonlinear CPFSK schemes with $h \neq 1/M$, where the inevitable merging event of general CPFSK has been overcome and, for a given number of trellis phase states, the maximum memory length has been reached.

4.4.1 Binary nonlinear CPFSK ($M = 4$, $h = 1/6$)

Rewriting (3.9) with $h = 1/6$, we have

$$\phi_n = \phi_{n-1} + \frac{n\pi}{6}(x_n - x_{n-1}), \tag{4.20}$$

where x_n, $x_{n-1} \in \{\pm 1, \pm 3\}$ for all integer values of n. Therefore ϕ_n can take only six values:

$0, \pi/3, 2\pi/3, \pi, 4\pi/3, 5\pi/3$ (modulo 2π). The four tones transmitted corresponding to the quaternary symbols -3, -1, 1 and 3 are $(f_0 - 1/4T)$, $(f_0 - 1/12T)$, $(f_0 + 1/12T)$ and $(f_0 + 1/4T)$, respectively. It is assumed that the lowest tone $(f_0 - 1/4T)$ goes through an integral number of cycles during one signalling interval. Thus

$$\begin{aligned}
-3 &: \ 2\pi(f_0 - 1/4T)T = \ 2n\pi = 0 \ \ (\text{modulo} - 2\pi) \\
-1 &: \ 2\pi(f_0 - 1/12T)T = \ \pi/3 \ \ (\text{modulo} - 2\pi) \\
+1 &: \ 2\pi(f_0 + 1/12T)T = \ 2\pi/3 \ \ (\text{modulo} - 2\pi) \\
+3 &: \ 2\pi(f_0 + 1/4T)T = \ \pi \ \ (\text{modulo} - 2\pi)
\end{aligned} \tag{4.21}$$

Clearly, the symbols -3, -1, 1 and 3 are associated with 0, $\pi/3$, $2\pi/3$ and π, respectively. As before we can obtain the phase trellis and the state transition diagram. Every trellis state has four branches leaving, each of which is related to one of -3, -1, 1 or 3. Twenty-four different waveforms are possible depending

on the state of the modulator and the quaternary input symbol. The phase trellis and the state diagram are shown in Figure 4.7. The state transition matrix, S_6, for $h = 1/6$, 4-CPFSK is given by:

$$S_6 = \begin{bmatrix} -3 & 0 & 0 & 3 & 1 & -1 \\ -1 & -3 & 0 & 0 & 3 & 1 \\ 1 & -1 & -3 & 0 & 0 & 3 \\ 3 & 1 & -1 & -3 & 0 & 0 \\ 0 & 3 & 1 & -1 & -3 & 0 \\ 0 & 0 & 3 & 1 & -1 & -3 \end{bmatrix}. \tag{4.22}$$

For 4-CPFSK with $h = 1/6$, the state sequence can be $(0, \pi/3, 2\pi/3, \pi, 4\pi/3, 5\pi/3)$ $(\pi/3, 2\pi/3, \pi, 4\pi/3, 5\pi/3, 0)$; $(2\pi/3, \pi, 4\pi/3, 5\pi/3, 0, \pi/3)$; $(\pi, 4\pi/3, 5\pi/3, 0, \pi/3, 2\pi/3)$; $(4\pi/3, 5\pi/3, 0, \pi/3, 2\pi/3, \pi)$ or $(5\pi/3, 0, \pi/3, 2\pi/3, \pi, 4\pi/3)$, all of which produce the same distance profile.

To construct a binary nonlinear CPFSK trellis modulation code with $h = 1/6$ it is necessary to find a six by six matrix, T_6, with two 1s in every row which satisfies (4.2). That is

$$L_{6,2} = (T_6)^2 = \begin{bmatrix} 1 & 1 & 1 & 1 & 1 & 1 \\ 1 & 1 & 1 & 1 & 1 & 1 \\ 1 & 1 & 1 & 1 & 1 & 1 \\ 1 & 1 & 1 & 1 & 1 & 1 \\ 1 & 1 & 1 & 1 & 1 & 1 \\ 1 & 1 & 1 & 1 & 1 & 1 \end{bmatrix} \tag{4.23}$$

In this case it is not possible to find a pattern in the matrix that satisfies the above equation and also maximises the distance. However, several good $h = 1/6$, binary nonlinear CPFSK trellis modulation codes have been found and they are shown in Figure 4.8.

In all the above codes the first merge takes place after only two signalling intervals. In other words we have not been able to overcome the inevitable merging event. On the other hand if we heuristically construct a four-state code as shown in Figure 4.9, it is possible to overcome the inevitable merging events, simultaneously

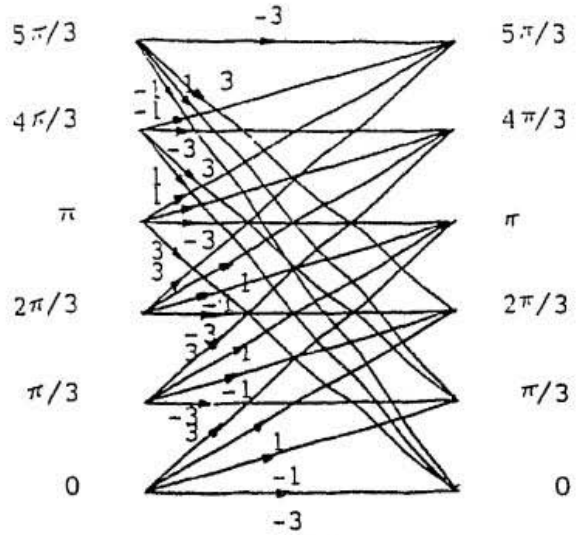

Trellis

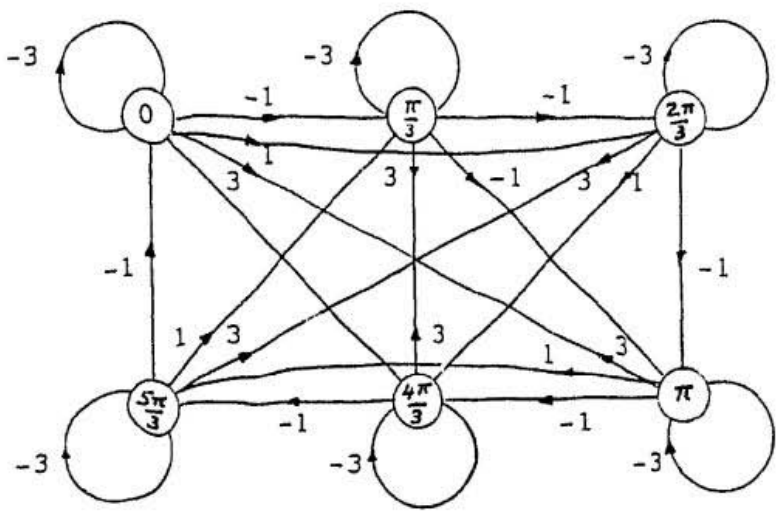

State diagram

Figure 4.7 Treliis and state diagram of 4-CPFSK, h=1/6.

$$S_6 = \begin{bmatrix} -3 & 0 & 0 & 3 & 0 & 0 \\ -1 & 0 & 0 & 0 & 0 & 1 \\ 0 & 0 & -3 & 0 & 0 & 3 \\ 0 & 1 & -1 & 0 & 0 & 0 \\ 0 & 3 & 0 & 0 & -3 & 0 \\ 0 & 0 & 0 & 1 & -1 & 0 \end{bmatrix}$$

$$d^2_{min} = 0.346$$

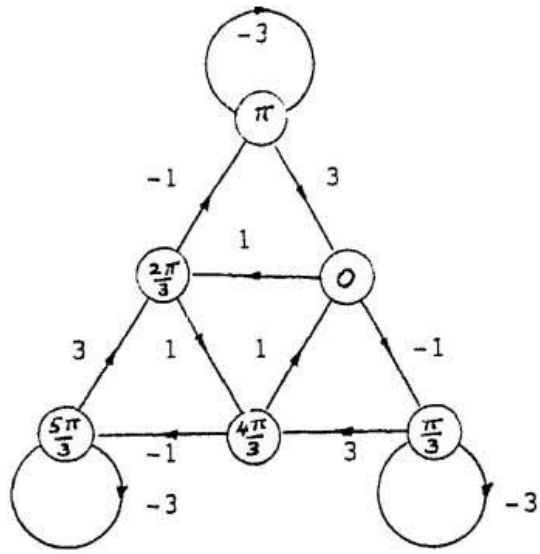

(a)

$$S_6 = \begin{bmatrix} -3 & 0 & 0 & 0 & 0 & -1 \\ 0 & 0 & 0 & 0 & 3 & 1 \\ 0 & -1 & -3 & 0 & 0 & 0 \\ 3 & 1 & 0 & 0 & 0 & 0 \\ 0 & 0 & 0 & -1 & -3 & 0 \\ 0 & 0 & 3 & 1 & 0 & 0 \end{bmatrix}$$

$$d^2_{min} = 0.346$$

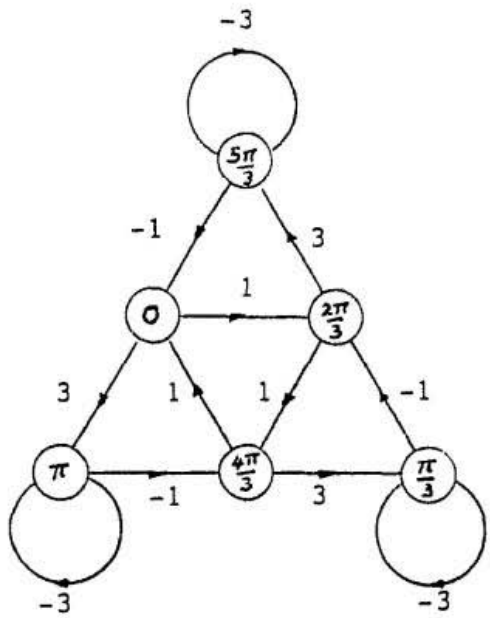

(b)

Figure 4.8 Binary nonlinear CPFSK (M=4, q=6)

$$S_6 = \begin{bmatrix} 0 & 0 & 0 & 0 & 1 & -1 \\ 0 & -3 & 0 & 0 & 3 & 0 \\ 1 & -1 & 0 & 0 & 0 & 0 \\ 3 & 0 & 0 & -3 & 0 & 0 \\ 0 & 0 & 1 & -1 & 0 & 0 \\ 0 & 0 & 3 & 0 & 0 & -3 \end{bmatrix}$$

$d^2_{min} = 0.346$

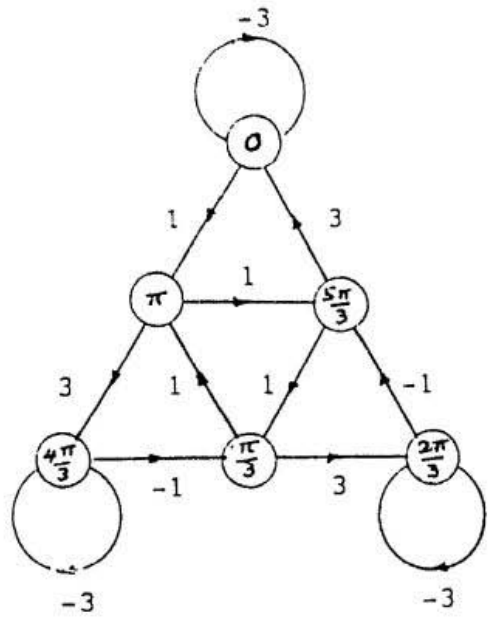

(c)

$$S_6 = \begin{bmatrix} 0 & 0 & 0 & 3 & 1 & 0 \\ 1 & -3 & 0 & 0 & 0 & 0 \\ 1 & 0 & 0 & 0 & 0 & 3 \\ 0 & 0 & -1 & -3 & 0 & 0 \\ 0 & 3 & 1 & 0 & 0 & 0 \\ 0 & 0 & 0 & 0 & -1 & -3 \end{bmatrix}$$

$d^2_{min} = 0.346$

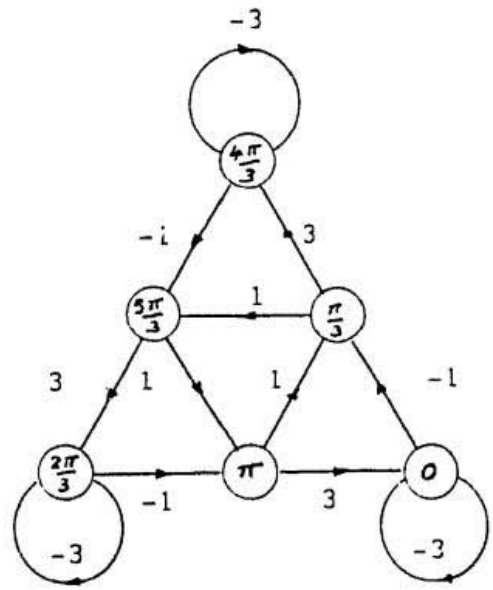

(d)

Figure 4.8 (Contd.) Binary nonlinear CPFSK (M=4, q=6).

achieving a memory length of three. This is the maximum memory length that can be gained according to (4.1). Nevertheless, the above realisation with $h = 1/6$ results in a minimum squared Euclidean distance of only 1.7595 compared with a minimum squared Euclidean distance of 2 for MSK signalling. Thus it is inferior to MSK signalling.

4.4.2 Binary nonlinear CPFSK ($M = 4$, $h = 1/8$)

In Section 4.3.2 we considered 8-CPFSK with $h = 1/8$. The trellis states can take the same set of phase values for 4-CPFSK with $h = 1/8$. Namely 0, $\pi/4$, $\pi/2$, $3\pi/4$,, π, $5\pi/4$, $3\pi/2$ and $7\pi/4$ (modulo-2π). However, only four tones are transmitted in the case of 4-CPFSK. The four tones and the associated phase shifts are as follows:

$$\begin{aligned}
-3: \ & 2\pi(f_0 - 3/16T)T = \ \ 0 \quad (\text{modulo} - 2\pi) \\
-1: \ & 2\pi(f_0 - 1/16T)T = \ \ \pi/4 \quad (\text{modulo} - 2\pi) \\
+1: \ & 2\pi(f_0 + 1/16T)T = \ \ \pi/2 \quad (\text{modulo} - 2\pi) \\
+3: \ & 2\pi(f_0 + 3/16T)T = \ \ 3\pi/4 \quad (\text{modulo} - 2\pi)
\end{aligned} \tag{4.24}$$

The phase trellis and the state transition diagram are shown in Figure 4.10. Every state has four transitions leaving, each of which is related to one of -3, -1, 1, or 3. Thus a total of thirty-two different waveforms are possible. The state transition matrix is given by:

$$S_8 = \begin{bmatrix}
-3 & 0 & 0 & 0 & 0 & 3 & 1 & -1 \\
-1 & -3 & 0 & 0 & 0 & 0 & 3 & 1 \\
1 & -1 & -3 & 0 & 0 & 0 & 0 & 3 \\
3 & 1 & -1 & -3 & 0 & 0 & 0 & 0 \\
0 & 3 & 1 & -1 & -3 & 0 & 0 & 0 \\
0 & 0 & 3 & 1 & -1 & -3 & 0 & 0 \\
0 & 0 & 0 & 3 & 1 & -1 & -3 & 0 \\
0 & 0 & 0 & 0 & 3 & 1 & -1 & -3
\end{bmatrix}. \tag{4.25}$$

$$S_6 = \begin{bmatrix} -3 & 0 & 0 & 0 & 0 & -1 \\ 0 & 0 & 0 & 0 & 0 & 0 \\ 1 & 0 & 0 & 0 & 0 & 3 \\ 0 & 0 & -1 & -3 & 0 & 0 \\ 0 & 0 & 0 & 0 & 0 & 0 \\ 0 & 0 & 3 & 1 & 0 & 0 \end{bmatrix}$$

State transition matrix

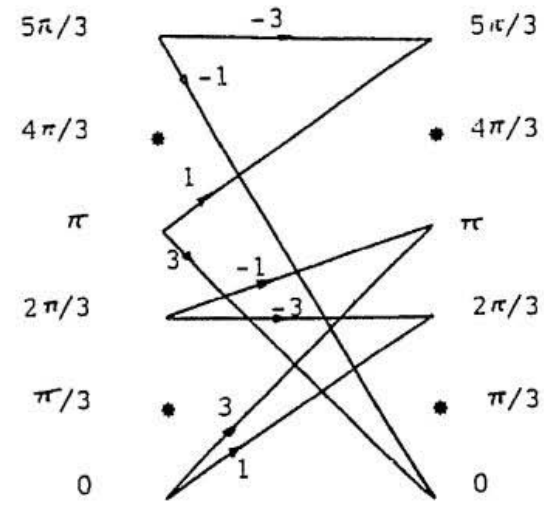

Trellis

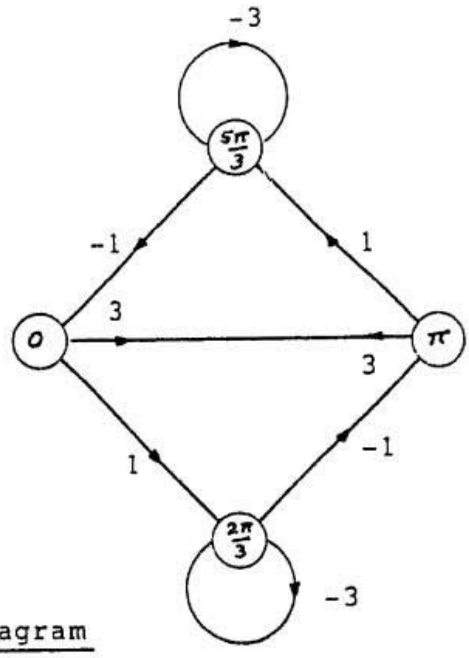

State diagram

Figure 4.9 Optimum binary nonlinear CPFSK (M=4, q=6).

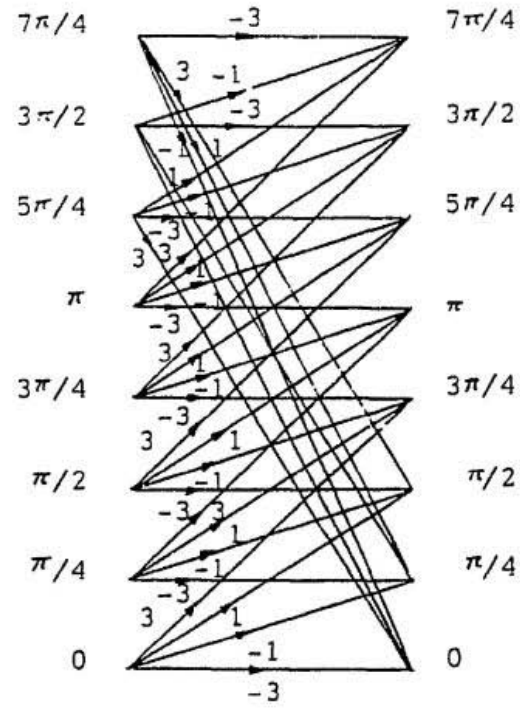

Trellis

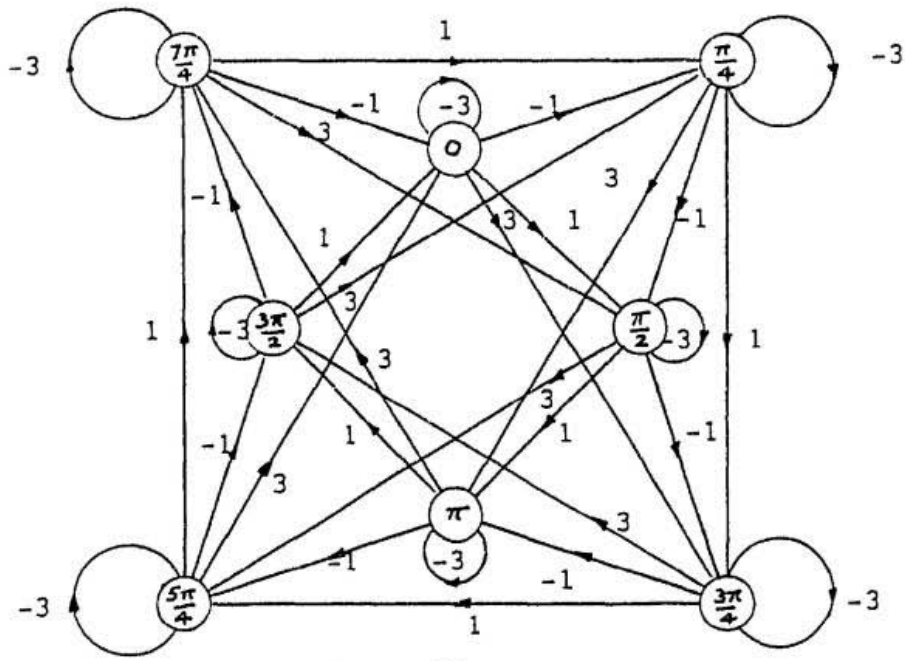

State diagram

Figure 4.10 Trellis and state diagram of 4-CPFSK, h=1/8.

$$S_8 = \begin{bmatrix} 0 & 0 & 0 & 0 & 0 & 3 & 0 & -1 \\ -1 & 0 & 0 & 0 & 0 & 0 & 3 & 0 \\ 1 & 0 & -3 & 0 & 0 & 0 & 0 & 0 \\ 0 & 1 & 0 & -3 & 0 & 0 & 0 & 0 \\ 0 & 3 & 0 & -1 & 0 & 0 & 0 & 0 \\ 0 & 0 & 3 & 0 & -1 & 0 & 0 & 0 \\ 0 & 0 & 0 & 0 & 1 & 0 & -3 & 0 \\ 0 & 0 & 0 & 0 & 0 & 1 & 0 & -3 \end{bmatrix}$$

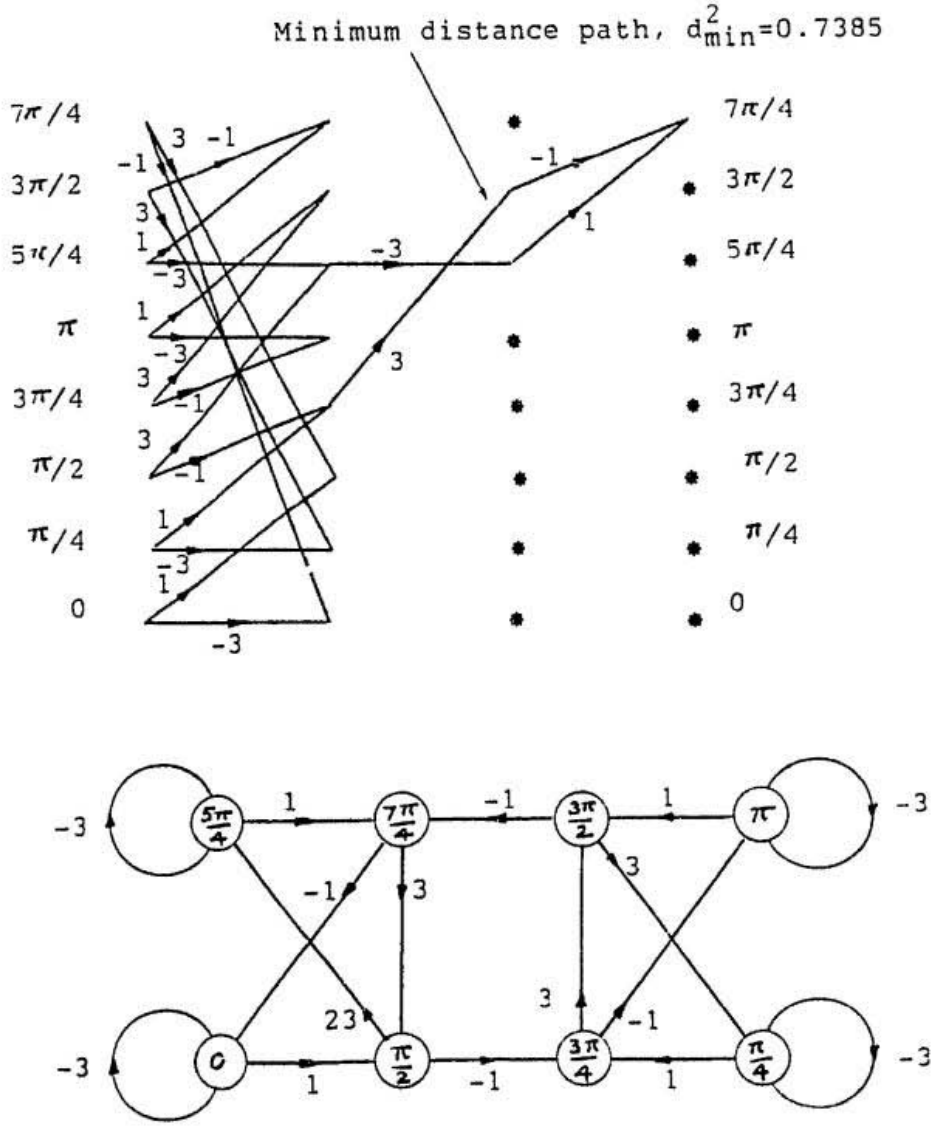

Figure 4.11 Optimum binary nonlinear CPFSK (M=4, q=8).

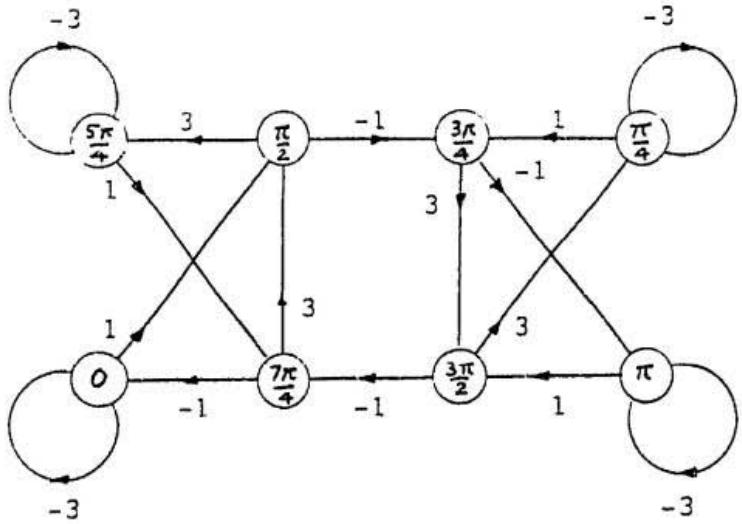

Minimum distance path

ϕ_n: $\pi/2 \longrightarrow 3\pi/4 \longrightarrow 3\pi/2 \longrightarrow 7\pi/4$

ϕ'_n: $\pi/2 \longrightarrow 5\pi/4 \longrightarrow 5\pi/4 \longrightarrow 7\pi/4$; $d^2_{min}=0.7385$

$$S_8 = \begin{bmatrix} 0 & 0 & 0 & 0 & 0 & 3 & 0 & -1 \\ -1 & 0 & 0 & 0 & 0 & 0 & 3 & 0 \\ 1 & 0 & -3 & 0 & 0 & 0 & 0 & 0 \\ 0 & 1 & 0 & -3 & 0 & 0 & 0 & 0 \\ 0 & 3 & 0 & -1 & 0 & 0 & 0 & 0 \\ 0 & 0 & 3 & 0 & -1 & 0 & 0 & 0 \\ 0 & 0 & 0 & 0 & 1 & 0 & -3 & 0 \\ 0 & 0 & 0 & 0 & 0 & 1 & 0 & -3 \end{bmatrix}$$

Figure 4.12 Binary nonlinear CPFSK equivalent to that of Figure 4.11

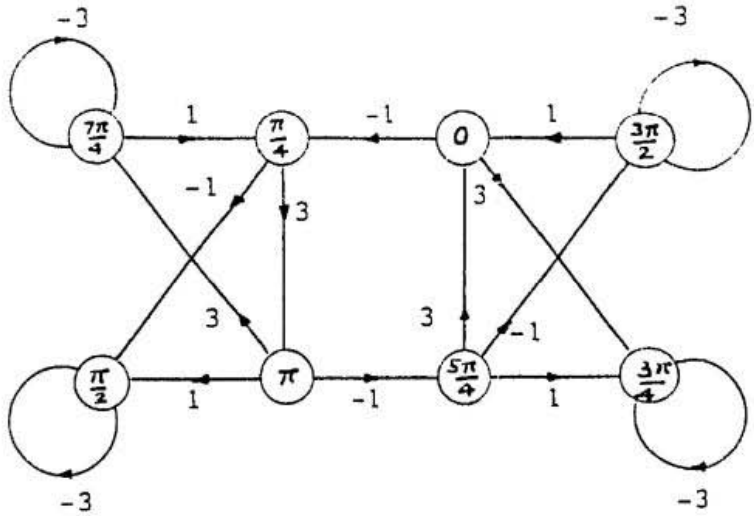

Minimum Distance Path

ϕ_n: $0 \longrightarrow \pi/4 \longrightarrow \pi \longrightarrow 5\pi/4$

ϕ'_n: $0 \longrightarrow 3\pi/4 \longrightarrow 3\pi/4 \longrightarrow 5\pi/4$; $d^2_{min}=0.7385$

$$S_8 = \begin{bmatrix} -3 & 0 & 0 & 0 & 0 & 0 & 1 & 0 \\ 0 & -3 & 0 & 0 & 0 & 0 & 0 & 1 \\ 0 & -1 & 0 & 0 & 0 & 0 & 0 & 3 \\ 3 & 0 & -1 & 0 & 0 & 0 & 0 & 0 \\ 0 & 0 & 1 & 0 & -3 & 0 & 0 & 0 \\ 0 & 0 & 0 & 1 & 0 & -3 & 0 & 0 \\ 0 & 0 & 0 & 3 & 0 & -1 & 0 & 0 \\ 0 & 0 & 0 & 0 & 3 & 0 & -1 & 0 \end{bmatrix}$$

Figure 4.12 (Contd.) Binary nonlinear CPFSK equivalent to that of Figure 4.11

We were unable to find a regular pattern to the best matrix for $M = 4$, $h = 1/8$ binary nonlinear CPFSK trellis modulation codes. Also, the maximum memory length of four predicted by (4.1) could not be achieved with an alphabet size of four owing to high connectivity between the trellis phase states. The best codes that we could find resulted in a memory length of only three and a minimum squared Euclidean distance of 0.738. In terms of the minimum squared Euclidean distance, MSK signals are 4.33 dB better than this trellis modulation code. Figure 4.11 shows the minimum distance path-pair for one of the best binary nonlinear CPFSK trellis modulation codes with $M = 4$ and $h = 1/8$. Two equivalent codes are given in Figure 4.12.

4.4.3 Binary nonlinear CPFSK ($M = 4$, $h = 1/10$)

In this case the phase trellis consists of ten phase angles: 0, $\pi/5$, $2\pi/5$, $3\pi/5$, $4\pi/5$, π, $6\pi/5$, $7\pi/5$, $8\pi/5$ and $9\pi/5$. It can be shown that the four symbols -3, -1, 1 and 3 are associated with phase changes 0, $\pi/5$, $2\pi/5$ and $3\pi/5$, respectively. The phase trellis, state diagram and state transition matrix are shown in Figure 4.13. Several good binary nonlinear CPFSK trellis modulation codes found for $h = 1/10$ are shown in Figure 4.14. The two codes given in Figures 4.14 (a) and 4.14(b) are rotationally invariant to carrier phase ambiguities of $2\pi/5$ radians, but not to other phase ambiguities of the uncoded signal set. Thus, none of the codes found are fully transparent to carrier phase ambiguities. In Section 4.6 the rotational symmetry property of nonlinear CPFSK trellis modulation codes will be considered in detail.

4.5 Numerical results

Table 4.1 lists the minimum squared Euclidean distances and coding gains for optimum correlation detection of binary nonlinear CPFSK trellis modulation codes

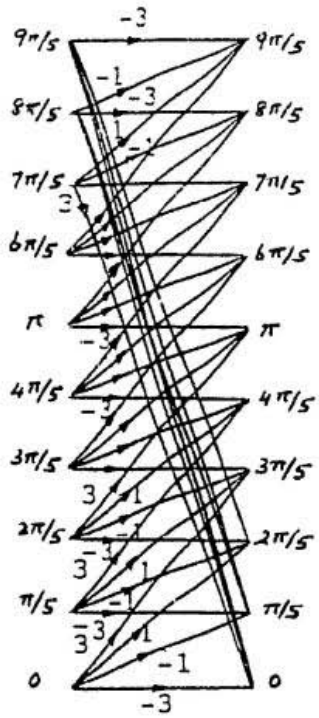

trellis

$$S_{10}= \begin{bmatrix} -3 & 0 & 0 & 0 & 0 & 0 & 0 & 3 & 1 & -1 \\ -1 & -3 & 0 & 0 & 0 & 0 & 0 & 0 & 3 & 1 \\ 1 & -1 & -3 & 0 & 0 & 0 & 0 & 0 & 0 & 3 \\ 3 & 1 & -1 & -3 & 0 & 0 & 0 & 0 & 0 & 0 \\ 0 & 3 & 1 & -1 & -3 & 0 & 0 & 0 & 0 & 0 \\ 0 & 0 & 3 & 1 & -1 & -3 & 0 & 0 & 0 & 0 \\ 0 & 0 & 0 & 3 & 1 & -1 & -3 & 0 & 0 & 0 \\ 0 & 0 & 0 & 0 & 3 & 1 & -1 & -3 & 0 & 0 \\ 0 & 0 & 0 & 0 & 0 & 3 & 1 & -1 & -3 & 0 \\ 0 & 0 & 0 & 0 & 0 & 0 & 3 & 1 & -1 & -3 \end{bmatrix}$$

transition matrix

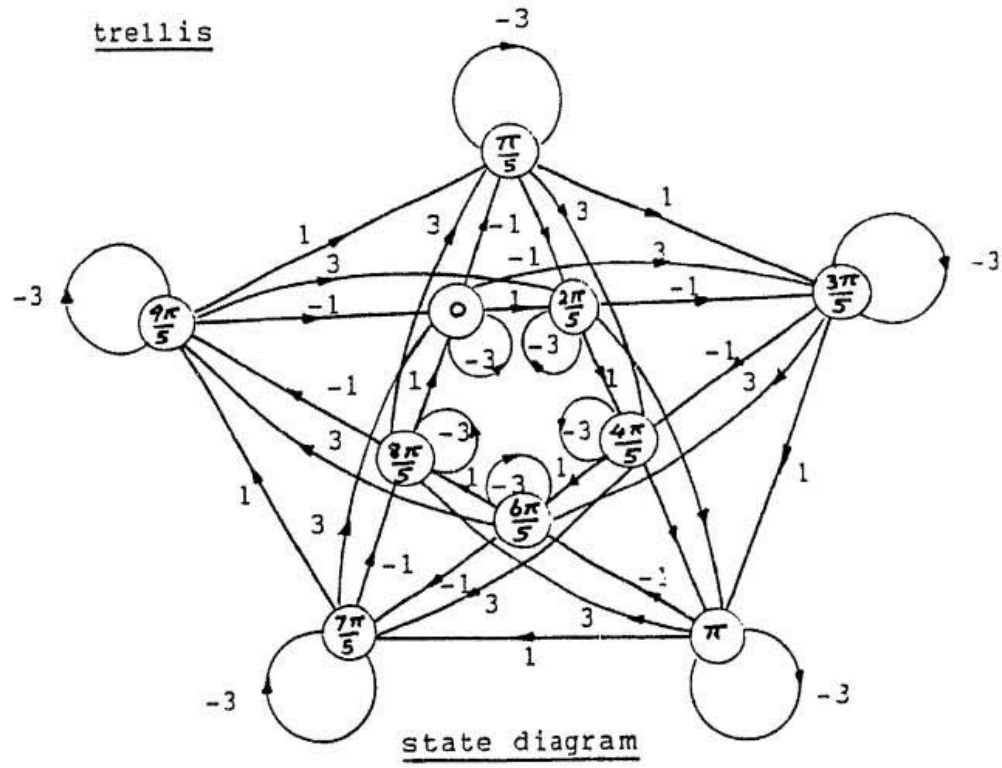

state diagram

Figure 4.13 Trellis, state diagram and state transition matrix for 4-CPFSK, h=1/10.

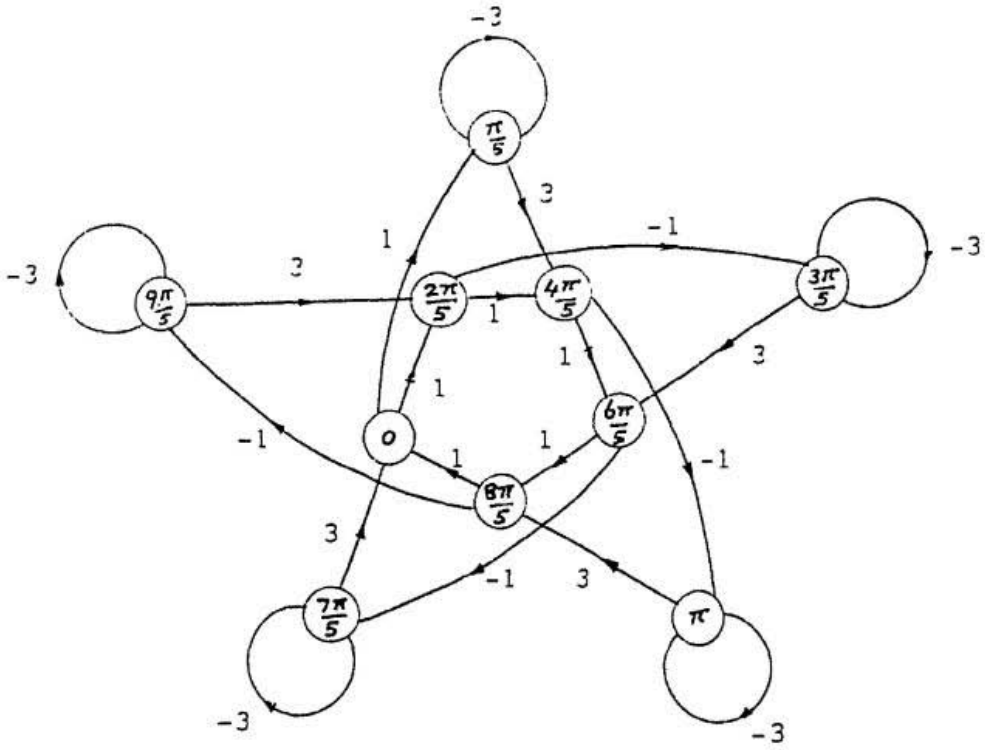

$$S_{10} = \begin{bmatrix} -3 & 0 & 0 & 0 & 0 & 0 & 0 & 3 & 0 & 0 \\ -1 & 0 & 0 & 0 & 0 & 0 & 0 & 0 & 0 & 1 \\ 0 & 0 & -3 & 0 & 0 & 0 & 0 & 0 & 0 & 3 \\ 0 & 1 & -1 & 0 & 0 & 0 & 0 & 0 & 0 & 0 \\ 0 & 3 & 0 & 0 & -3 & 0 & 0 & 0 & 0 & 0 \\ 0 & 0 & 0 & 1 & -1 & 0 & 0 & 0 & 0 & 0 \\ 0 & 0 & 0 & 3 & 0 & 0 & -3 & 0 & 0 & 0 \\ 0 & 0 & 0 & 0 & 0 & 1 & -1 & 0 & 0 & 0 \\ 0 & 0 & 0 & 0 & 0 & 3 & 0 & 0 & -3 & 0 \\ 0 & 0 & 0 & 0 & 0 & 0 & 0 & 1 & -1 & 0 \end{bmatrix}$$

Minimum distance path

ϕ_n: $4\pi/5 \longrightarrow 6\pi/5 \longrightarrow 8\pi/5$

ϕ'_n: $4\pi/5 \longrightarrow \pi \longrightarrow 8\pi/5$; $d^2_{min} = 0.486$

Figure 4.14(a) Equivalent binary nonlinear CPFSK(M=4,q=10).

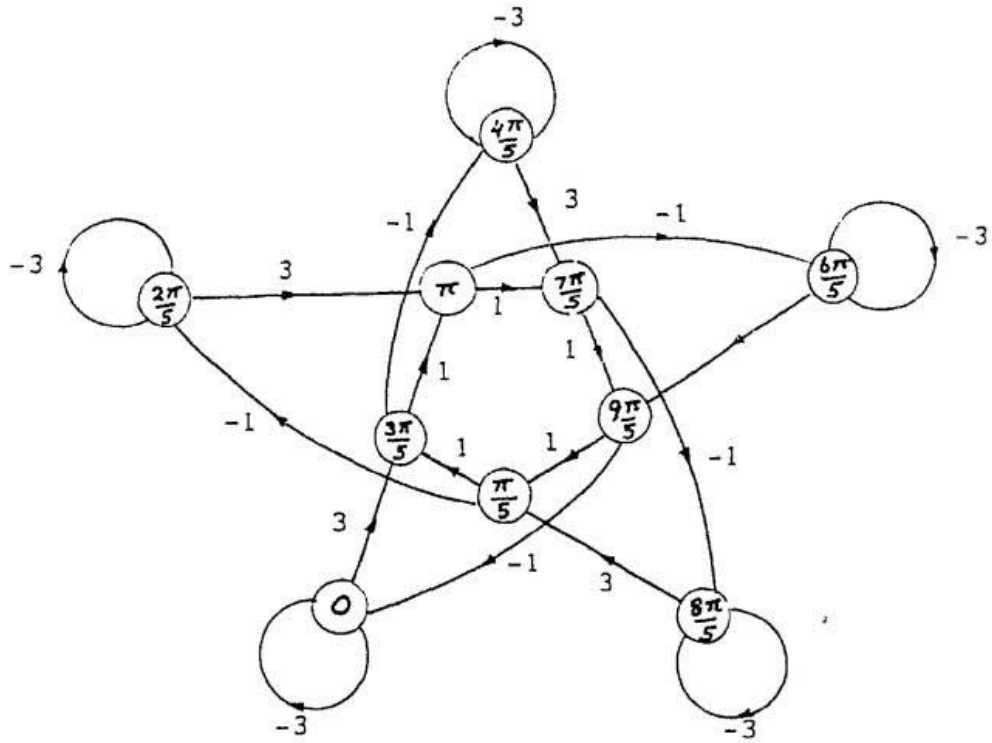

$$S_{10} = \begin{bmatrix} 0 & 0 & 0 & 0 & 0 & 0 & 0 & 0 & 1 & -1 \\ 0 & -3 & 0 & 0 & 0 & 0 & 0 & 0 & 3 & 0 \\ 1 & -1 & 0 & 0 & 0 & 0 & 0 & 0 & 0 & 0 \\ 3 & 0 & 0 & -3 & 0 & 0 & 0 & 0 & 0 & 0 \\ 0 & 0 & 1 & -1 & 0 & 0 & 0 & 0 & 0 & 0 \\ 0 & 0 & 3 & 0 & 0 & -3 & 0 & 0 & 0 & 0 \\ 0 & 0 & 0 & 0 & 1 & -1 & 0 & 0 & 0 & 0 \\ 0 & 0 & 0 & 0 & 3 & 0 & 0 & -3 & 0 & 0 \\ 0 & 0 & 0 & 0 & 0 & 0 & 1 & -1 & 0 & 0 \\ 0 & 0 & 0 & 0 & 0 & 0 & 3 & 0 & 0 & -3 \end{bmatrix}$$

Minimum distance path

ϕ_n: $\pi \longrightarrow 7\pi/5 \longrightarrow 9\pi/5$

ϕ_n': $\pi \longrightarrow 6\pi/5 \longrightarrow 9\pi/5$; $d^2_{min} = 0.486$

Figure 4.14(b) Equivalent binary nonlinear CPFSK (M=4,q=10).

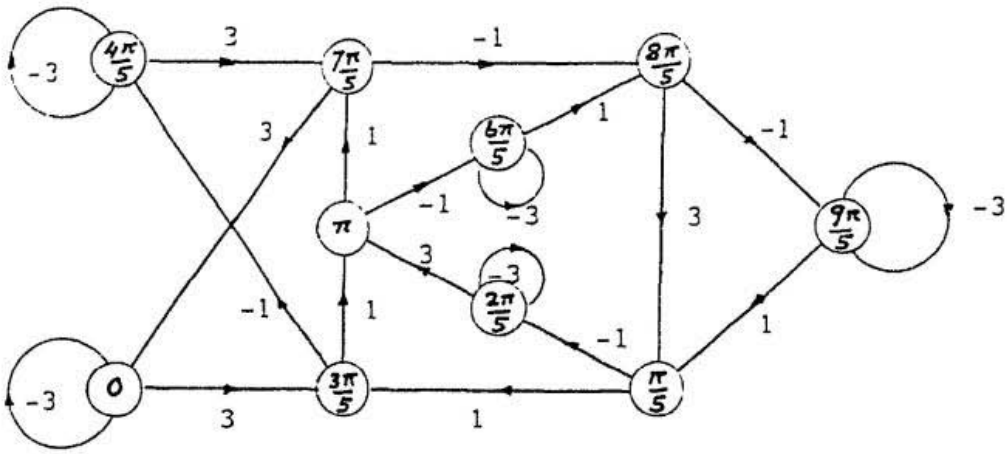

$$S_{10} = \begin{bmatrix}
-3 & 0 & 0 & 0 & 0 & 0 & 0 & 0 & 1 & 0 \\
-1 & 0 & 0 & 0 & 0 & 0 & 0 & 0 & 3 & 0 \\
0 & -1 & 0 & 0 & 0 & 0 & 0 & 0 & 0 & 3 \\
0 & 1 & 0 & -3 & 0 & 0 & 0 & 0 & 0 & 0 \\
0 & 0 & 1 & -1 & 0 & 0 & 0 & 0 & 0 & 0 \\
0 & 0 & 3 & 0 & 0 & -3 & 0 & 0 & 0 & 0 \\
0 & 0 & 0 & 0 & 1 & -1 & 0 & 0 & 0 & 0 \\
0 & 0 & 0 & 0 & 3 & 0 & 0 & -3 & 0 & 0 \\
0 & 0 & 0 & 0 & 0 & 0 & 1 & -1 & 0 & 0 \\
0 & 0 & 0 & 0 & 0 & 0 & 3 & 0 & 0 & -3
\end{bmatrix}$$

Minimum distance path:

$\phi_n: \pi \longrightarrow 7\pi/5 \longrightarrow 8\pi/5$

$\phi_n': \pi \longrightarrow 6\pi/5 \longrightarrow 8\pi/5$

; $d^2_{min} = 0.486$

Figure 4.14(c) Equivalent binary nonlinear CPFSK (M=4,q=10).

found in the previous sections. When $h = 1/M$, it was always possible to find a regular pattern in the state transition matrix. Also, it was always possible to avoid the inevitable merging of path-pairs after only two signalling intervals that is a characteristic of general CPFSK signals. Any particular pattern to the transition matrix could not be found when $h \neq 1/M$.

It is seen from the numerical results that the binary nonlinear CPFSK schemes with $h = 1/M$ achieve higher minimum squared Euclidean distances and memory lengths than MSK signalling. Thus they can be expected to perform better compared with MSK signalling in additive white Gaussian noise channels at high-SNR. Numerical results also show that when $h \neq 1/M$, although binary nonlinear schemes can be found with larger memory lengths, their minimum squared Euclidean distances are inferior to that of MSK signalling.

The spectral occupancy of each binary nonlinear scheme will be very similar to their general CPFSK counterparts. However, the complexity of the transmitter is increased owing to the sequential digital logic circuits of the finite-state machine that is needed to make the transmitted symbols depend on the state of the modulator. Another disadvantage of binary nonlinear CPFSK schemes, namely, the rotational non-invariance, will be considered in the following section. Unlike the binary multi-h schemes studied in [40] these binary nonlinear CPFSK schemes have a constant modulation index.

4.6 Rotational symmetry of nonlinear CPFSK

Coherent detection techniques rely on the ability of the receiver to regenerate reference signals in exact phase coherence with the transmitted signal. There are several ways of obtaining reference signals at the receiver. Irrespective of the technique, an

Table 4.1 Coding gain and minimum squared Euclidean distance of binary nonlinear CPFSK.

Modulation Index	M	N	v	d^2_{min}	Coding Gain (dB)
1/4	4	4	3	2.151	0.316
1/6	4	4	3	1.759	-0.558
1/8	4	8	3	0.738	-4.329
1/10	4	10	2	0.486	-6.144
1/8	8	8	4	2.514	0.993
1/16	16	16	5	3.356	2.248
1/32	32	32	6	2.640	1.205

ambiguity always remains concerning the true carrier-phase. This is particularly the case when the signal set has rotational symmetries (*e.g.* QAM, PSK) and the demodulator has no knowledge of which of the symmetries transmitted. Thus the demodulator arbitrarily selects the symmetry in which to demodulate the received signal with the possibility of being locked onto the wrong phase. The result of such imperfect reference signals is a degraded detection performance.

In mobile communication systems transmission of signals over multipath fading channels with Doppler frequency shifts can lead to frequent losses of carrier phase synchronisation in the receiver. The time required to re-establish the correct phase for decoding can cause signal loss during considerable periods of time. It is therefore desirable to find rotationally invariant (self-transparent) trellis modulation codes, which allow prompt resynchronisation after signal fades. The aspect of rotational invariance of trellis modulation codes has recently come under increasing study in the search for good combined coded-modulation schemes [24, 58, 78, 100, 99, 102, 96].

In uncoded memoryless systems the problem of carrier phase ambiguity can be overcome by differential encoding and decoding of the data [58]. For example, with uncoded BPSK modulation, transparency to carrier-phase ambiguities of π radians in the receiver is easily accomplished by differential encoding and decoding. The same is true for $\pi/2$ phase ambiguity in the case of uncoded QPSK. However, in linear rate-1/2 coded QPSK it is only possible to achieve rotational invariance under π radians, whereas, with other codes no such invariance exist [78]. The lack of invariance under $\pi/2$ phase rotation requires that QPSK signals are demodulated with the correct phase before trellis decoding can be performed [27]. A design procedure for fully transparent QPSK signal constellations is given in [78].

For trellis modulated systems the rotational invariance is much more involved

because we are dealing with sequences of symbols. The code space or the group of allowable symbol sequences in trellis modulation codes can be infinite in size unlike in the case of block codes, where the code space consists of a finite number of independent symbols. If a coded symbol sequence has been phase rotated, the resulting sequence may or may not fall in the code space. A trellis modulation code is said to be *rotationally invariant* or transparent to carrier-phase ambiguities of θ (θ not equal to zero) if all code sequences can be rotated by θ such that all rotated sequences are still in the code space [78]. In other words all rotated versions of the transmitted sequence will be decoded into the same source sequence or input symbol sequence. Such codes are also known as *self-transparent phase-invariant* codes [58] or simply as self-transparent codes. We shall use the term *self-transparent* in this work.

By considering the state transition matrix of M-ary CPFSK with $h = p/q$, it is easy to show that M-ary CPFSK signals are rotationally invariant to phase shifts of $2\pi h$, $4\pi h$, ..., $2(M-1)\pi h$ (modulo-2π). For example, consider the state transition matrix of $h = 1/4$, 4-CPFSK:

$$S_4 = \begin{array}{c} \\ 3\pi/2 \\ \pi \\ \pi/2 \\ 0 \end{array} \begin{array}{c} \begin{array}{cccc} 3\pi/2 & \pi & \pi/2 & 0 \end{array} \\ \begin{bmatrix} -3 & 3 & 1 & -1 \\ -1 & -3 & 3 & 1 \\ 1 & -1 & -3 & 3 \\ 3 & 1 & -1 & -3 \end{bmatrix} \end{array}. \tag{4.26}$$

A rotational shift of $\pi/2$ rad. makes the state transition matrix

$$S_{4,\frac{\pi}{2}} = \begin{array}{c} \\ 0 \\ 3\pi/2 \\ \pi \\ \pi/2 \end{array} \begin{array}{c} \begin{array}{cccc} 0 & 3\pi/2 & \pi & \pi/2 \end{array} \\ \begin{bmatrix} -3 & 3 & 1 & -1 \\ -1 & -3 & 3 & 1 \\ 1 & -1 & -3 & 3 \\ 3 & 1 & -1 & -3 \end{bmatrix} \end{array}. \tag{4.27}$$

S_4 is identical with $S_{4,\frac{\pi}{2}}$. Similarly it can be verified that $S_4 = S_{4,\frac{\pi}{2}} = S_{4,\pi} = S_{4,\frac{3\pi}{2}}$. Therefore carrier phase shifts of $\pi/2$, π and $3\pi/2$ do not affect the decoding process. As a second example, consider the state transition matrix and the $\pi/3$ phase rotated

matrix of $h = 1/6$, 4-CPFSK shown below.

$$S_6 = \begin{array}{c} \\ 5\pi/3 \\ 4\pi/3 \\ \pi \\ 2\pi/3 \\ \pi/3 \\ 0 \end{array} \begin{array}{c} \begin{array}{cccccc} 5\pi/3 & 4\pi/3 & \pi & 2\pi/3 & \pi/3 & 0 \end{array} \\ \begin{bmatrix} -3 & 0 & 0 & 3 & 1 & -1 \\ -1 & -3 & 0 & 0 & 3 & 1 \\ 1 & -1 & -3 & 0 & 0 & 3 \\ 3 & 1 & -1 & -3 & 0 & 0 \\ 0 & 3 & 1 & -1 & -3 & 0 \\ 0 & 0 & 3 & 1 & -1 & -3 \end{bmatrix} \end{array} \tag{4.28}$$

$$S_{6,\frac{\pi}{3}} = \begin{array}{c} \\ 0 \\ 5\pi/3 \\ 4\pi/3 \\ \pi \\ 2\pi/3 \\ \pi/3 \end{array} \begin{array}{c} \begin{array}{cccccc} 0 & 5\pi/3 & 4\pi/3 & \pi & 2\pi/3 & \pi/3 \end{array} \\ \begin{bmatrix} -3 & 0 & 0 & 3 & 1 & -1 \\ -1 & -3 & 0 & 0 & 3 & 1 \\ 1 & -1 & -3 & 0 & 0 & 3 \\ 3 & 1 & -1 & -3 & 0 & 0 \\ 0 & 3 & 1 & -1 & -3 & 0 \\ 0 & 0 & 3 & 1 & -1 & -3 \end{bmatrix} \end{array} \tag{4.29}$$

Clearly, S_6 and $S_{6,\frac{\pi}{3}}$ are identical. Similarly $S_{6,\frac{2\pi}{3}}$ and $S_{6,\pi}$ are also identical with S_6. Thus the trellis decoder can tolerate carrier-phase ambiguities of $\pi/3$, $2\pi/3$ and π rad. (modulo-2π). The general conclusion is that, since the state transition matrix of M-CPFSK with $h = p/q$ is invariant to rotational phase shifts of integer multiples of $2\pi h$, the Viterbi algorithm in the trellis decoder can resolve carrier-phase ambiguities of $2\pi h$, $4\pi h$, ..., $2(M-1)\pi h$.

The state transition matrix of the optimum binary nonlinear CPFSK ($M = 4$, $h = 1/4$) trellis modulation code found in Section 4.3.1 and the state transition matrices of the same code when the carrier-phase is rotated by $\pi/2$, π and $3\pi/2$ radians, respectively, are shown below.

$$S_4 = \begin{array}{c} \\ 3\pi/2 \\ \pi \\ \pi/2 \\ 0 \end{array} \begin{array}{c} \begin{array}{cccc} 3\pi/2 & \pi & \pi/2 & 0 \end{array} \\ \begin{bmatrix} -3 & 0 & 1 & 0 \\ -1 & 0 & 3 & 0 \\ 0 & -1 & 0 & 3 \\ 0 & 1 & 0 & -3 \end{bmatrix} \end{array} \tag{4.30}$$

$$S_{4,\frac{\pi}{2}} = \begin{array}{c} \\ 0 \\ 3\pi/2 \\ \pi \\ \pi/2 \end{array} \begin{array}{c} \begin{array}{cccc} 0 & 3\pi/2 & \pi & \pi/2 \end{array} \\ \begin{bmatrix} -3 & 0 & 1 & 0 \\ -1 & 0 & 3 & 0 \\ 0 & -1 & 0 & 3 \\ 0 & 1 & 0 & -3 \end{bmatrix} \end{array} \tag{4.31}$$

$$S_{1,\pi} = \begin{array}{c} \\ \pi/4 \\ 0 \\ \pi/4 \\ \pi \end{array} \begin{array}{c} \begin{array}{cccc} \pi/4 & 0 & \pi/4 & \pi \end{array} \\ \begin{bmatrix} -3 & 0 & 1 & 0 \\ -1 & 0 & 3 & 0 \\ 0 & -1 & 0 & 3 \\ 0 & 1 & 0 & -3 \end{bmatrix} \end{array} \tag{4.32}$$

$$S_{1,\frac{3\pi}{2}} = \begin{array}{c} \\ \pi \\ \pi/4 \\ 5\pi/4 \\ \pi \end{array} \begin{array}{c} \begin{array}{cccc} \pi & \pi/4 & 0 & 5\pi/4 \end{array} \\ \begin{bmatrix} -3 & 0 & 1 & 0 \\ -1 & 0 & 3 & 0 \\ 0 & -1 & 0 & 3 \\ 0 & 1 & 0 & -3 \end{bmatrix} \end{array} \tag{4.33}$$

Unlike in the case of general CPFSK, the above transition matrices are different from the original, indicative of the trellis decoder's inability to resolve carrier-phase ambiguities in the case of binary nonlinear CPFSK.

Similarly, binary nonlinear CPFSK with $M = 8$, $h = 1/8$ can be affected by phase ambiguities of $\pi/4$, $\pi/2$, $3\pi/4$, π, $5\pi/4$, $3\pi/2$ and $7\pi/4$ radians. And the state transition matrix of the optimum trellis modulation code given in (4.16) when phase rotated by the above phase angles results in different matrices. Further, since all phase states do not follow the same state transition pattern, there is no rotational invariance in the above code. In general, all optimum (in maximum memory length sense) binary nonlinear CPFSK trellis modulation codes found in Sections 4.3 and 4.4 are rotationally non-invariant and a phase ambiguity of $2\pi/M$ radians cannot be allowed in the carrier-phase recovery.

4.7 Conclusions

In this chapter we have considered a class of fixed-h binary nonlinear CPFSK trellis modulation codes for the additive white Gaussian noise channel. It was shown that binary nonlinear CPFSK schemes can be designed so that they achieve larger minimum squared Euclidean distances and memory lengths than MSK signalling. A systematic method for the construction of binary nonlinear CPFSK schemes that achieve the maximum memory length allowed by the number of trellis phase states

when $h = 1/M$ has been presented. Several codes were shown to overcome the inevitable merging events of general CPFSK. The coding gains of optimum binary nonlinear CPFSK ranged from 0.3 dB to 2.2 dB compared with MSK signalling. Delaying of merging events does not necessarily lead to a larger minimum squared Euclidean distance, although, it results in a larger time diversity. The optimal binary nonlinear CPFSK trellis modulation codes that achieved maximum memory lengths were shown to be rotationally non-invariant, therefore, they are not preferable for coherent demodulation with carrier-phase ambiguities.

Chapter 5

Suboptimum Coherent Detection of CPFSK Trellis Modulation Codes on Non-Gaussian Channels

5.1 Introduction

Suboptimum coherent detection of CPFSK trellis modulation codes on non-Gaussian channels is considered in this chapter. Two non-Gaussian channels are considered: the AWGN channel with carrier phase offsets and the mobile satellite channel.

First, the communication system and channel models used in the study will be described. Then the suboptimum coherent phase detection and trellis decoding receiver is introduced. Next, based on a generalisation of the Euclidean distance, a decoding metric (equivalent distance) will be derived for phase detection and trellis decoding of CPFSK trellis modulation codes. This equivalent distance is applicable to channels with carrier phase offsets and channels with independent amplitude-only fading.

Application of CPFSK trellis modulation codes for data transmission through multipath fading channels is considered in the second part of the chapter. The satellite-based mobile communication channel has received much attention in the recent literature because of its potential for providing reliable voice and data com-

munication to sparsely populated areas. Owing to the presence of a stable line-of-sight component, the fading in mobile satellite channels is less severe than that encountered in land-mobile communication channels. Therefore, coherent detection, with the assistance of a pilot tone or pilot symbols, is feasible on such channels. It is well known that when coherently detected, CPFSK signals are both more power- and bandwidth-efficient than PSK signals.

Instead of the widely used error probability criterion, the channel cutoff rate has been recently suggested as a more reasonable modulation system design criterion that allows comparison of different coded-modulation schemes under changing channel noise conditions or among different channel models. In many cases, the computation of the error probability is extremely difficult, especially when combined coding and modulation is employed. The channel cutoff rate R_0 can be used as the performance measure on interleaved mobile satellite channels.

5.2 Communication system and channel models

In the study of communication systems and data transmission the most frequently assumed model for a waveform channel is the AWGN channel model. However, for many practical communication systems the AWGN channel is a poor model and we must resort to more accurate and complicated models. Two types of non-Gaussian channel models which frequently occur in practice are the carrier phase offset channel and the multipath fading channel.

5.2.1 Carrier phase offset channel

The phase difference between the regenerated reference carrier at the receiver and the noise-free demodulated signal is called the carrier phase offset. In practical communication systems carrier phase offsets and carrier phase rotations (as pre-

viously discussed in Section 4.6) can occur due to transmission impairments such as impulse noise and imperfect coherent demodulators. When the phase tracking scheme of the receiver cannot track the disturbance of the carrier phase instantly a carrier phase offset would result.

The general model of the carrier phase offset channel considered in this work is shown in Fig. 5.1. A binary data sequence is encoded using a rate-1/2 or rate-2/3, $N = 2^{\nu}$ state trellis code, where ν is the memory length of the code. The output of the encoder is fed to an M-ary mapper followed by an ideal symbol interleaver with infinite interleaving depth. The interleaved symbols are then passed-on to the CPFSK modulator. At the receiver the CPFSK signal is coherently demodulated and deinterleaved to restore the original encoded data sequence. For analytical purposes, the above coded-modulation scheme with the ideal interleaver and deinterleaver pair can be replaced by a memoryless channel model [70].

The channel output y_n at discrete time $t = nT$ can be written as:

$$y_n = \rho_n x_n + n_n, \tag{5.1}$$

where $n_n = \Re\{n_n\} + j\Im\{n_n\}$ is a complex-valued zero-mean Gaussian random noise process. $\Re\{n_n\}$ and $\Im\{n_n\}$ are zero-mean, statistically independent Gaussian random variables each having a variance of $\sigma^2/2$, and $\rho_n = e^{j\theta_n}$ with an arbitrary carrier phase offset θ_n. A maximum-likelihood sequence decoder employs the Viterbi algorithm [43] to determine the most likely binary input sequence or equivalently the most likely coded symbol sequence $\mathbf{x}$. The decoding metric or the equivalent distance used in the decoder will be derived in Section 5.5 and will be shown to be suboptimum.

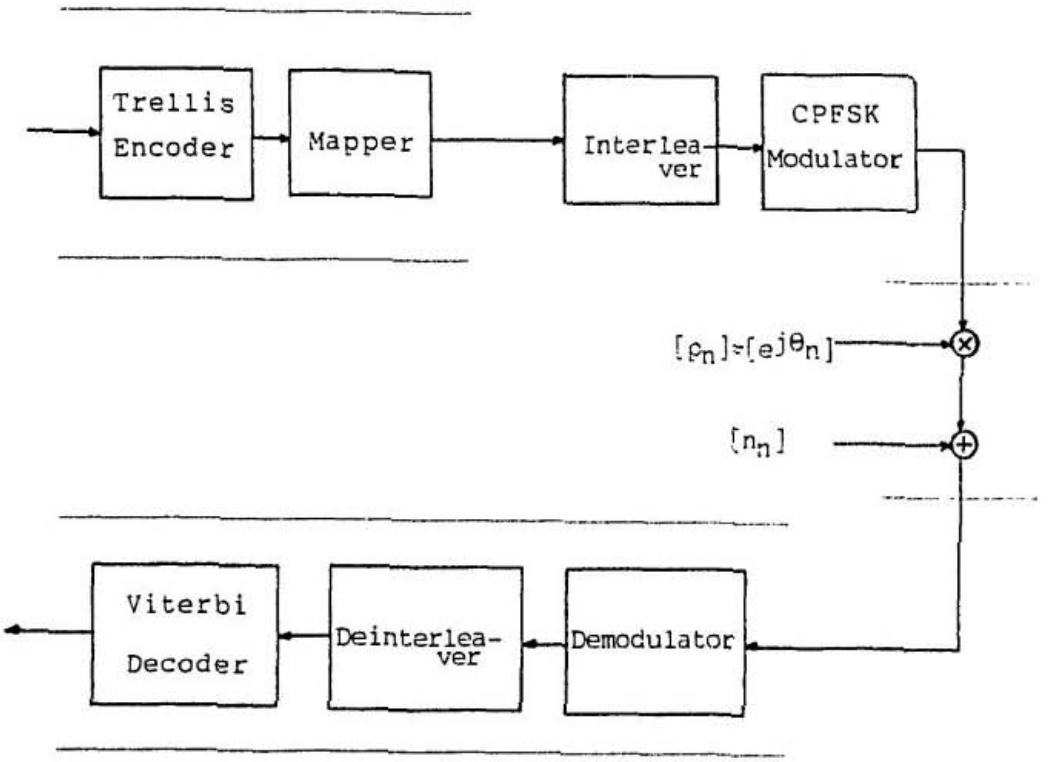

Figure 5.1 General model of carrier-phase offset channel.

5.2.2 Mobile satellite channel

As agreed by the WARC'92, held in Torremolinos, Spain, future mobile satellite systems (MSS) based on geostationary satellites will operate in the following bands of frequencies: (Global primary) 1980 2010 MHz (down link)/ 2170 2200 MHz (up link) and 2500 2520 MHz/ 2670 2690 MHz; (US/Canada) 1525 1559 MHz/ 1626.5 1660.5 MHz [83]. With the present technological developments it is expected that mobile satellite systems will operate with a channel spacing of 5 kHz, and transmit data and digitized-voice at low data rates, nominally at 2.4 4.2 kb/s.

Due to the presence of a direct path between the satellite and a mobile terminal, the fading conditions in the mobile satellite channel will not be severe as in land-mobile communication. Therefore, coherently detected, power and bandwidth-efficient coded-modulation schemes have been considered for application in these channels. Considerable effort has also been devoted to the measurement and characterization of the mobile satellite channel [30, 68] as these channel characterizations are important in the selection of suitable coded-modulation techniques for future mobile satellite communication systems.

In mobile satellite communication the mobile terminals will use small antennas having gain between 2–12 dB and broad beam-widths [30]. Therefore these antennas will pick multipath reflections of the satellite down-link signal thereby giving rise to multipath fading. Multipath fading imposes random amplitude and phase variations into the transmitted waveform. In other words, fading will cause the channel to exhibit time-varying behaviour in the received signal. Besides Gaussian noise, it is perhaps the most serious impairment that degrades the performance of data transmission through a mobile satellite channel. For reliable performance, the system must be able to combat short fades and recover promptly from long fades.

Fading also makes the problem of carrier synchronisation more difficult.

When an information-bearing signal is transmitted through a fading channel, if *coherence bandwidth* is small in comparison to the bandwidth of the transmitted signal, the channel is said to be *frequency selective* or fast fading [80]. (Coherence bandwidth is defined as the frequency separation for which two signals transmitted from the same base station are strongly correlated. This means if the frequency separation is large enough the statistical properties of the two signals at the receiver will be independent). Frequency-selective channels severely distort signals. The mobile satellite channel is assumed to be frequency-nonselective or slow fading in contrast to land-mobile communication channels where the fading is almost always frequency-selective.

Countermeasures for multipath fading

Because multipath fading can severely degrade the performance of data transmission in mobile satellite channels, it is required to use fading compensation techniques to combat the fading. There are several methods available to compensate for fading in general. All these methods involve some form of diversity reception: *space diversity*, *frequency diversity*, or *time diversity*. Both space diversity and frequency diversity have to be ruled out in most mobile satellite terminals owing to

1. the small size of the mobile terminal,

2. the large *coherence bandwidth* encountered in the mobile satellite channel [30].

Time diversity, however, can be incorporated through coded-modulation schemes employing various trellis modulation codes.

There are two major difficulties in using trellis modulation codes in multipath fading channels. First, much less is known about good bandwidth efficient codes

for burst noise channels. Second, the Viterbi decoder is sensitive to burst errors caused by multipath fading [70] and coding cannot achieve diversity improvement so long as the fading process is strongly correlated over the decoder constraint length. The conventional solution–and the most robust solution available yet–to these two problems is to interleave the encoded symbol sequence prior to transmission and to deinterleave the corresponding received symbol sequence at the demodulator [27, 70]. If the depth of interleaving is sufficiently long, then the interleaved channel (the combination of interleaver, multipath fading channel and deinterleaver) may be considered memoryless [70], thereby enabling the use of trellis modulation codes for data transmission.

The operation of interleaving permutes the ordering of a sequence of symbols in a deterministic way. The inverse permutation operation at the deinterleaver restores the ordering. There are two main types of interleavers commonly used: *periodic* and *pseudorandom*. A periodic interleaver is an interleaver for which the interleaving permutation is a periodic function of time [27]. In pseudorandom interleavers the permutation pattern is pseudorandom. In practice, periodic interleavers are preferred because of their simplicity. However, they are less robust than the pseudorandom interleavers [27]. Where there can be no substantial variation in burst characteristic, such as the mobile satellite channel, periodic interleavers are adequate [27].

In addition to multipath fading, there is a number of sources of performance degradation in the mobile satellite channel, namely, *shadowing, Doppler effect, channel nonlinearity* and *adjacent channel interference.*

Shadowing

Shadowing gives rise to much slower changes in the signal level than multipath fading. It is caused by changes in the topography such as buildings, hills and foliage. In contrast to severe shadowing encountered in land-mobile communication channels, a line-of-sight path frequently exists in satellite-based mobile communication channels. Therefore shadowing is mild in mobile satellite channels. A frequently used model for the Canadian mobile satellite channel with light, average and heavy shadowing can be found in [68].

Doppler effect

In aeronautical and satellite-based mobile communication systems a Doppler frequency shift f_d causes the received signal sequence to accumulate a phase shift or phase rotation of $2\pi f_d T$ radian, where T is the symbol duration, with respect to the transmitted signal sequence. This gives rise to carrier phase ambiguity problems.

Channel nonlinearity

In general, to achieve higher efficiency, the RF power amplifiers in a mobile terminal as well as on-board the satellite (for example the travelling-wave-tube amplifiers) will have to operate in the nonlinear region. This will cause some signal compression at the output. Applying, for instance, 6 dB backoff to an amplifier in order to make it linear enough for a code based on QAM, can remove that code's advantage over a constant-envelope modulation code [10]. Coded-modulation schemes with amplitude variations (for instance QAM) need Class B or AB power amplifiers in the mobile unit. They are 2–3 dB less efficient than the Class C amplifiers needed by PSK and CPM [10] which are impervious to channel nonlinearities in so far as the

amplitude is concerned. This 2–3 dB can be counted as a gain for constant-envelope schemes relative to variable-envelope schemes. Therefore constant-envelope modulation schemes are preferred in mobile satellite channels.

Adjacent channel interference

Adjacent channel interference is a major impairment for terrestrial land-mobile communications because the received signal may sometimes be weaker than a signal in the next channel or even a neighbouring channel. Adjacent channel interference can be reduced by proper frequency assignment. For satellite-based systems, however, all signals arrive approximately from the same distance and, hence, the differences in signal levels are primarily due to multipath fading. Therefore adjacent channel interference is not expected to be a major impairment in mobile satellite channels.

Channel model

A simplified block diagram of the satellite-based mobile communication system is shown in Fig. 5.2. While the mobile satellite channel is very difficult to treat mathematically, models have steadily been developed where they describe the physical channel with considerable accuracy [30, 68].

The fading channel introduces a multiplicative distortion on the received signal and it can be represented as [36, 80]:

$$\mathbf{y} = \rho \cdot \mathbf{x} + \mathbf{n}, \tag{5.2}$$

where the random process $\mathbf{n}$ is zero mean white Gaussian noise with double-sided power spectral density $N_0/2$. $\mathbf{x} = (x_1, x_2, \ldots, x_n)$ is a possible transmitted symbol sequence and $\mathbf{y} = (y_1, y_2, \ldots, y_n)$ is the corresponding received symbol sequence. ρ

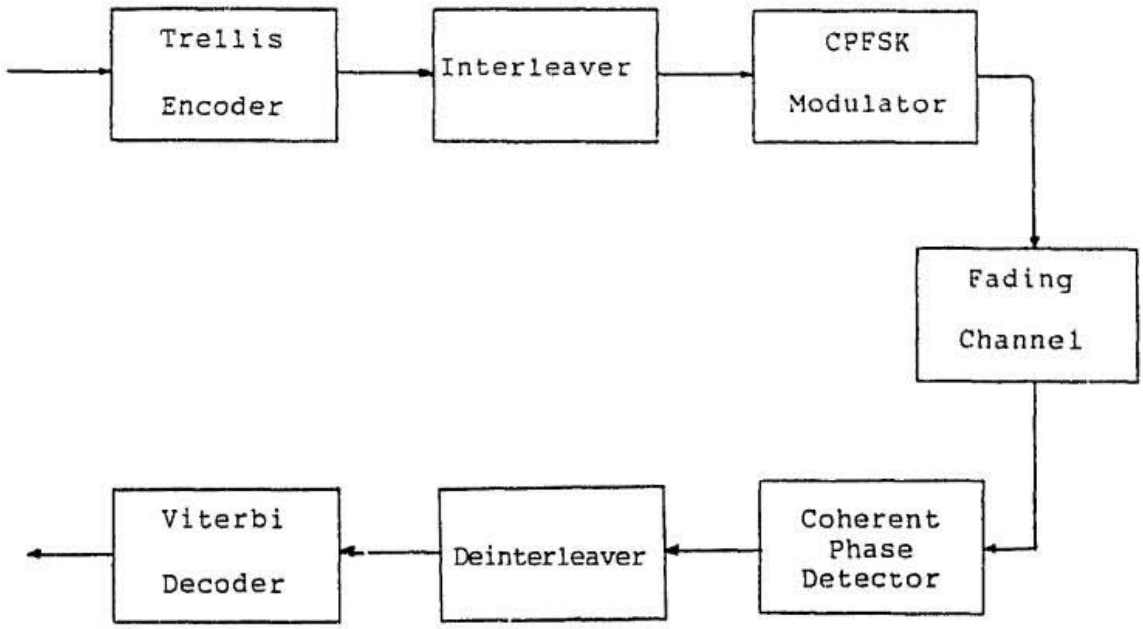

(a) Simplified block diagram

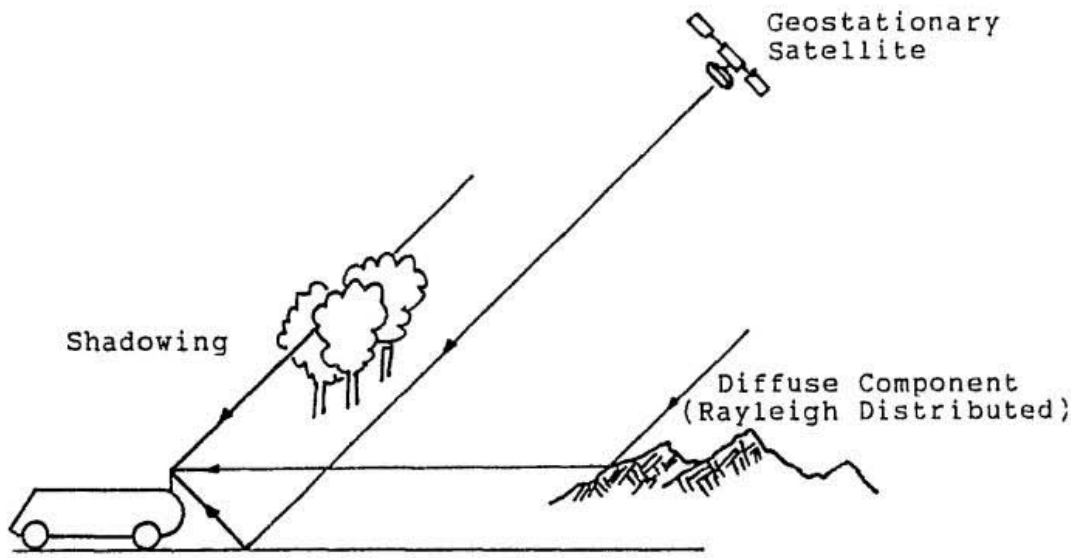

(b) Mobile satellite channel model

Figure 5.2: Mobile satellite communication system model (a) Simplified block diagram (b) Channel model.

denotes the normalized signal envelope (also known in the literature as the random fading amplitude [24, 36]) at the receiver input. Thus, depending on the severity of multipath fading, the channel acts to multiply each received signal's amplitude by a Rician or Rayleigh distributed random variable.

The received signal at the mobile terminal can be modelled as the sum of three vectors, shown in Fig. 5.2(b), consisting of two coherent components (the direct wave or the line-of-sight component and the ground-reflected wave or the specular component) and a non-coherent (diffuse) component. Analysis and field experiments [30, 68] have shown that the power of the diffuse component at the mobile terminal is 10 20 dB below that of the unshadowed direct wave. Often the ground-reflected wave is either ignored or combined with the coherent component [30]. The envelope of the diffuse component is Rayleigh distributed and the phase is uniformly ditributed between 0 and 2π radian [30]. Hence, the diffuse component has a frequency-nonselective Rayleigh fading waveform [30]. The vector sum of the direct wave (unshadowed) and the Rayleigh fading diffuse component results in a Rician distributed signal envelope [68].

A multipath fading channel can be roughly classified as Rayleigh, Rician, or non-fading depending on K, where K is a propagation parameter or fading factor defined as the ratio of powers of the coherent to non-coherent (random fading) components. For values of K not exceeding 0 dB the channel is Rayleigh distributed. The values of K roughly between 0 and 13 dB represent Rician distribution and for K greater than about 13 dB the channel can be approximately considered as nonfading [31].

The mobile satellite channel is assumed to be Rician distributed. The probability density function of ρ for Rician fading is given by [24, 36]:

$$p(\rho) = 2\rho(1+K)\exp\{-K-(1+K)\rho^2\}I_0[2\rho\sqrt{K(1+K)}], \quad \rho \geq 0 \qquad (5.3)$$

where K denotes the Rician factor with the same definition as in the previous paragraph and $I_0[.]$ denotes the modified Bessel function of the first kind of order zero [46]. For a Rayleigh fading channel (5.3) reduces to

$$p(\rho) = 2\rho e^{-\rho^2}, \quad \rho \geq 0. \tag{5.4}$$

While the above model of a mobile satellite channel accounts for the effect of the fading on the amplitude of the received signal, the effect of the fading on the phase of the received signal will be assumed to be fully compensated for. In other words, under the assumption of perfect coherence at the receiver, only amplitude fades affect the system performance. The channel symbols will be interleaved prior to transmission and the corresponding received symbol sequence will be deinterleaved at the receiver. Since there is only one symbol per trellis branch this amounts to a branch-by-branch interleaving. As stated before, the ideal interleaving process transforms the burst noise channel into a memoryless channel with random noise, and the depth of interleaving is assumed to be infinite for analytical purposes.

5.3 Phase detection and trellis decoding

The schematic block diagram of the suboptimum coherent phase detector considered in this chapter is shown in Fig. 5.3. This method has been directly adapted from the well known detection technique for PSK signalling. It consists of a coherent symbol-by-symbol phase detector followed by a trellis decoder. The CPFSK signal is treated as a PSK signal and its phase is measured after every signalling interval [61]. In this method, the received signal is first demodulated by multiplying by two coherent reference carriers in quadrature. The resulting inphase and quadrature-phase waveforms are low-pass filtered and sampled synchronously with the transmitter. The phase is computed from the inphase and quadrature-phase

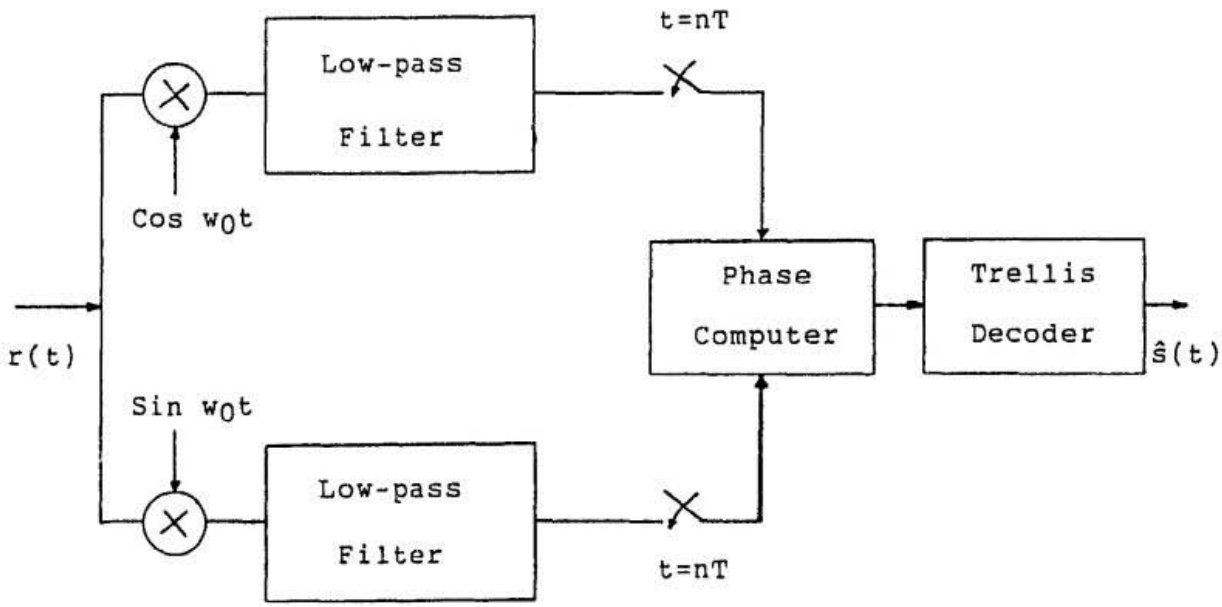

Figure 5.3: Phase detection and trellis decoding.

samples. The trellis decoder then uses this information to decode the most-likely transmitted sequence using the Viterbi algorithm. Since the continuity property of the phase, and hence the phase trellis, is not used in the demodulator, the receiver is suboptimum in an AWGN channel. The receiver is also unaffected by the use of a deinterleaver which destroys the memory of the CPFSK signal.

The number of calculations per signalling interval performed in the Viterbi decoder grows linearly with the number of states in the 'product' trellis or the 'super' trellis that is formed by multiplying the number of states of the CPFSK scheme by the number of states of the trellis precode. Clearly, the required speed of the processor in the receiver is proportional to the value qM in a correlation receiver, where q is the denominator of the rational value modulation index $h = p/q$ and M is the number of signalling levels.

Realisation of the suboptimum receiver is significantly simpler than that of the correlation receiver because the complexity does not grow with the number of signalling levels, since now, the number of states is only that of the coding scheme and is not multiplied by the number of states of CPFSK. The complexities involved in practical realization of this receiver is also similar to a PSK receiver. However, one would expect any error in the estimation of symbol transition instants to cause performance degradation in the case of CPFSK, while PSK is impervious to sampling errors [38]. The reason for this is the piecewise-continuous nature of the CPFSK phase. In PSK the phase remains constant over a signalling interval. An important advantage of phase detection and trellis decoding is that, as mentioned before, it can be used on interleaved multipath fading channels such as the mobile satellite channel. Throughout this work we assume an ideal receiver in order to keep the analysis tractable.

5.4 Trellis decoding on channels with finite memory

As stated before, the combination of a trellis modulation code and a channel with finite memory can be modelled as a single system with finite memory [70]. It has been shown by Massey [70] that it is possible to perform maximum-likelihood decoding on such a channel as easily as on a discrete channel without memory such as the classical additive white Gaussian noise channel.

Consider a Rician or Rayleigh fading channel with slow fading. Here 'slow fading' means that the fading bandwidth is small compared to the signal bandwidth so that the receiver can track the phase variations [48].

Let the input symbol sequence be denoted by $\mathbf{x} = (x_1, x_2, \ldots, x_n)$ and the output sequence by $\mathbf{y} = (y_1, y_2, \ldots, y_n)$. In the n^{th} signalling interval the transmitted signal is multiplied by the amplitude factor ρ_n, which is, depending on the channel conditions, a Rician or Rayleigh distributed random variable, and the carrier phase is shifted by an amount θ_n radians. The phase shift θ_n is assumed to be uniformly distributed between 0 and 2π radians. The sequence (ρ_n, θ_n) is a slow-varying random process not affected by the transmitted information sequence and it can be closely estimated at the receiver. It is assumed that the synchronisation is achieved between transmitter and receiver, and there is no feedback from receiver to transmitter so that

$$P(x_n \mid x_1, y_1, \ldots, x_{n-1}, y_{n-1}) = P(x_n \mid x_1, x_2, \ldots, x_{n-1}). \tag{5.5}$$

For this type of channel, the channel output can be written as [70]:

$$y_n = (y'_n, s_n), \tag{5.6}$$

where s_n is the channel state (that is the instantaneous fading depth) and y'_n is the

quasi-output of the channel.

The channel state accounts for the finite memory of the channel. That is,

$$P(y'_n \mid x_1, x_2, \ldots, x_n, y'_1, y'_2, \ldots, y'_{n-1}, s_1, s_2, \ldots, s_n) = P(y'_n \mid x_n, s_n). \quad (5.7)$$

The state of the channel evolves independent of the channel input. Therefore we have,

$$P(s_n \mid x_1, x_2, \ldots, x_n, y'_1, y'_2, \ldots, y'_{n-1}, s_1, s_2, \ldots, s_{n-1}) = P(s_n \mid s_1, s_2, \ldots, s_{n-1}). \quad (5.8)$$

The state s_n along with the quasi-output y'_n convey full information about the transmitted information sequence. When the state s_n is a suitably quantized representation of (ρ_n, θ_n), the resulting discrete channel is completely described by (5.6) and (5.7) [70]. The decoding metric for such a channel has also been derived by Massey [70] as shown below.

It follows from (5.6), (5.7) and (5.8) that

$$\begin{aligned} P(y_1, y_2, \ldots, y_N \mid x_1, x_2, \ldots, x_N) &= P(y'_1, \ldots, y'_N, s_1, \ldots, s_N \mid x_1, x_2, \ldots, x_N) \\ &= P(s_1, s_2, \ldots, s_N) \prod_{n=1}^{N} P(y'_n \mid x_n, s_n) \quad (5.9) \end{aligned}$$

The factor $P(s_1, s_2, \ldots, s_N)$ in (5.9) does not depend on the transmitted sequence $x_1, x_2, \ldots, x_N$ and therefore the maximum-likelihood decoding rule reduces to choosing $x_1, x_2, \ldots, x_N$ as that encoded sequence which maximises a suitable distance function or decoding metric.

From an implementation point of view, it is desirable to have the total decoding metric for a sequence of symbols to be equal to the sum of the decoding metrics for each channel input and output pair [27]. Such a decoding metric is known as an additive metric or an additive distance [27].

The distance function:

$$\sum_{n=1}^{N} d_n(x_n;\, y'_n, s_n). \tag{5.10}$$

where

$$d_n(x_n;\, y'_n, s_n) = A\,\{\log P(y'_n \mid x_n, s_n) - f_n(y'_n, s_n)\} \tag{5.11}$$

satisfies the additive requirement. The function f_n is selected arbitrarily and A is an arbitrary positive constant. For convenience of implementation of the decoder, one usually chooses [27]

$$f_n(y'_n,\, s_n) = \min_{x_n}\, \log P(y'_n \mid x_n,\, s_n) \tag{5.12}$$

so that the incremental distance given by (5.10) is never negative and generally the constant A is chosen so that these distance metrics are well approximated by small integers [27, 70]. In other words, when f_n and A are chosen as given above, the minimum of the decoding metric is zero and all other values of d_n lie in some convenient positive range.

When the channel state is given, the above model of a fading channel behaves as a memoryless channel (random noise channel) between its input and its quasi-output [70]. However, a decoding metric appropriate for the particular channel model has to be used. For example, in the case of memoryless channels in the presence of additive, white Gaussian noise we would use the Euclidean distance metric in the trellis decoder, where the squared Euclidean distance is given by

$$d^2(y_n,\, x_n) = -|y_n - x_n|^2. \tag{5.13}$$

On the other hand, for fading channels the appropriate decoding distance becomes [36]:

$$d^2(y_n,\, x_n) = -|y_n - \rho_n\, x_n|^2, \tag{5.14}$$

where ρ_n is the random fading amplitude [36, 70] during the n^{th} signalling interval as defined in (5.3) and (5.4).

The above principle enables one to build a maximum-likelihood decoder to be used with any kind of demodulator (optimum or suboptimum) when the decoder utilises comparisons of encoded sequences of the same length [70]. The Viterbi decoder satisfies the above condition and thus can be used to decode trellis modulation codes in channels with finite memory.

5.5 Distance metric for phase detection and trellis decoding of CPFSK signals

In this section we consider the determination of a suitable decoding metric (equivalent distance) for the decoder to use in phase detection and trellis decoding of CPFSK signals. This is based on a generalisation of the Euclidean distance used for transmission over the AWGN channel with maximum-likelihood detection (correlation detection and trellis decoding). The new equivalent distance is applicable to suboptimum coherent phase detection of CPFSK trellis modulation codes. The analysis done here closely follows the work of Divsalar and Simon [36], and Biglieri and McLane [25]. It uses the well known Chernoff bounding technique [105] to upper bound the symbol error probability of trellis modulated schemes on memoryless channels.

Consider transmission of information using trellis modulation codes over a memoryless channel that is not necessarily Gaussian. We have considered two examples of such channels before, namely, (i) AWGN channels with carrier phase offsets and (ii) independent, amplitude-only fading channels [25, 36].

Let $\mathbf{x}_N$ and $\mathbf{x}'_N$ denote two sequences of transmitted channel symbols of length N. *(While the symbol N has been used before in chapters 3 and 4 to denote the*

number of states in a trellis modulation code, there is no relation between that and the length of an error event as considered in this section. Which parameter N denotes will be clear from the context.) Corresponding to the two symbol sequences, there will be two trellis paths through the state trellis. An error-event of length N is said to occur when the trellis decoder output is $\mathbf{x}'_N (\neq \mathbf{x}_N)$ whenever $\mathbf{x}_N$ is transmitted. The probability of occurrence of an error-event of any length is upper bounded by [25, 36]:

$$P_E \leq \sum_{N=1}^{\infty} \sum_{\mathbf{x}_N} \sum_{\mathbf{x}'_N (\neq \mathbf{x}_N)} P[\mathbf{x}_N] P_E[\mathbf{x}_N \rightarrow \mathbf{x}'_N], \tag{5.15}$$

where $P_E[\mathbf{x}_N \rightarrow \mathbf{x}'_N]$ denotes the pairwise probability of error that the decoder chooses $\mathbf{x}'_N$ when in fact $\mathbf{x}_N$ was transmitted and $P[\mathbf{x}_N]$ is the a priori probability of transmitting $\mathbf{x}_N$.

Let $m(\mathbf{y}_N, \mathbf{x}_N)$ and $m(\mathbf{y}_N, \mathbf{x}'_N)$ denote the decoding metrics used by the trellis decoder for the correct sequence and the incorrect sequence, respectively. The trellis decoder makes an error whenever

$$m(\mathbf{y}_N, \mathbf{x}_N) \geq m(\mathbf{y}_N, \mathbf{x}'_N) \ \forall \ \mathbf{x}'_N \neq \mathbf{x}_N. \tag{5.16}$$

Assuming an additive metric, (5.16) can be written as:

$$\sum_{n=1}^{N} m(y_n, x'_n) \geq \sum_{n=1}^{N} m(y_n, x_n) \quad \forall \ x'_n \neq x_n. \tag{5.17}$$

Then, the pairwise probabilty of error $P_E[\mathbf{x}_N \rightarrow \mathbf{x}'_N]$ is given by:

$$P_E[\mathbf{x}_N \rightarrow \mathbf{x}'_N] = P\{\sum_{n=1}^{N} m(y_n, x'_n) \geq \sum_{n=1}^{N} m(y_n, x_n) \mid \mathbf{x}_N\}. \tag{5.18}$$

Next we apply the well known Chernoff bound [105] to (5.18). According to Chernoff bound if x is a continuous random variable, then,

$$P\{x \geq 0\} \leq \mathrm{E}\{e^{\lambda x}\}, \tag{5.19}$$

where $\lambda(\geq 0)$ is a parameter to be optimized. When x is the sum of N independent continuous random variables $x_1, x_2, \ldots, x_N$, the Chernoff bound becomes

$$P\{\sum_{n=1}^{N} x_n \geq 0\} \leq \prod_{n=1}^{N} \mathrm{E}\{e^{\lambda x_n}\}. \tag{5.20}$$

Therefore, corresponding to (5.18) we have,

$$\begin{aligned} P_E[\mathbf{x}_N \rightarrow \mathbf{x}'_N] \leq & \ \mathrm{E}\{e^{\lambda \sum_{n=1}^{N}[m(y_n, x'_n) - m(y_n, x_n)]} \mid \mathbf{x}_N\}, \\ = & \ \prod_{n=1}^{N} \mathrm{E}\{e^{\lambda[m(y_n, x'_n) - m(y_n, x_n)]} \mid x_n\}, \end{aligned} \tag{5.21}$$

where the equality in (5.21) follows from the assumption that the channel is memoryless. In (5.21), E denotes the statistical expectation operation and $\lambda(\geq 0)$ is the Chernoff bound parameter to be chosen such that the bound is optimised.

Furthermore, the analysis can be simplified by defining a quantity $\Delta_\lambda(x_n, x'_n)$ as follows [36]:

$$e^{-\Delta_\lambda(x_n, x'_n)} \triangleq \mathrm{E}\{e^{\lambda[m(y_n, x'_n) - m(y_n, x_n)]} \mid x_n\}. \tag{5.22}$$

Then, from (5.15), we have

$$P_E \leq \sum_{N=1}^{\infty} \sum_{\mathbf{x}_N} \sum_{\mathbf{x}'_N (\neq \mathbf{x}_N)} P[\mathbf{x}_N] \prod_{n=1}^{N} e^{-\Delta_\lambda(x_n, x'_n)}. \tag{5.23}$$

It is assumed that, as the signal-to-noise ratio increases, for any input and output signal pair (x_n, x'_n), the value of $\Delta_\lambda(x_n, x'_n)$ increases as well. Thus, asymptotically for high-SNR the error probability is approximately upper bounded by a term of the form

$$P_E \leq \mathcal{A} e^{-d_f^2}, \tag{5.24}$$

where $\mathcal{A}$ is a constant,

$$d_f^2 = \min_{N} \min_{\mathbf{x}'_N \neq \mathbf{x}_N} \sum_{n=1}^{N} d^2(x_n, x'_n), \tag{5.25}$$

$$d^2(x_n, x'_n) = \Delta_{\lambda_0}(x_n, x'_n). \tag{5.26}$$

and λ_0 is the optimum value of λ such that it minimises the probability of error. The constant $\mathcal{A}$ is dependent on the multiplicity of error events at distance d_f^2. Usually, $\mathcal{A}$ is a small constant and it is ignored (at a slight expense in tightness of the upper bound) at high signal-to-noise ratios [37].

To minimise the upper bound given in (5.23) we must select λ_0 such that $\sum_{n=1}^{N} \Delta_\lambda(x_n, x'_n)$ is maximised. However, selection of a value for λ_0 should be done within the additivity constraint, that is, $d^2(.,.)$ results in an additive distance. While in some cases the optimum λ_0 results in an additive distance, in others it fails to do so and, therefore, one must choose a suboptimum value for λ. Fortunately, as in the case of most engineering design, it is not necessary to use an optimum value for λ to obtain a useful upper bound to the error probability.

5.5.1 Additive white Gaussian noise channel

Under the assumption of an ideal, additive, white Gaussian noise channel, the received signal y_n at time $t = nT$ is given by,

$$y_n = x_n + n_n, \tag{5.27}$$

where n_n is a zero mean Gaussian noise process with variance σ^2 and probability density function

$$p(n_n) = \frac{1}{\sqrt{2\pi\sigma^2}} e^{-|y_n - x_n|^2/2\sigma^2} \tag{5.28}$$

The maximum-likelihood decoding metric, $m(y_n, x_n)$, for the AWGN channel is given by [36, 80]:

$$m(y_n, x_n) = \Re\{\mathbf{y}\mathbf{x}^*\} = -|y_n - x_n|^2, \tag{5.29}$$

where, for simplicity, the factor $\frac{1}{2\sigma^2}$ has been ignored since it can eventually be combined with the Chernoff bound parameter λ.

Substituting (5.29) into (5.22) and assuming that the real and imaginary parts, $\Re\{n_n\}$ and $\Im\{n_n\}$, respectively, of the complex noise random variable n_n are zero-mean statistically independent Gaussian random variables each having a variance of $\sigma_N^2 = \sigma^2/2$, it can be shown that [36]

$$\begin{aligned} P_E[\mathbf{x}_N \rightarrow \mathbf{x}'_N] &\leq \prod_{n=1}^{N} e^{-\lambda|x_n - x'_n|^2} \cdot \mathrm{E}\{e^{2\lambda\Re\{n_n(x_n - x'_n)^*\}}\}, \\ &\leq \prod_{n=1}^{N} e^{-\lambda|x_n - x'_n|^2(1-2\lambda\sigma_N^2)}. \end{aligned} \tag{5.30}$$

Since σ_N^2 is independent of the discrete time n, we have

$$\frac{\partial}{\partial\lambda}\{-\lambda|x_n - x'_n|^2(1 - 2\lambda\sigma_N^2)\} = |x_n - x'_n|^2(-1 + 4\lambda\sigma_N^2)$$

and

$$\frac{\partial}{\partial\lambda}\{|x_n - x'_n|^2(-1 + 4\lambda\sigma_N^2)\} = 4\sigma_N^2\,|x_n - x'_n|^2 > 0.$$

Therefore,

$$-1 + 4\lambda\sigma_N^2 = 0$$

is the condition which minimises the bound given in (5.30). That is,

$$\lambda_0 = \frac{1}{4\sigma_N^2} = \frac{1}{2\sigma^2} \tag{5.31}$$

is the optimised Chernoff bound parameter. Substitution of λ_0 in (5.30) gives the required upper bound to the pairwise probability of error for the AWGN channel, which is

$$P_E[\mathbf{x}_N \rightarrow \mathbf{x}'_N] \leq \prod_{n=1}^{N} e^{-\frac{1}{4\sigma^2}|x_n - x'_n|^2}. \tag{5.32}$$

Finally, (5.32) can be written as:

$$P_E[\mathbf{x}_N \rightarrow \mathbf{x}'_N] \leq e^{-\frac{1}{4\sigma^2}d_f^2}, \tag{5.33}$$

where

$$d_f^2 \triangleq \sum_{n=1}^{N} |x_n - x'_n|^2 \tag{5.34}$$

represents the squared Euclidean distance between the two channel symbol sequences $\mathbf{x}_N$ and $\mathbf{x}'_N$.

Next, we specialize the results of the preceding paragraphs to phase detection and trellis decoding of CPFSK signals on the AWGN channel.

The received signal corresponding to (5.27) becomes

$$y_n = \sqrt{2E_s}e^{j\phi_n} + n_n. \tag{5.35}$$

where E_s is the symbol energy and ϕ_n is the phase of the CPFSK signal at time $t = nT$. It was shown in Chapter 3 that,

$$\phi_n \in \{0,\ 2\pi/q,\ 4\pi/q, \ldots,\ 2(M-1)\pi/q\} \quad (\text{modulo} - 2\pi).$$

where q is the denominator of the rational value modulation index h.

The decoding metrics corresponding to (5.16) and (5.17) becomes

$$m(y_n, x_n) = \sqrt{2E_s} + \Re\{n_n e^{-j\phi_n}\} \tag{5.36}$$

for the correct sequence, and

$$m(y_n, x'_n) = \sqrt{2E_s}\cos(\phi_n - \phi'_n) + \Re\{n_n e^{-j\phi'_n}\} \tag{5.37}$$

for the incorrect sequence.

Substituting (5.36) and (5.37) into (5.21), we get the required upper bound for the pairwise probability of error as:

$$P_E[\mathbf{x}_N \rightarrow \mathbf{x}'_N] \leq \prod_{n=1}^{N} e^{-\Delta_\lambda(x_n, x'_n)}, \tag{5.38}$$

where

$$\begin{aligned} e^{-\Delta_\lambda(x_n, x'_n)} &= \mathrm{E}\{e^{\lambda\sqrt{2E_s}[\cos(\phi_n - \phi'_n) - 1] + \lambda\Re\{n_n(e^{-j\phi'_n} - e^{-j\phi_n})\}}\}, \\ &= e^{\lambda\sqrt{2E_s}[\cos(\phi_n - \phi'_n) - 1]} \cdot \mathrm{E}\{e^{\lambda\Re\{n_n(e^{-j\phi'_n} - e^{-j\phi_n})\}}\}, \\ &= e^{-\lambda\sqrt{2E_s}[1 - \cos(\phi_n - \phi'_n)] + \lambda^2\sigma^2[1 - \cos(\phi_n - \phi'_n)]}. \end{aligned} \tag{5.39}$$

Since n_n is a Gaussian random variable, the random variable $\Re\{n_n(e^{-j\phi'_n} - e^{-j\phi_n})\}$ is also Gaussian with zero mean and variance $\sigma^2[1 - \cos(\phi_n - \phi'_n)]$ [45]. Therefore (5.39) can be simplified as:

$$e^{-\Delta_\lambda(x_n, x'_n)} = e^{-[1-\cos(\phi_n - \phi'_n)]\lambda(\sqrt{2E_s} - \lambda\sigma^2)} \tag{5.40}$$

with the Chernoff bound parameter λ to be selected so that the upper bound for the pairwise probability of error is minimised. Minimisation of the exponent of the right hand side of (5.38) over λ gives

$$\lambda_0 = \frac{\sqrt{2E_s}}{2\sigma^2}. \tag{5.41}$$

Substituting λ_0 in (5.40), and from (5.38) we have:

$$P_E[\mathbf{x}_N \rightarrow \mathbf{x}'_N] \leq \prod_{n=1}^{N} e^{-\frac{E_s}{2\sigma^2}[1-\cos(\phi_n - \phi' n)]}, \tag{5.42}$$

which gives an expression for the incremental decoding distance as:

$$d^2(x_n, x'_n) = \frac{E_s}{N_0}[1 - \cos(\phi_n - \phi'_n)]. \tag{5.43}$$

This can be used as a squared distance to evaluate the error performance of CPFSK trellis modulation codes with suboptimum phase detection and trellis decoding on AWGN channels.

5.5.2 Carrier phase offset channel

In this section we derive an equivalent distance for suboptimum phase detection and trellis decoding of CPFSK signals when demodulated with a carrier phase offset of θ. The relevant channel model was described in Section 5.2.1. Typically the carrier phase offset would be a function of time. In the study, however, we assume that the carrier phase offset is static or constant over the duration of the error-events under consideration in the trellis decoder.

For carrier phase offset channels, the received signal y_n is given by [45, 93]:

$$y_n = \sqrt{2E_s}e^{j(\phi_n+\theta_n)} + n_n. \tag{5.44}$$

where E_s and ϕ_n are, as before, the symbol energy and phase angle of the signal at time $t = nT$, respectively. The carrier phase offset during the n^{th} signalling interval is denoted by θ_n.

The Viterbi decoder operates on the sequence given by (5.44) and the decoding metric must take phase offsets into account and, in general, can be written as $\Re\{\mathbf{y}\mathbf{x}^* e^{j\theta}\}$ [93], where θ is the carrier phase offset. Accordingly, the decoding metrics are

$$m(y_n, x_n) = \sqrt{2E_s}\cos\theta_n + \Re\{n_n e^{j(\theta_n-\phi_n)}\} \tag{5.45}$$

for the correct sequence, and

$$m(y_n, x'_n) = \sqrt{2E_s}\cos[(\phi'_n - \phi_n) + \theta_n] + \Re\{n_n e^{j(\theta_n-\phi'_n)}\} \tag{5.46}$$

for the incorrect sequence. Corresponding decoding metrics for the AWGN channel with no carrier phase offsets were given in (5.36) and (5.37).

For the special case of a static phase offset, $\theta_n = \theta =$ constant for all n over an error-event of length N and the pairwise probability of error can be upper bounded as:

$$P_E[\mathbf{x}_N \to \mathbf{x}'_N] \le \prod_{n=1}^{N} e^{-\Delta_\lambda(x_n, x'_n)}, \tag{5.47}$$

where

$$\begin{aligned} e^{-\Delta_\lambda(x_n,x'_n)} &= \mathrm{E}\{e^{\lambda[m(y_n,x'_n)-m(y_n,x_n)]} \mid x_n\} \\ &= \mathrm{E}\{e^{\lambda\sqrt{2E_s}\{\cos(\phi_n-\phi'_n+\theta)-\cos\theta\}+\Re[n_n\{e^{j(\theta-\phi'_n)}-e^{j(\theta-\phi_n)}\}]}\} \\ &= e^{\lambda\sqrt{2E_s}[\cos(\phi_n-\phi'_n+\theta)]} \cdot \mathrm{E}\{e^{\lambda\Re[n_n\{e^{j(\theta-\phi'_n)}-e^{j(\theta-\phi_n)}\}]}\}. \end{aligned} \tag{5.48}$$

Since n_n is a Gaussian random variable with zero-mean and variance σ^2, the random variable $\Re\,[n_n\{e^{j(\theta-\phi'_n)} - e^{j(\theta-\phi_n)}\}]$ is also Gaussian with zero-mean and variance $\sigma^2[1-\cos(\phi_n-\phi'_n)]$ and therefore (5.40) can be written as:

$$e^{-\Delta_1(x_n,x'_n)} = e^{-\{\lambda\sqrt{2E_s}[\cos\theta-\cos(\phi_n-\phi'_n+\theta)]-\lambda^2\sigma^2[1-\cos(\phi_n-\phi'_n)]\}} \tag{5.49}$$

with the Chernoff bound parameter λ to be chosen so that the upper bound is minimised. It can be shown that the value of λ that minimises the upper bound given in (5.47) is equal to

$$\lambda_0 = \frac{\sqrt{2E_s}}{N_0}\cdot\frac{[\cos\theta-\cos(\phi_n-\phi'_n+\theta)]}{[1-\cos(\phi_n-\phi'_n)]}. \tag{5.50}$$

If this value of λ is chosen for the upper bound, we get

$$\sum_{n=1}^{N} d^2(x_n,x'_n) = \frac{E_s}{N_0}\cdot\frac{\sum_{n=1}^{N}[\cos\theta-\cos(\phi_n-\phi'_n+\theta)]^2}{\sum_{n=1}^{N}[1-\cos(\phi_n-\phi'_n)]}. \tag{5.51}$$

However, the above distance does not produce an additive metric. Therefore, for the carrier phase offset channel, a suboptimum λ is chosen so that the distance metric is additive. Choosing $\lambda = \frac{\sqrt{2E_s}}{N_0}$ instead, which is the optimum value of λ obtained in (5.41) for the ideal AWGN channel, we have

$$\sum_{n=1}^{N} d^2(x_n,x'_n) = \sum_{n=1}^{N}\frac{E_s}{N_0}\{2[\cos\theta-\cos(\phi_n-\phi'_n+\theta)]-[1-\cos(\phi_n-\phi'_n)]\}. \tag{5.52}$$

This is an additive metric; therefore, similar to the Euclidean distance given by (1.6) for correlation detection

$$d_n^2 = 2E_s\{2[\cos\theta-\cos(\phi_n-\phi'_n+\theta)]-[1-\cos(\phi_n-\phi'_n)]\} \tag{5.53}$$

can be used as an equivalent distance to evaluate the asymptotic error performance of suboptimum detected CPFSK trellis modulation codes on channels with a constant carrier phase offset. This distance is also sometimes referred to as a generalized Euclidean distance in the literature.

5.6 Cutoff rate R_0 for a general interleaved channel with amplitude only fading

The channel cutoff rate R_0 is an indicator of the potential performance of a coded-modulation scheme. It has been shown that R_0 is a fundamental parameter of a channel which gives a simple lower bound to Shannon Capacity [69]. The cutoff rate is also closely related to the performance of convolutional codes on the Binary Symmetric Channel (BSC) and to computational cutoff rate R_{comp} of sequential decoding [69]. Several researchers [69, 105, 106] contend that R_0 is a better performance criterion than the widely used bit error probability criterion for channels, where coded-modulation schemes have been used for information transmission.

Consider two codewords $x_i(t)$ and $x_j(t)$ that have been selected at random from an M-ary modulation scheme. Assuming maximum-likelihood decoding on an AWGN channel with double-sided noise power spectral density $N_0/2$, the probability of error between these two codewords can be written as,

$$P_E[x_i(t), x_j(t)] = Q\{\frac{d(x_i(t) - x_j(t))}{\sqrt{2N_0}}\}, \tag{5.54}$$

where

$$d(x_i(t) - x_j(t)) = \sqrt{\int_{-\infty}^{\infty} (x_i(t) - x_j(t))^2 dt}$$

and

$$Q(x) = \frac{1}{\sqrt{2\pi}} \int_x^{\infty} e^{-y^2/2} dy.$$

The ensemble average probability of error or the expected value of (5.54), where the average is taken over all possible codeword pairs, can then be found to be [105],

$$\overline{P_E[x_i(t), x_j(t)]} = 2^{-NR_0}, \tag{5.55}$$

where N is the length of each codeword in M-ary symbols and the channel cutoff

rate R_0 (in bits per waveform or bits per signalling interval T) is given by,

$$R_0 = -\frac{1}{N} \log_2 \overline{Q\{\frac{d(x_i(t) - x_j(t))}{\sqrt{2N_0}}\}}. \tag{5.56}$$

The expectation in (5.56) is taken over the set of all possible M-ary signals.

If the information transmission rate is R bits per symbol (or bits per signalling interval), then, there would be a total of 2^{NR} codewords. According to the well known property that the probability of a union of events is upper bounded by the sum of the probability of these events (union bound of probability) [105] the overall probability of error for randomly selected codewords is upper bounded by $2^{NR} \cdot \overline{P_F[x_i(t), x_j(t)]}$. Therefore, the average probability of error using the above modulation scheme can be upper bounded as:

$$\overline{P_E[x_i(t), x_j(t)]} \leq 2^{N(R-R_0)}. \tag{5.57}$$

The same bound must apply to all transmitted sequences since the choice of sequences is identically distributed.

Although above coding bounds are obtained assuming memoryless modulation, it is widely held that the same type of union bound holds for interleaved channels with finite memory because, as previously shown in Sec. 5.4, combination of interleaver, modulator, waveform channel, demodulator, and deinterleaver can be considered as a discrete memoryless channel (DMC) [70]. The union bound, however, does not provide a clue to find good coded-modulation schemes for a given channel. Instead, it simply indicates that if the cutoff rate is high for a particular modulation scheme the potential for coding gain is also high. The cutoff rate for a general interleaved channel with amplitude-only fading will be derived next.

The cutoff rate R_0 for a general interleaved channel with amplitude-only fading can be derived using the Chernoff bound technique as follows. With the notation

and definitions of Sec. 5.4, the pairwise probability of error between two sequences $\mathbf{x}_N$ and $\mathbf{x}'_N$ can be written as

$$P_E[\mathbf{x}_N \rightarrow \mathbf{x}'_N] = P\{\sum_{n=1}^{N} m(y_n, x'_n) \geq \sum_{n=1}^{N} m(y_n, x_n) \mid \mathbf{x}_N\}. \tag{5.58}$$

Applying the Chernoff bound [105], (5.58) becomes:

$$\begin{aligned} P_E[\mathbf{x}_N \rightarrow \mathbf{x}'_N] &\leq \mathrm{E}\{e^{\lambda \sum_{n=1}^{N}[m(y_n,x'_n)-m(y_n,x_n)]} \mid \mathbf{x}_N\}. \\ &= \prod_{n=1}^{N} \mathrm{E}\{e^{\lambda \sum_{n=1}^{N}[m(y_n,x'_n)-m(y_n,x_n)]} \mid x_n\}. \\ &= \prod_{n=1}^{N} e^{-\Delta_\lambda(x_n,x'_n)}. \end{aligned} \tag{5.59}$$

where

$$e^{-\Delta_\lambda(x_n,x'_n)} \triangleq \mathrm{E}\{e^{\lambda[m(y_n,x'_n)-m(y_n,x_n)]} \mid x_n\}.$$

Since a bound of the type (5.57) must apply to all transmitted sequences $\mathbf{x}_N$, where the channel symbols are independently selected, if we assume that the N pairs of symbols forming $\mathbf{x}_N$ and $\mathbf{x}'_N$ are randomly selected from an M-ary signal set, the average probablity of error can then be upper bounded using the union bound [105] as:

$$\begin{aligned} \overline{P_E[\mathbf{x}_N \rightarrow \mathbf{x}'_N]} &\leq \overline{\sum_{n=1}^{N} e^{-\Delta_\lambda(x_n,x'_n)}}, \\ &= 2^{-NR_0}, \end{aligned} \tag{5.60}$$

where

$$R_0 = -\log_2 \overline{e^{-\Delta_\lambda(x_n,x'_n)}},$$

and

$$\overline{e^{-\Delta_\lambda(x_n,x'_n)}} = \frac{1}{M^2} \sum_{x_n} \sum_{x'_n} e^{-\Delta_\lambda(x_n,x'_n)}.$$

R_0 depends on the Chernoff bound parameter λ, and for AWGN channels the optimum value of λ was found in (5.31) to be $\lambda_0 = 1/2\sigma^2$. Using the above value

of λ and assuming M-ary modulation with perfect knowledge of the random fading amplitude ρ, it has been shown in [36] that

$$\overline{P_E[\mathbf{x}_N \rightarrow \mathbf{x}'_N]} \leq \prod_{n=1}^{N} \overline{e^{-\frac{1}{4\sigma^2}\rho_n^2|x_n - x'_n|^2}}. \tag{5.61}$$

Therefore, the cutoff rate R_0 for a general interleaved channel with amplitude-only fading is given by

$$R_0 = -\log_2\{\frac{1}{M^2}\sum_{x_n}\sum_{x'_n}\overline{e^{-\frac{1}{4\sigma^2}\rho_n^2|x_n - x'_n|^2}}\}. \tag{5.62}$$

This expression will be used in Chapter 7 to evaluate the performance bounds of CPFSK trellis modulation codes on fading multipath channels.

5.7 Conclusions

In this chapter we have considered suboptimum coherent phase detection of CPFSK trellis modulation codes on two non-Gaussian channels: (i) the carrier phase offset channel and (ii) the mobile satellite channel. A suitable decoding metric (equivalent distance) for the decoder to use in phase detection and trellis decoding of CPFSK signals on AWGN channels has been derived. Next, this equivalent distance was modified to take phase offsets into account, so that it can be used on AWGN channels with carrier phase offsets. In amplitude only fading mutipath channels, such as the mobile satellite channels, instead of the widely used error probability criterion, the channel cutoff rate R_0 has been considered as a suitable performance criterion for the comparison of coded-modulations. The cutoff rate R_0 for a general interleaved channel with amplitude-only fading has been derived.

Chapter 6

Performance Evaluation of CPFSK Trellis Modulation Codes on Carrier Phase Offset Channels

6.1 Introduction

This chapter is concerned with the performance evaluation of CPFSK trellis modulation codes with suboptimum coherent detection on AWGN channels with carrier phase offsets. A computer search is performed for the optimum self-transparent 4-CPFSK ($h \leq 1/4$) and 8-CPFSK ($h \leq 1/8$) trellis modulation codes with suboptimum coherent detection. The matrix description of CPFSK signals introduced in Chapter 3 is used to limit the search to rotationally invariant state transition matrices. Next, the equivalent distance derived in Chapter 5 for suboptimum coherent phase detection and trellis decoding of CPFSK signals is used to study the effect of static carrier phase offsets on the performance of CPFSK trellis modulation codes.

The general model of the carrier phase offset channel was described in Section 5.2.1, and a simplified block diagram was given in Fig. 5.1. In Section 5.5.2, an additive metric (equivalent distance) was derived for use on such channels with suboptimum coherent detection of M-CPFSK signals. The Viterbi algorithm is used to decode the signal and the equivalent distance takes phase offsets into account.

In our case the phase offset is assumed to remain constant over an error event and the phase detector is assumed to be ideal. Only self-transparent 4-CPFSK and 8-CPFSK trellis modulation codes are considered here and, therefore, the problem of carrier phase ambiguity resolution does not arise.

The equivalent distance derived in (5.53) also provides an analytical tool for evaluating the effect of carrier phase offsets on the performance of CPFSK trellis modulation codes. The conventional method of computing the reduction in minimum equivalent distance (MED) for various carrier phase offsets could give an idea of trends in performance degradation. However, it must be emphasized that the results would be valid only asymptotically at high SNR.

The error performance of trellis-coded 8-PSK in the presence of carrier phase offsets has been evaluated in [45, 93] and references therein. For rate 1/2, ν=2, and ν=3 convolutional-coded 8-PSK, it has been shown by simulation that the SNR required to maintain an event error probability of 10^{-5} asymptotically increases until $\theta = 22.5°$, while in the case of uncoded 4-PSK, the operating range extends to $\theta = 45°$. This is only a typical case. It is known that trellis coded schemes in general are more susceptible to carrier phase offsets than uncoded schemes. This greater susceptibility has been ascribed to the formation of long segments of received signals at the same distance from two or more distinct trellis paths. At that point the code exhibits catastrophic error properties and the decoder would then fail.

To find the best self-transparent trellis modulation codes on carrier phase offset channels, we use the suboptimum equivalent distance given in (5.53) instead of the maximum-likelihood metric (Euclidean distance) in the code search program. Codes achieving the largest minimum squared equivalent distance (MED) for a given code complexity and modulation index were searched for. For 4-CPFSK signals the search was limited to $h \leq 1/4$ and $N \leq 256$, where N is the number

of states in the overall trellis modulation code. For 8-CPFSK signals the limiting values were $h \leq 1/8$ and $\mathcal{N} \leq 128$.

6.2 Computer search for self-transparent 4-CPFSK trellis modulation codes

An exhaustive search for optimum codes involves an enormous amount of computer time. Lindell et al. [53, 57, 55], among others, have carried-out such a search for the optimum combinations of convolutional codes and M-CPFSK, so that for a given code-rate (R), memory length (ν) and modulation index (h), such a combination will yield the largest minimum Euclidean distance. However, finding the optimum code (in the sense of largest minimum Euclidean distance) is computationally infeasible for large values of ν.

Although most researchers have been content to find optimum convolutional codes for CPFSK, better codes may be obtained by searching over a more general set of trellis codes. In other words, the outer code need not be necessarily convolutional as has always been considered in the literature; perhaps, better outer trellis codes exist not based on convolution. The assumption that the encoder is a general trellis encoder generalizes the convolutional encoder on which prior work on coded-CPFSK has concentrated.

Usually, good codes can be obtained by limiting the search to a subset of the codes that possess certain desirable properties. It is generally accepted that good codes possess symmetry and that M-ary symbols occur with equal frequency and with regularity. The following heuristic code design rules that are similar to those of [94] for set-partition codes are proposed for self-transparent 4-CPFSK trellis modulation codes.

- The state of the CPFSK trellis modulation code is expressed as $X_n = \{C_n, \phi_n\}$, where $C_n = (x_{n-1}, x_{n-2}, \ldots\ldots, x_{n-\nu})$ and $\phi_n \in \{0, 2\pi h, 4\pi h, \ldots\ldots, 2(M-1)\pi h\}$. ν is the memory length of the trellis code and h is the rational value modulation index. The state X_n is called a pair-state in the literature and it has been frequently used in trellis search algorithms.

- The $N \times N$ state transition matrix that describes the overall CPFSK trellis modulation code is partitioned into $2^{2\nu}$ $q \times q$ sub-matrices.

- Each sub-matrix is either an all-zero matrix or a more sparse version (so that it has only one of a kind of the M-ary symbols) of the $q \times q$ state transition matrix of the uncoded M-CPFSK scheme. This condition makes all phase states to follow identical state transition patterns. If not, the code will be transparent to only some of the carrier-phase ambiguities.

- Every row and column of the $N \times N$ matrix should have two and only two symbols.

- The output symbol distribution is restricted to be uniform. This means that each M-ary symbol should occur with equal frequency, and the set of symbols is equally distributed over the branches of the trellis. That is, each M-ary symbol will appear $q\,2^{\nu}$ times within the $N \times N$ matrix.

A search for codes satisfying the above constraints was performed. The search was limited to codes with even number of states $N \leq 256$. With these constraints imposed on the state transition matrix many poor codes (those codes with small minimum Euclidean distances) are discarded, and the set of codes that must be searched becomes reasonable because only rotationally invariant state transition matrices are input to the search algorithm.

Since the CPFSK trellis modulation codes are nonlinear, the largest minimum Euclidean distance between CPFSK signal sequences through the trellis does not necessarily occur between the signal sequences corresponding to the all-zero binary input sequence of the trellis code and a sequence diverging from and remerging later with this sequence. The merging events occur not only when the phase states but also the symbol states of the sequences become identical. In the code search program, an efficient algorithm due to Mulligan [75] was adapted, which computed d^2_{min} among all possible pairs of sequences diverging in some pair-state and remerging later in another pair-state.

Although the minimum Euclidean distance itself can be used to determine the symbol error probability P_e at high-SNR as discussed previously, it is really not sufficient to describe the overall performance in every situation. This is because in the calculation of minimum Euclidean distance we always compute the distance between two paths merging at the shortest error event (memory length), but in most codes examined above there exist some trellis paths that are not yet merged at the memory length but have smaller distances between them than the minimum Euclidean distance found. If the length of the observation interval at the demodulator is not long enough, there is a possibility that these smaller distances will eventually dominate the error probabilty. Therefore, the receiver path memory (N_R) should at least be equal to the minimum number of symbol intervals required to ensure that the distance between any two paths is greater than the minimum Euclidean distance of signals.

Receiver path memory is one of several factors that affect trellis decoder performance. Decoder memory and decoder synchronisation are two other factors critical for maximum-likelihood decoding. Since there are at least $N = q\,2^{\nu}$ states in the state transition matrix of a CPFSK trellis modulation code, the decoder must

reserve N words of storage for survivors in the Viterbi algorithm. The Viterbi algorithm examines every state in the trellis, then, a matched filter operation is performed for each signal possibility in the n^{th} interval, and the results compared among themselves to find the maximum-likelihood trellis path into each state at the $(n+1)^{\text{th}}$ interval. Therefore each word must be able to store the survivor path and its accumulated distance. Since the storage requirements increase exponentially with the memory length ν, in practice, it is not possible to use trellis modulation codes with very large N. Since the number of calculations per symbol interval in the Viterbi decoder grows linearly with N, it is obvious that the required speed of the processor in the receiver is proportional to the value of q.

Code search results for the optimum self-transparent 4-CPFSK trellis modulation codes is shown in Table 6.1. The asymptotic coding gain for each code over uncoded 4-CPFSK is also shown. Among codes with the same minimum Euclidean distance for a given number of states, the code with the shortest receiver path memory was selected as the optimum code. Table 6.1 lists the results for only those codes achieving larger minimum Euclidean distances than MSK signals, because, MSK is our reference scheme. Based on the results of this search, it was possible to identify a pattern in the optimum state transition matrix so that the CPFSK trellis modulation code is transparent to all carrier-phase ambiguities of the uncoded CPFSK scheme.

Table 6.1 Coding gain of optimum self-transparent 4-CPFSK trellis modulation codes on an AWGN channel.

Matrix states N	Receiver path memory N_R	Uncoded minimum distance	Coded minimum distance	Coding gain relative to 4-CPFSK (dB)	Coding gain relative to MSK (dB)
8	3	1.454	3.000	3.146	1.761
10	3	0.973	2.298	3.732	0.603
16	10	1.454	4.302	4.711	3.326
20	12	0.973	3.202	5.173	2.044
24	12	0.692	2.416	5.430	0.821
32	16	1.454	5.241	5.568	4.184
40	18	0.973	3.863	5.988	2.859
48	18	0.692	2.900	6.223	1.614
56	19	0.516	2.234	6.364	0.480
64	21	1.454	6.151	6.264	4.879
80	21	0.973	4.427	6.580	3.451
96	23	0.692	3.400	6.914	2.304
112	24	0.516	2.611	7.042	1.158
128	21	1.454	6.331	6.389	5.004
160	26	0.973	4.797	6.929	3.800
192	26	0.692	3.573	7.129	2.520
224	28	0.516	2.740	7.251	1.367
256	23	1.454	6.515	6.514	5.129

Consider the best rotationally invariant state transition matrix for eight-state 4-CPFSK trellis modulation code shown below.

$$\begin{bmatrix} 0 & -1 & 0 & 0 & 0 & 0 & 0 & 3 \\ 0 & 0 & -1 & 0 & 3 & 0 & 0 & 0 \\ 0 & 0 & 0 & -1 & 0 & 3 & 0 & 0 \\ -1 & 0 & 0 & 0 & 0 & 0 & 3 & 0 \\ 0 & 0 & 1 & 0 & -3 & 0 & 0 & 0 \\ 0 & 0 & 0 & 1 & 0 & -3 & 0 & 0 \\ 1 & 0 & 0 & 0 & 0 & 0 & -3 & 0 \\ 0 & 1 & 0 & 0 & 0 & 0 & 0 & -3 \end{bmatrix} \tag{6.1}$$

When the states S_0 and S_1 are represented as the binary equivalents of the shift register contents, it also can be identified as the state transition matrix of a usual binary convolutional code with constraint length two, naturally mapped onto a 4-CPFSK scheme with $h = 1/4$. Therefore the overall 4-CPFSK trellis modulation code can be implemented by a convolutional outer code followed by a natural binary mapping rule as shown in Fig. 6.1. Comparing this with the previously published results [53, 55, 57, 79] it can be concluded that the optimum eight-state 4-CPFSK trellis modulation code is also the best self-transparent code.

As another example, consider the best 64-state self-transparent 4-CPFSK trellis modulation code, the transition matrix of which is given in Figure 6.2(a). This can be implemented as a convolutional code of constraint length five followed by a natural binary mapping rule and $h = 1/4$ 4-CPFSK as shown in Figure 6.2(b). This trellis modulation code achieves a coding gain of 4.879 dB relative to MSK signalling on AWGN channels. More bandwidth-efficient 64-state codes can be obtained by choosing $h = 1/32$, $h = 1/16$ or $h = 1/8$ 4-CPFSK with convolutional codes of constraint length 2, 3 and 4, respectively. However, they are less power-efficient than the one in the example owing to their smaller modulation index. Table 6.2 lists different implementations of 4-CPFSK trellis modulation codes at a given number of states. The coefficients of the code polynomials are specified in

		S_0				S_1			
		$3\pi/2$	π	$\pi/2$	0	$3\pi/2$	π	$\pi/2$	0
S_0	$3\pi/2$	0	-1	0	0	0	0	0	3
	π	0	0	-1	0	3	0	0	0
	$\pi/2$	0	0	0	-1	0	3	0	0
	0	-1	0	0	0	0	0	3	0
S_1	$3\pi/2$	0	0	1	0	-3	0	0	0
	π	0	0	0	1	0	-3	0	0
	$\pi/2$	1	0	0	0	0	0	-3	0
	0	0	1	0	0	0	0	0	-3

state transition matrix

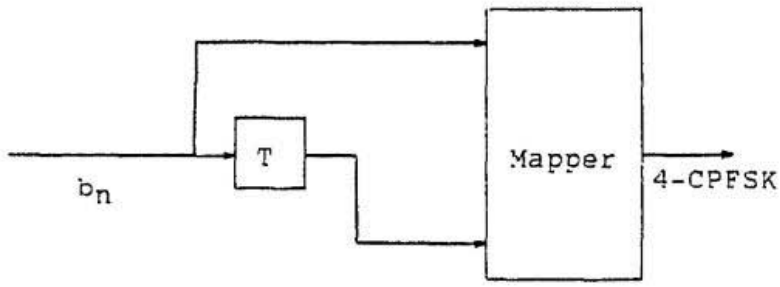

rate 1/2 code:

$g_1 = [2]_8$

$g_0 = [1]_8$

00	-3
01	-1
10	1
11	3

(natural binary)

Figure 6.1 Implementation of the optimum eight-state self-transparent 4-CPFSK, h=1/4 trellis modulation code.

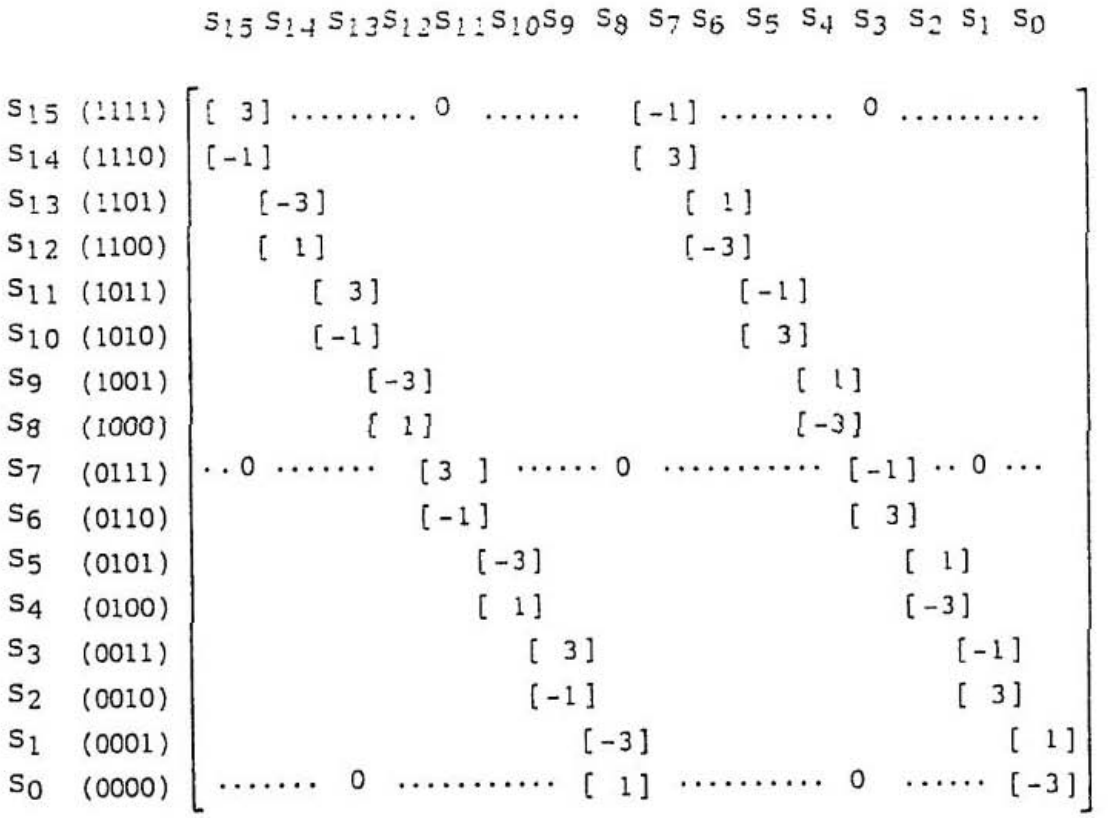

$$[-3] = \begin{bmatrix} -3 & 0 & 0 & 0 \\ 0 & -3 & 0 & 0 \\ 0 & 0 & -3 & 0 \\ 0 & 0 & 0 & -3 \end{bmatrix}_{4X4} \qquad [-1] = \begin{bmatrix} 0 & 0 & 0 & -1 \\ -1 & 0 & 0 & 0 \\ 0 & -1 & 0 & 0 \\ 0 & 0 & -1 & 0 \end{bmatrix}_{4X4}$$

$$[1] = \begin{bmatrix} 0 & 0 & 1 & 0 \\ 0 & 0 & 0 & 1 \\ 1 & 0 & 0 & 0 \\ 0 & 1 & 0 & 0 \end{bmatrix}_{4X4} \qquad [3] = \begin{bmatrix} 0 & 3 & 0 & 0 \\ 0 & 0 & 3 & 0 \\ 0 & 0 & 0 & 3 \\ 3 & 0 & 0 & 0 \end{bmatrix}_{4X4}$$

Figure 6.2(a) State transition matrix of the optimum 64-state self-transparent 4-CPFSK code.

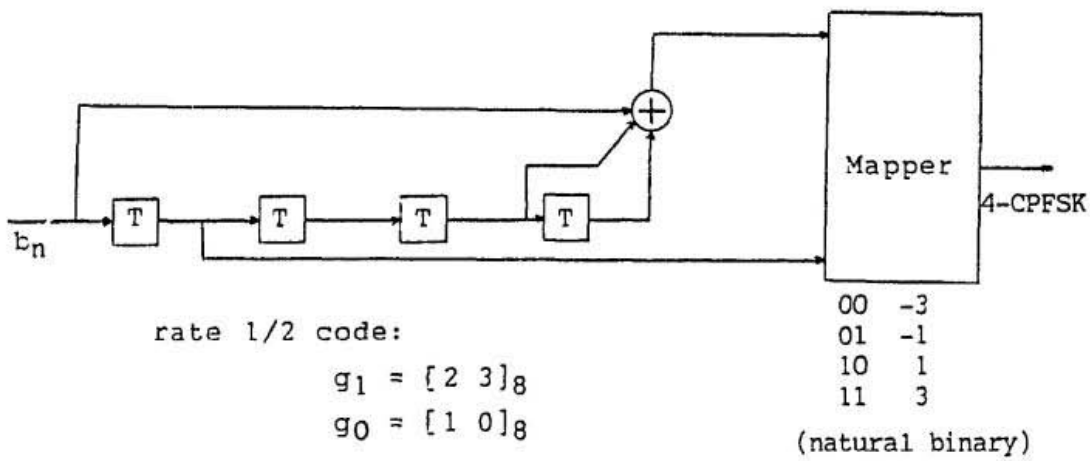

Figure 6.2(b) Implementation of the optimum 64-state self-transparent 4-CPFSK trellis modulation code.

Table 6.2 Implementation of self-transparent 4-CPFSK trellis modulation codes with convolutional codes.

Matrix states	Modulation index	Code	Generator
N	h	$[g_1]_8$	$[g_0]_8$
8	1/4	2	1
10	1/5	2	1
16	1/4	7	2
20	1/5	7	2
24	1/6	7	2
32	1/4	15	02
40	1/5	15	02
48	1/6	15	02
56	1/7	15	02
64	1/4	23	10
80	1/5	23	10
96	1/6	23	10
112	1/7	23	10
128	1/4	61	02
160	1/5	61	02
192	1/6	61	02
224	1/7	61	02
256	1/4	141	002

octal notation. The natural binary mapping rule has been used throughout. The implementation of the convolutional codes at each memory length is shown in Fig. 6.3.

Every optimum 4-CPFSK trellis modulation code for suboptimum coherent detection (except when $\nu = 1$) involves the natural binary mapping rule. Clearly, the effect a phase rotation has on CPFSK trellis modulation codes depends on the signal set mapping, and only the natural binary mapping is consistent with self-transparent codes. Pietrobon et al. [78] have shown that this is the case with trellis-coded QPSK and 8-PSK. In the case of $\nu = 1$, however, the mapping rule of the best code for suboptimum coherent detection was different from that found in the literature for AWGN channels. The optimum code for $\nu = 1$ and $h \leq 1/4$ is shown in Fig. 6.4(a). The two other codes shown in Fig. 6.4(b) and (c) resulted in the same minimum squared equivalent distance, but the optimum code required a decoder memory of three as opposed to four for the other two codes.

Based on the results of the code search performed above, we can identify a generalised state transition matrix to construct self-transparent 4-CPFSK trellis modulation codes at any even number of states. The generalised state transition matrix is shown in Fig. 6.5, and it is valid for any modulation index $h \leq 1/M$. $2^{\nu}(2^{\nu} - 2)$ submatrices of the $N \times N$ matrix will be all-zero matrices and therefore the matrix is sparse. The above results lead us to conclude that for self-transparent 4-CPFSK trellis modulation codes the best codes have a convolutional outer code. For an N state CPFSK trellis modulation code, the maximum memory length of the convolutional precoder is given by $\nu = \log_2(N/q)$.

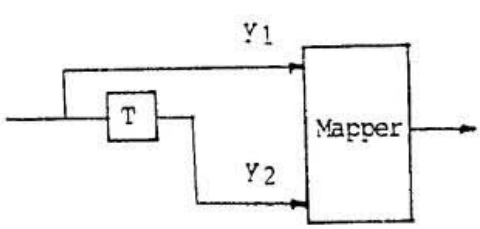

(a) v=1

y_1	y_2	symbol
0	0	-3
0	1	-1
1	0	+1
1	1	+3

Natural Binary

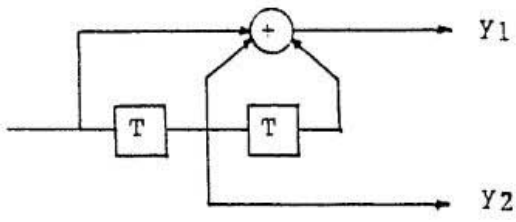

(b) v=2

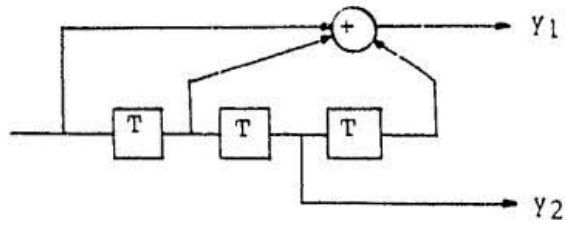

(c) v=3

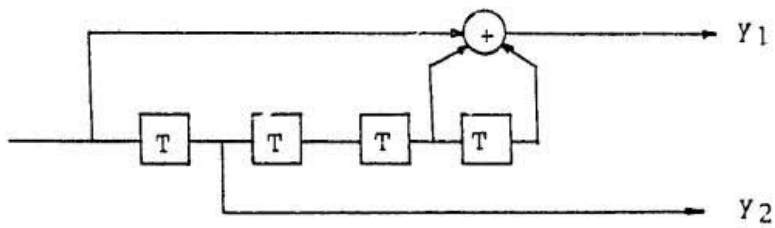

(d) v=4

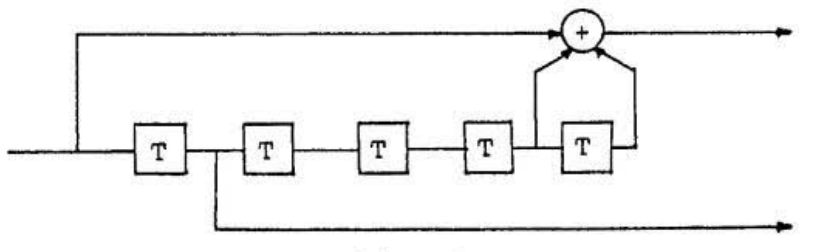

(e) v=5

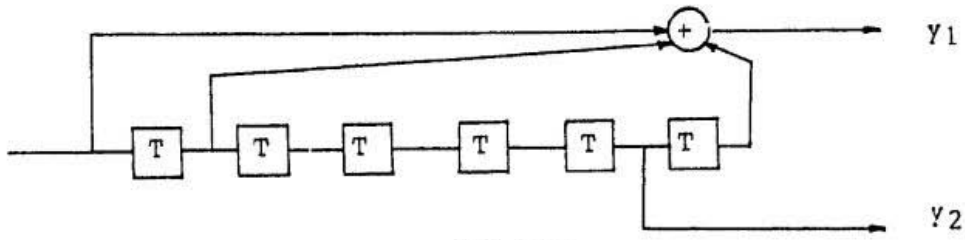

(f) v=6

Figure 6.3 Optimum codes for suboptimum coherent phase detection of 4-CPFSK signals with $h \leq \frac{1}{4}$ on carrier phase offset channel.

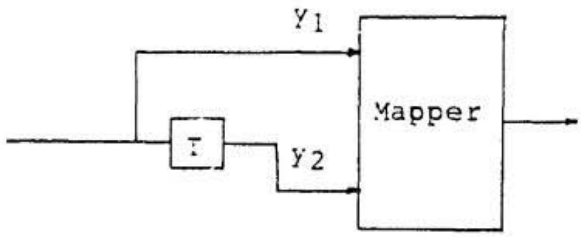

y_1	y_2	symbol
0	0	-1
0	1	-3
1	0	3
1	1	1

(a) Suboptimum phase detection

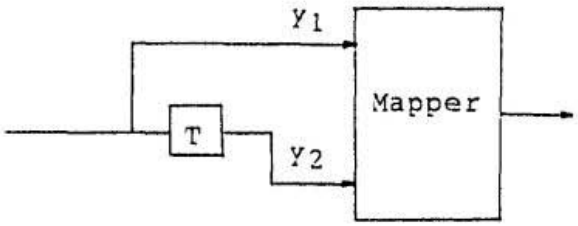

y_1	y_2	symbol
0	0	-3
0	1	-1
1	0	1
1	1	3

Natural Binary

(b) Optimum correlation detection

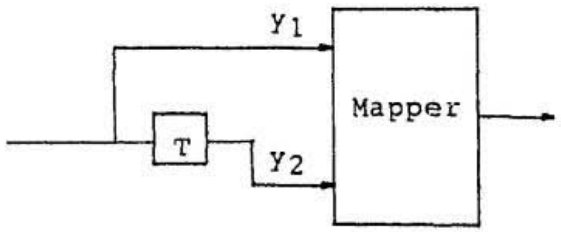

y_1	y_2	symbol
0	0	-3
0	1	1
1	0	-1
1	1	3

(c) Equivalent code to that of (b)

Figure 6.4 Optimum 4-CPFSK trellis modulation codes for rate 1/2, v=1 and $h \leq 1/4$ on carrier phase offset channels.

Figure 6.5 State transition matrix for optimal self-transparent 4-CPFSK trellis modulation codes when $h \leqslant 1/4$.

$$
\begin{array}{c}
 \\
S_{2^{V}-1} \\
S_{2^{V}-2} \\
S_{2^{V}-3} \\
S_{2^{V}-4} \\
\vdots \\
S_{3} \\
S_{2} \\
S_{1} \\
S_{0}
\end{array}
\begin{array}{c}
\begin{array}{cccccccccc}
S_{2^{V}-1} & & & \cdots\cdots\cdots & & & S_{2^{V-1}-1} & S_{2^{V-1}-2} & \cdots S_{1} & S_{0}
\end{array} \\
\left[\begin{array}{cccccccccc}
\left[(+3)\right]_{qxq} & \cdots\cdots & 0 & \cdots\cdots & & & \left[(-1)\right]_{qxq} & \cdots\cdots & 0 & \cdots\cdots \\
\left[(-1)\right] & \cdots\cdots & 0 & \cdots\cdots & & & \left[(+3)\right] & \cdots\cdots & 0 & \cdots\cdots \\
0 & \left[(-3)\right] & \cdots\cdots & 0 & \cdots\cdots & & \left[(+1)\right] & \cdots & 0 & \cdots\cdots \\
0 & \left[(+1)\right] & \cdots\cdots & 0 & \cdots\cdots & & \left[(-3)\right] & \cdots & 0 & \cdots\cdots \\
 & \cdots\cdots & & & & & \cdots\cdots & & & \\
\cdots & 0 & \cdots\cdots & \left[(+3)\right] & \cdots\cdots & 0 & \cdots\cdots & \left[(-1)\right] & 0 & \\
\cdots & 0 & \cdots\cdots & \left[(-1)\right] & \cdots\cdots & 0 & \cdots\cdots & \left[(+3)\right] & 0 & \\
\cdots\cdots & 0 & \cdots\cdots & \left[(-3)\right] & \cdots\cdots & 0 & \cdots\cdots & \left[(+1)\right] & & \\
\cdots\cdots & 0 & \cdots\cdots & \left[(+1)\right] & \cdots\cdots & 0 & \cdots\cdots & \left[(-3)\right] & &
\end{array}\right]_{NxN}
\end{array}
$$

6.3 Computer search for self-transparent 8-CPFSK trellis modulation codes

Here we apply the heuristic design rules given in Section 6.2 to find the optimum 8-CPFSK trellis modulation codes on AWGN channels with carrier phase offsets. In this case the number of symbols in every row and column of the $N \times N$ state transition matrix is equal to four. The coding operation above is equivalent to encoding the least-significant-bit (LSB) of the binary data sequence with a rate-1/2 trellis code and then mapping on to an 8-CPFSK signal set. The overall code-rate would be 2/3. As before, the $N \times N$ state transition matrix is partitioned into $2^{2\nu}$ sub-matrices. Each sub-matrix is obtained from the state transition matrix of the uncoded $h = 1/q$ ($q \geq 8$) 8-CPFSK so that each sub-matrix has only two of a kind of the 8-ary symbols. For example, sub-matrices for $h = 1/8$ 8-CPFSK is shown in Fig. 6.6.

A search for 8-CPFSK trellis modulation codes satisfying the above conditions was carried out. To reduce the computational complexity, the search was limited to codes with states $N \leq 128$. Since the state transition matrices of 8-CPFSK trellis modulation codes would have twice as many symbols as in the case of 4-CPFSK codes, the computational effort is substantially larger. The results are summarised in Table 6.3 and Fig. 6.7. Only those codes achieving minimum Euclidean distances larger than MSK signals are listed in Table 6.3.

$$[(-7,1)] = \begin{bmatrix} -7 & 0 & 0 & 0 & 1 & 0 & 0 & 0 \\ 0 & -7 & 0 & 0 & 0 & 1 & 0 & 0 \\ 0 & 0 & -7 & 0 & 0 & 0 & 1 & 0 \\ 0 & 0 & 0 & -7 & 0 & 0 & 0 & 1 \\ 1 & 0 & 0 & 0 & -7 & 0 & 0 & 0 \\ 0 & 1 & 0 & 0 & 0 & -7 & 0 & 0 \\ 0 & 0 & 1 & 0 & 0 & 0 & -7 & 0 \\ 0 & 0 & 0 & 1 & 0 & 0 & 0 & -7 \end{bmatrix}_{8X8}$$

$$[(3,-5)] = \begin{bmatrix} 0 & 0 & 0 & 3 & 0 & 0 & 0 & -5 \\ -5 & 0 & 0 & 0 & 3 & 0 & 0 & 0 \\ 0 & -5 & 0 & 0 & 0 & 3 & 0 & 0 \\ 0 & 0 & -5 & 0 & 0 & 0 & 3 & 0 \\ 0 & 0 & 0 & -5 & 0 & 0 & 0 & 3 \\ 3 & 0 & 0 & 0 & -5 & 0 & 0 & 0 \\ 0 & 3 & 0 & 0 & 0 & -5 & 0 & 0 \\ 0 & 0 & 3 & 0 & 0 & 0 & -5 & 0 \\ 0 & 0 & 0 & 3 & 0 & 0 & 0 & -5 \end{bmatrix}_{8X8}$$

$$[(-1,7)] = \begin{bmatrix} 0 & 7 & 0 & 0 & 0 & -1 & 0 & 0 \\ 0 & 0 & 7 & 0 & 0 & 0 & -1 & 0 \\ 0 & 0 & 0 & 7 & 0 & 0 & 0 & -1 \\ -1 & 0 & 0 & 0 & 7 & 0 & 0 & 0 \\ 0 & -1 & 0 & 0 & 0 & 7 & 0 & 0 \\ 0 & 0 & -1 & 0 & 0 & 0 & 7 & 0 \\ 0 & 0 & 0 & -1 & 0 & 0 & 0 & 7 \\ 7 & 0 & 0 & 0 & -1 & 0 & 0 & 0 \end{bmatrix}_{8X8}$$

$$[(5,-3)] = \begin{bmatrix} 0 & 0 & 5 & 0 & 0 & 0 & -3 & 0 \\ 0 & 0 & 0 & 5 & 0 & 0 & 0 & -3 \\ -3 & 0 & 0 & 0 & 5 & 0 & 0 & 0 \\ 0 & -3 & 0 & 0 & 0 & 5 & 0 & 0 \\ 0 & 0 & -3 & 0 & 0 & 0 & 5 & 0 \\ 0 & 0 & 0 & -3 & 0 & 0 & 0 & 5 \\ 5 & 0 & 0 & 0 & -3 & 0 & 0 & 0 \\ 0 & 5 & 0 & 0 & 0 & -3 & 0 & 0 \end{bmatrix}_{8X8}$$

Figure 6.6 Sub-matrices for self-transparent 8-CPFSK, h=1/8.

Table 6.3 Coding gain of optimum self-transparent 8-CPFSK trellis modulation codes on an AWGN channel.

Matrix states N	Receiver path memory N_R	Coded minimum distance	Uncoded minimum distance	Coding gain relative to 8-CPFSK (dB)	Coding gain relative to MSK (dB)
32	12	2.555	0.598	6.307	1.064
36	12	2.070	0.476	6.384	0.149
64	18	3.282	0.598	7.394	2.151
72	18	2.660	0.476	7.473	1.239
80	18	2.194	0.387	7.535	0.402

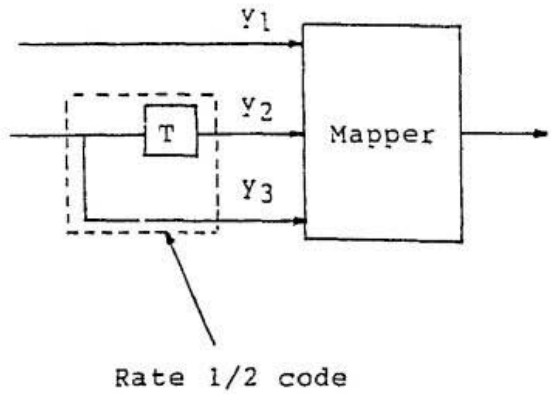

y_1	y_2	y_3	symbol
0	0	0	-7
0	0	1	-5
0	1	0	-3
0	1	1	-1
1	0	0	1
1	0	1	3
1	1	0	5
1	1	1	7

Natural Binary

(a) Optimum rate 2/3, v=1 code and natural binary mapping rule.

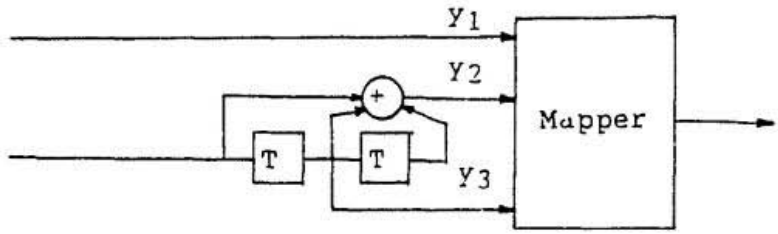

(b) Optimum rate 2/3, v=2 code

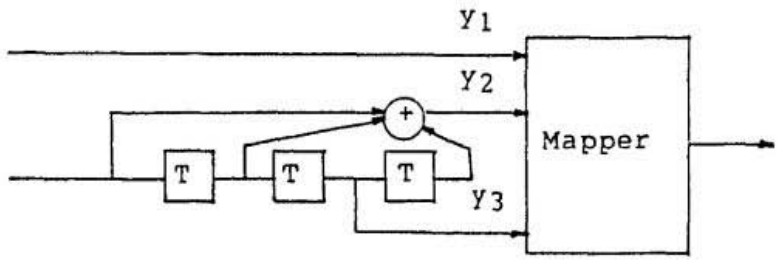

(c) Optimum rate 2/3, v=3 code

Figure 6.7 Optimum codes for suboptimum coherent phase detection of 8-CPFSK signals with $h \leq 1/8$ on carrier phase offset channels.

Table 6.4 Implementation of self-transparent 8-CPFSK trellis modulation codes with convolutional codes.

Matrix states	Modulation index	Code	Generator
N	h	$[g_1]_8$	$[g_0]_8$
32	1/8	7	2
36	1/9	7	2
64	1/8	1 5	0 2
72	1/9	1 5	0 2
80	1/10	1 5	0 2
128	1/8	3 1	0 2

Consider the state transition matrix of the best self-transparent 16-state 8-CPFSK trellis modulation code given below.

$$\begin{bmatrix}
0 & 7 & 0 & 0 & 1 & 0 & 0 & 0 & 0 & 0 & 0 & 3 & 0 & 0 & 0 & -5 \\
0 & 0 & 7 & 0 & 0 & 1 & 0 & 0 & -5 & 0 & 0 & 0 & 3 & 0 & 0 & 0 \\
0 & 0 & 0 & 7 & 0 & 0 & 1 & 0 & 0 & -5 & 0 & 0 & 0 & 3 & 0 & 0 \\
0 & 0 & 0 & 0 & 7 & 0 & 0 & 1 & 0 & 0 & -5 & 0 & 0 & 0 & 3 & 0 \\
1 & 0 & 0 & 0 & 0 & 7 & 0 & 0 & 0 & 0 & 0 & -5 & 0 & 0 & 0 & 3 \\
0 & 1 & 0 & 0 & 0 & 0 & 7 & 0 & 3 & 0 & 0 & 0 & -5 & 0 & 0 & 0 \\
0 & 0 & 1 & 0 & 0 & 0 & 0 & 7 & 0 & 3 & 0 & 0 & 0 & -5 & 0 & 0 \\
7 & 0 & 0 & 1 & 0 & 0 & 0 & 0 & 0 & 0 & 3 & 0 & 0 & 0 & -5 & 0 \\
0 & 0 & 5 & 0 & 0 & 0 & -3 & 0 & -7 & 0 & 0 & 0 & 1 & 0 & 0 & 0 \\
0 & 0 & 0 & 5 & 0 & 0 & 0 & -3 & 0 & -7 & 0 & 0 & 0 & 1 & 0 & 0 \\
-3 & 0 & 0 & 0 & 5 & 0 & 0 & 0 & 0 & 0 & -7 & 0 & 0 & 0 & 1 & 0 \\
0 & -3 & 0 & 0 & 0 & 5 & 0 & 0 & 0 & 0 & 0 & -7 & 0 & 0 & 0 & 1 \\
0 & 0 & -3 & 0 & 0 & 0 & 5 & 0 & 1 & 0 & 0 & 0 & -7 & 0 & 0 & 0 \\
0 & 0 & 0 & -3 & 0 & 0 & 0 & 5 & 0 & 1 & 0 & 0 & 0 & -7 & 0 & 0 \\
5 & 0 & 0 & 0 & -3 & 0 & 0 & 0 & 0 & 0 & 1 & 0 & 0 & 0 & -7 & 0 \\
0 & 5 & 0 & 0 & 0 & -3 & 0 & 0 & 0 & 0 & 0 & 1 & 0 & 0 & 0 & -7
\end{bmatrix} \tag{6.2}$$

The above state transition matrix can be implemented with the rate-1/2 convolutional code of Figure 6.7(a) followed by the natural binary mapping rule and an 8-CPFSK modulator with $h = 1/8$. The states S_0 and S_1 are represented by the binary contents of the delay units of the convolutional code. This matches the best rate-1/2, constraint length two convolutional coded 8-CPFSK found in the literature [75]. Therefore, the best 16-state 8-CPFSK trellis modulation code is also the best self-transparent code. The above trellis modulation code achieves a coding gain of 3.927 dB relative to general 8-CPFSK with $h = 1/8$. However, it is inferior to MSK signalling because it has a minimum squared Euclidean distance of only 1.477. Table 6.4 lists different implementations of selected self-transparent 8-CPFSK trellis modulation codes with convolutional codes followed by the natural binary mapping onto 8-CPFSK. Similar to 4-CPFSK, only the natural binary mapping rule was consistent with the rotational invariance property.

Figure 6.8 State transition matrix for optimal self-transparent 8-CPFSK trellis modulation codes when $h \leqslant 1/8$.

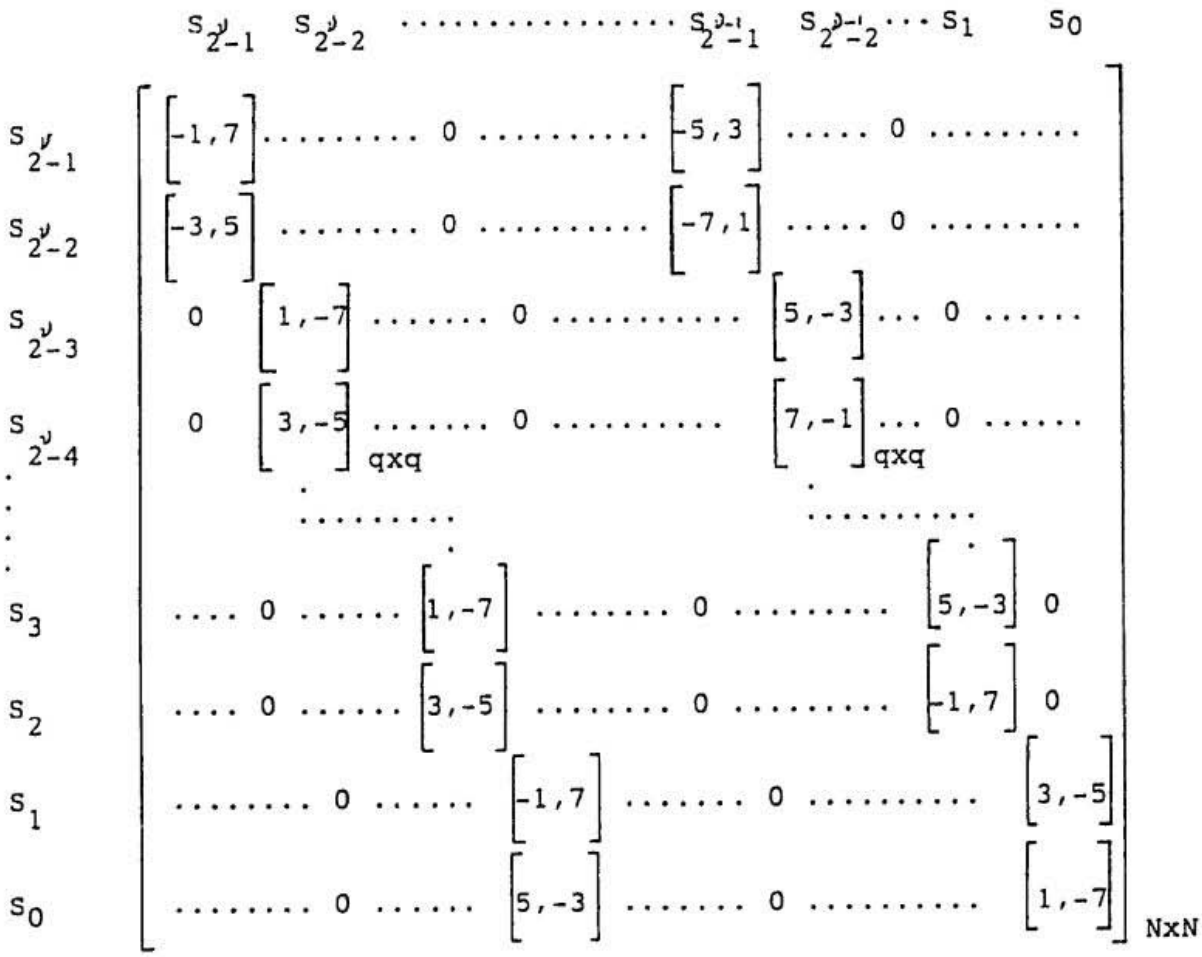

Based on the above findings, it is possible to identify a generalised state transition matrix that may be used to construct self-transparent 8-CPFSK trellis modulation codes for the carrier phase offset channel. The generalised state transition matrix is given in Fig. 6.8 and it is valid for self-transparent 8-CPFSK trellis modulation codes with any even number of states and $h \leq 1/8$. We conclude that the best self-transparent 8-CPFSK trellis modulation codes are also based on convolutional outer codes.

6.4 Distance properties of CPFSK trellis modulation codes on carrier phase offset channels

An important property of the equivalent distance used in suboptimum coherent detection of CPFSK trellis modulation codes was evident during the code search. In AWGN channels it is well known that the squared Euclidean distance is strictly greater than zero for all error events irrespective of their length. In other words, the squared Euclidean distance grows monotonically with time along the length of the error event. Unfortunately, this does not hold true for the suboptimum equivalent distance derived for the carrier phase offset channel. For small carrier phase offset values, the equivalent distance remained nondecreasing for all error events. For example, in the case of optimum rate 1/2, ν=1 4-CPFSK trellis modulation code, the equivalent distance retained its nondecreasing property for all $h \leq 1/4$ and $\theta \leq 5°$. In rate 1/2, ν=2 4-CPFSK trellis modulation codes the equivalent distances were positive for all error events until $\theta \approx 2.5°$. In general, for $h \leq 1/4$ 4-CPFSK trellis modulation codes the equivalent distance remained nondecreasing for all memory lengths considered in the study only below $\theta \approx 2.5°$.

Table 6.5 Minimum equivalent distance for 4-CPFSK trellis modulation codes with h=1/4 on carrier phase offset channels.

θ	v=1			v=2			v=3		
deg	MED	m	N_R	MED	m	N_R	MED	m	N_R
0	3.000	3	3	5.000	4	10	6.000	6	16
1	2.964	3	3	4.964	4	11	5.928	6	16
2	2.927	3	3	4.924	4	11	5.853	6	16
3	2.887	3	3	4.882	4	11	5.774	6	16
4	2.846	3	3	4.836	4	11	5.692	6	16
5	2.803	3	3	4.788	4	11	5.606	6	16
6	2.758	3	3	4.736	4	11	5.516	6	16
7	2.712	3	3	4.682	4	11	5.423	6	16
8	2.663	3	3	4.624	4	11	5.327	6	16
9	2.613	3	3	4.564	4	11	5.227	6	16
10	2.562	3	3	4.501	4	14	5.123	6	20
11	2.508	3	3	4.435	4	14	5.016	6	20
12	2.453	3	3	4.366	4	14	4.906	6	20
13	2.396	3	3	4.294	4	14	4.793	6	20
14	2.338	3	3	4.219	4	17	4.676	6	24
15	2.278	3	3	4.142	4	17	4.556	6	24
16	2.216	3	3	4.061	4	17	4.433	6	24
17	2.153	3	3	3.978	4	20	4.306	6	28
18	2.088	3	3	3.893	4	23	4.177	6	32
19	2.022	3	3	3.804	4	26	4.044	6	36
20	1.954	3	3	3.713	4	32	3.908	6	44
21	1.885	3	3	3.619	4	38	3.769	6	52
22	1.814	3	3	3.523	4	53	3.628	6	72
23	1.742	3	3	3.424	4	89	3.483	6	120
24	1.668	3	3	3.322	4	368	3.336	6	492

Table 6.5 (Contd.) Minimum equivalent distance for 4-CPFSK trellis modulation codes with h=1/4 on carrier phase offset channels.

θ	v=4			v=5			v=6		
deg	MED	m	N_R	MED	m	N_R	MED	m	N_R
0	7.000	8	18	7.000	7	15	8.000	12	24
1	6.893	8	18	6.963	7	19	7.928	12	24
2	6.782	8	18	6.922	7	19	7.851	12	24
3	6.667	8	18	6.876	7	19	7.769	12	24
4	6.547	8	18	6.826	7	19	7.682	12	24
5	6.424	8	18	6.772	7	19	7.590	12	24
6	6.296	8	18	6.714	7	22	7.494	12	25
7	6.164	8	18	6.652	7	22	7.393	12	25
8	6.029	8	18	6.585	7	22	7.288	12	25
9	5.889	8	18	6.515	7	22	7.177	12	25
10	5.745	8	21	6.368	10	26	7.062	12	31
11	5.598	8	21	6.180	10	26	6.943	12	31
12	5.447	8	21	5.987	10	26	6.819	12	36
13	5.291	8	21	5.790	10	26	6.690	12	36
14	5.133	8	21	5.589	10	30	6.503	17	39
15	4.970	8	25	5.384	10	30	6.213	17	39
16	4.804	8	25	5.175	10	30	5.918	17	39
17	4.634	8	28	4.962	10	34	5.618	17	43
18	4.461	8	32	4.745	10	38	5.313	17	50
19	4.284	8	35	4.524	10	42	5.004	17	53
20	4.104	8	42	4.299	10	50	4.690	17	64
21	3.920	8	49	4.070	10	58	4.371	17	71
22	3.733	8	67	3.838	10	78	4.048	17	95
23	3.543	8	109	3.602	10	126			
24	3.349	8	434	3.363	10	498			

Table 6.6 Minimum equivalent distances for 4-CPFSK trellis modulation codes with h=1/5 on carrier phase offset channels.

θ deg	v=1			v=2			v=3		
	MED	m	N_R	MED	m	N_R	MED	m	N_R
0	2.500	3	3	3.618	3	10	4.309	4	14
1	2.487	3	3	3.576	3	10	4.275	4	14
2	2.472	3	3	3.532	3	10	4.237	4	14
3	2.455	3	3	3.485	3	10	4.198	4	16
4	2.437	3	3	3.436	5	13	4.155	4	18
5	2.418	3	3	3.386	5	13	4.110	4	18
6	2.397	3	3	3.333	5	13	4.063	4	18
7	2.374	3	3	3.278	5	13	4.013	4	20
8	2.350	3	3	3.220	5	13	3.960	4	20
9	2.325	3	3	3.161	5	16	3.905	6	24
10	2.298	3	3	3.100	5	16	3.779	6	24
11	2.270	3	3	3.036	5	16	3.642	6	28
12	2.240	3	3	2.971	5	19	3.502	6	28
13	2.208	3	3	2.904	5	22	3.359	6	32
14	2.176	3	3	2.834	5	22	3.214	6	36
15	2.142	3	3	2.763	5	31	3.066	6	44
16	2.106	3	3	2.690	5	37	2.916	6	52
17	2.069	3	3	2.614	5	55	2.763	6	76
18	2.031	3	3	2.537	5	109	2.608	6	148

Table 6.6 (Contd.) Minimum equivalent distances for 4-CPFSK trellis modulation codes with h=1/5 on carrier phase offset channels.

θ deg	v=4			v=5			v=6		
	MED	m	N_R	MED	m	N_R	MED	m	N_R
0	5.000	5	15	5.691	6	18	6.118	8	23
1	4.932	5	15	5.590	6	19	6.021	8	23
2	4.861	5	15	5.485	6	19	5.921	8	23
3	4.787	5	18	5.377	6	22	5.817	8	23
4	4.710	5	18	5.265	6	22	5.710	8	24
5	4.630	5	18	5.150	6	22	5.598	8	24
6	4.548	5	18	5.032	6	22	5.484	8	27
7	4.462	5	20	4.911	6	25	5.360	7	28
8	4.373	5	20	4.786	6	25	5.199	7	28
9	4.282	5	25	4.658	6	30	5.035	7	32
10	4.119	8	25	4.459	10	30	4.798	12	32
11	3.944	8	27	4.247	10	33	4.550	12	38
12	3.767	8	27	4.032	10	33	4.298	12	38
13	3.587	8	32	3.814	10	38	4.042	12	40
14	3.404	8	34	3.593	10	41	3.783	12	43
15	3.218	8	41	3.369	10	49	3.521	12	53
16	3.029	8	48	3.142	10	57	3.255	12	61
17	2.838	8	69	2.912	10	81	2.987	12	85
18	2.644	8	132	2.680	10	166	2.715	12	164

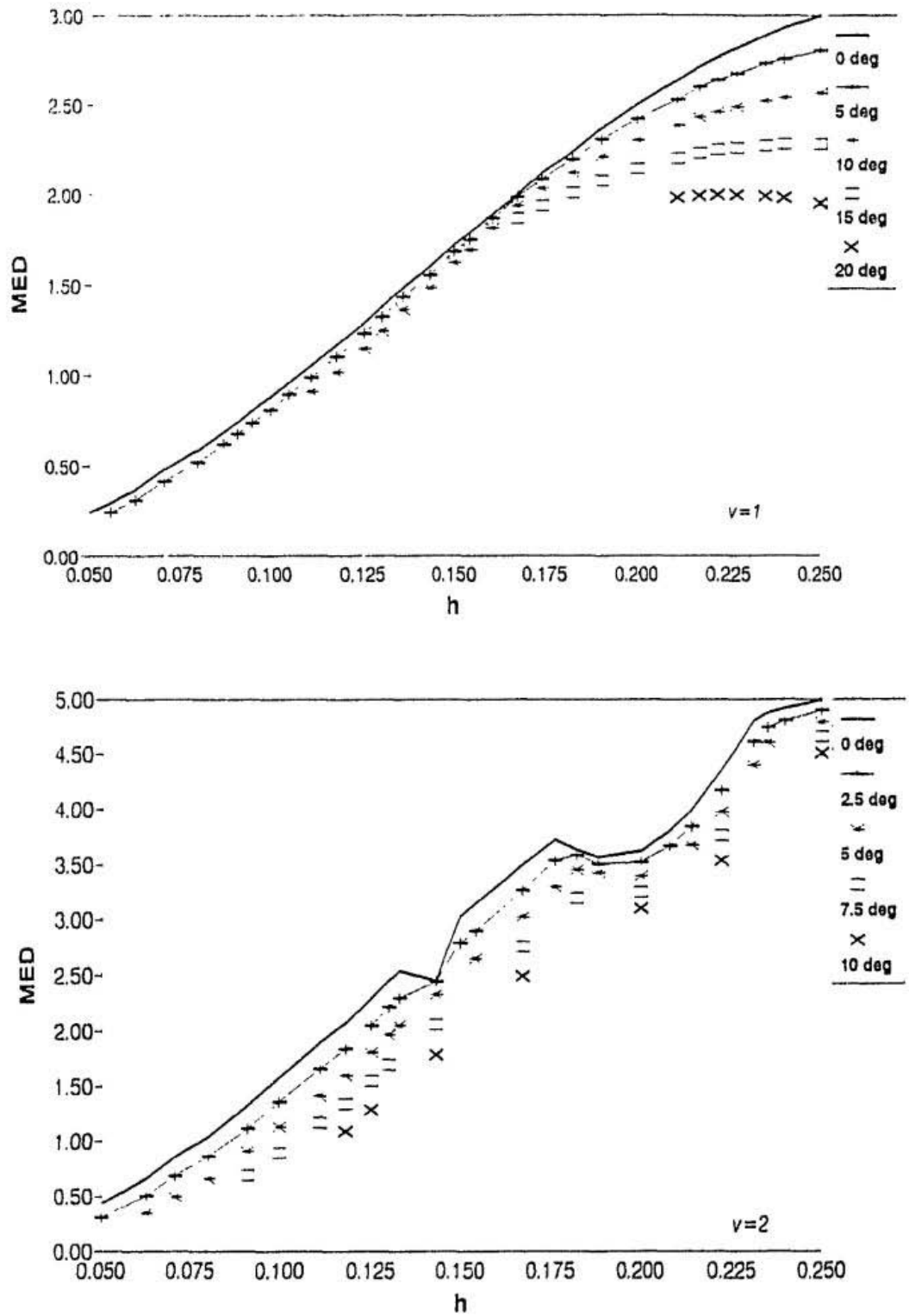

Figure 6.9 Minimum equivalent distance versus modulation index for 4-CPFSK trellis modulation codes on carrier phase offset channels.

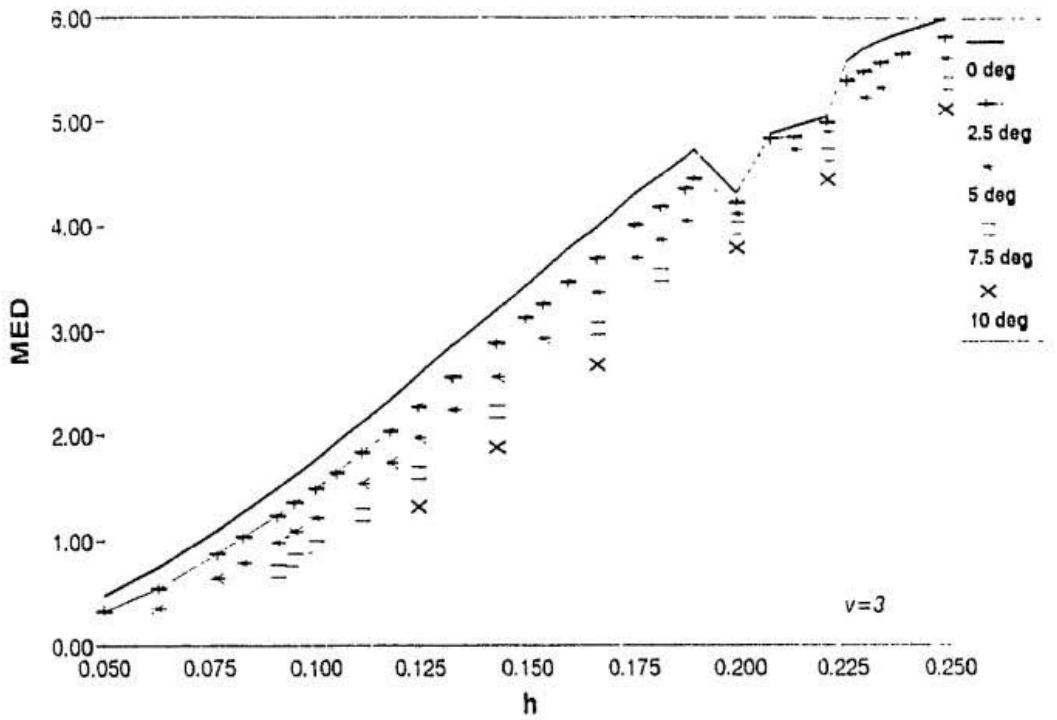

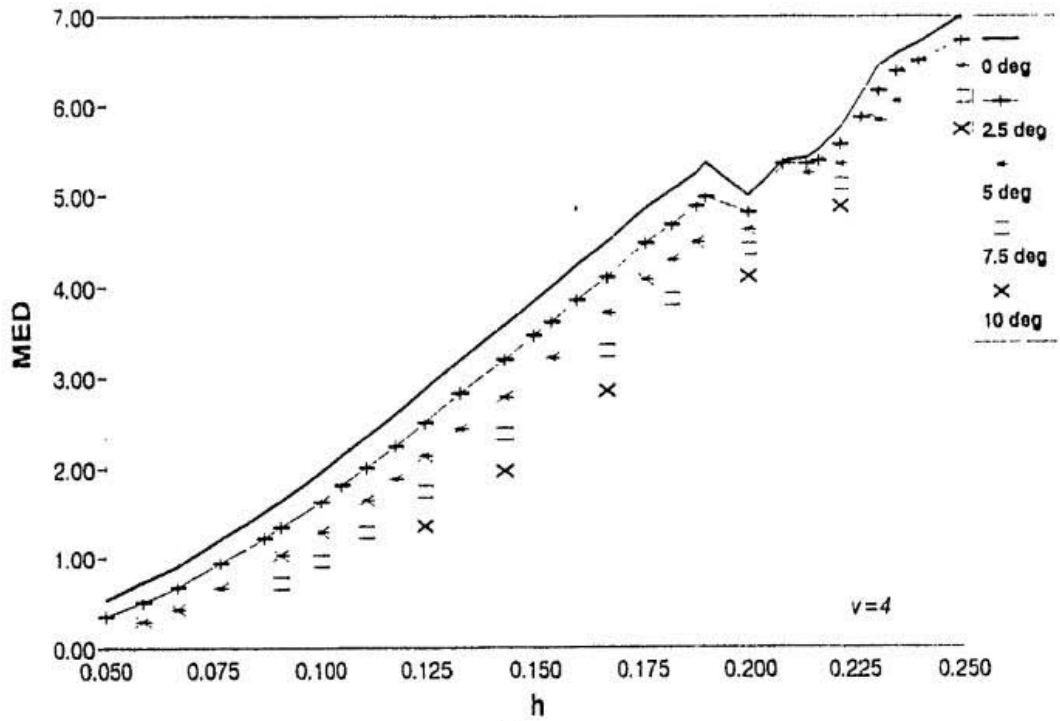

Figure 6.9 (Contd.) Minimum equivalent distance v^s modulation index for 4-CPFSK trellis modulation codes on carrier phase offset channels.

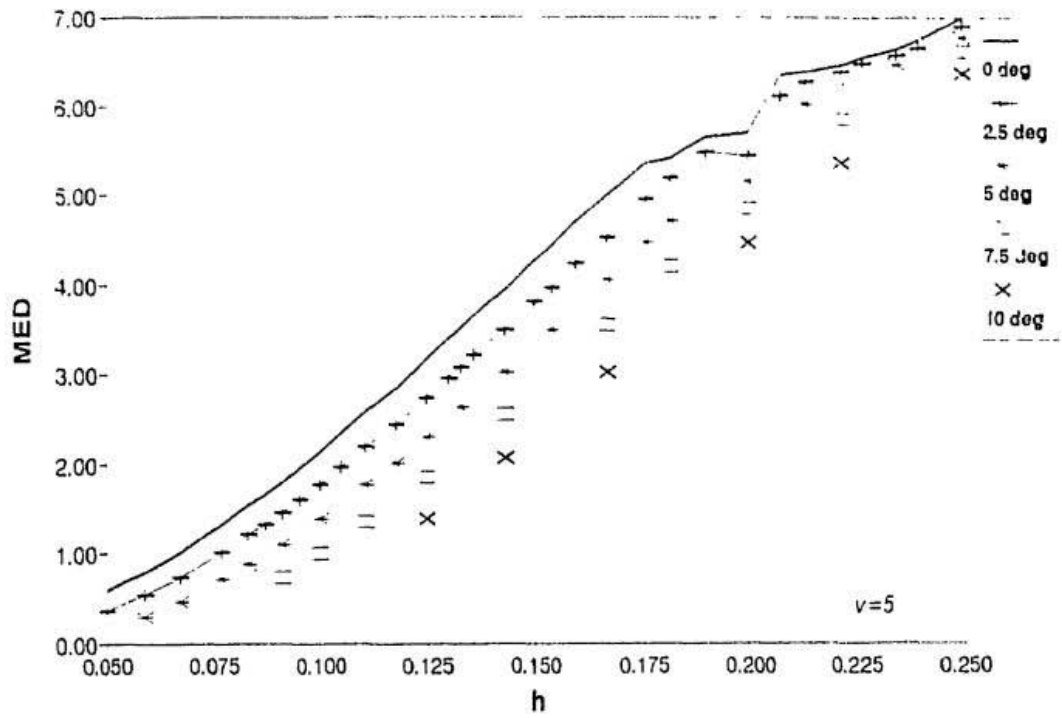

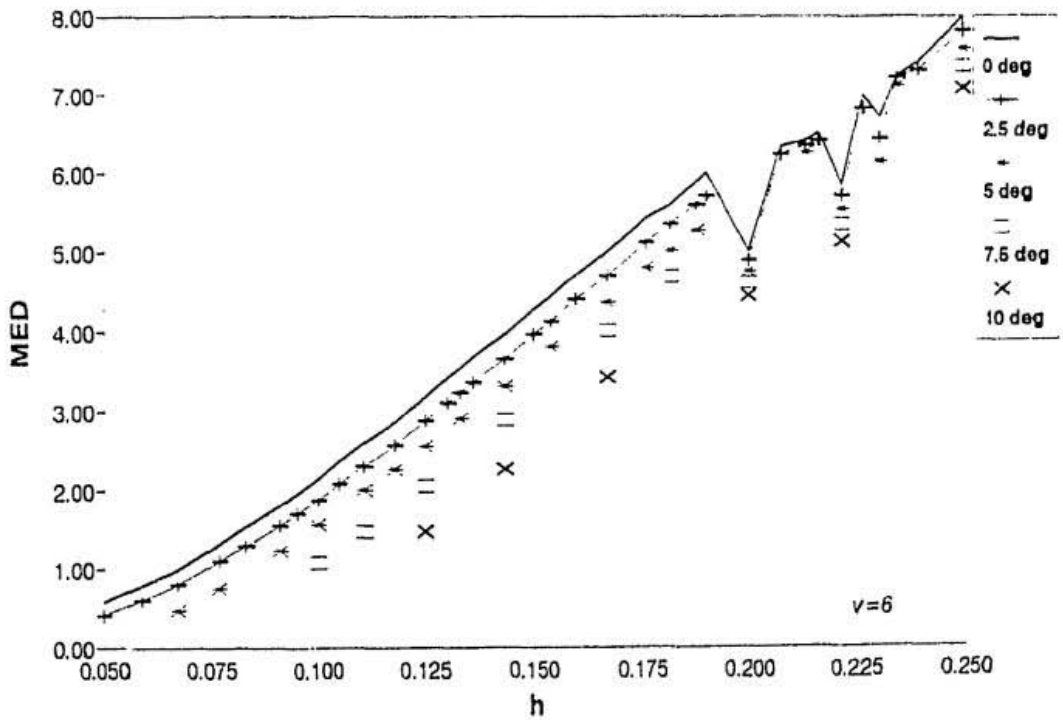

Figure 6.9 (Contd.) Minimum equivalent distance vs modulation index for 4-CPFSK trellis modulation codes on carrier phase offset channels.

6.4.1 Numerical results

Numerical values for the minimum squared equivalent distance (MED) for suboptimum coherent detection of 4-CPFSK trellis modulation codes with $h = 1/4$ is given in Table 6.5. Recall m is the length of the minimum distance error event and N_R is the receiver path memory. The optimum code given in Fig. 6.2(a) was used to encode the 4-CPFSK signal. The maximum carrier phase offset θ_{max} with this scheme is 24° for memory lengths $1 \leq \nu \leq 5$. When $\nu = 6$, θ_{max} reduces to 22°. The memory length and hence the minimum distance error event remains the same for $\nu = 1, 2, 3, 4$. For $\nu = 5$, beyond $\theta = 10°$ a different error event gives the minimum distance. For $\nu = 6$ a different minimum distance error event occurs only after $\theta = 14°$. Also, it can be seen that the decoder memory or receiver path memory required to ensure all unmerged paths have a larger distance than the minimum distance path increases exponentially as θ_{max} is approached. MEDs for the same code with $h = 1/5$ 4-CPFSK are given in Table 6.6. For $h = 1/5$, θ_{max} reduces to 18.5°. The receiver path memory increases exponentially as θ approaches 18.5°. The maximum receiver path memory allowed by the code search program was 500 levels.

In Fig. 6.9 we have plotted MED versus modulation index for suboptimum coherent detection of 4-CPFSK trellis modulation codes on carrier phase offset channels. The heavy solid line corresponds to the zero phase offset channel or the ideal AWGN channel. The other solid line represents the MED values for $\theta = 5°$ in the case of $\nu = 1$ and, $\theta = 2.5°$ when $2 \leq \nu \leq 6$. Moreover, the continuous line indicates that no locally decreasing error events occur for all rational modulation indexes $h \leq 1/4$. It should be noted, however, that although we connect the points in a continuous line, the minimum equivalent distances are computed

only at rational value modulation indexes and consequently the curve is inherently discontinuous. The distances obtained for $\theta = 0°$ (AWGN) are not the same as for correlation detection because the equivalent distance defined in (5.53) is applicable only to suboptimum coherent phase detection of M-CPFSK. The dip in the MED observed in Fig. 6.9 for rate 1/2, $\nu = 2$ code is due to a minimum distance error event of length four occuring at $h = 1/7$. Another gradual reduction in MED is seen around $h = 1/5$ owing to a minimum distance error event of length three. The MEDs for optimum 8-CPFSK trellis modulation codes with $h = 1/8$ and $h = 1/10$ on carrier phase offset channels are given in Table 6.7 and Table 6.8, respectively. For both the cases rate 2/3, $\nu = 1$ code behaves differently from $\nu = 2$ and $\nu = 3$ codes. This is because the connectivity of the trellis at $\nu = 1$ is more than for larger memory length codes. The minimum distance error event is of length three in the case of $\nu = 1$, and of length four when $\nu = 2$ and $\nu = 3$. For the $\nu = 1$ code, the maximum carrier phase offset before equivalent distance becomes negative is $\theta_{max} = 5°$ and this value increases to $\theta_{max} = 11°$ for $\nu = 2$ and $\nu = 3$ codes. For $h = 1/8$, the same error event produces the minimum distance for all three memory lengths considered. As θ_{max} is approached the receiver path memory increases exponentially. In the case of 8-CPFSK, the receiver path memory is limited to 100 levels in the code search program. Variation of MED against modulation index for rate 2/3, ν= 1, 2, 3, 8-CPFSK trellis modulation codes on carrier phase offset channels is shown in Fig. 6.10.

The variation of receiver path memory (N_R) with carrier phase offset for suboptimum coherent phase detection of 4-CPFSK with $h = 1/4$ and $h = 1/8$ is shown in Fig. 6.11. For rate 1/2, $\nu = 1$ codes the receiver path memory remains constant until the carrier phase offset reaches the critical angle θ_{max}, while for other memory lengths N_R grows exponentially as θ_{max} is approached. The critical angle for rate

1/2. $\nu = 1, 2, 3, 4, 5$ coding of 4-CPFSK signals with $h \leq 1/4$ is 24°. Fig. 6.12 shows the variation of receiver path memory for suboptimum coherent detection of 8-CPFSK trellis modulation codes with $h = 1/8$ and $h = 1/10$. θ_{max} values for 8-CPFSK trellis modulation codes are substantially less than θ_{max} values for 4-CPFSK trellis modulation codes for small modulation indexes. Maximum carrier phase offsets (critical angles) tolerable with suboptimum coherent phase detection of CPFSK trellis modulation codes with small modulation indexes are summarized in Tables 6.9 and 6.10. The equivalent minimum distance derived in (5.53) cannot be used to evaluate performance above the critical angles because the squared distance becomes negative and causes error events to have decreasing distances. Also, it was seen that larger the denominator q of the rational value modulation index, smaller the critical angles would be. When q is large the code is more complex and the number of different possible error events is also increased. On the basis of minimum equivalent distance results 8-CPFSK trellis modulation codes are more sensitive to carrier phase offsets than 4-CPFSK trellis modulation codes. However, the above results are valid only for decoding with an ideal phase detector on an AWGN channel with constant carrier phase offsets.

Table 6.7 Minimum equivalent distances for 8-CPFSK trellis modulation codes with h=1/8 on carrier phase offset channels.

θ	v=1			v=2			v=3		
deg	MED	m	N_R	MED	m	N_R	MED	m	N_R
0.0	2.586	3	3	4.000	2	11	4.000	2	12
0.5	2.466	3	3	3.999	2	11	3.999	2	12
1.0	2.344	3	3	3.998	2	11	3.998	2	12
1.5	2.221	3	3	3.997	2	14	3.997	2	16
2.0	2.097	3	3	3.995	2	14	3.995	2	16
2.5	1.971	3	3	3.992	2	14	3.992	2	16
3.0	1.844	3	3	3.989	2	17	3.989	2	20
3.5	1.715	3	3	3.907	4	17	3.985	2	20
4.0	1.585	3	3	3.808	4	17	3.981	2	20
4.5	1.454	3	3	3.708	4	17	3.975	2	24
5.0	1.321	3	3	3.607	4	17	3.942	6	24
5.5				3.506	4	20	3.815	6	28
6.0				3.404	4	20	3.687	6	28
6.5				3.301	4	20	3.559	6	28
7.0				3.198	4	23	3.430	6	32
7.5				3.094	4	23	3.300	6	36
8.0				2.989	4	26	3.170	6	36
8.5				2.884	4	29	3.039	6	40
9.0				2.779	4	35	2.908	6	48
9.5				2.673	4	41	2.776	6	56
10.0				2.566	4	53	2.643	6	72
10.5				2.459	4	74	2.510	6	100
11.0				2.351	4	146	2.376	6	196

Table 6.8 Minimum equivalent distances for 8-CPFSK trellis modulation codes with h=1/10 on carrier phase offset channels.

θ	v=1			v=2			v=3		
deg	MED	m	N_R	MED	m	N_R	MED	m	N_R
0.0	1.764	3	3	3.146	4	14	3.528	6	20
0.5	1.656	3	3	3.059	4	14	3.420	6	20
1.0	1.547	3	3	2.971	4	14	3.312	6	20
1.5	1.437	3	3	2.883	4	17	3.203	6	24
2.0	1.326	3	3	2.794	4	17	3.094	6	24
2.5	1.214	3	3	2.705	4	17	2.984	6	24
3.0	1.101	3	3	2.616	4	17	2.874	6	24
3.5	0.988	3	3	2.526	4	17	2.763	6	24
4.0	0.873	3	3	2.436	4	20	2.652	6	28
4.5	0.758	3	3	2.345	4	20	2.540	6	28
5.0				2.254	4	20	2.428	6	28
5.5				2.162	4	23	2.315	6	32
6.0				2.070	4	26	2.202	6	36
6.5				1.978	4	29	2.089	6	40
7.0				1.885	4	35	1.975	6	48
7.5				1.792	4	41	1.861	6	56
8.0				1.699	4	56	1.746	6	76
8.5				1.605	4	95	1.631	6	128
9.0				1.510	4	479	1.515	6	>500

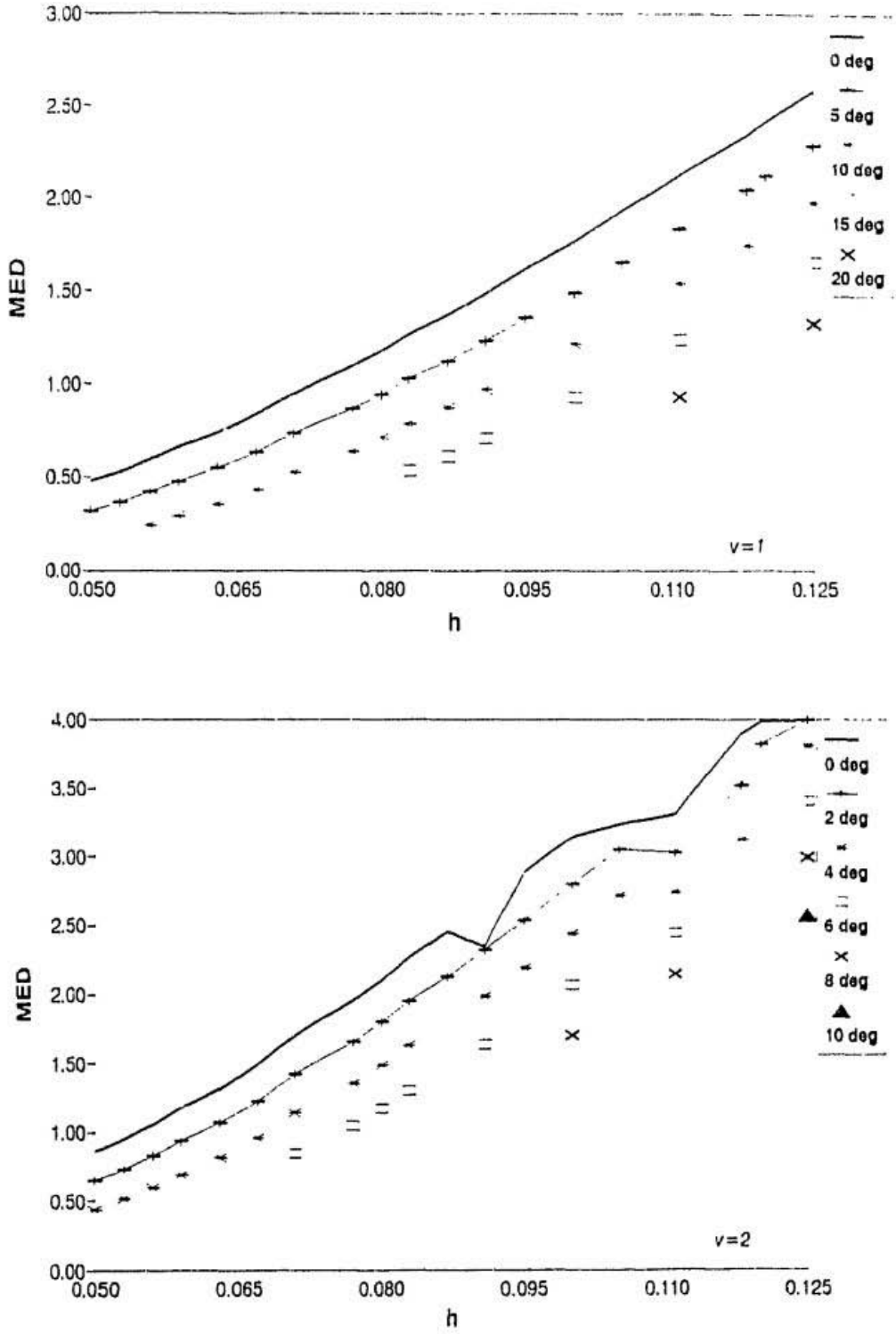

Figure 6.10 Minimum equivalent distance v^s modulation index for 8-CPFSK trellis modulation codes on carrier phase offset channels.

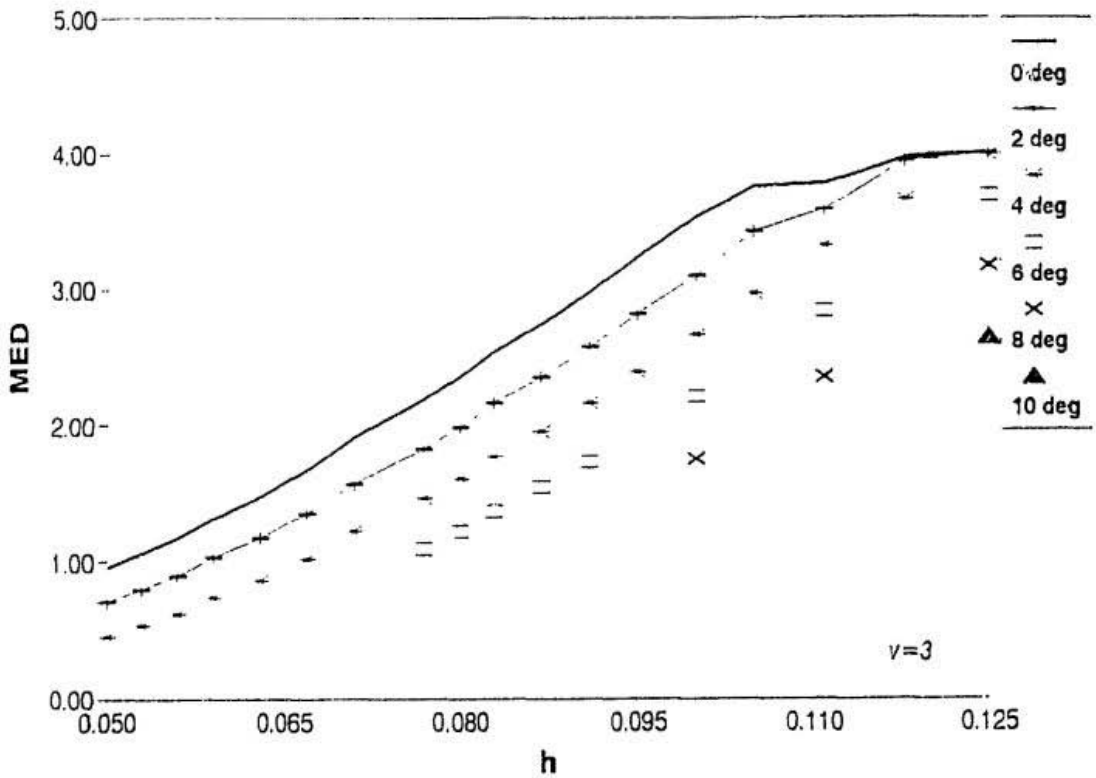

Figure 6.10(Contd.) Minimum equivalent distance v^s modulation index for 8-CPFSK trellis modulation codes on carrier phase offset channels.

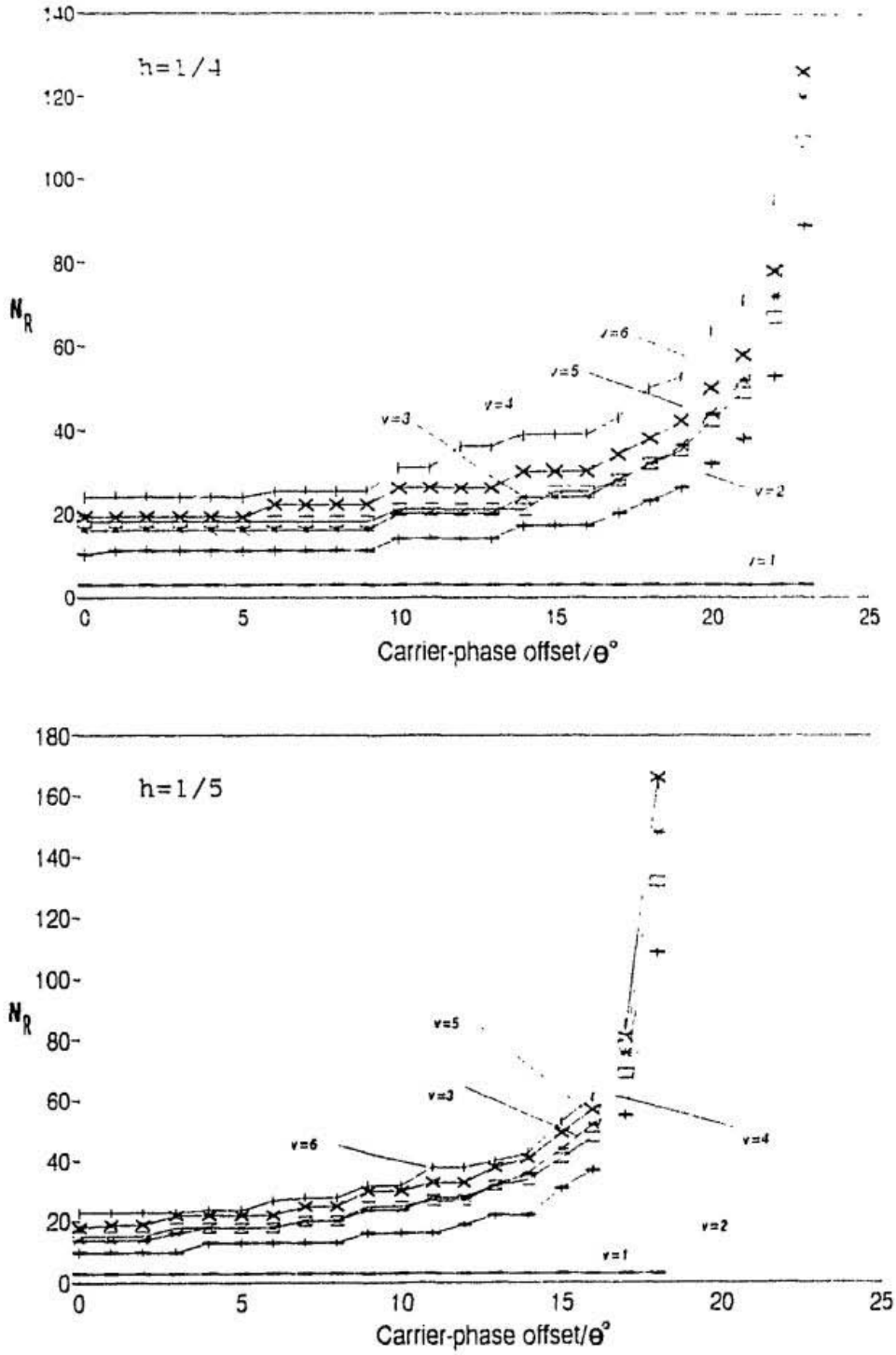

Figure 6.11 Receiver path memory v^S carrier phase offset for 4-CPFSK trellis modulation codes.

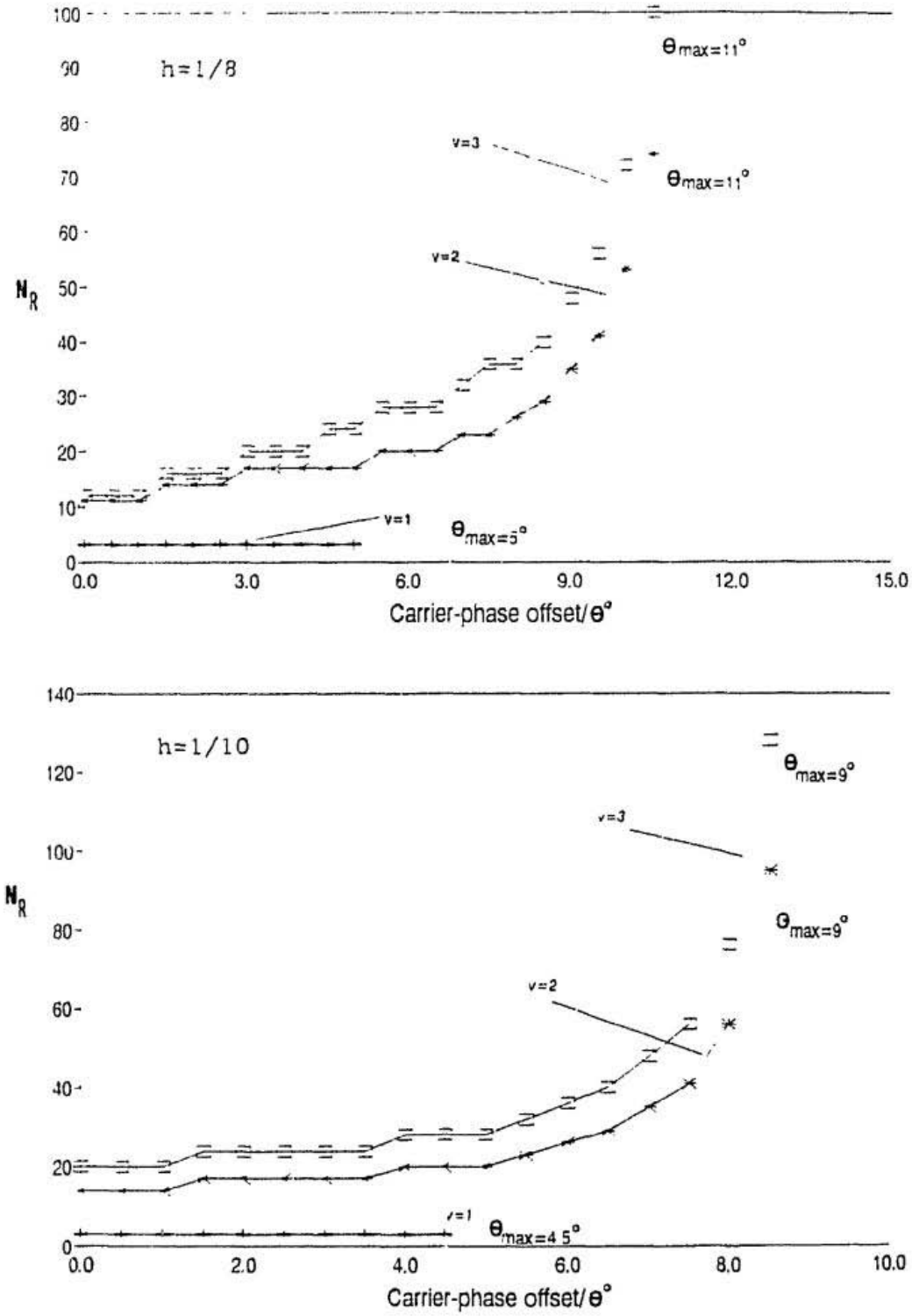

Figure 6.12 Receiver path memory v^s carrier phase offset for 8-CPFSK trellis modulation codes.

Table 6.9 Critical angles for suboptimum coherent detection of 4-CPFSK trellis modulation codes on carrier phase offset channels.

h	θ°_{max}					
	v=1	v=2	v=3	v=4	v=5	v=6
1/4	24.0	24.0	24.0	24.0	24.0	24.0
1/5	18.5	18.5	18.5	18.5	18.5	18.5
1/6	15.5	15.5	15.5	15.5	15.5	15.5
1/7	13.0	13.0	13.0	13.0	13.0	13.0
1/8	11.0	11.0	11.0	11.0	11.0	11.0

Table 6.10 Critical angles for suboptimum coherent detection of 8-CPFSK trellis modulation codes on carrier phase offset channels.

h	θ°_{max}		
	v=1	v=2	v=3
1/8	5.0	11.0	11.0
1/9	5.0	10.0	10.0
1/10	4.5	9.0	9.0
1/11	4.0	8.0	8.0
1/12	3.5	7.5	7.5

6.5 Conclusions

In this chapter we have considered suboptimum coherent detection of CPFSK trellis modulation codes on AWGN channels with carrier phase offset. An equivalent distance that takes phase offsets into account derived in Chapter 5 was used in the Viterbi algorithm to decode the signal. It was found that, this distance cannot be used for large phase offset values because, then error events with locally decreasing minimum distances occur. A computer search for the best self-transparent 4-CPFSK and 8-CPFSK trellis modulation codes was also carried out. The best codes for the carrier phase offset channel were identical with those found in the literature for AWGN channels, except when the memory length of the trellis code was one. 8-CPFSK trellis modulation codes were found to be more sensitive to carrier phase offsets than 4-CPFSK trellis modulation codes.

Chapter 7

Performance Evaluation of CPFSK Trellis Modulation Codes on Multipath Fading Channels

7.1 Introduction

Performance evaluation of suboptimum coherent detection of CPFSK trellis modulation codes on multipath fading channels is considered in this chapter. Specifically, the performance is evaluated on a mobile satellite channel, which is modelled as a Rician distributed fading channel with a steady line-of-sight component. The fading conditions on such channels are less severe than in land-mobile communication channels and therefore permits pilot tone or pilot symbol assisted coherent detection of CPFSK signals. Instead of the error probability criterion, the channel cutoff rate described in Chapter 5 is used as the performance measure. Cutoff rate bounds are computed for suboptimum coherent detection of 4-CPFSK, 8-CPFSK, and 16-CPFSK signals. The results are compared with cutoff rates for PSK signals on AWGN channels and Rician fading channels. They provide useful information about the relative performance of CPFSK trellis modulation codes under different fading channel conditions.

7.2 R_0 calculation for PSK

The cutoff rate R_0 for a general interleaved channel with amplitude-only fading was derived in Section 5.6. Here we specialize the above results to coherent detection of PSK signals on AWGN channels.

The PSK modulation scheme is a memoryless scheme: therefore calculation of R_0 for PSK is easier than the calculation of R_0 for signalling schemes with memory, such as CPFSK.

In the case of AWGN channels (5.62) reduces to

$$R_0 = -\log_2 \frac{1}{M^2} \sum_{i=1}^{M} \sum_{j=1}^{M} e^{-d^2\{s_i(t), s_j(t)\}/4\sigma^2}. \tag{7.1}$$

where $s_i(t)$ and $s_j(t)$ are randomly selected M-ary PSK signals (corresponding to channel signals x_n and x'_n) which are assumed to be equiprobable.

Let

$$s_i(t) = \sqrt{\frac{2E_s}{T}} \cos\left(2\pi f_0 t + \frac{\pi}{M} x_i\right), \; i = \overline{1, M} \tag{7.2}$$

and

$$s_j(t) = \sqrt{\frac{2E_s}{T}} \cos\left(2\pi f_0 t + \frac{\pi}{M} x_j\right), \; j = \overline{1, M}, \tag{7.3}$$

where x_i and x_j can take any value of the M-ary set

$$\{(2n - M - 1), \; n = \overline{1, M}\} = \{\pm 1, \pm 3, \ldots, \pm(M-1)\}.$$

The squared Euclidean distance d_{ij}^2 between $s_i(t)$ and $s_j(t)$ is given by

$$\begin{aligned}
d_{ij}^2 &= \frac{2E_s}{T} \int_0^T \left[\cos\left\{2\pi f_0 t + \frac{\pi}{M}(2i - M - 1)\right\} - \cos\left\{2\pi f_0 t + \frac{\pi}{M}(2j - M - 1)\right\}\right]^2 dt \\
&= \frac{2E_s}{T} \int_0^T \left[\cos^2\left\{2\pi f_0 t + \frac{\pi}{M}(2i - M - 1)\right\} + \cos^2\left\{2\pi f_0 t + \frac{\pi}{M}(2j - M - 1)\right\}\right. \\
&\quad \left. -2\cos\left\{2\pi f_0 t + \frac{\pi}{M}(2i - M - 1)\right\} \cos\left\{2\pi f_0 t + \frac{\pi}{M}(2j - M - 1)\right\}\right] dt \\
&= \frac{2E_s}{T} \int_0^T \left[\frac{1}{2}\left\{2 + \cos\left\{4\pi f_0 t + \frac{2\pi}{M}(2i - M - 1)\right\} + \cos\left\{4\pi f_0 t + \frac{2\pi}{M}(2j - M - 1)\right\}\right\}\right. \\
&\quad \left. - \cos\left\{\frac{2\pi}{M}(i - j)\right\} - \cos\left\{4\pi f_0 t + \frac{2\pi}{M}(i - j - M - 1)\right\}\right] dt
\end{aligned}$$

Assuming $f_0 >> \frac{1}{T}$, we have

$$\begin{aligned} d_{ij}^2 &= \frac{2E_s}{T}\int_0^T \{1-\cos\frac{2\pi}{M}(i-j)\}dt, \\ &= 2E_s\{1-\cos\frac{2\pi}{M}(i-j)\}. \end{aligned} \tag{7.4}$$

By substituting d_{ij}^2 in (7.1) we can obtain the expression for R_0 for coherent detection of M-PSK signals on AWGN channels.

$$R_{0(PSK)} = -\log_2 \frac{1}{M^2}\sum_{i=1}^{M}\sum_{j=1}^{M} e^{-\frac{E_s}{2\sigma^2}\{1-\cos\frac{2\pi}{M}(i-j)\}} \tag{7.5}$$

When calculating R_0 for PSK signalling on Rician fading channels, the exponential term in the right hand side of (7.1) has to be averaged over the fading amplitude. The fading amplitude ρ has a Rician distribution given by [36]

$$p(\rho) = 2\rho(1+K)e^{-K-(1+K)\rho^2} I_0[2\rho\sqrt{K(1+K)}];\ \ \rho \geq 0, \tag{7.6}$$

where $I_0[.]$ is the zero-order modified Bessel function of the first kind.

Therefore, the cutoff rate R_0 for PSK signalling on Rician fading channels is given by

$$R_0 = -\log_2 \frac{1}{M^2}\sum_{i=1}^{M}\sum_{j=1}^{M}\int_0^\infty e^{-\frac{1}{4\sigma^2}\rho^2 d_{ij}^2} p(\rho)d\rho, \tag{7.7}$$

where $d_{ij}^2 = 2E_s\{1-\cos\frac{2\pi}{M}(i-j)\}$.

The integral in the above expression for R_0 can be evaluated as follows:

$$\begin{aligned} \mathcal{I} &= \int_0^\infty e^{-\frac{1}{4\sigma^2}\rho^2 d_{ij}^2} p(\rho)d\rho, \\ &= \int_0^\infty e^{-\frac{1}{4\sigma^2}\rho^2 d_{ij}^2} 2\rho(1+K)e^{-\{K+(1+K)\rho^2\}} I_0[2\rho\sqrt{K(K+1)}]d\rho. \end{aligned} \tag{7.8}$$

Since the modified Bessel function of first kind of order ν, $I_\nu(\rho)$, is related to Bessel function of order ν through $I_\nu[\rho] = (\sqrt{-1})^{-\nu} J_\nu[(\sqrt{-1})\rho]$, we have

$$\begin{aligned} \mathcal{I} &= \int_0^\infty e^{-\frac{1}{4\sigma^2}\rho^2 d_{ij}^2} 2\rho(1+K)e^{-K+(1+K)\rho^2} J_0[(\sqrt{-1})\,2\rho\sqrt{K(1+K)}]d\rho, \\ &= 2(1+K)e^{-K}\int_0^\infty \rho e^{-(1+K+d_{ij}^2)\rho^2} J_0[(\sqrt{-1})2\rho\sqrt{K(1+K)}]d\rho. \end{aligned} \tag{7.9}$$

From tables of integrals for Bessel functions of order ν [1],

$$\int_0^\infty \rho^{\nu+1} e^{-\alpha^2\rho^2} J_\nu(\beta\rho)d\rho = \frac{\beta^\nu}{(2\alpha^2)^{\nu+1}} e^{-\beta^2/4\alpha^2}. \tag{7.10}$$

Also, changing $\beta\rho$ to $\sqrt{-1}\beta\rho$ does not affect the convergence of the integral [46] and the integral $\mathcal{I}$ evaluates as:

$$\mathcal{I} = 2(1+K)\frac{1}{2(1+K+d_{ij}^2/4\sigma^2)} e^{-\frac{Kd_{ij}^2/4\sigma^2}{1+K+d_{ij}^2/4\sigma^2}}. \tag{7.11}$$

Therefore, the desired expression for R_0 for coherent detection of PSK signals on Rician fading channels is given by

$$R_{0(PSK)} = -\log_2 \frac{1}{M^2} \sum_{i=1}^{M} \sum_{j=1}^{M} \frac{1+K}{1+K+d_{ij}^2/4\sigma^2} e^{-\frac{Kd_{ij}^2/4\sigma^2}{1+K+d_{ij}^2/4\sigma^2}}, \tag{7.12}$$

where

$$d_{ij}^2/4\sigma^2 = \frac{E_b}{2N_0}\log_2 M\{1-\cos\frac{2\pi}{M}(i-j)\},\ i,j = \overline{1,M}$$

and K is the Rician factor defined as the ratio of coherent to noncoherent power.

7.3 R_0 calculation for CPFSK

Channel cutoff rate calculations for coherent maximum-likelihood detection (correlation detection) of CPFSK signals on AWGN channels can be found in [11]. In suboptimum coherent detection the CPFSK signal is treated as a PSK signal and, therefore, the cutoff rate calculation is similar to PSK signals done in the previous section.

For the classical AWGN channel, R_0 for suboptimum coherent detection of CPFSK signals reduces to

$$R_{0(CPFSK)} = -\log_2 \frac{1}{M^2} \sum_{i=1}^{M} \sum_{j=1}^{M} e^{-d_{ij}^2/4\sigma^2}, \tag{7.13}$$

where d_{ij}^2 is the distance between two CPFSK signals treated as PSK signals.

The transmitted signal for CPFSK signals was given in (3.5) as

$$s(t) = \sqrt{\frac{2E_s}{T}} \cos(2\pi f_0 t + \frac{\pi h x_n t}{T} + o_n). \tag{7.14}$$

It was shown in Chapter 3 that the phase of the CPFSK signal at symbol transition instants, o_n, can take any value of the set

$$\Phi = \{0, 2\pi h, 4\pi h, \ldots, 2(M-1)\pi h\}.$$

An ideal coherent phase detector has exact knowledge of these phase values and, therefore, as far as the trellis decoder is concerned, the CPFSK signal can be represented as a PSK signal, which is mathematically given by

$$s(t) = \sqrt{\frac{2E_s}{T}} \cos(2\pi f_0 t + \frac{\pi h x_n t}{T}), \tag{7.15}$$

where x_n can take any value of the M-ary set $\{(2n - M - 1), n = 1, M\}$.

The Euclidean distance between two such signals

$$s_i(t) = \sqrt{\frac{2E_s}{T}} \cos(2\pi f_0 t + \frac{\pi h x_i t}{T}),$$
$$s_j(t) = \sqrt{\frac{2E_s}{T}} \cos(2\pi f_0 t + \frac{\pi h x_j t}{T}),$$

where x_i and x_j are randomly selected from the M-ary set given above can be written as:

$$d_{ij}^2 = \frac{2E_s}{T} \int_0^T [\cos\{2\pi f_0 t + \frac{\pi h(2i - M - 1)t}{T}\} - \cos\{2\pi f_0 t + \frac{\pi h(2j - M - 1)t}{T}\}]^2 dt. \tag{7.16}$$

Assuming $f_0 >> \frac{1}{T}$, it can be shown that the above equation simplifies to

$$d_{ij}^2 = 2E_s\{1 - \frac{\sin 2\pi h(i-j)}{2\pi h(i-j)}\}. \tag{7.17}$$

This distance can also be deduced from the squared Euclidean distance derived in Appendix for correlation detection of CPFSK signals, by removing the dependence on σ_n and σ_n', which is

$$\begin{aligned} d_{ij}^2 &= 2E_s[1 - \frac{\sin\frac{\pi h\{(2i-M-1)-(2j-M-1)\}}{2}}{\frac{\pi h\{(2i-M-1)-(2j-M-1)\}}{2}} \cos\frac{\pi h\{(2i-M-1)-(2j-M-1)\}}{2}]. \\ &= 2E_s\{1 - \frac{\sin 2\pi h(i-j)}{2\pi h(i-j)}\}. \\ &= 2E_s\{1 - \operatorname{sinc} 2h(i-j)\}. \end{aligned} \tag{7.18}$$

where $\operatorname{sinc} x$ is defined as $\frac{\sin \pi x}{\pi x}$. Therefore the desired expression for R_0 for suboptimum coherent detection of M-CPFSK signals on AWGN channels is given by:

$$R_{0(CPFSK)} = -\log_2 \frac{1}{M^2} \sum_{i=1}^{M} \sum_{j=1}^{M} e^{-\frac{2E_s}{4\sigma^2}\{1-\operatorname{sinc} 2h(i-j)\}}. \tag{7.19}$$

The cutoff rate for suboptimum coherent detection of CPFSK on Rician fading channels can be obtained by averaging the exponential term in (5.62) over the Rician distribution. Similar to the expression for $R_{0(PSK)}$ on Rician fading channels derived in (7.12), we have for CPFSK:

$$R_{0(CPFSK)} = -\log_2 \frac{1}{M^2} \sum_{i=1}^{M} \sum_{j=1}^{M} \frac{1+K}{1+K+d_{ij}^2/4\sigma^2} e^{-\frac{Kd_{ij}^2/4\sigma^2}{1+K+d_{ij}^2/4\sigma^2}}. \tag{7.20}$$

where

$$d_{ij}^2/4\sigma^2 = \frac{E_b}{2N_0} \log_2 M\{1 - \operatorname{sinc} 2h(i-j)\},$$

and K is the Rician factor.

7.4 Numerical Results

Numerical values of R_0 for coherently detected PSK signals on AWGN channels obtained by evaluating (7.5) are given in Table 7.1. Variation of R_0 with E_s/N_0 (average signal-to-noise ratio) is shown in Fig. 7.1. E_s is related to E_b (energy per bit in the transmitted signal) through the relation

$$E_s = E_b \log_2 M. \tag{7.21}$$

From the plot of R_0 versus E_s/N_0 it is clear that at high SNR, higher-order modulations have better coding potential because they have a larger channel cutoff rate. However, at low SNR, 4-PSK has a coding potential comparable to any higher-order M-PSK modulation scheme. Therefore, on AWGN channels under low SNR conditions, theoretically, it is sufficient to use simple PSK modulation schemes such as QPSK.

Table 7.2 shows the cutoff rates for suboptimum coherent detection of 4-CPFSK on AWGN channels for modulation indexes ranging from $h = 1/9$ to $h = 1/2$. Only rational value modulation indexes with small denominators (i.e. small q values, where $h = p/q$ and $h \leq 1/2$) are of interest to us because the complexity of the receiver becomes impractical for large q values. R_0 increases with E_b/N_0 and saturates at the rate of 2 bit/T–the maximum rate of information a 4-ary signalling scheme can carry.

In Fig. 7.2 R_0 values for suboptimum coherent phase detection of 4-CPFSK signals are compared with coherently detected 4-PSK on the AWGN channel. For all modulation indexes ($h \leq 1/2$) it can be seen that R_0 for 4-CPFSK is less than or equal to R_0 for 4-PSK. In other words, for all signal-to-noise ratios, 4-PSK has a better coding potential than 4-CPFSK with suboptimum coherent phase detection. The difference between the two schemes is pronounced at low E_b/N_0 values. For

Table 7.1 Cutoff rate R_0 of M-PSK on an AWGN channel.

E_s/N_0 (dB)	R_0			
	M=2	M=4	M=8	M=16
0.0	0.548	0.632	0.633	0.633
1.0	0.639	0.768	0.769	0.769
2.0	0.731	0.922	0.925	0.925
3.0	0.816	1.094	1.100	1.100
4.0	0.887	1.277	1.291	1.291
5.0	0.940	1.460	1.491	1.491
6.0	0.973	1.630	1.692	1.692
7.0	0.990	1.774	1.891	1.891
8.0	0.997	1.880	2.082	2.082
9.0	0.999	1.946	2.264	2.267
10.0	0.999	1.981	2.438	2.446
11.0	1.000	1.995	2.599	2.621
12.0	1.000	1.999	2.740	2.794
13.0	1.000	1.999	2.852	2.966
14.0	1.000	1.999	2.929	3.136
15.0	1.000	2.000	2.972	3.304
16.0	1.000	2.000	2.992	3.469
17.0	1.000	2.000	2.998	3.624
18.0	1.000	2.000	2.999	3.760
19.0	1.000	2.000	2.999	3.866
20.0	1.000	2.000	3.000	3.937

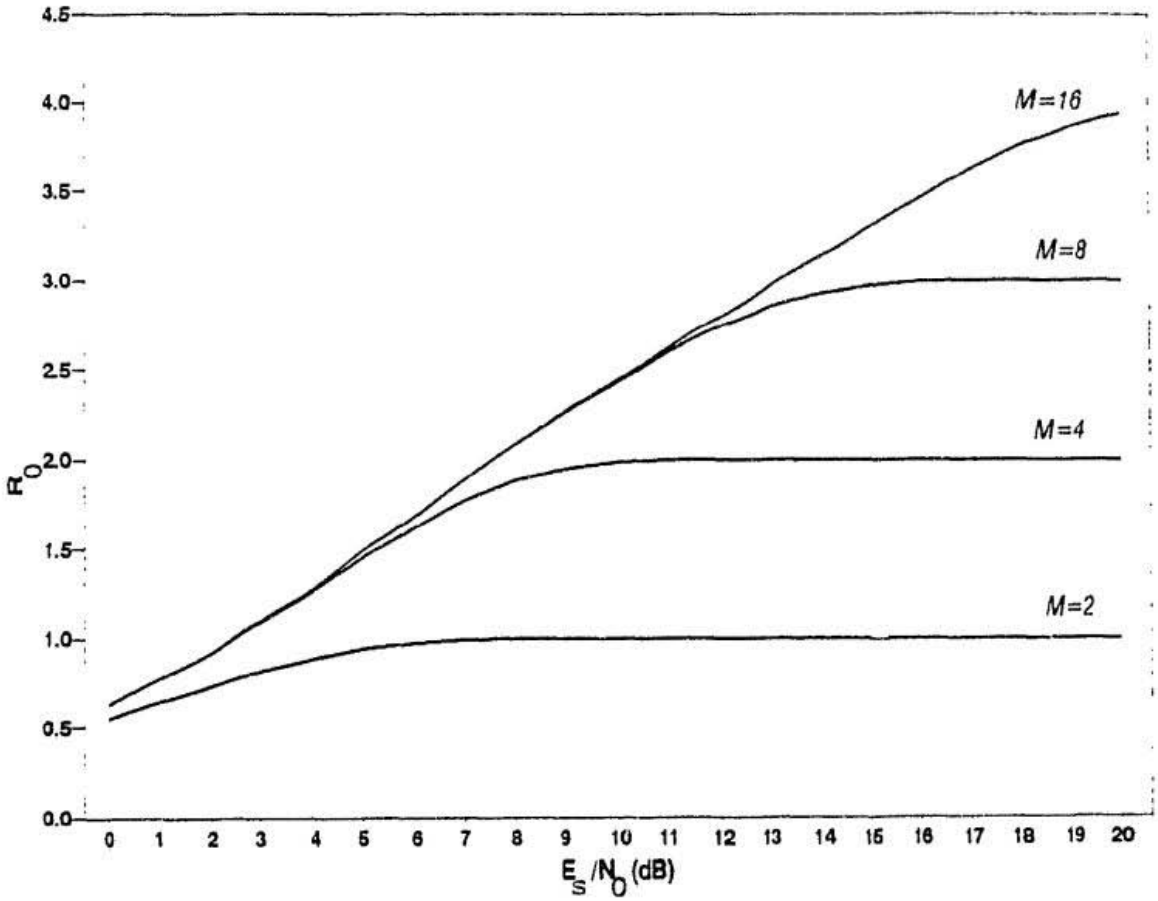

Figure 7.1 Cutoff rate R_0 against signal-to-noise ratio E_S/N_0 for M-PSK on an AWGN channel.

Table 7.2 Cutoff rate R_0 of 4-CPFSK with sub-optimum coherent detection on an AWGN channel.

E_b/N_0 (dB)	R_0						
	h=2/7	h=1/3	h=3/8	h=2/5	h=3/7	h=4/9	h=1/2
1.0	0.859	0.945	1.000	1.028	1.056	1.071	1.111
2.0	1.016	1.119	1.183	1.216	1.248	1.265	1.309
3.0	1.184	1.301	1.374	1.409	1.445	1.462	1.506
4.0	1.355	1.481	1.558	1.594	1.629	1.645	1.686
5.0	1.519	1.646	1.719	1.752	1.782	1.795	1.828
6.0	1.667	1.782	1.844	1.869	1.891	1.900	1.921
7.0	1.789	1.882	1.926	1.942	1.955	1.960	1.971
8.0	1.882	1.946	1.971	1.979	1.985	1.988	1.992
9.0	1.943	1.979	1.991	1.994	1.996	1.997	1.998
10.0	1.978	1.994	1.998	1.999	1.999	2.000	2.000
11.0	1.993	1.999	2.000	2.000	2.000	2.000	2.000
12.0	1.998	2.000	2.000	2.000	2.000	2.000	2.000
13.0	2.000	2.000	2.000	2.000	2.000	2.000	2.000
14.0	2.000	2.000	2.000	2.000	2.000	2.000	2.000
15.0	2.000	2.000	2.000	2.000	2.000	2.000	2.000
16.0	2.000	2.000	2.000	2.000	2.000	2.000	2.000
17.0	2.000	2.000	2.000	2.000	2.000	2.000	2.000
18.0	2.000	2.000	2.000	2.000	2.000	2.000	2.000
19.0	2.000	2.000	2.000	2.000	2.000	2.000	2.000
20.0	2.000	2.000	2.000	2.000	2.000	2.000	2.000

Table 7.2 Cutoff rate R_0 of 4-CPFSK with sub-optimum coherent detection on an AWGN channel.

E_b/N_0 (dB)	R_0						
	h=1/9	h=1/8	h=1/7	h=1/6	h=1/5	h=2/9	h=1/4
1.0	0.283	0.339	0.409	0.501	0.620	0.692	0.772
2.0	0.346	0.411	0.494	0.601	0.739	0.822	0.915
3.0	0.419	0.495	0.591	0.713	0.869	0.963	1.069
4.0	0.504	0.591	0.700	0.836	1.009	1.112	1.229
5.0	0.600	0.698	0.818	0.967	1.155	1.265	1.388
6.0	0.706	0.814	0.945	1.105	1.302	1.416	1.540
7.0	0.822	0.939	1.078	1.246	1.448	1.561	1.677
8.0	0.945	1.069	1.215	1.387	1.587	1.692	1.794
9.0	1.074	1.203	1.353	1.526	1.713	1.804	1.884
10.0	1.207	1.340	1.491	1.657	1.821	1.890	1.944
11.0	1.342	1.476	1.623	1.773	1.902	1.948	1.978
12.0	1.478	1.608	1.743	1.867	1.955	1.980	1.993
13.0	1.609	1.730	1.844	1.923	1.983	1.994	1.998
14.0	1.731	1.833	1.913	1.972	1.995	1.999	2.000
15.0	1.833	1.910	1.964	1.991	1.999	2.000	2.000
16.0	1.911	1.960	1.987	1.998	2.000	2.000	2.000
17.0	1.960	1.985	1.997	2.000	2.000	2.000	2.000
18.0	1.986	1.996	1.999	2.000	2.000	2.000	2.000
19.0	1.996	1.999	2.000	2.000	2.000	2.000	2.000
20.0	1.999	2.000	2.000	2.000	2.000	2.000	2.000

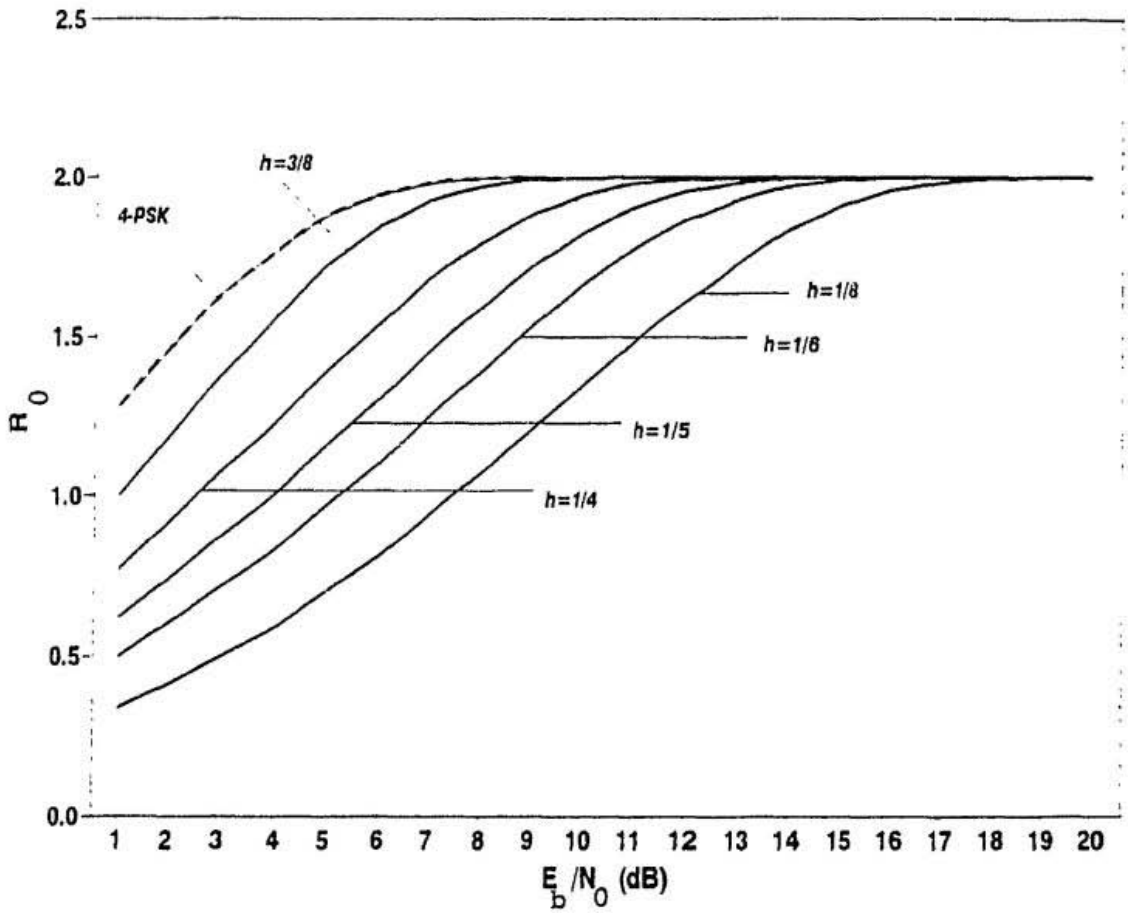

Figure 7.2 Comparison of cutoff rate R_0 of 4-PSK with coherent detection and 4-CPFSK with sub-optimum coherent detection on an AWGN channel.

$E_b/N_0 < 7$ dB. 4-PSK has approximately 0.5 bit/T advantage over 4-CPFSK with $h = 1/4$.

Table 7.3 shows the cutoff rates for suboptimum coherent phase detection of 8-CPFSK signals on the AWGN channel. 8-CPFSK has larger cutoff rates than 4-CPFSK for the same modulation index. The maximum cutoff rate of 3 bit/T for $h = 1/8$, 8-CPFSK is reached approximately at $E_b/N_0 = 17$ dB. In Fig. 7.3 we have compared R_0 for suboptimum coherent phase detection of 8-CPFSK with coherently detected 8-PSK on the AWGN channel. In this case, when modulation index is greater than about 1/4, 8-CPFSK exhibits a larger cutoff rate than 8-PSK. Therefore 8-CPFSK with $h = 1/4$ has theoretically a better coding potential than 8-PSK for $E_b/N_0 > 2$ dB. However, for $E_b/N_0 < 9$ dB, suboptimum coherent phase detection of 8-CPFSK with $h = 1/8$ is inferior to coherently detected 8-PSK by approximately 0.5 bit/T.

Channel cutoff rates for 16-CPFSK with suboptimum coherent phase detection on AWGN channels are listed in Table 7.4. For small modulation indexes, 16-CPFSK achieves large cutoff rates only at large signal-to-noise ratios as much as $E_b/N_0 = 11.5$ dB is required to achieve 3 bit/T when $h = 1/16$. In Fig. 7.4 cutoff rates for 16-CPFSK at several h values are compared with cutoff rates for coherent 16-PSK. It can be seen that for approximately $h > 1/8$, 16-CPFSK has larger R_0 values compared with 16-PSK for $E_b/N_0 < 15$ dB. Similar to $h = 1/4$, 4-CPFSK and $h = 1/8$, 8-CPFSK on AWGN channels, $h = 1/16$, 16-CPFSK results in an R_0 value some 0.5 bit/T less than coherently detected 16-PSK.

Clearly, suboptimum coherent detection of $h = 1/M$, M-CPFSK is inferior to coherent detection of M-PSK by approximately 0.5 bit/T on AWGN channels for all M values. Also, on the basis of channel cutoff rate, suboptimum coherent detection of 4-CPFSK is inferior to 4-PSK for all modulation indexes $h \leq 1/2$, while

Table 7.3 Cutoff rate R_0 of 8-CPFSK with sub-optimum coherent detection on an AWGN channel.

E_b/N_0 (dB)	R_0						
	h=2/7	h=1/3	h=3/8	h=2/5	h=3/7	h=4/9	h=1/2
1.0	1.693	1.786	1.849	1.879	1.907	1.921	1.958
2.0	1.974	2.086	2.159	2.193	2.224	2.239	2.278
3.0	2.249	2.374	2.451	2.485	2.515	2.530	2.566
4.0	2.493	2.619	2.690	2.719	2.744	2.756	2.784
5.0	2.689	2.798	2.853	2.874	2.890	2.898	2.915
6.0	2.828	2.909	2.943	2.955	2.963	2.967	2.974
7.0	2.917	2.966	2.983	2.988	2.991	2.992	2.995
8.0	2.966	2.990	2.996	2.997	2.998	2.999	2.999
9.0	2.989	2.998	2.999	3.000	3.000	3.000	3.000
10.0	2.997	3.000	3.000	3.000	3.000	3.000	3.000
11.0	3.000	3.000	3.000	3.000	3.000	3.000	3.000
12.0	3.000	3.000	3.000	3.000	3.000	3.000	3.000
13.0	3.000	3.000	3.000	3.000	3.000	3.000	3.000
14.0	3.000	3.000	3.000	3.000	3.000	3.000	3.000
15.0	3.000	3.000	3.000	3.000	3.000	3.000	3.000
16.0	3.000	3.000	3.000	3.000	3.000	3.000	3.000
17.0	3.000	3.000	3.000	3.000	3.000	3.000	3.000
18.0	3.000	3.000	3.000	3.000	3.000	3.000	3.000
19.0	3.000	3.000	3.000	3.000	3.000	3.000	3.000
20.0	3.000	3.000	3.000	3.000	3.000	3.000	3.000

Table 7.3 Cutoff rate R_0 of 8-CPFSK with sub-optimum coherent detection on an AWGN channel.

E_b/N_0	R_0						
(dB)	h=1/9	h=1/8	h=1/7	h=1/6	h=1/5	h=2/9	h=1/4
1.0	0.950	1.055	1.171	1.297	1.435	1.514	1.601
2.0	1.102	1.221	1.353	1.500	1.665	1.759	1.863
3.0	1.261	1.390	1.537	1.703	1.893	2.002	2.122
4.0	1.422	1.560	1.718	1.898	2.109	2.229	2.359
5.0	1.582	1.726	1.892	2.083	2.306	2.430	2.561
6.0	1.741	1.889	2.059	2.256	2.481	2.602	2.722
7.0	1.899	2.050	2.222	2.419	2.635	2.743	2.841
8.0	2.056	2.208	2.380	2.571	2.765	2.852	2.921
9.0	2.212	2.364	2.532	2.708	2.867	2.926	2.967
10.0	2.367	2.516	2.673	2.823	2.936	2.970	2.989
11.0	2.517	2.657	2.794	2.907	2.975	2.990	2.997
12.0	2.658	2.781	2.887	2.959	2.992	2.998	3.000
13.0	2.782	2.878	2.948	2.986	2.998	3.000	3.000
14.0	2.878	2.942	2.981	2.996	3.000	3.000	3.000
15.0	2.942	2.978	2.994	2.999	3.000	3.000	3.000
16.0	2.978	2.993	2.999	3.000	3.000	3.000	3.000
17.0	2.993	2.999	3.000	3.000	3.000	3.000	3.000
18.0	2.999	3.000	3.000	3.000	3.000	3.000	3.000
19.0	3.000	3.000	3.000	3.000	3.000	3.000	3.000
20.0	3.000	3.000	3.000	3.000	3.000	3.000	3.000

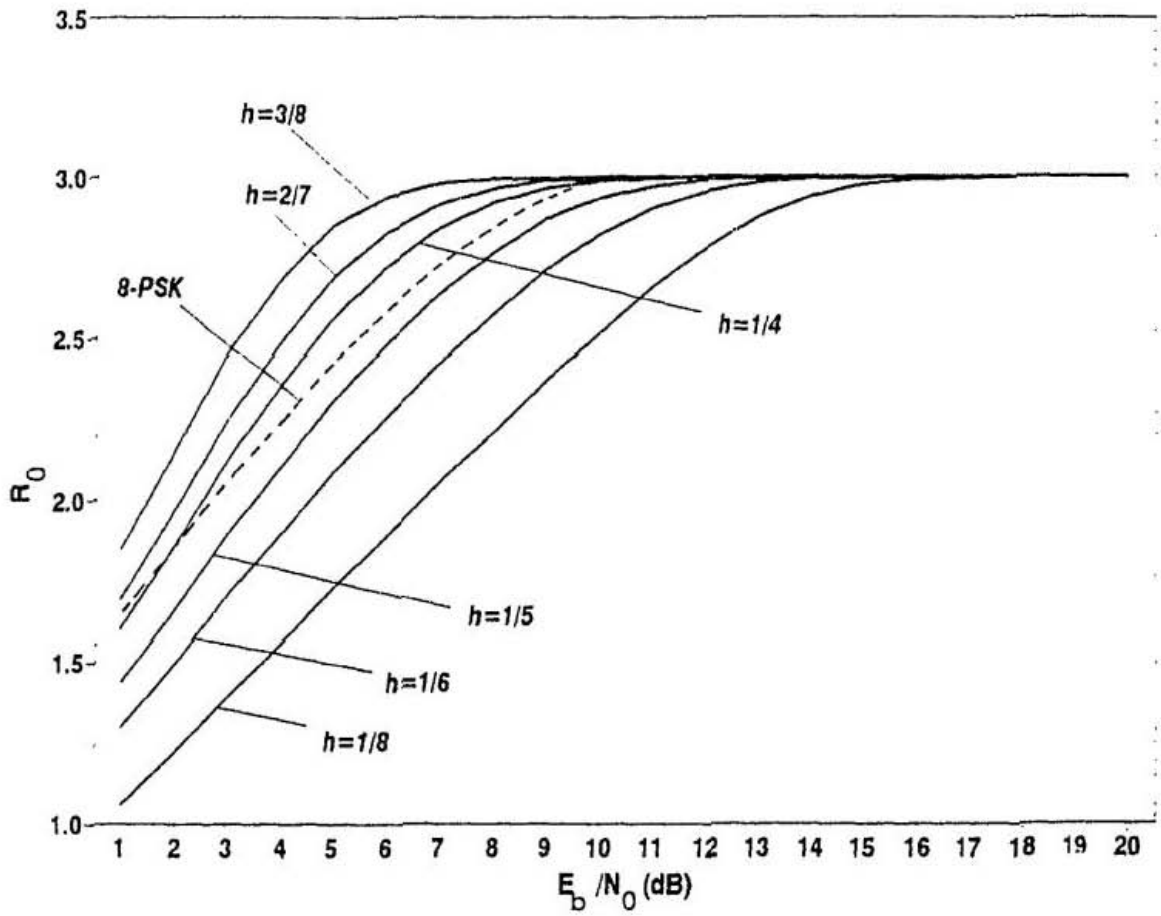

Figure 7.3 Comparison of cutoff rate R_0 of 8-PSK with coherent detection and 8-CPFSK with sub-optimum coherent detection on an AWGN channel.

Table 7.4 Cutoff rate R_0 of 16-CPFSK with sub-optimum coherent detection on an AWGN channel.

E_b/N_0 (dB)	R_0						
	h=1/4	h=2/7	h=1/3	h=3/8	h=2/5	h=3/7	h=1/2
1.0	2.521	2.613	2.706	2.763	2.789	2.813	2.856
2.0	2.906	3.020	3.132	3.197	3.225	3.251	3.295
3.0	3.252	3.380	3.499	3.563	3.588	3.611	3.647
4.0	3.526	3.652	3.758	3.809	3.827	3.842	3.864
5.0	3.722	3.827	3.903	3.935	3.944	3.952	3.962
6.0	3.851	3.924	3.968	3.983	3.987	3.989	3.992
7.0	3.930	3.972	3.992	3.997	3.998	3.998	3.999
8.0	3.973	3.991	3.998	4.000	4.000	4.000	4.000
9.0	3.992	3.998	4.000	4.000	4.000	4.000	4.000
10.0	3.998	4.000	4.000	4.000	4.000	4.000	4.000
11.0	4.000	4.000	4.000	4.000	4.000	4.000	4.000
12.0	4.000	4.000	4.000	4.000	4.000	4.000	4.000
13.0	4.000	4.000	4.000	4.000	4.000	4.000	4.000
14.0	4.000	4.000	4.000	4.000	4.000	4.000	4.000
15.0	4.000	4.000	4.000	4.000	4.000	4.000	4.000
16.0	4.000	4.000	4.000	4.000	4.000	4.000	4.000
17.0	4.000	4.000	4.000	4.000	4.000	4.000	4.000
18.0	4.000	4.000	4.000	4.000	4.000	4.000	4.000
19.0	4.000	4.000	4.000	4.000	4.000	4.000	4.000
20.0	4.000	4.000	4.000	4.000	4.000	4.000	4.000

Table 7.4 Cutoff rate R_0 of 16-CPFSK with sub-optimum coherent detection on an AWGN channel.

E_b/N_0 (dB)	R_0						
	h=1/16	h=1/10	h=1/8	h=1/7	h=3/16	h=1/5	h=2/9
1.0	1.269	1.732	1.943	2.065	2.297	2.350	2.433
2.0	1.440	1.961	2.205	2.349	2.630	2.695	2.797
3.0	1.611	2.177	2.447	2.609	2.932	3.007	3.125
4.0	1.778	2.375	2.664	2.837	3.187	3.268	3.395
5.0	1.942	2.557	2.856	3.036	3.396	3.478	3.602
6.0	2.103	2.730	3.033	3.215	3.570	3.646	3.755
7.0	2.264	2.897	3.203	3.383	3.716	3.779	3.864
8.0	2.424	3.062	3.367	3.542	3.832	3.879	3.936
9.0	2.585	3.226	3.525	3.686	3.915	3.944	3.975
10.0	2.745	3.387	3.670	3.808	3.964	3.979	3.993
11.0	2.905	3.542	3.795	3.898	3.988	3.994	3.998
12.0	3.065	3.686	3.890	3.955	3.997	3.999	4.000
13.0	3.225	3.807	3.950	3.984	4.000	4.000	4.000
14.0	3.384	3.898	3.982	3.996	4.000	4.000	4.000
15.0	3.539	3.955	3.995	3.999	4.000	4.000	4.000
16.0	3.682	3.984	3.999	4.000	4.000	4.000	4.000
17.0	3.804	3.996	4.000	4.000	4.000	4.000	4.000
18.0	3.896	3.999	4.000	4.000	4.000	4.000	4.000
19.0	3.954	4.000	4.000	4.000	4.000	4.000	4.000
20.0	3.984	4.000	4.000	4.000	4.000	4.000	4.000

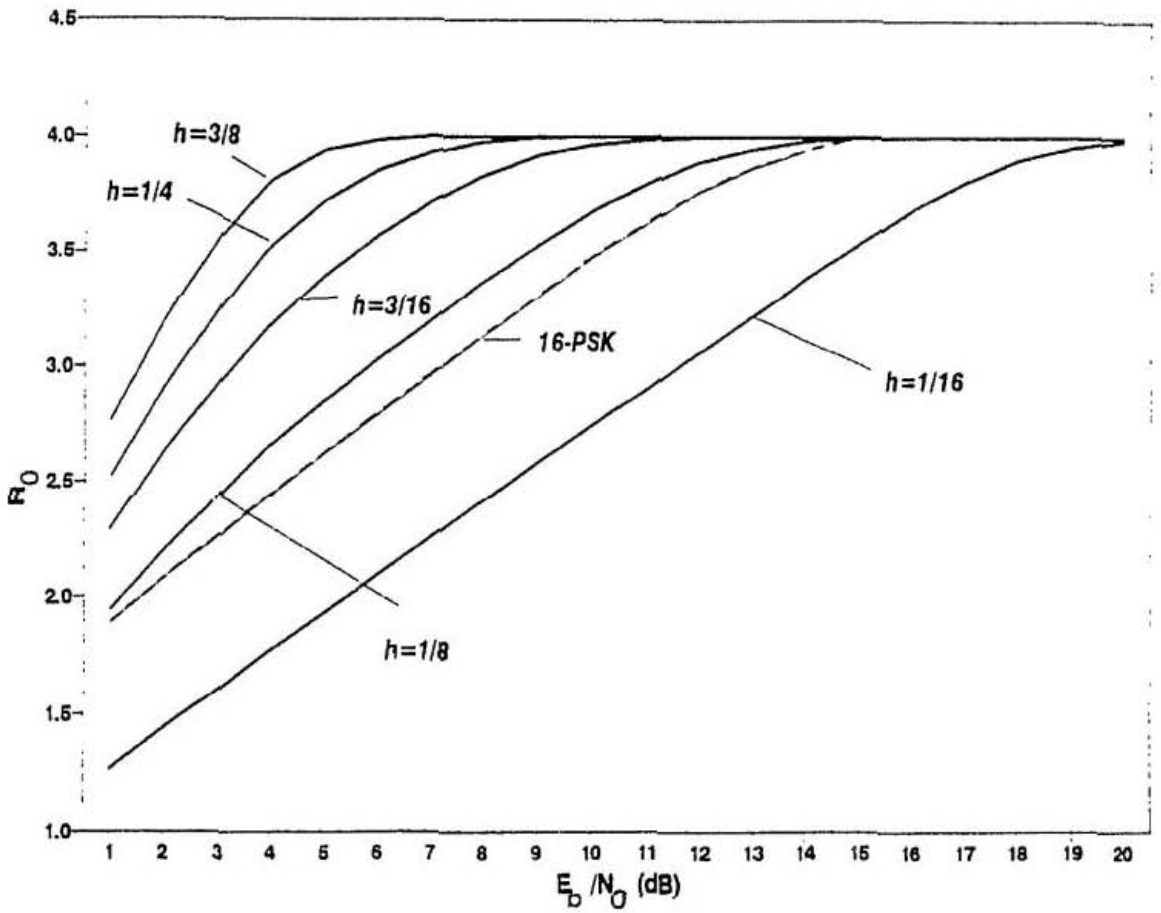

Figure 7.4 Comparison of cutoff rate R_0 of 16-PSK with coherent detection and 16-CPFSK with sub-optimum coherent detection on an AWGN channel.

suboptimum coherent detection of 8-CPFSK and 16-CPFSK are inferior to their PSK counterparts when approximately $h \leq 1/4$ and $h \leq 1/8$, respectively. More exact modulation index figures are of no practical value because CPFSK signalling schemes are always implemented with small rational modulation indexes $h \leq 1/2$.

The channel cutoff rates for coherent detection of PSK and suboptimum coherent detection of CPFSK for mobile satellite channels is computed next. For mobile satellite channels $R_0(PSK)$ is computed using (7.12) and $R_0(CPFSK)$ using (7.20). In a recent study [2] R_0 values have been obtained for both coherent and noncoherent suboptimum detection of CPM on Rician and Rayleigh fading channels. Our results are in exact agreement with the results of [2].

Experiments have shown that for low angles of elevation to the geosynchronous satellite (such as the Canadian mobile satellite channel, where the angle of elevation is less than about twenty degrees) the Rician fading model is described by a Rician factor (K) of less than 20 dB. However, a more conservative estimate for K at low elevation angles has been 10 dB [31]. In the presence of an unshadowed direct path between the satellite and the mobile, the channel could be modelled as Rician distributed with $K = 20$ dB. When $K \leq 0$ dB, the fading in the mobile satellite channel is Rayleigh distributed. Since a Rayleigh fading channel is too hostile for coherent demodulation cutoff rates are computed for Rician factors ranging from 0 to 20 dB corresponding to light- or no-shadowing in the line-of-sight component.

Numerical values of R_0 for coherently detected M-PSK signals and suboptimum coherent detected M-CPFSK signals with modulation index $h = 1/M$ on K=0 dB, 5 dB, 10 dB and 20 dB Rician fading channels are given in Tables 7.5–7.7. Fig. 7.5 illustrates the cutoff rate R_0 versus E_b/N_0 for suboptimum coherent detection of M-CPFSK with $h = 1/M$ compared with R_0 for coherent detection of M-PSK. The thick line shows R_0 for $h = 1/M$, M-CPFSK, whereas, the thin line

Table 7.5 Cutoff rate of 4-PSK, and h=1/4, 4-CPFSK with suboptimum coherent detection on Rician fading channels.

E_b/N_0	R_0 (4-PSK)				R_0 (4-CPFSK, h=1/4)			
(dB)	K=0	K=5	K=10	K=20	K=0	K=5	K=10	K=20
0	0.825	0.919	1.016	1.086	0.525	0.569	0.610	0.640
1	0.938	1.054	1.177	1.267	0.614	0.671	0.727	0.767
2	1.054	1.192	1.341	1.448	0.710	0.782	0.855	0.908
3	1.169	1.328	1.498	1.617	0.812	0.902	0.994	1.060
4	1.280	1.454	1.640	1.760	0.919	1.028	1.140	1.218
5	1.384	1.568	1.757	1.868	1.029	1.156	1.287	1.377
6	1.480	1.666	1.847	1.938	1.139	1.283	1.432	1.528
7	1.566	1.746	1.910	1.976	1.247	1.405	1.567	1.666
8	1.640	1.809	1.950	1.992	1.350	1.518	1.687	1.783
9	1.705	1.858	1.973	1.998	1.446	1.619	1.786	1.874
10	1.759	1.895	1.986	2.000	1.533	1.705	1.863	1.936
11	1.805	1.922	1.993	2.000	1.611	1.775	1.917	1.973
12	1.842	1.942	1.997	2.000	1.679	1.831	1.953	1.991
13	1.873	1.957	1.998	2.000	1.737	1.874	1.975	1.998
14	1.898	1.967	1.999	2.000	1.786	1.907	1.987	2.000
15	1.919	1.975	2.000	2.000	1.827	1.931	1.993	2.000
16	1.935	1.981	2.000	2.000	1.860	1.949	1.997	2.000
17	1.948	1.985	2.000	2.000	1.888	1.961	1.998	2.000
18	1.959	1.989	2.000	2.000	1.910	1.971	1.999	2.000
19	1.967	1.991	2.000	2.000	1.928	1.978	2.000	2.000
20	1.974	1.993	2.000	2.000	1.942	1.983	2.000	2.000
21	1.979	1.995	2.000	2.000	1.954	1.987	2.000	2.000
22	1.983	1.996	2.000	2.000	1.963	1.990	2.000	2.000
23	1.987	1.997	2.000	2.000	1.971	1.992	2.000	2.000
24	1.989	1.997	2.000	2.000	1.977	1.994	2.000	2.000
25	1.992	1.998	2.000	2.000	1.982	1.995	2.000	2.000
26	1.993	1.998	2.000	2.000	1.985	1.996	2.000	2.000
27	1.995	1.999	2.000	2.000	1.988	1.997	2.000	2.000
28	1.996	1.999	2.000	2.000	1.991	1.998	2.000	2.000
29	1.997	1.999	2.000	2.000	1.993	1.998	2.000	2.000
30	1.997	1.999	2.000	2.000	1.994	1.999	2.000	2.000

Table 7.6 Cutoff rate of 8-PSK, and h=1/8, 8-CPFSK with suboptimum coherent detection on Rician fading channels.

E_b/N_0	R_0 (8-PSK)				R_0 (8-CPFSK, h=1/8)			
(dB)	K=0	K=5	K=10	K=20	K=0	K=5	K=10	K=20
0	1.061	1.193	1.332	1.431	0.701	0.771	0.841	0.891
1	1.198	1.353	1.519	1.632	0.807	0.894	0.982	1.046
2	1.340	1.519	1.708	1.831	0.920	1.025	1.134	1.210
3	1.485	1.688	1.898	2.024	1.039	1.163	1.292	1.379
4	1.632	1.856	2.083	2.209	1.164	1.307	1.453	1.548
5	1.779	2.021	2.261	2.386	1.294	1.454	1.617	1.715
6	1.923	2.179	2.427	2.550	1.427	1.604	1.780	1.878
7	2.062	2.327	2.577	2.697	1.562	1.755	1.941	2.039
8	2.192	2.460	2.705	2.817	1.699	1.905	2.101	2.198
9	2.312	2.576	2.807	2.904	1.835	2.054	2.256	2.354
10	2.421	2.673	2.881	2.958	1.969	2.198	2.406	2.505
11	2.517	2.751	2.932	2.985	2.098	2.334	2.546	2.646
12	2.601	2.813	2.963	2.996	2.221	2.460	2.670	2.770
13	2.673	2.860	2.980	2.999	2.335	2.571	2.774	2.867
14	2.733	2.895	2.990	3.000	2.439	2.666	2.855	2.934
15	2.783	2.921	2.995	3.000	2.531	2.745	2.913	2.973
16	2.825	2.941	2.997	3.000	2.612	2.807	2.951	2.991
17	2.859	2.955	2.999	3.000	2.681	2.855	2.973	2.998
18	2.887	2.966	2.999	3.000	2.740	2.892	2.986	3.000
19	2.909	2.974	3.000	3.000	2.789	2.919	2.993	3.000
20	2.928	2.980	3.000	3.000	2.829	2.939	2.997	3.000
21	2.942	2.984	3.000	3.000	2.863	2.954	2.998	3.000
22	2.954	2.988	3.000	3.000	2.890	2.965	2.999	3.000
23	2.963	2.990	3.000	3.000	2.912	2.974	3.000	3.000
24	2.971	2.993	3.000	3.000	2.929	2.980	3.000	3.000
25	2.977	2.994	3.000	3.000	2.944	2.984	3.000	3.000
26	2.981	2.995	3.000	3.000	2.955	2.988	3.000	3.000
27	2.985	2.996	3.000	3.000	2.964	2.991	3.000	3.000
28	2.988	2.997	3.000	3.000	2.971	2.993	3.000	3.000
29	2.991	2.998	3.000	3.000	2.977	2.994	3.000	3.000
30	2.993	2.998	3.000	3.000	2.982	2.995	3.000	3.000

Table 7.7 Cutoff rate of 16-PSK, and h=1/16,16-CPFSK with suboptimum coherent detection on Rician fading channels.

E_b/N_0 (dB)	R_0 (16-PSK)				R_0 (16-CPFSK, h=1/16)			
	K=0	K=5	K=10	K=20	K=0	K=5	K=10	K=20
0	1.234	1.395	1.566	1.682	0.838	0.930	1.024	1.092
1	1.378	1.562	1.756	1.880	0.953	1.064	1.178	1.259
2	1.527	1.733	1.946	2.072	1.075	1.204	1.339	1.429
3	1.679	1.906	2.134	2.257	1.202	1.350	1.502	1.599
4	1.835	2.079	2.317	2.437	1.334	1.499	1.667	1.766
5	1.993	2.252	2.498	2.613	1.469	1.651	1.831	1.931
6	2.152	2.424	2.675	2.786	1.608	1.805	1.995	2.093
7	2.312	2.596	2.849	2.958	1.750	1.960	2.157	2.254
8	2.471	2.765	3.021	3.128	1.894	2.116	2.319	2.414
9	2.630	2.931	3.189	3.296	2.040	2.272	2.480	2.574
10	2.784	3.091	3.351	3.460	2.187	2.429	2.640	2.735
11	2.934	3.243	3.503	3.614	2.336	2.586	2.801	2.895
12	3.076	3.383	3.639	3.749	2.485	2.742	2.961	3.055
13	3.208	3.508	3.753	3.856	2.634	2.898	3.120	3.215
14	3.328	3.615	3.842	3.929	2.781	3.051	3.276	3.373
15	3.436	3.704	3.905	3.971	2.924	3.198	3.427	3.527
16	3.532	3.775	3.946	3.991	3.061	3.337	3.567	3.670
17	3.614	3.830	3.971	3.998	3.190	3.464	3.690	3.792
18	3.684	3.872	3.985	4.000	3.310	3.575	3.792	3.885
19	3.742	3.904	3.992	4.000	3.418	3.670	3.869	3.946
20	3.791	3.928	3.996	4.000	3.514	3.748	3.923	3.979
21	3.832	3.945	3.998	4.000	3.598	3.809	3.957	3.994
22	3.865	3.958	3.999	4.000	3.670	3.857	3.977	3.998
23	3.891	3.968	3.999	4.000	3.731	3.893	3.988	4.000
24	3.913	3.975	4.000	4.000	3.781	3.920	3.994	4.000
25	3.930	3.981	4.000	4.000	3.823	3.939	3.997	4.000
26	3.944	3.985	4.000	4.000	3.858	3.954	3.998	4.000
27	3.956	3.988	4.000	4.000	3.886	3.965	3.999	4.000
28	3.965	3.991	4.000	4.000	3.909	3.973	4.000	4.000
29	3.972	3.993	4.000	4.000	3.927	3.979	4.000	4.000
30	3.978	3.994	4.000	4.000	3.942	3.984	4.000	4.000

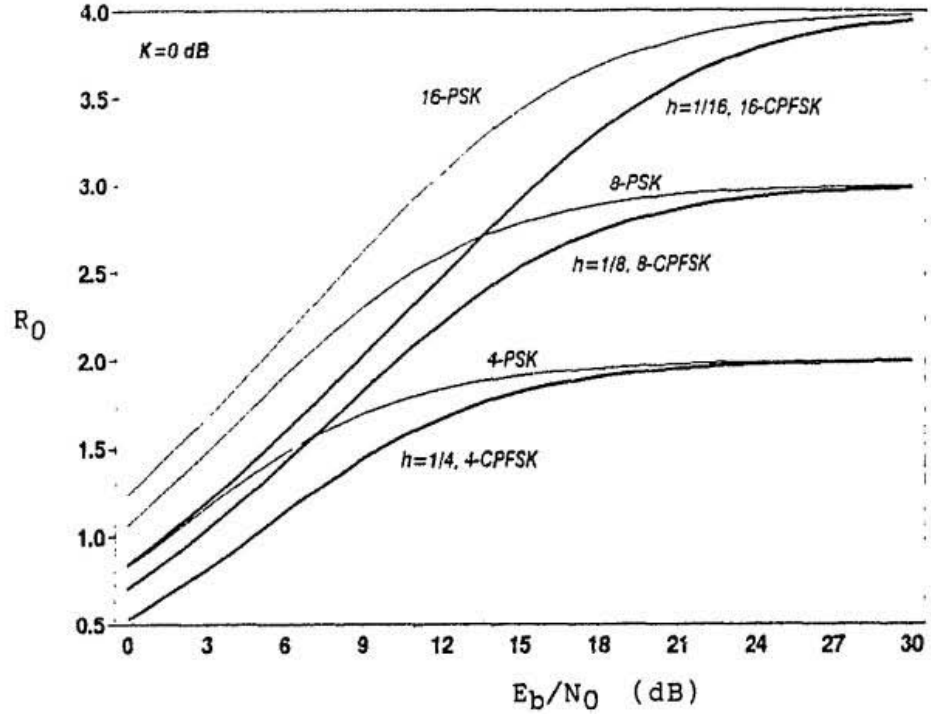

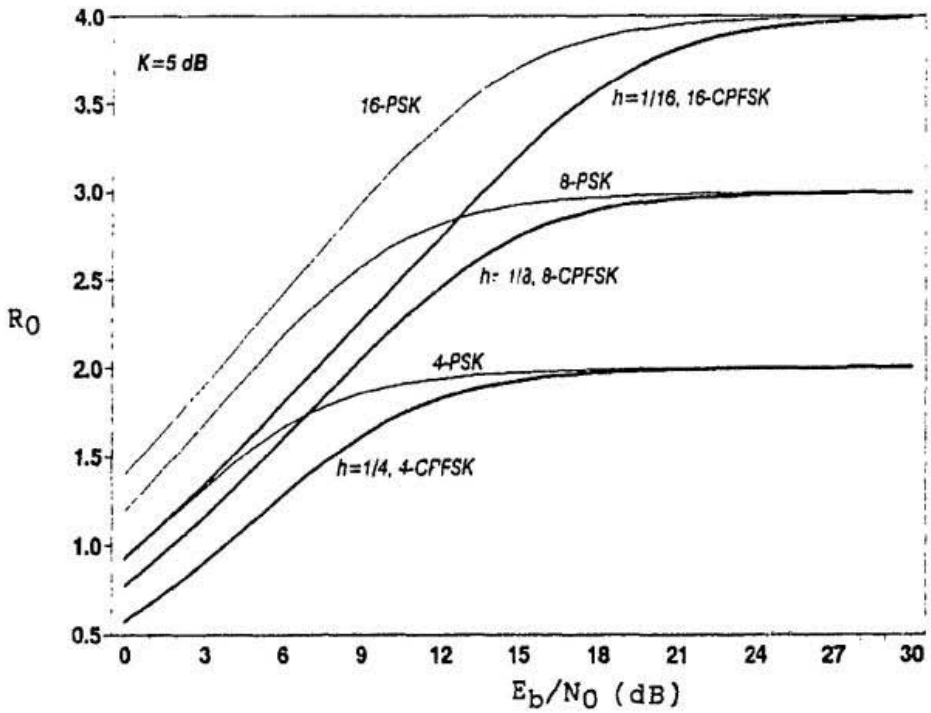

Figure 7.5 Comparison of cutoff rate bounds for suboptimum coherent detection of CPFSK and coherent PSK on mobile satellite channels.

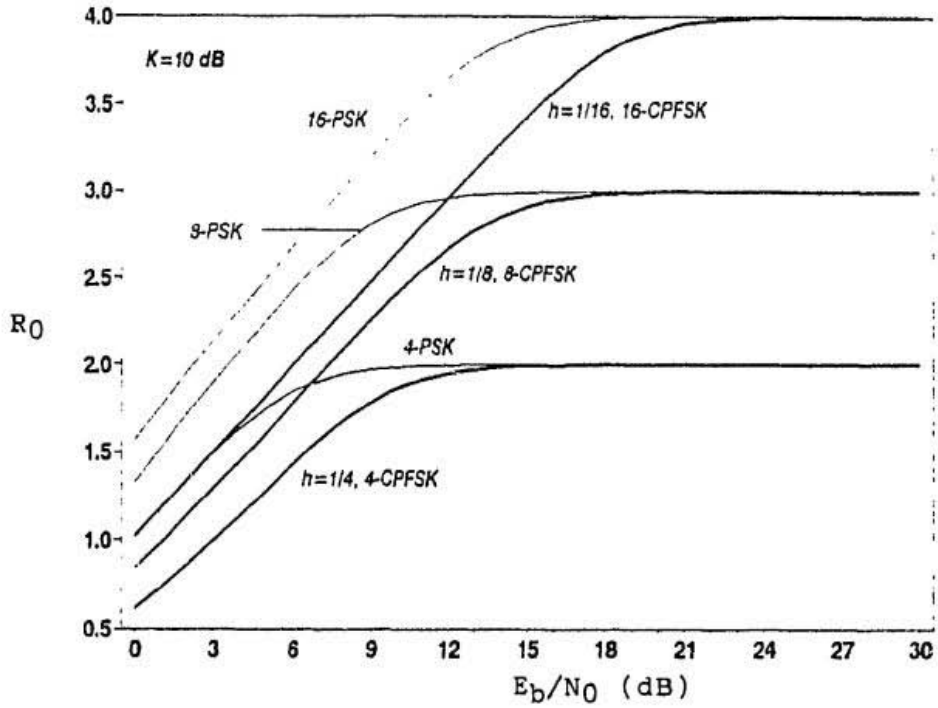

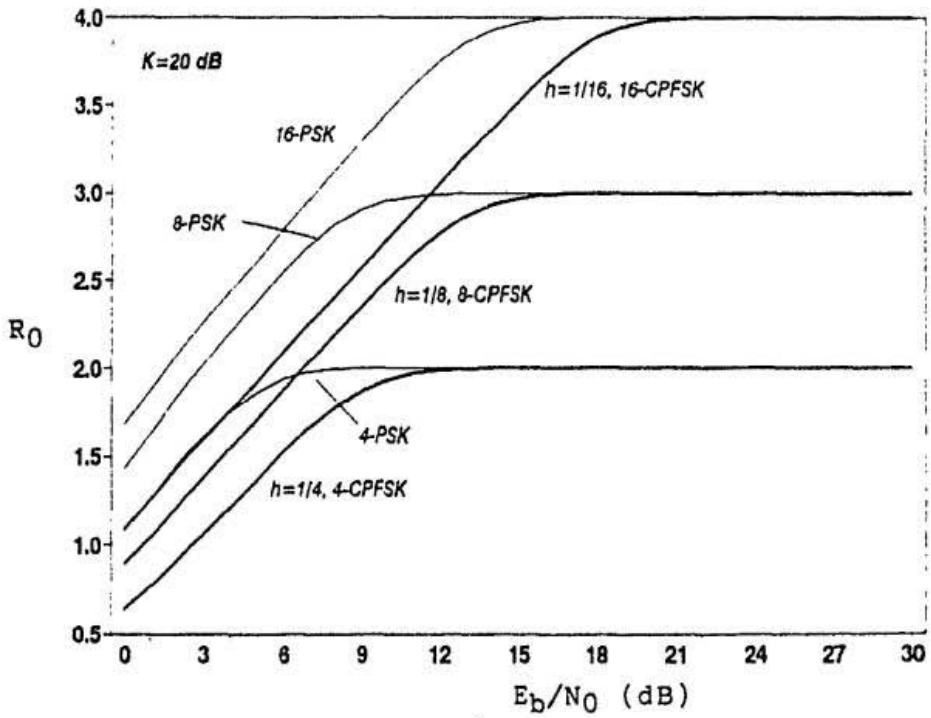

Figure 7.5 (Contd.) Comparison of cutoff rate bounds for suboptimum coherent detection of CPFSK and coherent PSK on mobile satellite channels.

shows R_0 for M-PSK. For all three modulations, namely 4-CPFSK, 8-CPFSK, and 16-CPFSK, when $h = 1/M$, the cutoff rates are smaller than cutoff rates for the corresponding M-PSK signals. Therefore, under the mobile satellite channel conditions also suboptimum coherent detection of M-CPFSK with $h = 1/M$ has less coding potential and hence would be less effective than coherent M-PSK signalling.

The M-CPFSK signal would normally be precoded with a rate $r = (m-1)/m$ trellis code, where $M = 2^m$, and in the case of 4-CPFSK the code rate is $r = 1/2$ and the system would be required to transmit on average 1 bit/signalling interval or 1 bit/T. The cutoff rate of $h = 1/4$, 4-CPFSK signals is equal to 1 bit/T at E_b/N_0=5 dB with K=0 dB, and E_b/N_0=3 dB with K=10 dB. In the case of 8-CPFSK signals the required information rate would be 2 bit/T and on Rician fading channels with K=0 dB this is achieved at $E_b/N_0 \approx 10$ dB. For average shadowed channels with K=10 dB the required E_b/N_0 is 7.5 dB. For $h = 1/16$, 16-CPFSK signals, 3 bit/T can be achieved on K=10 dB Rician fading channels at $E_b/N_0 \approx 12$ dB.

In Fig. 7.6 we have plotted R_0 versus E_b/N_0 with modulation index $h(\leq 1/2)$ as a parameter for 4-CPFSK with suboptimum coherent phase detection on mobile satellite channels. For all E_b/N_0 values and K values, 4-PSK has a larger channel cutoff rate than 4-CPFSK. This was true for suboptimum coherent phase detection of 4-CPFSK on AWGN channels as well. Therefore, on the basis of channel cutoff rate, suboptimum coherent phase detection of 4-CPFSK at any modulation index ($h \leq 1/2$) is inferior to coherently detected 4-PSK on mobile satellite channels.

In Fig. 7.7 channel cutoff rates for suboptimum coherent detection of 8-CPFSK on mobile satellite channels with K=0, 5, 10 and 20 dB are plotted against E_b/N_0 for several small modulation indexes. For small K values (K=0 dB and K=5 dB) the cutoff rates for 8-PSK and $h = 1/4$ 8-CPFSK are almost equal. For

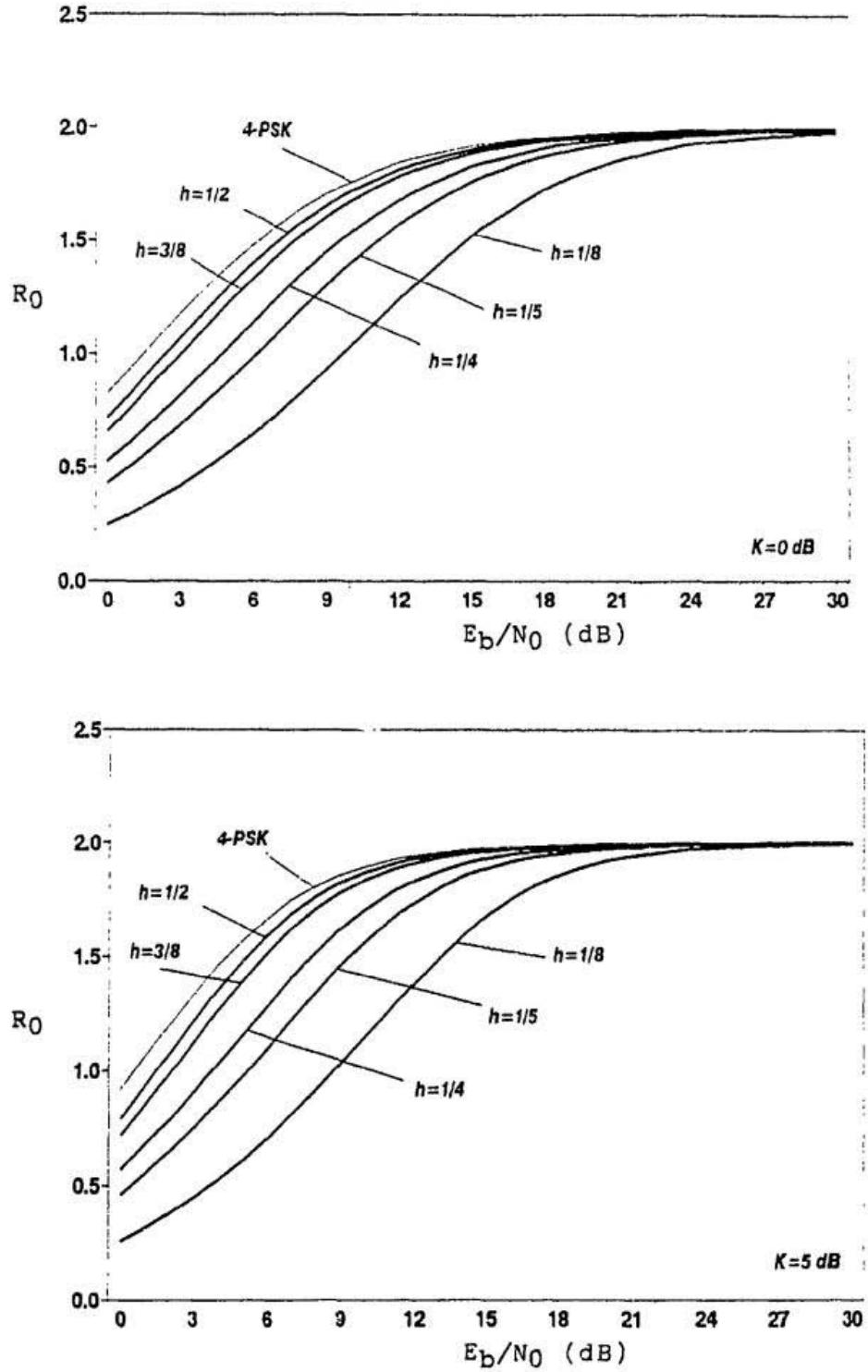

Figure 7.6 Channel cutoff rate R_0 vs E_b/N_0 for suboptimum coherent detection of 4-CPFSK on mobile satellite channel.

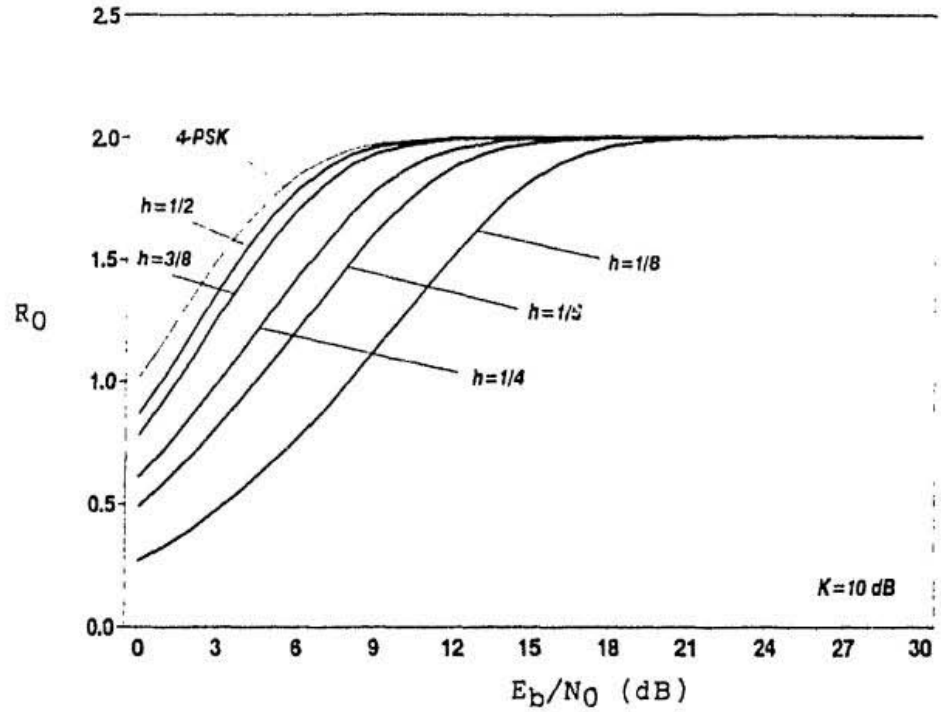

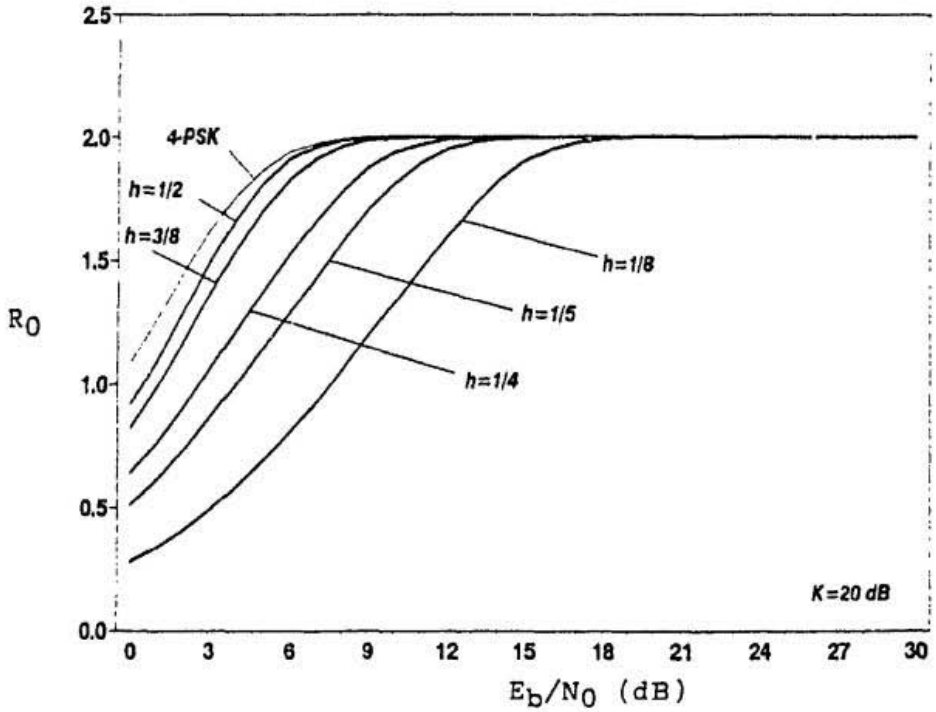

Figure 7.6 (Contd.) Channel cutoff rate R_0 vs E_b/N_0 for suboptimum coherent detection of 4-CPFSK on mobile satellite channels.

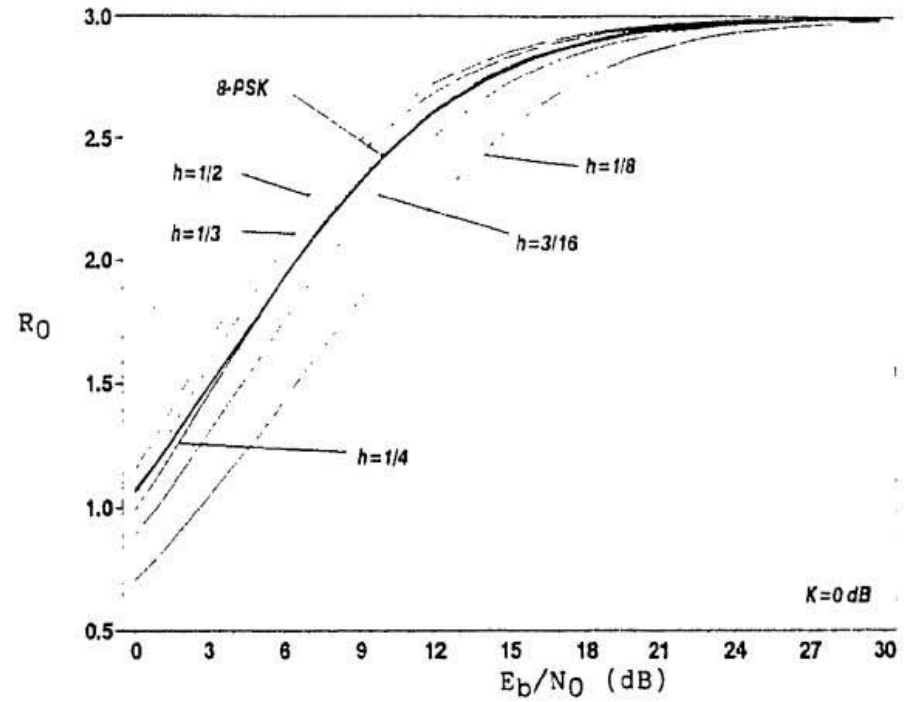

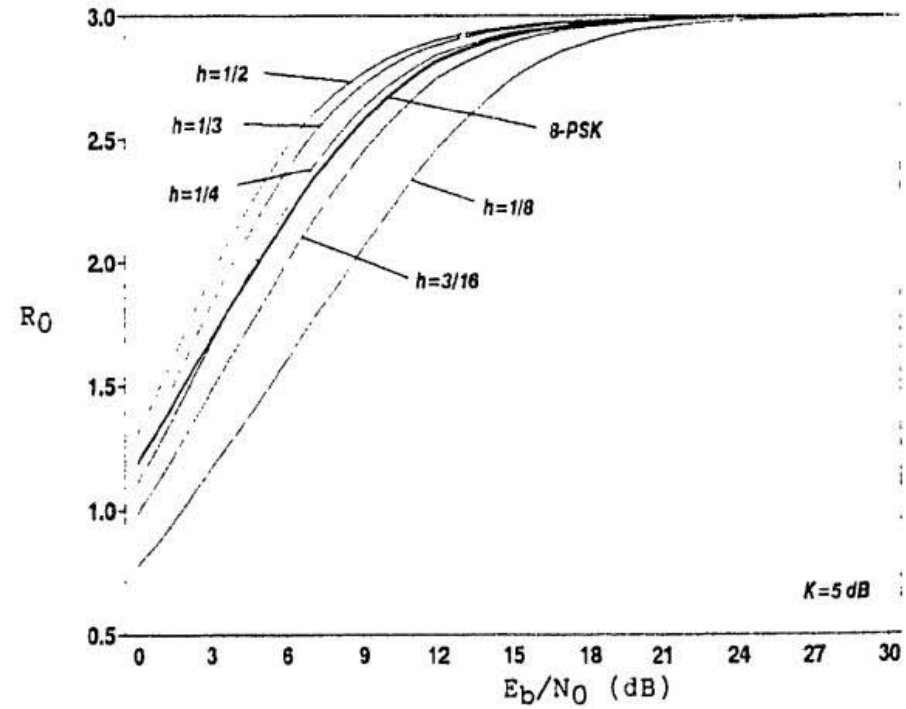

Figure 7.7 Channel cutoff rate R_0 vs E_b/N_0 for suboptimum coherent detection of 8-CPFSK on mobile satellite channels.

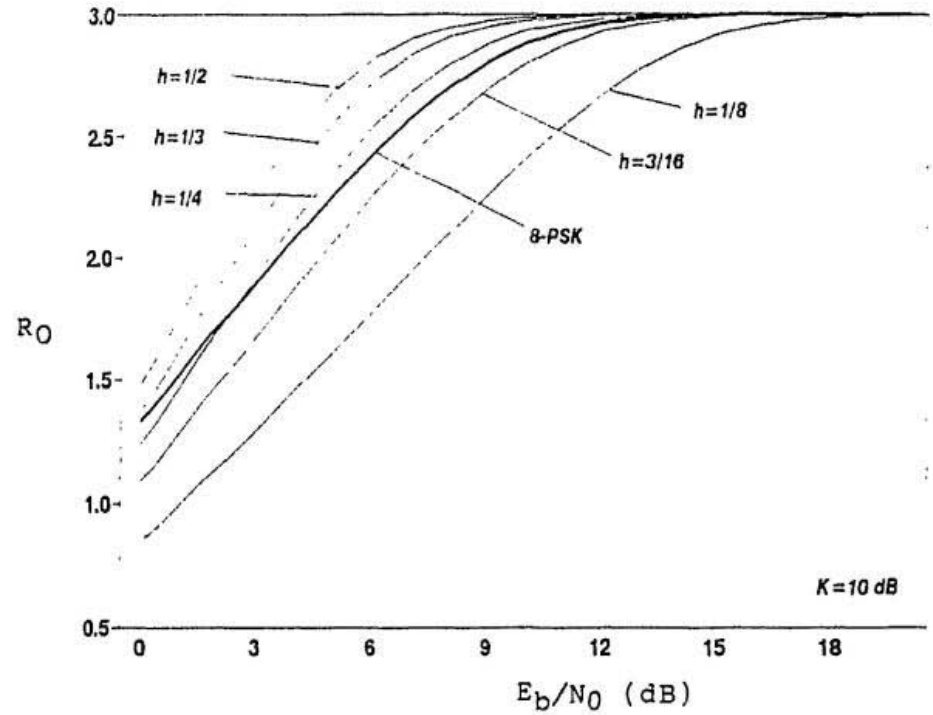

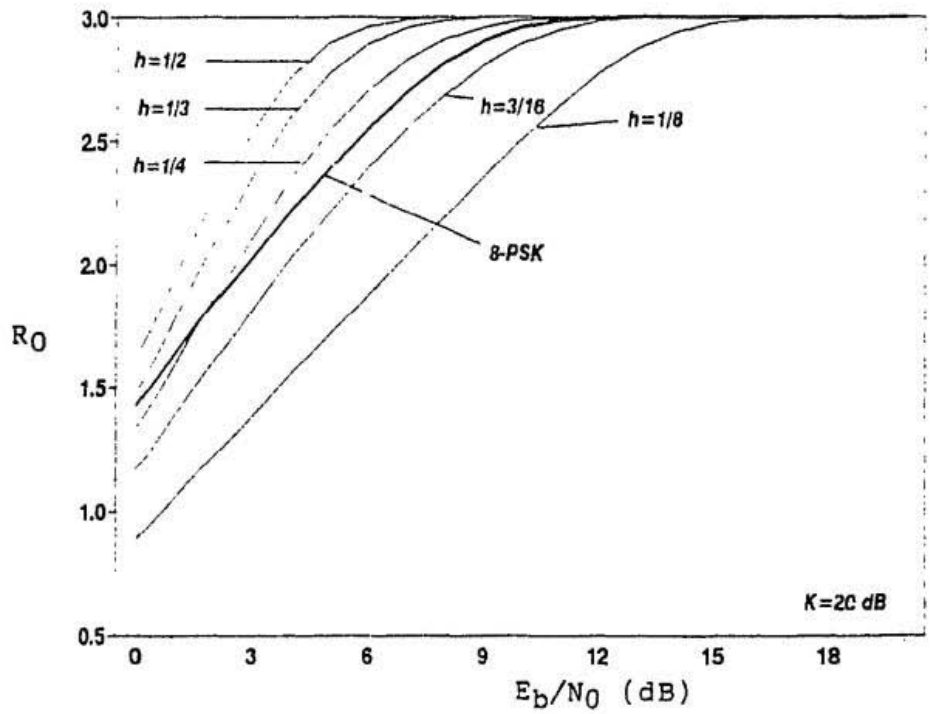

Figure 7.7 (Contd.) Channel cutoff rate R_0 vs E_b/N_0 for suboptimum coherent detection of 8-CPFSK on mobile satellite channels.

Rician fading channels with K=10 dB and 20 dB. $h = 1/4$. 8-CPFSK has a larger cutoff rate than 8-PSK beyond about E_b/N_0=2.5 dB and E_b/N_0=2 dB, respectively. Smaller modulation indexes result in smaller R_0 values than 8-PSK at every K. However, 8-CPFSK schemes with modulation indexes larger than $h = 1/4$ have a better coding potential than 8-PSK.

R_0 values for suboptimum coherent detection of 16-CPFSK signals on Rician fading channels are illustrated in Fig. 7.8. For almost all channel conditions of interest, 16-CPFSK with $h = 1/8$ outperforms coherent 16-PSK. This was also true on AWGN channels. CPFSK schemes with modulation indexes larger than $h = 1/8$ achieve larger cutoff rates than 16-PSK. This is more pronounced in channels with higher K values. For example, on Rician fading channels with K=10 dB, the channel cutoff rate of suboptimum detected 16-CPFSK with $h = 1/2$ can be as much as 1.1 bit/T more than 16-PSK at E_b/N_0=6 dB.

Summarizing the results for mobile satellite channels it can be concluded that on the basis of channel cutoff rate, suboptimum coherent detection of 4-CPFSK is inferior to 4-PSK in both light- and average-fading conditions for all rational $h \leq 1/2$. Suboptimum coherent detection of 8-CPFSK with $1/4 \leq h \leq 1/2$ outperforms coherently detected 8-PSK, and 16-CPFSK with $1/8 \leq h \leq 1/2$ has better coding potential than 16-PSK for average signal-to-noise ratios.

It is important to note that the channel cutoff rates calculated in this section are upper bounds to the actual cutoff rate of the channel. This is because of the assumptions we made regarding the infinitely interleaved channel as well as the ideal receiver. Nevertheless, these channel cutoff rate bounds provide useful information about the relative performance under different channel conditions and with different trellis modulation codes.

For analytical purposes, we have assumed that the depth of interleaving is infi-

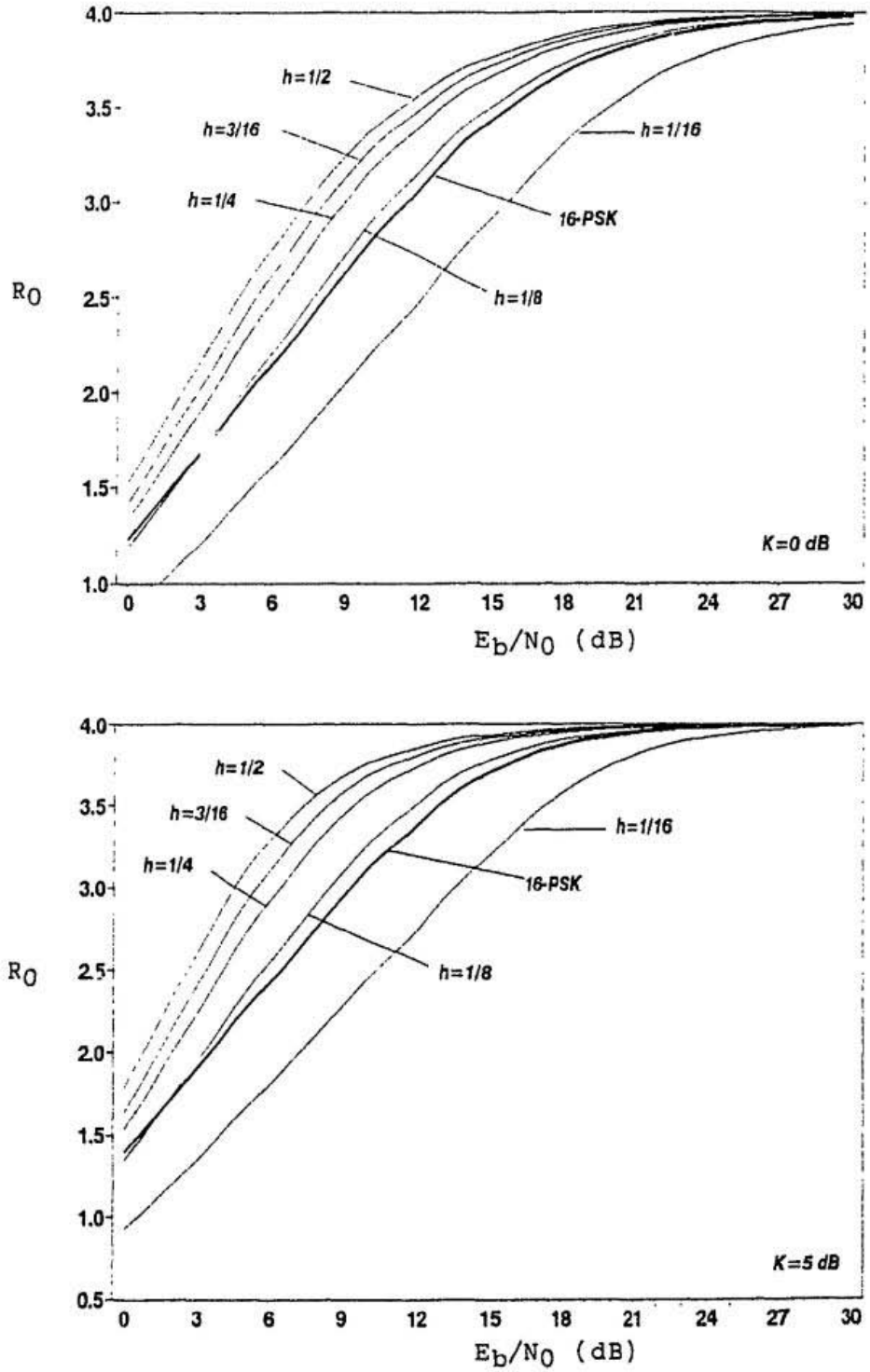

Figure 7.8 Channel cutoff rate R_0 v^s E_b/N_0 for suboptimum coherent detection of 16-CPFSK on mobile satellite channels.

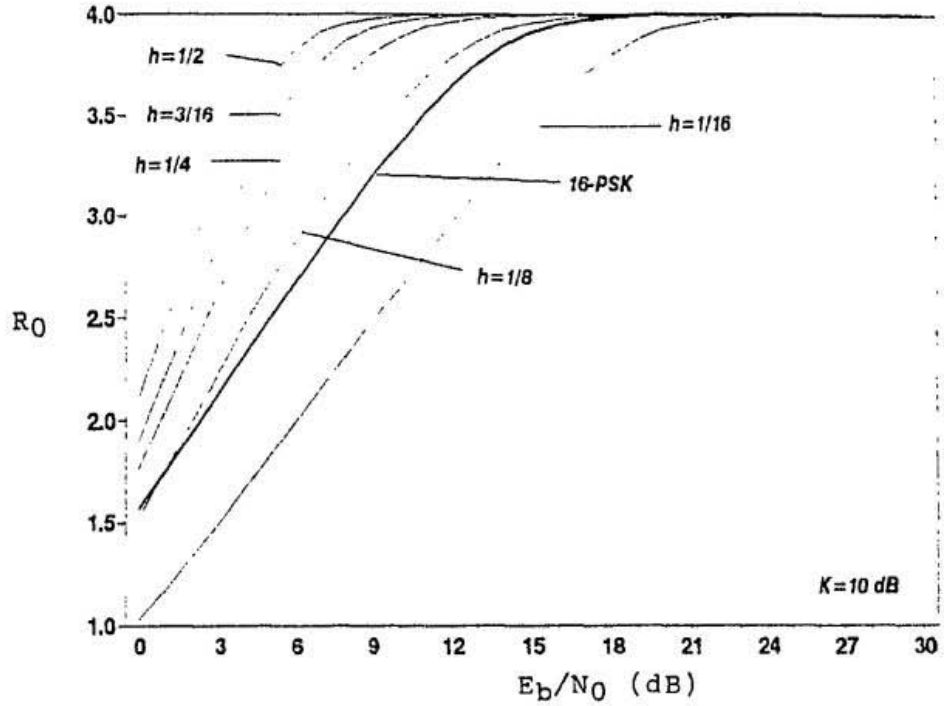

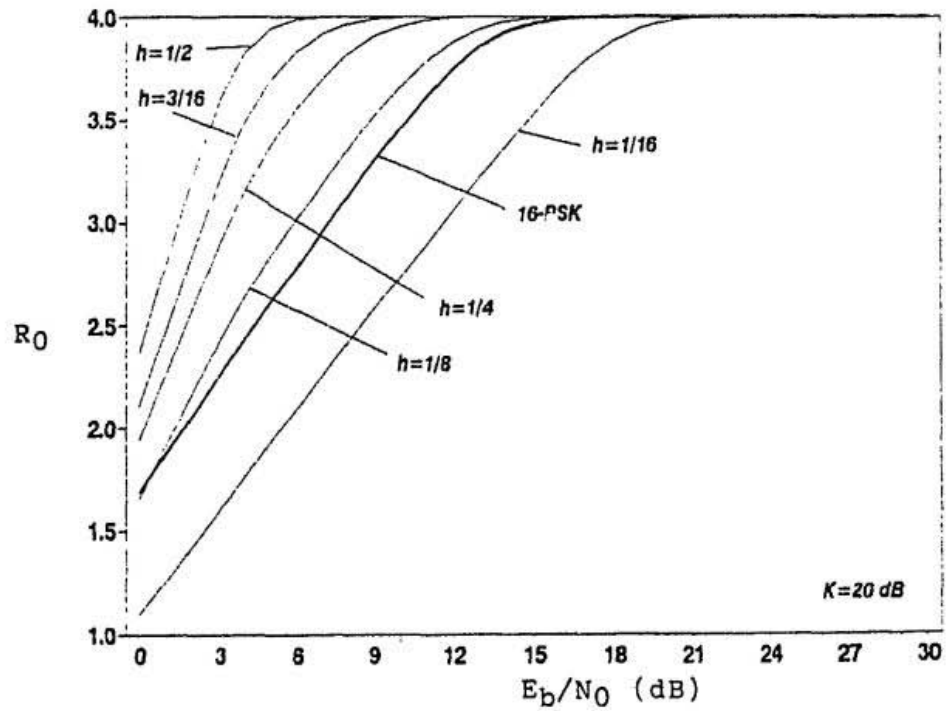

Figure 7.8 (Contd.) Channel cutoff rate R_0 vs E_b/N_0 for suboptimum coherent detection of 16-CPFSK on mobile satellite channels.

nite. But, in practice, the depth of interleaving must be finite. Symbol interleaving and deinterleaving introduces an unavoidable delay to the received signal. For digitized speech transmission it is well known that a delay of more than about 60 ms cannot be tolerated. If the depth of interleaving cannot exceed the maximum fade duration in a mobile communication channel the system performance would degrade because the Viterbi algorithm is sensitive to burst errors. The system designer should select a suitable depth of interleaving so that the delay is not perceivable, yet sufficient to combat the fading. But, if only data is to be transmitted then adequate interleaving could be provided. Considering the 60 ms delay restriction that has to be adhered to in voice transmission it seems interleaving is not suitable for voice transmission in the mobile satellite channel. Therefore, the main application of the CPFSK trellis modulation codes considered in this study would be for data transmission.

7.5 Conclusions

Performance of suboptimum coherent detection of CPFSK trellis modulation codes on mobile satellite channels was considered in this chapter. The channel was assumed to be Rician distributed with a steady line-of-sight component, and the receivers were assumed to be ideal. Instead of the error probability criterion, the channel cutoff rate R_0 was used as the performance measure. Upper bounds on R_0 were calculated for coherent detection of PSK signals and suboptimum coherent detection of CPFSK signals on AWGN channels and Rician fading channels. It was found that for both these channels suboptimum coherent detection of 4-CPFSK is inferior to 4-PSK in terms of R_0. But, suboptimum coherent detection of 8-CPFSK with $h \geq 1/4$ and 16-CPFSK with $h \geq 1/8$ offered better coding potential than coherent 8-PSK and 16-PSK, respectively. This makes suboptimum coherent detection of 8-CPFSK and 16-CPFSK more attractive alternatives to PSK signals on mobile satellite channels.

Chapter 8

Summary and Conclusions

The main contributions of this research can be summarized as follows:

A simplified, time-invariant finite-state trellis representation is introduced for CPFSK signals. According to the traditional finite-state trellis representation the number of phase states is equal to q if p is even and $2q$ if p is odd, where the modulation index $h = p/q$, with p and q relatively prime positive integers. By assuming that the lowest tone of the CPFSK signal goes through an integer multiple of cycles during a signalling interval, we have shown that the number of trellis phase states can always be made equal to q, irrespective of whether p is odd or even.

Based on the simplified finite-state trellis representation, a matrix representation is formulated for CPFSK signals, which is applicable to any M-CPFSK signal with $h \leq 1/M$. A state transition matrix can be defined for any CPFSK trellis modulation code when there are no parallel branches in the trellis. When $h \leq 1/M$, CPFSK signals do not have any parallel branches in the trellis. The state transition matrix indicates the presence or the absence of transitions between states in the trellis. The combination of state transition matrix and state location matrix defined at the end of every signalling interval gives rise to a matrix description for CPFSK signals. The matrix approach can be used to simplify trellis search procedures that compute minimum distance and other trellis parameters.

One of the goals of this research was to find ways of improving the error performance of CPFSK signals. The fixed-h binary nonlinear CPFSK signalling scheme introduced here can be considered as an improvement of the general CPFSK signals without resorting to multi-h type signalling. They differ from general CPFSK signals in that all transitions of general CPFSK are not allowed in binary nonlinear CPFSK, thereby decreasing the connectivity of the trellis and delaying the merging of path-pairs. Numerical results indicate that, for a given complexity, binary nonlinear CPFSK schemes can be designed so that they achieve larger minimum squared Euclidean distances and memory lengths than general binary CPFSK signals. A systematic method for the construction of binary nonlinear CPFSK trellis modulation codes that achieve the maximum memory length allowed by the number of states is given. The coding gains of these binary nonlinear schemes on the AWGN channel ranged from 0.3 dB to 2.2 dB compared with MSK signalling. They lacked the important property of rotational invariance, which would have enabled quick resynchronisation of signals after signal fades.

Suboptimum coherent phase detection and trellis decoding technique for CPFSK is a detection technique that has been directly adopted from PSK. The implementation of this receiver is simpler than that of the correlation receiver. The receiver has the added advantage that it can be used on interleaved channels. However, it is suboptimum because the inherent memory of CPFSK is unexploited. The performance of this receiver was studied on carrier phase offset channels. Using the well known Chernoff bounding technique, an equivalent distance that takes phase offsets into account was derived. It was found that this distance cannot be used for large phase offset values because, then error events with locally decreasing minimum distances occur. Based on a code search subject to a set of heuristic design rules, the optimum self-transparent 4-CPFSK and 8-CPFSK trellis modulation codes were

found for the carrier phase offset channel. It was found that for $h \leq 1/M$ the best codes were identical with those found in the literaure for AWGN channels, except when the memory length of the trellis code was one. Also, 8-CPFSK trellis modulation codes were found to be more sensitive to carrier phase offsets than 4-CPFSK trellis modulation codes.

Another goal of our research was to find how effective was the suboptimum coherent detection of CPFSK trellis modulation codes on mobile satellite channels. The mobile satellite channel was modelled as a Rician distributed fading channel with a steady line-of-sight component and the receiver was assumed to be ideal. Instead of the error probablity criterion, the channel cut off rate, R_0, was used as the performance measure. Bounds on R_0 were calculated for coherent detection of PSK signals and suboptimum coherent detection of CPFSK signals on AWGN channels and Rician fading channels. It was found that for both these channels, in terms of R_0, suboptimum coherent detection of 4-CPFSK is inferior to coherent detection of 4-PSK signals. But, for average signal-to-noise ratios, suboptimum coherent detection of 8-CPFSK with $h \geq 1/4$ and 16-CPFSK with $h \geq 1/8$ offered better coding potential than coherent 8-PSK and 16-PSK, respectively. This makes suboptimum coherent 8-CPFSK and 16-CPFSK more attractive alternatives to PSK signals on mobile satellite channels. The study was limited to $h \leq 1/2$. However, CPFSK signals have good spectral properties only in this range of h and hence is the region of interest for practical implementation.

A natural extension of this study would be to simulate the CPFSK trellis modulation codes in actual channel conditions to estimate the error performance. Critical parameters such as interleaving depth and channel model could then be selected to more accurately reflect the actual conditions. Instead of the Viterbi algorithm, one could use a suboptimum decoding algorithm, such as the M-algorithm, to decode

CPFSK signals in both Gaussian and non-Gaussian channels. We have mentioned that the spectra of binary nonlinear CPFSK would be close to the corresponding M-ary CPFSK signals. This could be verified by computing the spectra of nonlinear CPFSK by using a suitable method available in the literature. The performance on bandlimited channels, as well as the effects of co-channel and adjacent channel interference could also be studied. In coherent phase detection of CPFSK signals, the accuracy of the sampling instants is important because errors in sampling would cause performance degradation. An investigation of the effect of sampling errors on the performance of CPFSK trellis modulation codes on both the AWGN channel and non-Gaussian channels is also recommended.

References

[1] M. Abramowitz and I.A. Stegun (eds.).*Handbook of Mathematical Functions*, Dover Publications, New York, N.Y., U.S.A., 1972, p.486

[2] F. Abrishamkar and E. Biglieri, "Suboptimum Detection of Trellis-Coded CPM for Transmission on Bandwidth- and Power-Limited Channels." *IEEE Transactions on Communications*, vol. 39, no. 7, July 1991, pp. 1065 1074

[3] F. Abrishamkar and E. Biglieri, "Trellis-coded continuous phase modulation for satellite based mobile communications," in proceedings of the IEEE Global Telecommunications Conference, GLOBECOM'88, Holywood, FL, U.S.A., November 1988, pp. 1155 1159

[4] F. Abrishamkar and E. Biglieri, "Trellis coded CPM for satellite based mobile communications," in proceedings of the International Mobile Satellite Conference, Pasadena, CA, U.S.A., May 1988, pp. 263-270

[5] F. Amoroso, "The bandwidth of digital data signals," *IEEE Communications Magazine*, vol. 18, no. 6, November 1980, pp. 13-24

[6] J.B. Anderson, T. Aulin and C.-E. Sundberg, *Digital Phase Modulation*, Plenum Press, New York, N.Y., U.S.A., 1986

[7] J.B. Anderson and R. de Buda, "Better phase-modulation error performance using trellis phase codes," *Electronics Letters*, vol. 12, no. 22, October 1976, pp. 587-588

[8] J.B. Anderson, J. Hagenauer, C.-E.W. Sundberg, and R.E. Ziemer, "Bandwidth and power-efficient coded modulation," Guest editorial, *IEEE Journal on Selected Areas in Communications*, vol. SAC-7, no. 6, August 1989, pp. 1277-1279

[9] R.R. Anderson and J. Salz, "Spectra of digital FM," *Bell System Technical Journal*, vol. 44, July/August 1965, pp. 1165-1189

[10] J.B. Anderson and C.-E. W. Sundberg, "Advances in Constant Envelope Coded Modulation," *IEEE Communications magazine*, vol. 29, no. 12, December 1991, pp. 36-45

[11] J.B. Anderson, C.-E.W. Sundberg, T. Aulin, and N. Rydbeck, "Power-bandwidth performance of smooth phase modulation codes," *IEEE Transactions on Communications*, vol. COM-29, no. 2, February 1981, pp. 156-162

[12] J.B. Anderson and D.P. Taylor, "A bandwidth efficient class of signal space codes," *IEEE Transactions on Information Theory*, vol. IT-24, no. 6, November 1978, pp. 703–712

[13] T. Aulin, "Symbol error probabilty bounds for coherently Viterbi decoded continuous phase modulated signals," *IEEE Transactions on Communications*, vol. COM-29, no. 11, November 1981, pp. 1707-1714

[14] T. Aulin, N. Rydbeck, and C.-E.W. Sundberg, "Continuous phase modulation-Part II: Partial response signaling," *IEEE Transactions on Communications*, vol. COM-29, no. 3, March 1981, pp. 210–225

[15] T. Aulin and C.-E.W. Sundberg, "CPM- An efficient constant amplitude modulation scheme," *International Journal of Satellite Communications*, vol. 2, 1984, pp. 161–186

[16] T. Aulin and C.-E. Sundberg, "Partially coherent detection of digital full response continuous phase modulated signals," *IEEE Transactions on Communications*, vol. COM-30, no. 5, May 1982, pp. 1096–1117

[17] T. Aulin and C.-E. Sundberg, "Calculating digital FM spectra by means of autocorrelation," *IEEE Transactions on Communications*, vol. COM-30, no. 5, May 1982, pp. 1199–1208

[18] T. Aulin and C.-E. Sundberg, "Synchronization properties of continuous phase modulation," in proceedings of the *IEEE Global Telecommunications Conference, GLOBECOM'82*, Miami, FL, U.S.A., 1982, pp. D7.1.1-D7.1.7

[19] T. Aulin and C.-E.W. Sundberg,"Continuous phase modulation-Part I: Full response signaling," *IEEE Transactions on Communications*, vol. COM-29, no. 3, March 1981, pp. 196–209

[20] S. Benedetto, E. Biglieri, and V. Castellani, *Digital Transmission Theory*, Prentice-Hall, Englewood Cliffs, N.J., U.S.A., 1987

[21] S. Benedetto, M.A. Marsan, G. Albertengo, and E. Giachin, " Combined coding and modulation: Theory and applications, "*IEEE Transactions on Information Theory*, vol. 34, no. 2, March 1988, pp. 223–236

[22] V.K. Bhargava, D. Haccoun, R. Matyas, and P.P. Nuspl, *Digital Communications by Satellite*, John Wiley, New York, NY, U.S.A., 1981

[23] E. Biglieri, "High level modulation and coding for non-linear satellite channels," *IEEE Transactions on Communications*, vol. COM-32, no. 5, May 1984, pp. 616-626

[24] E. Biglieri, D. Divsalar, P.J. McLane, and M. K. Simon, *Introduction to Trellis-Coded Modulation with Applications*, McMillan Publishing Company, New York, NY, U.S.A., 1991

[25] E. Biglieri and P.J. McLane, "Uniform distance and error probabilty properties of TCM schemes," *IEEE Transactions on Communications*, vol. 39, no. 1, January 1991, pp. 41-53

[26] J.K. Cavers, "An Analysis of Pilot Symbol Assisted Modulation for Rayleigh Fading Channels," *IEEE Transactions on Vehicular Technology*, vol. 40, no. 4, November 1991, pp. 686-693

[27] G.C. Clark and J.B. Cain, *Error-Correction Coding for Digital Communications*, Plenum Press, New York, NY, U.S.A., 1981

[28] K. Clarke, R. Davis, and J. Roesch, "Development of a coded 16-ary CPFSK coherent demodulator," in conference record of the *International Mobile Satellite Conference*, Pasadena, CA, U.S.A., May 1988, pp. 317-322

[29] F. Davarian, "Mobile digital communications via tone calibration," *IEEE Transactions on Vehicular Technology*, vol. VT-36, May 1987, pp. 55-62

[30] F. Davarian, "Channel simulation to facilitate mobile-satellite communication research," *IEEE Transactions on Communications*, vol. COM-35, no. 1, January 1987, pp. 47–56

[31] F. Davarian, "Fade Margin Calculation for Channels Impaired by Rician Fading," *IEEE Transactions on Vehicular Technology*, vol. VT-34, no. 1, February 1985, pp. 41–44

[32] R. de Buda, "Fast FSK signals and their demodulation," *Canadian Electrical Engineering Journal*, vol. 1, no. 1, 1976, pp. 28–34

[33] R. de Buda, "Coherent demodulation of frequency-shift keying with low deviation ratio," *IEEE Transactions on Communications*, vol. COM-20, no. 3, June 1972, pp. 429–436

[34] D. Divsalar and M.K. Simon, "The design of trellis coded MPSK for fading channels: Performance criteria," *IEEE Transactions on Communications*, vol. COM-36, no. 9, September 1988, pp. 1004–1012

[35] D. Divsalar and M.K. Simon, "The design of trellis coded MPSK for fading channels," Set partitoning for optimum code design," *IEEE Transactions on Communications*, vol. COM-36, no. 9, September 1988, pp. 1013–1021

[36] D. Divsalar and M.K. Simon, "Trellis-coded modulation for 4800–9600 bit/s transmission over a fading mobile satellite channel," *IEEE Journal on Selected Areas in Communications*, vol. SAC-5, no. 2, February 1987, pp. 162–175

[37] D. Divsalar, M.K. Simon, and T. Jedrey,"Trellis coding techniques for mobile communications," in proceedings of the *IEEE Military Communications Conference, MILCOM'88*, San Diego, CA, U.S.A., October 1988

[38] N. Ekanayake, "M-ary continuous phase frequency shift keying with modulation index $1/M$." *IEE Proceedings*, vol. 131, Part F, no. 2, April 1984, pp. 173-178

[39] N. Ekanayake and R. Liyanapathirana, "Distance properties of trellis-coded M-ary CPFSK," presented at the *IEEE International Symposium on Information Theory*, Ann Arbor, Michigan, U.S.A., October 1986

[40] J.P. Fonseka, "Nonlinear Continuous Phase Frequency Shift Keying," *IEEE Transactions on Communications*, vol. 39, no. 10, October 1991, pp. 1473-1481

[41] J.P. Fonseka, "Adaptive CPFSK signaling," in proceedings of the *IEEE International Conference on Communications, ICC'90*, Atlanta, GA, U.S.A., April 1990, pp. 231.4.1-231.4.5

[42] J.P. Fonseka and G.R. Davis, "Cobined coded/multi-h CPFSK signaling," *IEEE Transactions on Communications*, vol. 38, no. 10, October 1990

[43] G.D. Forney, "The Viterbi Algorithm," *Proceedings of the IEEE*, vol. 61, no. 3, March 1973, pp. 268–278

[44] G.D. Forney, R.G. Gallager, G.R. Lang, F.M. Longstaff, and S. U. Qureshi, "Efficient modulation for band-limited channels," *IEEE Journal on Selected Areas in Communications*, vol. SAC-2, no. 5, September 1984, pp. 632-647

[45] T. Fujino, Y. Umeda, and E. Yamazaki, "Coded Octal PSK System Performance Disturbed by Imperfect Recovered Phase Reference," *Electronics and Communications in Japan*, Part I, vol. 68, no. 7, pp. 114–123 (Translated

from Denshi Tsushin Gakkai Ronbunshi, vol. 67-B, no. 10, October 1984, pp. 1095–1102)

[46] A. Gray and G.B. Mathews, *A Treatise on Bessel Functions*, Macmillan and Co., London

[47] S.A. Gronemeyer and A.L. McBride, "MSK and Offset QPSK Modulation," *IEEE Transactions on Communications*, vol. COM-24, no. 8, August 1976, pp. 809–819

[48] J. Hagenauer and E. Lutz, "Forward error correction coding for fading compensation in mobile satellite channels," *IEEE Journal on Selected Areas in Communications*, vol. SAC-5, no. 2, February 1987, pp. 215–225

[49] Conference record of the *International Mobile Satellite Conference, IMSC'88*, May 1988, Jet Propulsion Lab, Pasadena, CA, U.S.A.

[50] R.W. Kerr and P.J. McLane, "Coherent detection of interleaved trellis encoded CPFSK on shadowed mobile satellite channels," in proceedings of the *Canadian Conference on Electrical and Computer Engineering*, September 1989, pp. 83–88

[51] W.U. Lee, "Carrier synchronization of CPFSK signals," in proceedings of the *National Telecommunications Conference, NTC'77*, Los Angeles, CA, U.S.A., December 1977, pp. 30.2.1–30.2.4

[52] S. Lin and D.J. Costello, *Error Control Coding: Fundamentals and Applications*, Prentice-Hall, Englewood Cliffs, N.J.,U.S.A., 1983

[53] G. Lindell. *On Coded Continuous Phase Modulation*. Ph.D. Dissertation. Telecommunication Theory Department. University of Lund. Lund. Sweden. May 1985

[54] G. Lindell and C.-E.W. Sundberg. "An upper bound on the bit error probability of combined convolutional coding and continuous phase modulation." *IEEE Transactions on Information Theory*, vol. 34. no. 5. September 1988. pp. 1263–1269

[55] G. Lindell and C.-E.W. Sundberg, "Error probabilty of multilevel CPM with high rate convolutional codes." in conference record of the *International Zurich Seminar on Digital Communications*. Zurich. Switzerland. March 1984. pp. 93–100

[56] G. Lindell and C.-E. Sundberg, "Multi-level continuous-phase modulation with high-rate convolutional codes," in proceedings of the *IEEE Global Telecommunications Conference, GLOBECOM'83*. San Diego, CA. U.S.A., Nov. 29–Dec. 1, 1983. pp. 30.2.1–30.2.6

[57] G. Lindell, C.-E. Sundberg, and T. Aulin, "Minimum Euclidean distance for combinations of short rate-1/2 convolutional codes and CPFSK modulation," *IEEE Transactions on Information Theory*, vol. IT-30, no. 3, May 1984, pp. 509–519

[58] Y.-J. Liu and E. Biglieri, "Fully transparent phase/Doppler invariant trellis-coded modulation," *IEE Proceedings-I*, vol. 138, no. 2, April 1991, pp. 105-116

[59] R. Liyanapathirana and N. Ekanayake, "On the Exact Formula for the Minimum Squared Euclidean Distance of CPFSK," *IEEE Transactions on Communications*, vol. 42, no. 11, November 1994

[60] R. Liyanapathirana and N. Ekanayake, "Finite-state trellis representation of Continuous-Phase Modulation," *Electronics Letters*, vol. 28, no. 2, 16 January 1992, pp. 108–109

[61] R. Liyanapathirana and N. Ekanayake, "Phase detection and trellis decoding of CPFSK signals," in proceedings of the *International Conference on Communication Systems, ICCS'88*, Singapore, October 1988, p. 27.4

[62] R. Liyanapathirana and N. Ekanayake, "Correlation detection and trellis decoding of CPFSK signals," *Electronics Letters*, vol. 24, no. 21, 13 October 1988, pp. 1330–1331

[63] R. Liyanapathirana and S. Le-Ngoc, "Nonlinear CPFSK Trellis Modulation Codes," in proceedings of the *International Conference on Selected Topics in Wireless Communications*, Vancouver, B.C., Canada, June 1992

[64] R. Liyanapathirana, S. Le-Ngoc and N. Ekanayake, "Matrix representation of CPFSK trellis modulation codes," *Electronics Letters*, vol. 29, no. 9, 29 April 1993, pp. 757–758

[65] R. Liyanapathirana, S. Le-Ngoc and N. Ekanayake, "Nonlinear Continuous-Phase Frequency-Shift-Keying," *Electronics Letters*, vol. 28, no. 8, 9 April 1992, pp. 758–760

[66] J.H. Lodge and M.L. Moher. "Time diversity for mobile satellite channels using trellis-coded modulations." in proceedings of the *IEEE Global Communications Conference, GLOBECOM'87*. Tokyo, Japan. 1987. pp. 8.7.1 8.7.5

[67] J.H. Lodge, M.L. Moher and S.N. Crozier. "A comparison of data modulation techniques for land-mobile satellite channels". *IEEE Transactions on Vehicular Technology*, vol. VT-36, no. 1, February 1987,pp. 28 35

[68] C. Loo. "A statistical link for a land-mobile satellite link." *IEEE Transactions on Vehicular Technology*, vol. VT-34, no. 3, August 1985, pp. 122 127

[69] J.L. Massey. "Coding and modulation in digital communications." in conference record of the *International Zurich Seminar on Digital Communications*, Zurich, Switzerland, 1974, pp. E2(1)-E2(4)

[70] J.L. Massey. "The how and why of channel coding," in conference record of the *International Zurich Seminar on Digital Communications*, Zurich, Switzerland, 1983, pp. E 1.1–E 1.7

[71] J.P. McGeehan and A.J. Bateman,"Phase locked transparent tone-inband (TTIB): A new spectrum configuration particularly suited to the transmission of data over SSB mobile radio networks," *IEEE Transactions on Communications*, vol. COM-32, no. 1, January 1984, pp. 81-87

[72] P.J. McLane, P.H. Wittke, and P. Ho, "PSK and DPSK trellis codes for fast fading shadowed mobile satellite channels," *IEEE Transactions on Communications*, vol. COM-36, no. 11, November 1988, pp. 1242–1246

[73] H. Miyakawa, H. Harashima, and Y. Tanaka, "A new digital modulation scheme, multimode binary CPFSK," in proceedings of the *Third Interna-*

tional Conference on Digital Satellite Communication, Kyoto, Japan, November 1975, pp. 105–112

[74] M.L. Moher and J.H. Lodge, "TCMP–A modulation and coding strategy for Rician fading channels," *IEEE Journal on Selected Areas in Communications*, vol. 7, no. 9, December 1989, pp. 1347–1355

[75] M.G. Mulligan and S.G. Wilson, "An improved algorithm for evaluating trellis phase codes," *IEEE Transactions on Information Theory*, vol. IT-30, no. 3, May 1984, pp. 509–519

[76] W.P. Osborne and M.B. Luntz, "Coherent and non-coherent detection of CPFSK," *IEEE Transactions on Communications*, vol. COM-22, no. 8, August 1974, pp. 1023–1036

[77] M.G. Pelchat, R.C. Davis, and M.B. Luntz, "Coherent demodulation of continuous phase binary FSK signals," in proceedings of *International Telemetering Conference*, Washington, D.C., U.S.A., 1971, pp. 181–190

[78] S.S. Pietrobon, D.J. Costello, and G. Ungerboeck, "Rotationally Invariant Trellis Codes," presented at the *IEEE International Symposium on Information Theory*, San Diego, CA, U.S.A., January 1990

[79] S.V. Pizzi and S.G. Wilson, "Convolutional coding combined with continuous phase modulation," *IEEE Transactions on Communications*, vol. COM-33, no. 1, January 1985, pp. 20–29

[80] J.G. Proakis, *Digital Communications*, McGraw-Hill, New York, NY, U.S.A., 1989

[81] B. Rimoldi, "Exact Formula for the Minimum Squared Euclidean Distance of CPFSK," *IEEE Transactions on Communications*, vol. 39, no. 9, September 1991, pp. 1280–1282

[82] B.E. Rimoldi, "A decomposition approach to CPM," *IEEE Transactions on Information Theory*, vol. 34, no. 2, March 1988, pp. 260–270

[83] C.M. Rush, "How WARC'92 Will Affect Mobile Services," *IEEE Communications Magazine*, vol. 30, no. 10, October 1992, pp. 90–96

[84] C. Schlegel and D.J. Costello, "Bandwidth efficient coding for fading channels: Code construction and performance analysis," *IEEE Journal on selected areas in communications*, vol. 7, no. 9, Dec. 1989, pp. 1356–1368

[85] T.A. Schonhoff, "Symbol error probabilities for M-ary CPFSK: Coherent and noncoherent detection," *IEEE Transactions on Communications*, vol. COM-24, no. 6, June 1976, pp. 644–652

[86] M.K. Simon, "The performance of multilevel DPSK on a fading mobile satellite channel," *IEEE Transactions on Vehicular Technology*, vol. VT-37, no. 2, May 1988, pp. 78–91

[87] C.-E. Sundberg, "Continuous phase modulation," *IEEE Communications Magazine*, vol. 24, no. 4, April 1986, pp. 25–38

[88] C.-E. Sundberg, "On continuous phase modulation in digital cellular mobile radio systems," *The Bell System Technical Journal*, vol. 62, no. 7, September 1983, pp. 2067–2089

[89] A.B. Svennson, "On optimum and sub-optimum coherent detection of continuous phase modulation on a two-ray multipath fading channel," *IEEE*

Transactions on Communications, vol. COM-35, no. 10, October 1987, pp. 1041 1049

[90] A. Svensson, "Reduced state sequence detection of full response continuous-phase modulation," *Electronics Letters*, vol. 20, no. 10, May 1984, pp. 654-656

[91] J.M. Tennant and N. Kingsbury, "Use of the Viterbi algorithm to compute error events of trellis phase coding in order of increasing distance," *IEEE Transactions on Communications*, vol. COM-36, no. 10, October 1988, pp. 1166 117

[92] G. Ungerboeck, "Trellis-coded modulation with redundant signal sets, Part I: Introduction," *IEEE Communications Magazine*, vol. 25, no. 2, February 1987, pp. 5–11

[93] G. Ungerboeck, "Trellis-coded modulation with redundant signal sets, Part II: State of the art," *IEEE Communications Magazine*, vol. 25, no. 2, February 1987, pp. 12–21

[94] G. Ungerboeck, "Channel coding with multilevel/phase sigals," *IEEE Transactions on Information Theory*, vol. IT-18, no. 1, Jan. 1982, pp. 55–67

[95] G. Ungerboeck and I. Csajka, "On improving data link performance by increasing the channel alphabet and introducing sequence coding," presented at the *IEEE International Symposium on Information Theory*, Ronneby, Sweden, June 1976, p. 53

[96] G. Ungerboeck and S.S. Pietrobon, "Codes for QPSK modulation with invariance under 90° rotation," in conference record of the *Mobile Satellite Conference*, Pasadena, CA, U.S.A., May 1988, pp. 277–282

[97] A.J. Viterbi, "Wireless digital communication: A view based on three lessons learned," *IEEE Communications magazine*, vol. 29, no. 9, September 1991, p. 33

[98] A.J. Viterbi and J.K. Omura, *Principles of Digital Communication and Coding*, McGraw-Hill, New York, NY, U.S.A., 1979

[99] L.F. Wei, "Trellis-coded modulations with multidimensional constellations," *IEEE Transactions on Information Theory*, vol. IT-33, no. 4, July 1987, pp. 483–501

[100] L.F. Wei, "Rotationally Invariant Convolutional Channel Coding with Expanded Signal Space. Part II: Nonlinear Codes," *IEEE Journal on Selected Areas in Communications*, vol. SAC-2, 1984, pp. 672–686

[101] S.G. Wilson, "Bandwidth efficient modulation and coding: A survey of recent results," in proceedings of the *IEEE International Communications Conference, ICC'86*, New York, NY, U.S.A., June 1986, pp. 31.1.1–31.1.5

[102] S.G. Wilson, "Rate-5/6 trellis-coded 8-PSK," *IEEE Transactions on Communications*, vol. COM-34, no. 10, October 1986, pp. 1045–1049

[103] S.G. Wilson and C.-D. Hsu, "Joint MAP data/phase sequence estimation for trellis phase codes," in proceedings of the *International Conference on Communications, ICC'80*, Seattle, WA, U.S.A., June 1980, pp. 26.1.1–26.1.5

[104] S.G. Wilson, H.A. Sleeper II, P.J. Schottler, and M.T. Lyons, "Rate-3/4 convolutional coding of 16-PSK," *IEEE Transactions on Communications*, vol. COM-32, no. 12, December 1984, pp. 1308–1315

[105] J.M. Wozencraft and I.M. Jacobs, *Principles of Communication Engineering*, John Wiley, New York, NY, U.S.A., 1965

[106] J.H. Yuen, M.K. Simon, W. Miller, F. Pollara, C.R. Ryan, D. Divsalar, and J. Morakis, "Modulation and coding for satellite and space applications," *Proceedings of the IEEE*, vol. 78, no. 7, July 1990, pp. 1250–1266

APPENDIX

Minimum Euclidean distance for CPFSK signals

Consider an M-ary signal set consisting of M finite energy signals $s_1(t)$, $s_2(t)$, $s_3(t)$ ..... $s_M(t)$. One waveform from the set of M waveforms is transmitted every T seconds in relation to the data symbol and depending on the symbols in the preceding time intervals. The well known geometric interpretation of signals [14] allows representation of the above signals as linear combinations of N ($N \leq M$) orthonormal basis functions. This can be seen as an N-dimensional coordinate representation of a signal set, and is known as the signal space. The distance between two signal points in the signal space is the same as the Euclidean distance between those two points.

For CPFSK signals the incremental squared Euclidean distance between any two signals $s_n(t)$ and $s'_n(t)$ is defined as

$$D^2[s_n(t),\, s'_n(t)] \triangleq \int_{nT}^{(n+1)T} [s_n(t) - s'_n(t)]^2\, dt, \qquad (A.1)$$

where

$$s_n(t) = \sqrt{2E_s/T}\cos(2\pi f_0 t + \pi h a_n t/T + \phi_n), \quad nT \leq t \leq (n+1)T,$$

and

$$s'_n(t) = \sqrt{2E_s/T}\cos(2\pi f_0 t + \pi h a'_n t/T + \phi'_n), \quad nT \leq t \leq (n+1)T.$$

ϕ_n and ϕ'_n are the phase angles (reckoned in modulo–2π) of the two signals $s_n(t)$ and $s'_n(t)$ at $t = nT$ as shown in Fig. A.1. From Equation (A.1) we have

$$D^2(s_n,\, s'_n) = \int_{nT}^{(n+1)T} s_n^2(t)dt + \int_{nT}^{(n+1)T} s_n'^2(t)dt - \int_{nT}^{(n+1)T} 2s_n(t)s'_n(t)dt.$$

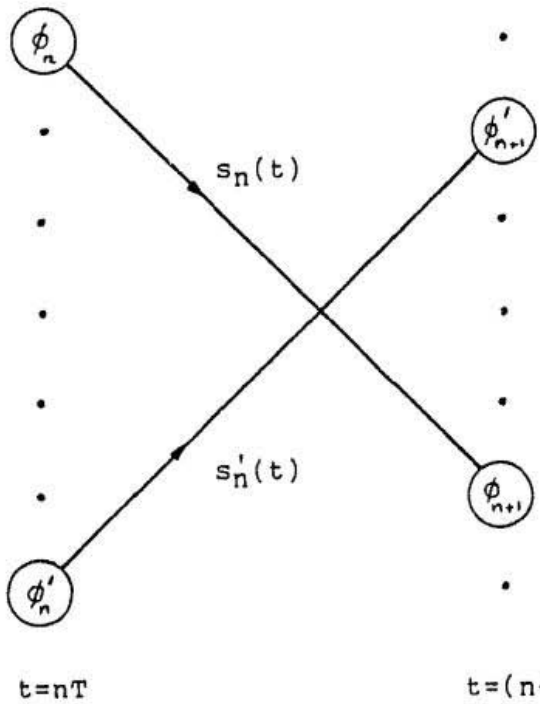

Figure A.1 Two signal paths of the CPFSK trellis.

The above equation reduces to

$$D^2(s_n,\, s'_n) = 2E_s - 2\int_{nT}^{(n+1)T} s_n(t)s'_n(t)dt.$$

Substituting for $s_n(t)$ and $s'_n(t)$ we get

$$\begin{aligned} D^2(s_n,\, s'_n) &= 2E_s - 2\int_{nT}^{(n+1)T} \sqrt{2E_s/T}\cos(2\pi f_0 t + \pi h a_n t/T + \phi_n) \times \\ &\qquad \sqrt{2E_s/T}\cos(2\pi f_0 t + \pi h a'_n t/T + \phi'_n)dt, \\ &= 2E_s - 2E_s/T\int_{nT}^{(n+1)T} \{\cos[\pi h(a_n - a'_n)t/T + \varphi_n - \phi'_n] + \\ &\qquad \cos[4\pi f_0 t + \pi h(a_n + a'_n)t/T + \varphi_n + \phi'_n]\}dt. \end{aligned}$$

Assuming $f_0 >> 1/T$,

$$D^2(s_n,\, s'_n) = 2E_s - 2E_s/T\int_{nT}^{(n+1)T} \cos[\pi h(a_n - a'_n)t/T + \phi_n - \phi'_n]dt + \epsilon$$

where $\epsilon \to 0$ as $f_0 \to \infty$.

$$\begin{aligned} D^2(s_n,\, s'_n) = 2E_s\{1 - \sin[\pi h(a_n - a'_n)/2]/[\pi h(a_n - a'_n)/2] \times \\ \cos[\pi h(a_n - a'_n)/2 + \phi_n - \phi'_n]\} + \epsilon \end{aligned}$$

Therefore the incremental squared Euclidean distance between any two signals $s_n(t)$ and $s'_n(t)$ is given by

$$D^2(s_n,\, s'_n) \approx 2E_s\{1 - \frac{\sin[\frac{\pi h(a_n - a'_n)}{2}]}{[\frac{\pi h(a_n - a'_n)}{2}]}\cos[\frac{\pi h(a_n - a'_n)}{2} + \phi_n - \phi'_n]\}.$$